Development of kaolin-based microporous membrane for energy efficient microalgal harvesting and effluent recycle under circular bioeconomic approach

Thesis submitted in partial fulfilment of the requirements for the degree of

DOCTOR OF PHILOSOPHY

By

ANKIT AGARWALLA

(186107002)

Department of Chemical Engineering

Indian Institute of Technology Guwahati

Assam- 781039, India

June 2024

Development of kaolin-based microporous membrane for energy efficient microalgal harvesting and effluent recycle under circular bioeconomic approach

-Ankit Agarwalla

Department of Chemical Engineering

Indian Institute of Technology Guwahati

Assam- 781039, India

CERTIFICATE

This is to certify that the thesis entitled **"Development of kaolin-based microporous membrane for energy efficient microalgal harvesting and effluent recycle under circular bioeconomic approach"** being submitted by **Mr. Ankit Agarwalla** for the award of the degree of Doctor of Philosophy has been carried out by him at Department of Chemical Engineering, Indian Institute of Technology Guwahati, under my guidance and supervision. This work has not been submitted to any other University or Institute for the award of any degree or diploma.

Date:

Place:

(Signature of Thesis Supervisor)

Prof. Kaustubha Mohanty

Department of Chemical Engineering

Indian Institute of Technology Guwahati

DEDICATION

This thesis is dedicated to my parents- Mr. Binod Agarwalla and Mrs. Champa Agarwalla and my wife Mrs. Priyanka Prajapati

Acknowledgement

First and foremost, I extend my deepest gratitude to my supervisor, **Prof. Kaustubha Mohanty** for his invaluable guidance, unwavering support, and constant encouragement throughout this journey. His expertise, patience, and dedication has been instrumental in shaping this research and fostering my intellectual growth.

I wish to extend my heartfelt appreciation to my doctoral committee members, **Prof. G.Pugazhenthi**, **Prof. Animes Kumar Golder**, and **Prof. Pankaj Kalita**, for their invaluable guidance and constructive feedback provided during my seminars and progress reviews. Their input has been instrumental in the accomplishment of my thesis.

I express my gratitude to **Prof. Kaustubha Mohanty**, the current Head of the Department of Chemical Engineering, and **Prof. Anugrah Singh**, the former Head, for their administrative support. Additionally, I appreciate the continuous encouragement and assistance received from all the staff members of the Chemical Engineering Department. I am thankful to the Department of Chemical Engineering, School of Energy Science and Engineering and the Central Instruments Facility at IIT Guwahati for granting access to instrumental facilities.

I am indebted to the selfless help and co-operation of my research group members, Mr. Om Prakash, Ms. Janaki Komandur, Ms. Anindita Das, Mr. Pikesh Kumar, Mr. Sanku Pratim Bora, Mr. Naveenkumar Ashok Yaranal, Mr. Abhishek kumar, (Bioenergy & Waste Management lab) and Dr. Sanjeev Mishra. Dr. Madonna Roy, Dr. Sounak Bera, Mr. Deepesh Singh Chauhan, Ms. Pooja Singh, Mr. Saptaswa Biswas, Ms. Suchetna Kushwah and Ms. Priyanka Tripathi, (Algal Biorefinery Lab group)

I would also like to acknowledge Mr. Anweshan Ghosh, Mrs. Ananya Bardhan, Dr. Prabhat Patel, Mrs. Deepti Nair, and Dr. Karan Kumar for their help and support.

My Ph.D. endeavour would not have been successful without the love, trust, support and blessings of my parents and family members. I owe my achievements to my family. I thank my sisters Swati Agarwal and Preeti Agarwal for their constant support and love. I thank my wife Mrs. Priyanka Prajapati for her immense care, encouragement and moral support in achieving this level and always standing by me in all phases of my life.

I am deeply grateful to God for His unwavering guidance and divine grace throughout the journey of completing this Ph.D. thesis. In moments of challenge and triumph, His presence has been my constant source of strength and inspiration.

Sincerely,

Ankit Agarwalla

Abstract

Biodiesel as a renewable energy source can provide an alternative to the alarmingly depleting energy from fossil fuels. Microalgae is an encouraging third-generation feedstock for the production of biodiesel as it has the capability of oil production throughout the year. Besides several advantages, commercial production of microalgal biomass feedstock is not considered sustainable due to its high production cost. In this context, recycling the culture media carry significant potential to reduce the overall cost for the long-term growth of microalgal industry. The first and most crucial step in the downstream processing of biomass is the recovery of microalgae from culture. Due to energy and capital costs, selecting and designing an appropriate harvest method for large-scale algae production facilities is crucial. The absence of chemicals permits the incorporation of membrane technology into the microalgae biorefinery, simplifying the process of extracting products from biomass and culture media recycling. Ceramic membranes exhibit superior chemical, thermal, and mechanical stability in contrast to polymeric membranes. But their application in microalgal harvesting is restricted due to the substantial capital cost, mainly contributed by the starting raw material. Also, activated carbon can adsorb organic compounds on its surface thereby limiting the inhibitor growth in the harvested media and improving the algal growth henceforth. Though several advantages, implementation in the recycling of microalgal culture medium is not studied significantly.

In this work, indigenous low-cost disc and tubular membranes were fabricated using naturally available kaolin as the key precursor. Different composition of kaolin (80-92 wt.%) and binder (8-20 wt.%) was used to optimize the raw material and binder composition. The optimized binder concentration in disc membrane was used to further fabricate tubular membranes. Moreover, calcium carbonate was added to enhance the porosity of the tubular membranes. Disc membranes were prepared by paste casting and tubular membranes by extrusion technique. In both cases, X-Ray Diffusion, X-Ray Fluorescence, particle size, Fourier Transform Infrared Spectroscopy,

Thermo-gravimetric, Field emission scanning electron microscopy, porosity, pore size, water permeability, mechanical strength and chemical strength analysis were employed to determine the optimum raw material, binder as well as poreformer composition.

With increase in binder percentage from 8% to 20% in disc membranes, the percentage porosity, average pore size and water permeability decreased from 34.52% to 21.5%, 2.28 µm to 0.195 µm and 6.12×10^{-9} to 1.69×10^{-9} m Pa^{-1} s^{-1} respectively while flexural strength increased slightly from 7.1 MPa to 9.4 MPa. Hence, binder percentage of 8% i.e., 2% boric acid, 2% sodium metasilicate and 4% sodium carbonate was found to be optimum. Thereafter, tubular membranes will be fabricated using this binder concentration. The fabricated tubular membranes had porosity of ~26% - 47%, a pore diameter of 0.123-0.182 µm, water permeability of 4.2×10^{-8} – 17.1×10^{-8} m^3 m^{-2} s^{-1} kPa^{-1}, along with good mechanical and chemical strength.

The optimized membrane (77% kaolin, 2% boric acid, 2% sodium metasilicate, 4% sodium carbonate, and 15% calcium carbonate) was tested for microfiltration of microalgae *Monoraphidium* sp. KMC4 with 1.5 g L^{-1} of initial concentration at a persistent cross-flow rate (1.11×10^{-5} m^3 s^{-1}) and various transmembrane pressures (69 kPa - 345 kPa). The separation results yielded an average permeate flux of 1.85×10^{-5} m^3 m^{-2} s^{-1} at an optimized transmembrane pressure of 276 kPa. The corresponding volume reduction factor and permeate recovery were 1.38 and 28.17%, respectively. Complete algal cell recovery and substantial nutrient passage (>88%) were observed within the pressure range of 69 kPa to 345 kPa. Fouling mechanism was explained by fitting four distinct pore-blocking models, of which the cake filtration model provided the most accurate fit as compared to the complete, intermediate and standard pore-blocking models. Additionally, the total organic carbon varied in the range of 31.6-63.2 mg L^{-1}. This essentially explained the source of pore blocking. The elongated shape of *Monoraphidium sp.* KMC4 might have contributed to the enhanced fouling of membrane. Lastly, the nitrate

passage was almost complete (~88% - 97%), highlighting the prospects of permeate stream in further cultivation process.

Henceforth, the suitability of cultivating *Monoraphidium* sp. KMC4 was exhibited in different effluent-based culture (EBC) media concentrations, the latter being treated with powdered activated carbon (PAC) with a loading of 5-50 mg L^{-1}. The optimum EBC media treated with 30 mg L^{-1} PAC enhanced the biomass yield by 21.9% as compared to the untreated one (1.21 g L^{-1}). A recyclability study performed in five batches resulted in an optimal growth up to three batches with an overall biomass yield of 4.21 g and a total water savings of 30%. Additionally, physico-chemical characterization and FAME profile of the biomass from the recyclability study validated feedstock's energy potential. Moreover, this study proposes a biorefinery model which could recover nutrient rich liquid effluent (3.1 million litres) and solid residue for various applications along with the generation of 5760 kg of biomass followed by 113 L d^{-1} biodiesel yield.

The economic feasibility of low-cost membrane fabrication, microalgal harvesting using the developed membrane and the energy efficient recycle process has been successfully assessed. The initial phase of cost estimation begins with assessing the expenses involved in membrane fabrication, which encompasses equipment costs and manufacturing expenses. The projected cost per square meter of membrane stands at 190.93 USD, falling within the category of low-cost membranes. Following this, the subsequent stage of cost estimation involves evaluating the cost of microalgal harvesting using the low-cost tubular kaolin membrane, both in lab scale as well as pilot scale. The lab scale setup consists of a single membrane with an effective filtration area of 15.71×10^{-4} m^2, while the pilot scale comprises three parallel membrane housings, each containing seven membranes, with an effective filtration area of 0.0989 m^2. For the lab scale process, the total cost of harvesting one litre of microalgal culture was estimated to be 0.648 USD/L which lowered to 0.04 USD/L for the pilot scale harvesting setup.

The final step of cost estimation involved the energy efficient recycle process, both in lab scale as well as pilot scale. The cost per gram of biomass was calculated to be 7.02 USD/g for the lab scale configuration while it dropped to 0.1195 USD/g for the pilot scale setup.

CONTENTS

List of Tables

List of Figures

NOMENCLATURE

Abbreviations

APHA	American Public Health Association
ASTM	American Society For Testing And Materials
AOM	Algalogenic Organic Matter
CFV	Cross Flow Velocity
CE	Cellulose Ether
DOC	Dissolved Organic Carbon
DCW	Dry Cell Weight
EBC	Effluent Based Culture
EPS	Extracellular Polysaccharides
EOM	Extracellular Organic Matter
FO	Forward Osmosis
FTIR	Fourier-Transform Infrared Spectroscopy
FAME	Fatty Acid Methyl Esters
GAC	Granular Activated Carbon
LOI	Loss on Ignition
MF	Microfiltration
MUFA	Monounsaturated Fatty Acids
OD	Optical Density
PAC	Powdered Activated Carbon
PSF	Polysulphone
PC	Polycarbonate
PMMA	Polymethyl Methacrylate
PEG	Polyethylene Glycol
PSS	Poly-(Styrenesulfonate)
PDADMAC	Poly-(Diallyldimethylammonium Chloride)
PESH	Polyethersulfone
PET	Polyethylene Terephthalate
PAC	Powdered Activated Carbon
PSD	Particle Size Distribution
PUFA	Polyunsaturated Fatty Acids
RO	Reverse Osmosis

RC	Regenerated Cellulose
sPSF	Sulfonated Polysulfone
SFA	Saturated Fatty Acid
TMP	Transmembrane Pressure
TOC	Total Organic Carbon
TGA	Thermogravimetric Analysis
UF	Ultrafiltration
USD	US Dollar
VRF	Volume Reduction Factor
XRD	X-Ray Diffraction
XRF	X-Ray Fluorescence

Notations

A	Membrane Area
b	Sample Width
B	Dry Cell Weight
C_0	Initial Feed Concentration
C_p	Permeate Concentration
d_i	Diameter of the i^{th} Pore
F	Fracture Point Load
J	Water Flux
L	Span Length
L_h	Hydraulic Permeability
n	Overall Count of Pores
n_i	Quantity of Pores with Diameter D_i
P	Pressure
Q	Permeation Volume
t	Sample Thickness
V_f	Final Feed Volumes
V_i	Initial Feed Volumes
V_m	Membrane Volume
V_p	Volume of Permeate Collected

W_{dry}	Weight of Dry Membrane
W_f	Final Weight
W_i	Initial Weight
W_{wet}	Weight of Wet Membrane
X	OD taken at 680 nm

Greek Symbols

σ	Flexural Strength
τ	Membrane Tortuosity
ε	Membrane Porosity
μ	Viscosity of Pure Water
π	Pi

Chapter 1

Introduction, Literature Survey and Objectives

CHAPTER 1

Introduction, Literature Survey and Objectives

The initial part of this chapter provides a concise overview of the basics and classification of membrane technology. The recent advances on the use of low-cost raw material for membrane fabrication are also highlighted with main focus on kaolin as the key precursor. This is succeeded by a detailed discussion on microalgal harvesting techniques with focus on the use of membrane technology for the same. This chapter also provides insights on the treatment of harvested effluent for energy efficient recycle. The meticulous literature review carried out here unveils potential scopes for further research in the above topic, which also shapes the objectives of the thesis. Finally, this chapter outlines the structure of the thesis.

1.1. Introduction to Membrane Technology

Membrane systems are acknowledged globally because of their cost-effectiveness, ease of use and exceptional energy efficiency. Bechhold's patent in 1907 [2] introduced nitrocellulose membranes with consistent pore sizes and subsequently researchers across the globe have enhanced the design. The first microporous membrane available for consumers was way back in 1930s. In the next 30 years, microfiltration membrane with cellulose acetate as precursor was developed using phase inversion technique by Loeb and Sourirajan [3]. Membrane production have blossomed with time solving various separation problems worldwide. It is a rapidly evolving field in chemical engineering and separation science that involves the use of semipermeable membranes to separate and purify various substances from a mixture [4]. These membranes typically made from polymers or ceramics act as sieves, allowing specific molecule to pass through while blocking others based on their charge, size or chemical properties [5].

Membrane technology offers several advantages in several industrial applications which include selectivity, energy efficiency, environmental sustainability, scalability, reduced chemical usage, reduced environmental impact and improved product quality [6].

1.1.1. Classification of membrane processes

The transport mechanism across a membrane takes place when a driving force is involved and applied to the feed components. Based on this driving force membrane separation processes are classified into four categories as shown in Fig. 1.1.

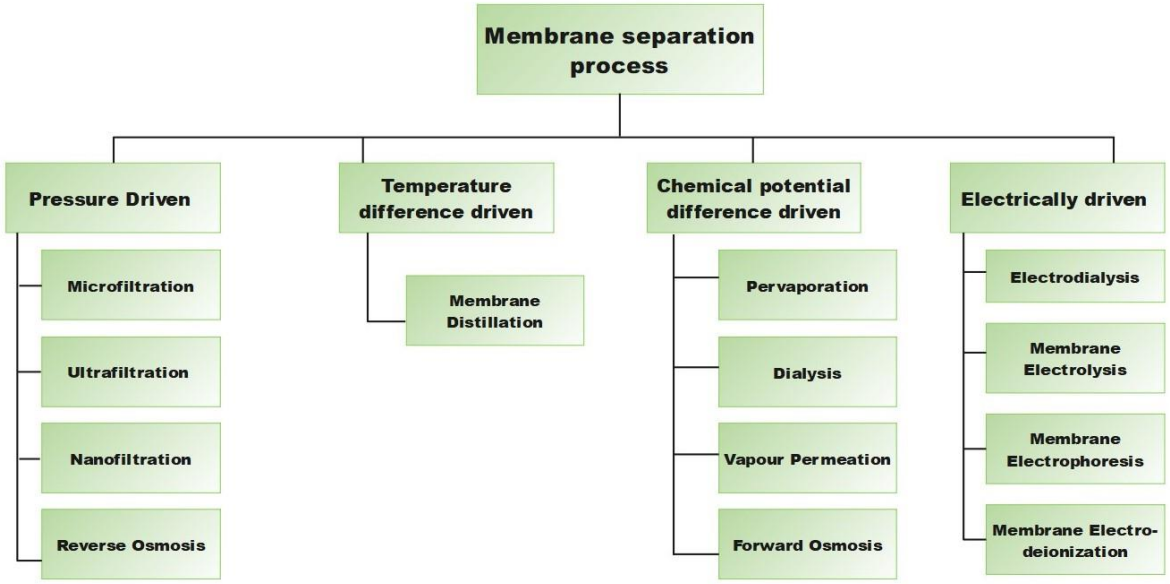

Fig. 1.1 Classification of membrane separation process based on driving force

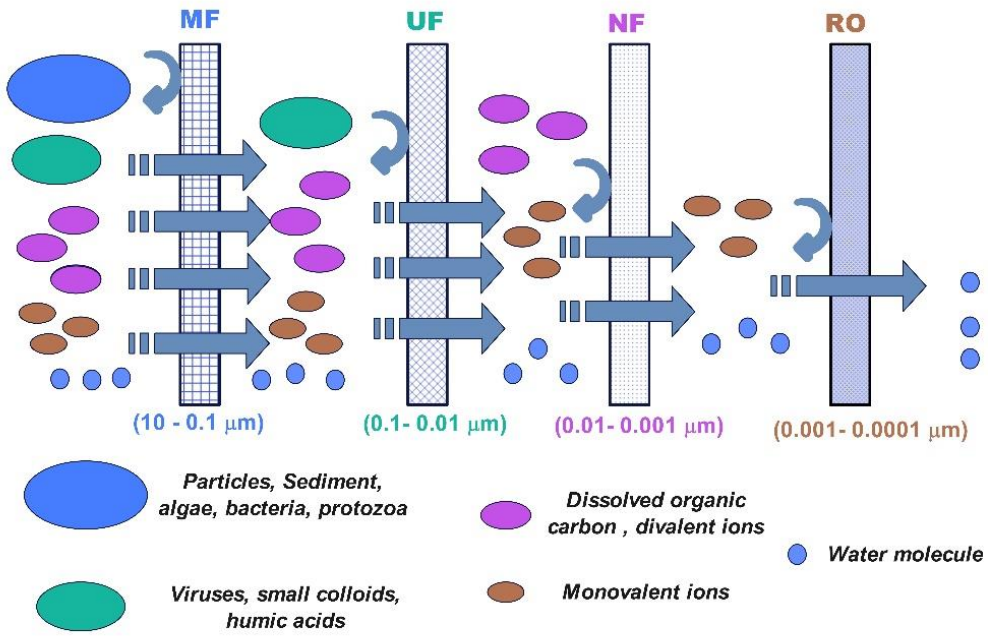

Fig. 1.2 Classification of pressure driven membrane process according to their pore size and components separated

Out of all the driving forces, pressure-driven membrane processes are attracting growing attention owing to their various benefits in comparison to their counterparts [7]. Water treatment membrane processes predominantly involve pressure-driven separation mechanisms, with the driving force being a pressure differential across the membrane [8]. Fig. 1.2 depicts different classes of pressure driven processes such as microfiltration, ultrafiltration, nanofiltration and reverse osmosis.

- ***Microfiltration (MF):***

  - The pore diameter of MF ranges from 10 µm to 0.1 µm. MF is one of the earliest pressure-driven membrane technology adopted in commercial applications.

- Focused on the principle of physical separation, MF is proficient at separating particles in micrometre range which includes suspended particles, viruses, bacteria, protozoa and algae.
- The wide range of pore size in MF membranes has facilitated its applications in various fields like wastewater treatment, food, biotechnology and desalination [8].

➢ ***Ultrafiltration (UF):***

- The pore size of UF membrane lies between 0.1 and 0.01 µm.
- Commonly employed in industries where removal of specific components is essential.
- UF membranes are operated in the pressure range of 1 to 10 bar.
- Can separate colloids, humic acids and viruses from the feed wastewater stream [9].

➢ ***Nanofiltration (NF):***

- NF membranes typically have pore size between 0.01 to 0.001 µm.
- NF membranes are designed to selectively separate ions, organic compounds and small molecules. They are highly effective at removing low molecular weight solutes and divalent ions.
- NF membranes are operated in the pressure range of 5 to 10 bar [10].

➢ ***Reverse Osmosis (RO):***

- RO membranes have typically small pores ranging between 0.001 to 0.0001 µm, allowing only water molecules to pass through and blocking dissolved salts and minerals.
- RO membranes are operated in the pressure range of 10 to 150 bar.
- RO is energy intensive and primarily used technology for water drinking water purification [11].

1.1.2. Polymeric membrane vs ceramic membranes

Polymeric and ceramic membranes are two distinct classes of materials used in membrane separation processes, each providing unique properties and applications. Polymeric membranes are typically composed of synthetic polymers such as polyamide, polyethersulfone, or polysulfone, offering cost-effectiveness and flexibility [12]. Polymeric membranes are typically used for processes where high selectivity and flux is desired. On the other hand, ceramic membranes are composed of inorganic materials such as alumina, zirconia, silica or titania, providing superior chemical, thermal and mechanical stability [13]. These membranes are often employed in wastewater treatment, gas separations and other applications involving harsh conditions. Ceramic membrane's robust nature and resistant to fouling make them ideal for demanding industrial processes [8]. Table 1.1 outlines the advantages and disadvantages of both polymeric and ceramic membranes.

Table 1.1 Advantages and disadvantages of polymeric and ceramic membranes

Property	Polymeric membrane	Ceramic membrane	Reference
Permeability	Higher	Lower	[12]
Chemical resistance	Sensitive	Resistant	[14]
Mechanical resistance	Lower	Higher	[14]
Thermal stability	Lower	Higher	[15]
Fouling sensitivity	More prone	Less prone	[5]
Cost	Low cost	High	[7]
Cleaning	Difficult	Easy	[5]
Lifetime	Short	Prolonged	[16]
Application	Suitable for less harsh environment	Suitable for harsh conditions	[12]

1.1.3. Raw materials involved in the fabrication of low-cost ceramic membrane

Out of the many advantages of ceramic membranes, the one drawback that catches considerable attention is the cost of ceramic membranes. Hence, to overcome this demerit, researchers across the globe have started to consider low-cost precursors as an alternative to high-cost silica, alumina, titania or zirconia. Fig. 1.3 presents the percentages of the number of articles that were published on different low-cost materials such as kaolin, flyash, ball clay, bentonite, rice husk ash etc.

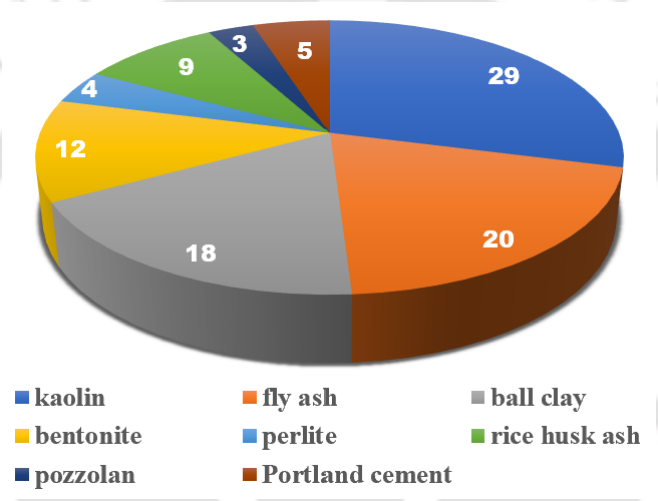

Fig. 1.3 Percentages of number of articles published in the period 2010-2023 on preparation of low-cost ceramic membranes using the above shown raw materials.

Among all of the low-cost raw materials, the use of kaolin in the fabrication of ceramic membrane was found to be the highest i.e., 29%. The several advantages associated to this widely used mineral are as follows: abundant and cost-effective raw material, porous structure, high absorption capacity, chemical inertness, thermal stability, high silica to alumina ratio, hydrophilic behaviour, high refractory properties and established industrial use [17].Therefore, owing to these advantages, the use of kaolin made ceramic membranes provide a new perspective into diverse separation and purification applications [18–23].

1.1.4. Types of membrane modules

Different types of membrane modules are shown in Fig. 1.4. Among the various membrane configurations developed till date, flat, spiral wound, hollow fibre and tubular membranes have been widely used in industrial processes.

A spiral wound membrane configuration is a spiral arrangement of flat sheet membrane and feed spacer around a permeate collection tube. These modules are typically used for reverse osmosis and nanofiltration applications. They provide high packing density but are susceptible to membrane fouling, making it difficult to clean the membrane module. Also, the pressure drop in spiral wound modules is significantly high [24]. Unlike spiral wound membranes, flat shaped membranes are typically designed as planar or flat sheets. Their main advantages include their ease of preparation and simplicity in design. Due to low packing density, this membrane category is specially used for lab scale experiments to perform preliminary separation experiments [15]. Hollow fibre membranes consist of small capillary sized tubes assembled together in a tubular module. They provide high surface area to volume ratio, making them suitable and efficient for various separation processes. However, they are very complex in design and can be prone to fouling requiring effective cleaning strategies [25]. Contrary to spiral wound and hollow fibre membrane types, tubular configurations have low tendency to fouling as a consequence of large diameters. Also, application of high cross flow velocity is permissible, allowing treatment of solutions with high ratio of suspended solids [26]. With the ease of installation, regenerability properties and versatility in applications, tubular membranes are used highly in industrial applications [27].

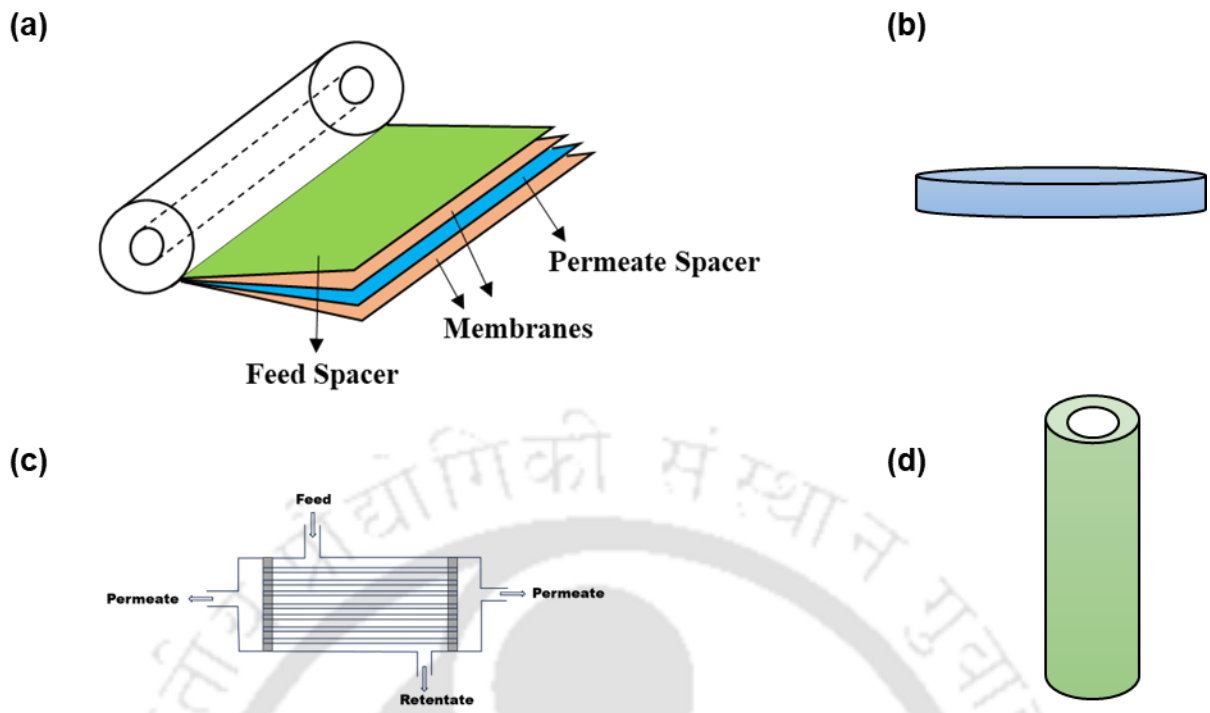

Fig. 1.4 Different membrane modules (a) Spiral wound (b) Flat membrane (c) Hollow fibre (d) Tubular

1.1.5. Ceramic membrane production

The fabrication method of membranes are diverse and tailored to meet specific performance requirement [28]. Ceramic membranes are generally produced in tubular and flat configurations. Various techniques such as extrusion, tape casting, phase inversion and pressing were used widely for fabricating ceramic membranes [29]. The detailed study on each method along with their schematic is given in the following section.

1.1.5.1. Types of fabrication methods

1.1.5.1.1. Extrusion

Extrusion is a well-known technique for fabrication of tubular membranes. In this technique, fine ceramic powders are mixed with binders, pore former and water to form a homogeneous paste [30]. The resulting paste is then passed through a die to shape the material into a tubular structure. Subsequently, the resulted membranes are sent to a drying process to remove the

solvent. The dried membranes are then sintered at higher temperatures to achieve the desired properties such as porosity, morphology, chemical and thermal stability. Ceramic powder characteristics, binder concentration, extrusion rate and pressure, drying and sintering conditions are some of the important factors affecting the fabrication process [31].

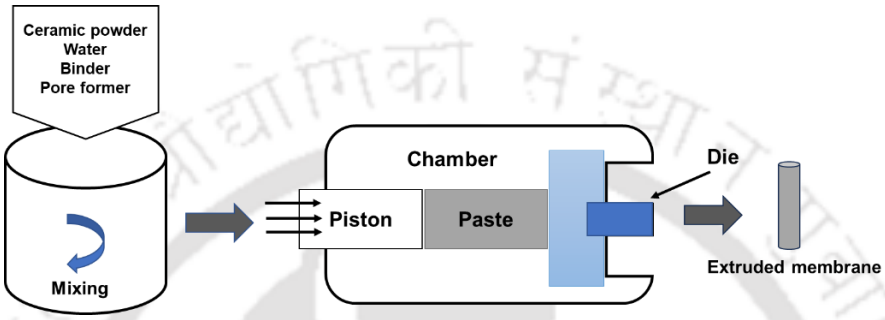

Fig. 1.5 Extrusion method of tubular membrane fabrication

1.1.5.1.2. Tape casting

The tape casting method is a widely employed technique for the production of flat ceramic sheets. Here, a ceramic slurry consisting of ceramic powder and binder solution is cast into a glass plate or plastic film [32]. A doctor blade is often used to control the thickness of the slurry to ensure even coating. After casting, the tape is allowed to dry resulting in a green ceramic sheet. The green sheet can be easily cut into desired shapes according to the specific application. The final step comprises of sintering the green sheet to get the densified ceramic structure with desired mechanical and thermal properties [33].

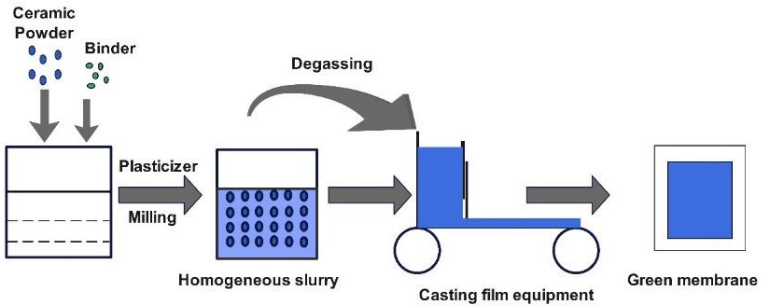

Fig. 1.6 Tape casting method of producing flat ceramic sheets

1.1.5.1.3. Phase inversion

In this method, a casting solution is first prepared by dissolving a polymer in a suitable solvent. The solution is then coated onto a support material. The phase inversion takes place during the solvent removal step where the polymer solution undergoes a composition change through immersion in non-solvent bath. The resulting change induces a phase separation giving rise to a porous structure [34]. The choice of solvent, non-solvent, composition of polymer solution and casting conditions determines the membrane performance, pore size distribution and morphology [35].

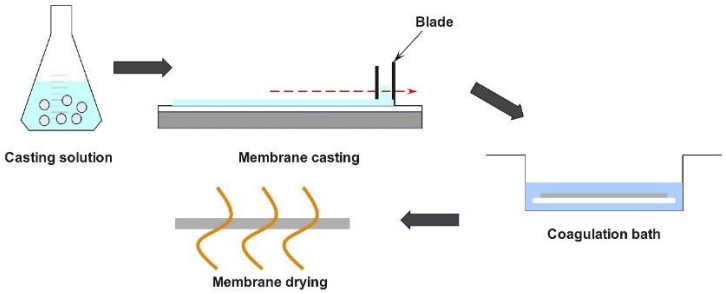

Fig. 1.7 Phase-inversion method

1.1.5.1.4. Pressing method

The pressing method is a membrane fabrication technique employed for the fabrication of ceramic membranes. Here, ceramic powder and binder are mixed and then pressed into a specific desired shape using mechanical pressure [28]. The pressed green membranes are subjected to high temperature sintering to achieve the final rigid structure. This method is valued for its simplicity, reproducibility and suitability for large volume production [29].

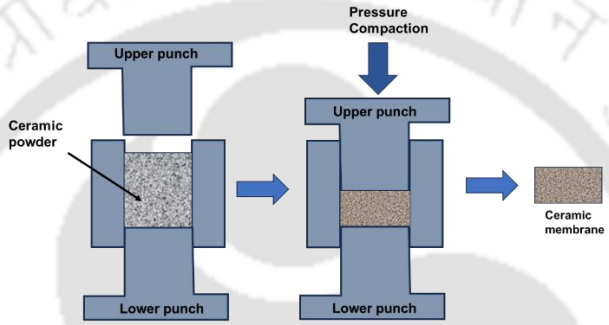

Fig. 1.8 Pressing method of ceramic membrane production

1.2. Introduction to Microalgal Harvesting

The process of algal harvesting involves extracting or separating algae from its growth medium. The harvesting method relies heavily on the density, cell size, end product specifications, and the viability of reusing the culture medium of the selected microalgae [36]. Challenges in harvesting arises due to factors such as growth of algae in dilute suspension, their small cell size, minimal density difference between microalgal cells and culture medium, negatively charged cell surfaces, and so on [37]. Efficient microalgal harvesting is essential for maximizing the productivity and sustainability of microalgae-based processes, making it an essential part to harness the potential of microalgae for diverse applications [38].

1.2.1. Classification of harvesting methods

The classification of microalgal harvesting methods is based on different principles keeping in consideration factors like biological, chemical and physical properties of microalgae [39].

Mechanical based methods such as sedimentation, filtration, and centrifugation rely on physical forces such as difference in size, density, or settling rates to separate microalgae from the culture medium [40]. Whereas, chemical methods make use of flocculants or coagulants to induce microalgal agglomeration, thereby facilitating microalgal separation [41]. Biological methods exploit the inherent characteristics of microalgae by the introduction of biopolymers or bio-flocculants, which interacts with microalgae, resulting in separation [42]. And, electrical methods harness the electrical properties of microalgae to efficiently separate microalgae from the culture medium [39]. The detailed classification of microalgal harvesting techniques is shown in Fig. 1.9.

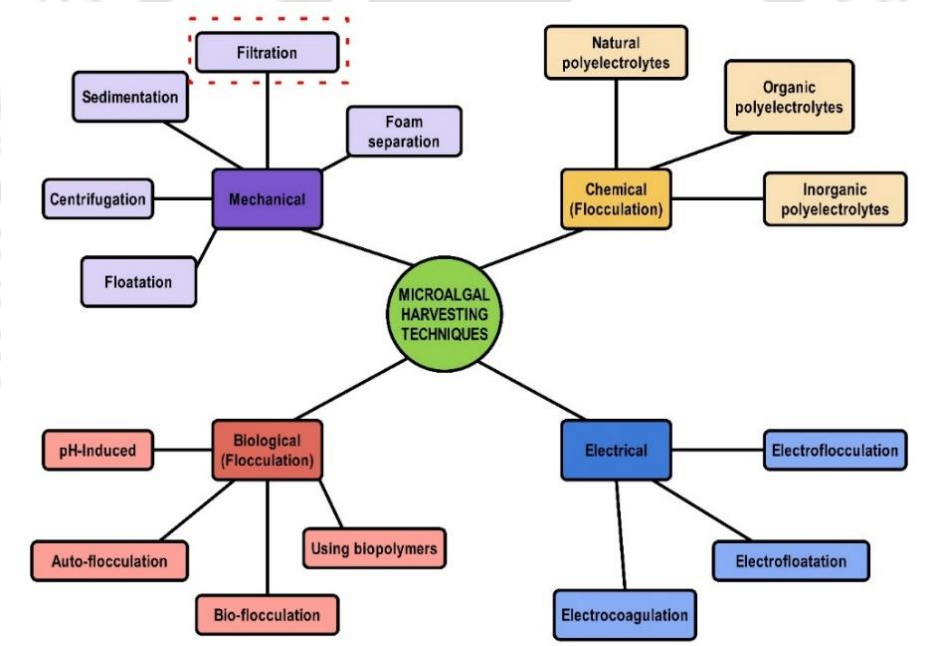

Fig. 1.9 Classification of microalgal harvesting techniques

1.2.1.1. Mechanical methods

Mechanical methods involve the use of physical forces to separate microalgae from their culture medium. The sedimentation method is a commonly used technique that uses gravitational force to settle microalgal cells [43]. However, if the density difference or

microalgal size is small, the separation force may be reduced. The use of the sedimentation process is not widely adopted because of lessened sedimentation rate for microalgae of 4-5 µm size on a large scale [42]. As sedimentation is species dependent, it is not suitable for smaller microalgal species such as chlorella and also for motile microalgae such as *Chlorogonium*, *Euglena* and *Pedinomonas* [44]. The sedimentation-based method is an economical, simple and effortless technique, requiring no input energy or chemical additives. However, it is time consuming, lacks reliability and hence retarding its viability in commercial application [45].

Centrifugation is the quickest method of harvesting microalgae, yet its use is restrained by its high cost and energy consumption [46]. There are also researches indicating the damage of microalgal cells due to high centrifugal shear forces. This method is species independent and results in a highly efficient microalgal cell recovery [47].

The floatation based microalgal harvesting is a technique that takes the advantage of the buoyancy forces of microalgae to assist the separation process. The floatation process relies on the low density of microalgal cells, which enables them to ascend upwards more easily rather than sedimenting downwards [48]. The process involves attachment of cells to gas bubbles, which help the cells to rise to the surface and then be removed and separated from the culture medium. Based on bubble generation, floatation method is categorized into froth floatation, dissolved air floatation, dispersed air floatation and electrolytic floatation. Advantages such as low operational costs, short operation times and less space requirement are associated with floatation method. However, high energy requirements and species dependency hinders its commercial application [49].

The filtration technique is a widely adopted method that uses the physical separation of microlalgal cells through a porous semi-permeable membrane [36]. In this process, microalgal culture is passed through membranes with specific pore size (MF, UF, NF or RO) allowing

water to pass through and retaining microalgal biomass. As membrane filtration is a chemical free method, the extraction of the desired product from microalgal biomass becomes an easy process. Filtration is a highly efficient and chemical-free method, maintaining cell integrity [37]. This technique is suitable for the microalgal species that are sensitive to high shear forces, additionally, the process aids the use of the culture medium in further recycle, which is a drawback in other chemical based process [50]. However, higher membrane costs and tendency of fouling are the underlying drawbacks of this harvesting method [51].

1.2.1.2. Chemical

Chemical methods involve use of different chemical agents to induce flocculation or precipitation of microalgal cells. Chemical flocculation is the primary approach for economically optimized microalgal harvesting [52]. The method is useful to process high volumes of microalgal culture and is also handy for diverse range of microalgal species. The flocculation step concentrates the medium by 20-100 times, which results in increased particle size of microalgal cells, thereby decreasing the energy requirement in further dewatering step [53]. The main principle in this technique is the neutralization of microalgal cell charge by the use of oppositely charged flocculants. Aluminium sulphate, ferric sulphate and ferric chloride are the three major inorganic flocculants that are widely used commercially [39]. Harvesting using inorganic flocculants is simple, economical and energy deprived process. However, the color and chemical composition of culture medium remains at stake in this technique, making it unsuitable for reuse. Organic flocculants can be cationic or anionic polymers with linear or branched chain structure. In contrast to inorganic flocculants, organic flocculants are highly efficient even at lower doses, generating lower sludge volumes [54]. Despite of the many advantages, the use of organic flocculants in commercial scale is limited due to their higher costs.

1.2.1.3. Biological

Biological-based methods mainly comprise of autoflocculation and bioflocculation. Autoflocculation, which is caused by a increase in pH of the culture, is an eco-friendly and cost-effective method [42]. It is devoid of use of flocculants and hence medium reuse is possible. The process may occur spontaneously in microalgal cultures exposed to sunlight and having a restricted CO_2 supply. The photosynthesis reaction causes use of CO_2 by the culture medium resulting in an enhanced pH. The use of calcium, magnesium and sodium hydroxide have stimulated this phenomenon of autoflocculation. However, this process is not suitable for commercial use as it is a slow, unreliable and suitable only for some selected microalgal species [55].

The use of bioflocculants for microalgal harvesting represents an eco-friendly and sustainable approach to biomass recovery. Bioflocculants are natural polymers produced by bacteria, fungi or any other microorganism. The use of bioflocculant negates the necessity of costly and hazardous chemical flocculants [56]. But, the co-cultivation of microalgal culture with bacteria or fungi-based flocculants may result in microbiological contamination, challenging the biomass suitability for feed or food applications. The effectiveness of microbial flocculation depends mainly on the release of EPS by bacteria and the capability of microalgae to get attached to them leading to floc formation [53].

1.2.1.4. Electrical-based methods

Though electrical methods of microalgal harvesting are not widely used, they exhibit versatility and applicable to varied range of microalgal species. With no addition of chemical required, these processes are termed to be environment friendly [39]. Since microalgal cells are charged negatively, the application of electric field in the culture medium results in their separation. Electrophoresis results in the precipitation of microalgal cells in the electrode whereas electroflocculation is the accumulation of the cells at the bottom of vessel. In contrast, electro-floatation involves the generation of hydrogen bubbles via water electrolysis [41]. The effectiveness of electrical based methods is primarily dependent on the choice of electrode materials. Aluminium and iron stand out as the predominant option for this type of process. While electrical methods offer numerous advantages, the equipment costs and high energy requirements limits its use in large scale [42].

Table 1.2 Advantages and limitations of major microalgal harvesting techniques

Harvesting technique	Advantages	Limitations	Ref.
Sedimentation	• Simple, low cost • No cell damage • No toxicity	• Low efficiency • Time consuming • Energy required for slurry pumping	[42,43]
Centrifugation	• High recovery efficiency • No chemical addition • Short process time	• Cell damage occurs • High cost involved • High energy	[46] [47]
Floatation	• Large scale application • Low space requirement • Short processing time	• Expensive equipment • Ozofloatation is costly	[48] [49]
Flocculation	• Less energy used • Large scale application suitable • Applicable to wide range of microalgal species	• Chemicals can be expensive • Culture medium recycling is hindered • Cell damage may occur	[52] [53] [54]
Magnetic Separation	• Rapid and simple • Low cost	• Expensive nanoparticles • Poor quality biomass	[39]

	• Less space requirement	• Metal contamination may occur	
Dead end filtration	• Simple operation • Highly efficient	• Fouling prone • Regular cleaning required • Not suitable for highly concentrated biomass	[41,57,58]
Cross flow filtration	• Turbulent flow • Low fouling tendency • Can be used for higher concentration of biomass • Less energy requirement than dead end filtration	• Energy required for feed pumping • Fouling may occur • Lower recovery rate	[59–61]
Submerged filtration	• Low operation cost • Reduced energy required • Low fouling risk	• Not operated in commercial scale • Slow recovery and rate	[62,63]
Dynamic filtration	• Foiling is low • Efficiency is enhanced	• Complex process • Expensive equipment required • Vibration energy requirement is high	[64–66]
Forward Osmosis	• Low risk of fouling • Low energy consumption	• Only for low biomass concentrations • Concentration polarization • Reverse salt flux is a concern	[66–68]

1.2.2. Advantages of membrane technology over others in microalgal harvesting

Since algae cells are only micrometres or tens of micrometres in size, harvesting and dewatering the biomass from cultivation media is a formidable task [50,69]. Traditionally, microalgae are grown in either closed photobioreactors or open ponds [70], necessitating substantial water volumes and a considerable energy input for harvesting and dewatering. This is because microalgal cell suspensions are typically dilute, with concentrations usually below 1 g L^{-1} [71]. Various methods have been utilized to concentrate microalgae biomass, such as coagulation, flocculation, flotation, and centrifugation [72–74]. However, these techniques either demand significant energy input or require substantial amounts of chemicals to achieve efficient biomass concentration. According to the literature, 90% of the equipment expenses

associated with these processes can be attributed to the cost of apparatus utilized for dewatering of microalgal biomass [75]. Simultaneously, the harvesting of microalgal biomass accounts for 20-30% of the total expenses involved in microalgae production [76]. The substantial capital and operational expenses pose a significant obstacle to commercializing large-scale microalgae production. At the same time, membrane filtration has been receiving increased interest due to its potential benefits in terms of performance, energy efficiency, and cost-effectiveness [19,77]. As compared to other separation methods such as centrifugation, floatation, and flocculation, membrane separations offer distinct advantages, which include ease of scalability, low energy consumption, and absence of any chemical usage [69,78,79]. The removal of chemical additions simplifies subsequent processes such as extraction, conversion, and refining, as well as the utilization of the residual algal biomass that is left over after oil extraction.

The main advantages are high selectivity, energy efficiency, continuous operation, scalability, gentle on cells, low chemical usage, minimal environmental impact, integration with downstream processing and reduced footprint.

1.2.3. Membrane configurations

Different filtration modes such as cross-flow, dead end flow, submerged systems, dynamic systems and forward osmosis are used for microalgal harvesting. Out of all the configurations, cross-flow type is widely used as it presents distinct advantages over other filtration modes [78]. In cross-flow mode, the liquid flow continuously parallel to the membrane surface, thus, minimizing fouling and ensuring a more effective separation. Submerged membranes are immersed directly into the feed solution, presenting direct contact between the membrane and substance to be filtered[80]. Forward osmosis (FO) is a process that transports water from the side with low osmotic pressure (the medium solution) to the side with higher osmotic pressure (the draw solution) [81,82]. This happens because of the difference in osmotic pressure between the two sides. The dynamic filtration process, also known as shear-enhanced filtration, involves the introduction of turbulence to cleanse foulants from the surface of the membrane through shaking, rotation, and vibration [83]. The major advantages and drawbacks of these configurations are presented in Table 1.3.

The cross-flow system for tubular membranes offers distinct advantages in various separation processes. One major advantage is the continuous tangential flow of feed stream along the surface of the tubular membrane. This flow pattern minimizes the risk of fouling by preventing the accumulation of contaminants or feed solute on the membrane surface [84]. Tubular configuration with cross-flow configuration is particularly suited for applications where fouling is a major concern, making it a reliable choice for processes such as microalgal harvesting and other wastewater treatment processes [85]. The recent works on microalgal harvesting using membrane in cross-flow configuration is summarized in Table 1.4.

Table 1.3 Schematic of various membrane configurations along with their advantages and disadvantages

Filtration type	Schematic	Advantages	Disadvantages
Dead-end	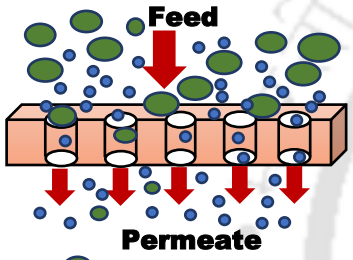	• Feed flow perpendicular to membrane • High recovery rate (95-98%) • Simple Operation	• Cake layer formation • Requires regular cleaning • Easily fouled membrane • Fast permeance drop • Inadequate for high biomass concentrated culture
Cross-flow	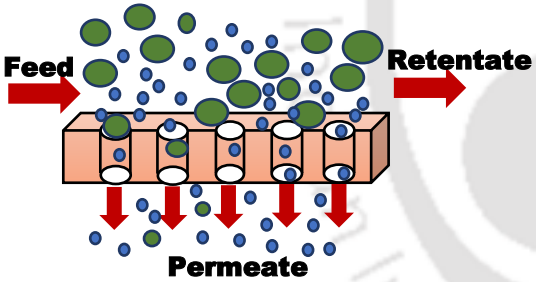	• Feed flow tangentially to membrane • Turbulence flow reduces fouling. • Most frequently used configuration for industrial applications. • Less energy required than dead-end	• Slow process • Energy requirement for feed pumping • Fouling • Risk of cell damage
Submerged	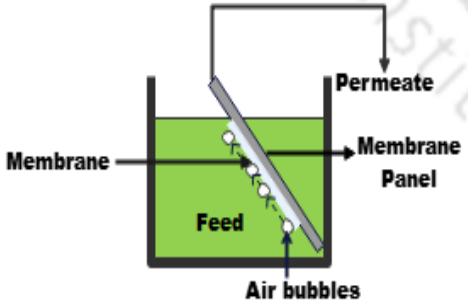	• Membrane module immersed in reactor • The principal source of shear is air bubbling. • Lesser energy required • Low operation cost • Lower fouling and cell damage	• Not suitable for open and continuous process • Slower rate and recovery • Hindered commercial applications

Forward Osmosis	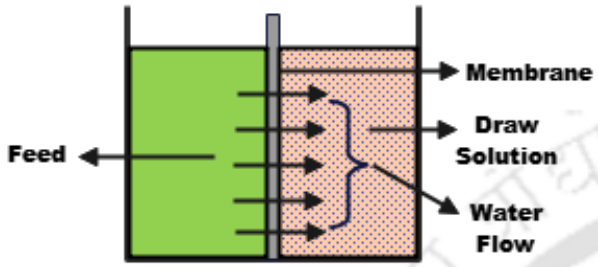	• Uses Osmotic pressure gradient • Water transport takes place • Low membrane fouling propensity • High cleaning efficiency • More productive than submerged filtration	• Low membrane permeance • low microalgal concentration • mild driving force • draw solute regeneration resulting high energy consumption • Concentration polarization
Dynamic	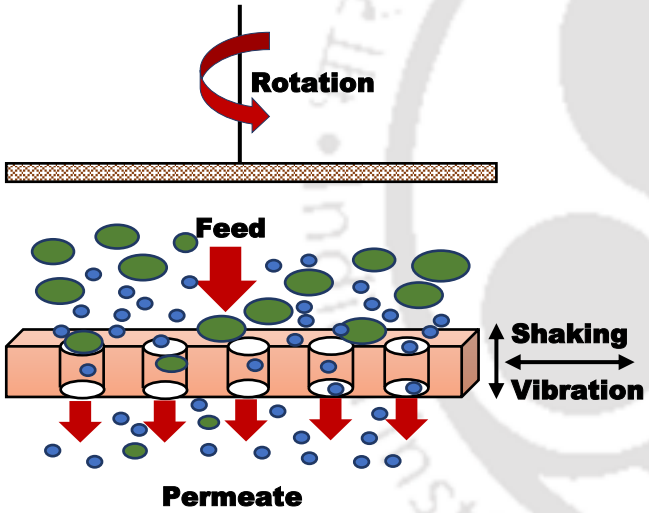	• Involves rotation, vibration and shaking of membrane surface • Uses turbulent flow to diminish the laminar boundary layer • Higher permeate flux • Higher productivity compared to submerged configuration	• Complicated process • Energy requirement is more for generating rotation and vibration • Equipment cost is high

Table 1.4 Recent works on microalgal harvesting using membrane in cross-flow systems

Membrane material and pore size	Configuration	Main parameters	Permeate flux (L/m^2 h bar)	Microalgal Species and initial concentration	Filtration area (m^2)	Biomass recovery (%)	Ref.
Ceramic 25 µm,	Flocculation assisted filtration	CFV: 0.1 m/s; TMP: 2 bar	27.75×10^3	*Chlorella sorokiniana* (1 g/L)	25	95.2	[86]
TiO_2 0.14 µm	Microalgal dewatering with simultaneous reuse of water	CFV: 2 m/s; TMP: 1 bar	70-120	*Scenedesmus obliquus* (1.6 g/L)	0.00471	100	[87]
(PSF)	Flocculation-assisted patterned membrane filtration	CFV: 0.0025 m/s; TMP: 1.5 bar;	590 ± 17	*Dictyosphaerium* sp.	0.004	N/A	[88]
N/A		PEG: 28 wt%,		(0.81 g/L)			
PSF	sPSF blend patterned PSF membranes	CFV: 0.0025 m/s; TMP: 2.5 bar;	1000	*Desmodesmus* sp.	0.004	100	[89]
N/A		sPSF: 4.5 wt%		(0.88 g/L)			
PC	PSS/PDADMAC	CFV: 15 L/min; TMP: 1 bar	133	*C. vulgaris*	0.0013	100	[90]
0.086	layer-by-layer PC membrane			(2×10^6 cell / mL)			
Ceramic	Electrochemical membrane filtration	TMP: 0.69 bar	762	*Scenedesmus dimorphus*	0.004	N/A	[91]
N/A				(0.05 g/L)			
CE	Microfiltration in presence of rigid particles (PMMA)	TMP: 0.2-0.6 bar; CFV: 0.43-1.11	34.5-132	*Chlorella* sp.	0.0004	N/A	[92]
0.22 µm		m/s; PMMA: 10-40 mg/L		(10 mg/L)			

CFV: Cross flow velocity; TMP: Transmembrane pressure; PSF: Polysulphone; sPSF: Sulfonated polysulfone; PC: Polycarbonate; CE: Cellulose ether; PMMA: polymethyl methacrylate; PEG: Polyethylene glycol; PSS: poly-(styrenesulfonate); PDADMAC: poly-(diallyldimethylammonium chloride)

1.2.4. Factors influencing microalgal harvesting using membrane

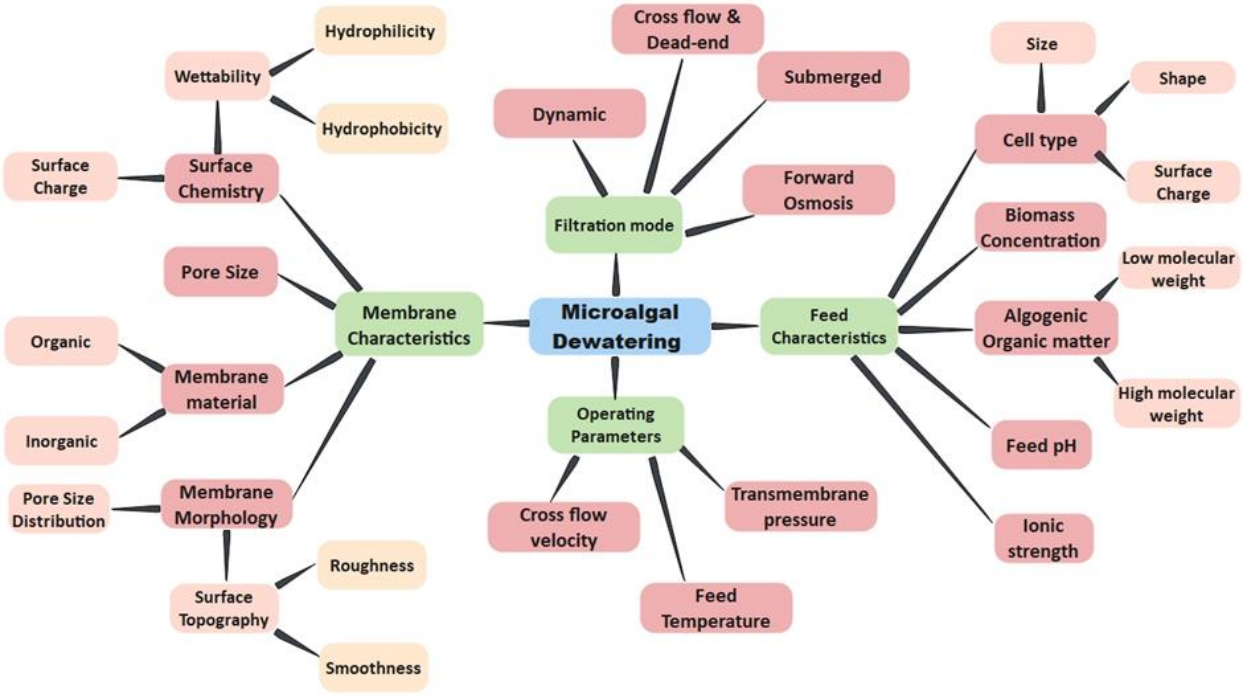

Fig. 1.10 Filtration mode and factors affecting membrane performance in microalgal dewatering

1.2.4.1. Membrane properties

A typical membrane comprises a thin active surface layer responsible for the necessary permeability, while a thicker and more open base provides structural integrity. Membranes fall into two categories: organic (polymeric) and inorganic (metallic or ceramic). The properties of both organic and inorganic membranes, along with their advantages and limitations, have been documented in a previous study [93]. Organic membranes, for instance, polyvinylidene fluoride (PVDF), polyacrylonitrile (PAN), polyether sulfone (PES), polysulfone (PS), cellulose acetate (CA), regenerated cellulose (RC), polyethylene terephthalate (PET), cellulose ester (CE), polyvinyl chloride (PVC), and others, are widely recognized and extensively utilized

within the microalgae industry due to their easy availability and cost-effectiveness [79,94–99]. Broadly speaking, membranes crafted from diverse materials and incorporating different additives exhibit distinct structures and characteristics (including surface charge and the balance between hydrophobic and hydrophilic traits). These factors, in turn, impact both membrane fouling tendencies and the overall efficiency of the dewatering process [79]. In most cases, an augmentation in the hydrophilic nature of a membrane can improve its ability to resist fouling [94,100]. To illustrate, Elcik and Cakmakci (2017) conducted experiments involving four distinct membranes of materials displaying varying degrees of hydrophilicity and hydrophobicity. The study revealed that the hydrophilic polyethersulfone (PESH) membrane exhibited the most favourable results. This outcome was attributed to the hydrophilic nature, which effectively impeded the development of permanent fouling and facilitated the straightforward removal of reversible fouling through backwashing [94].

The fouling of membrane is directly impacted by both the size and distribution of pores along with surface characteristics such as roughness or smoothness. Table 1.5 highlights the influence of different pore sizes on membrane fouling propensity. Susanto et al. in 2017 utilized ultrafiltration (UF) membranes of varying pore sizes to dewater microalgae [101]. Their findings revealed that the membrane featuring the smallest pore size (regenerated cellulose with a pore size of 10 kDa) exhibited the greatest normalized flux, implying that it experienced the least fouling. Conversely, Zhao et al. (2017) noted that membrane with a pore size of 0.1 µm exhibited the least transmembrane pressure and fouling among 0.05 µm, 0.03 µm, and 0.1 µm membranes [102]. Consequently, this membrane was identified as the most suitable for microalgal harvesting. These findings indicate that the influence of membrane pore size on membrane effectiveness is intricate, primarily relying on the relative size between microalgae and pore. For every microalgae species, there exists a critical pore size. Below this size, raising the membrane pore size results in augmentation of filtration flux.

1.2.4.2. Microalgae properties

Microalgal properties significantly influence the regulation of membrane fouling. These characteristics encompass factors such as type of microalgae, cell dimensions, particle size distribution, and rigidity. In one study, researchers utilized membrane technology to dewater three microalgal suspensions with comparable concentrations. *Chlorella* and *Phaeodactylum* possessing rigid cell walls demonstrated greater critical fluxes than *Nannochloropsis* lacking rigid cell walls [103]. It has been reported that the various shapes found in the microalgal species *Phaeodactylum tricornutum* are responsible for the loosely organized structure of the cake layer. These different shapes hamper the ability of the cells to pack closely together [79]. Apart from the microalgae's morphology, several other characteristics can significantly affect the membrane's performance and the effectiveness of the dewatering processes, such as concentration, structural integrity, and interactions with the membrane [104]. The negatively charged outer surface of microalgal cells significantly impacts the adhesion properties. These cells exhibit a strong affinity towards positively charged membrane surfaces, leading to severe fouling. On the other hand, fouling is less likely to happen on negatively charged membrane surfaces because surfaces with the same charge tend to repel each other [105]. In ideal conditions, feed concentration increases fouling due to solute pressure on the membrane. Hwang et al. [106] reported that an increase in the initial cell concentration during the cross-flow filtration of microalgae culture broth causes rapid fouling and decreases flux stabilization. Also, a high biomass concentration causes more extracellular polymeric substances (EPS) to be released, which contributes to the potential for membrane fouling [107].

The amount and composition of extracellular polymeric substances (EPS) and extracellular organic matter (EOMs) are critical variables that impact membrane fouling. Algal EOMs include polysaccharides and proteins with molecular weights up to 100 kDa. These compounds possess hydrophobic properties and can induce flux decline, thus contributing to reversible and

irreversible fouling [108,109]. The probability of fouling can differ amongst microalgae species because of differences in the amount and kind of EPS released. As an illustration, *Chlorella* sp. showed a higher flux than *P. purpureum* under comparable cultivation conditions. This difference was attributed to *Chlorella* sp. having less extracellular polymeric substances in their composition [69].

1.2.4.3. Operating parameters

Transmembrane pressure (TMP) is a critical parameter in membrane filtration that directly correlates with the permeate flux. Consequently, any elevation or reduction in TMP leads to a corresponding increase or decrease in permeate flux [69,78,110]. Yet, elevated TMP causes intensified fouling molecule convection across the membrane, leading to cake layer build up and concentration polarization. This results in reduced permeate flux and necessitates higher pressure to maintain a consistent flux flow. In this context, scientists have identified a critical flux where little minimum fouling occurs. Although higher TMP is suitable for enhanced permeate flux, keeping TMP below the critical flux is recommended. In studies conducted by various researchers [111,112] using UF membrane, it was observed that the permeate flux continued to increase up to a particular TMP, but after that, a noticeable flux decline occurred as TMP subsequently increased.

Cross-flow velocity (CFV) is another crucial factor in membrane microalgal harvesting. Higher CFV and the resultant shear stress on membrane surfaces can effectively reduce membrane fouling and result in increased permeate [78,79]. Furthermore, in cross-flow systems where diverse particle sizes are present in the feed, maintaining a high CFV is acknowledged for preventing larger particles from accumulating on the membrane surface. As a result, smaller particles are selectively retained, forming dense cake layers [113]. This principle directly applies to microalgae culture broth, where a diverse range of flocculants may be present, including microalgae cells, cell debris, and algalogenic organic matter.

Table 1.5 Summary of major findings investigating the influence of different parameters on microalgal harvesting using membrane

Parameter	Major findings (Influences)	Remarks	References
Membrane material	Organic: • Normally hydrophobic, • Susceptible to fouling, • Constant cleaning required • Low cost Inorganic: • More heat and, chemical stability and mechanical stability • Very expensive • Highly hydrophilic • Low fouling propensity	• Membranes made with various materials and additives possess different structures and properties (such as surface charge and hydrophobicity-hydrophilicity)	[99,100,114,115]
Surface Chemistry	Hydrophilic membranes: • Have low contact angle • More resistant to fouling • Form a tight water layer on their surfaces that reduces the adsorption site of foulant molecules Hydrophobic membranes: • High fouling propensity • High affinity to the hydrophobic foulants Negatively charged membrane surfaces: • Show higher permeability • Electrostatic repulsive force on negatively charged microalgae cells and other exopolysaccharides that cause fouling of membranes.	• When an excessive number of microalgal cells deposit on the membrane surface, the electrostatic repulsion effect diminishes, suggesting that negative charge can only be a supplementary method.	[105,113,116–119]

Morphology	Pore size/distribution: • MF membranes: susceptible to irreversible fouling • UF membranes: cake layer formation occurs, reversible fouling Roughness/Smoothness: • Rough surface have high fouling propensity • Poor flux permeability • Foulants attach in valleys of rough surface	• Membrane pore size should be optimized species-dependent (mainly depending on microalgal cell size) to reach maximum filtration performance.	[71,105,113,114,120–122]
Microalgae properties	Concentration: • High concentration ⇒fouling ↑, intense concentration polarization Cell size: • (3–30 μm) • Fouling due to cake or biofilm layer on surface Cell shape: • Influence nature of cake layer formed (Loosely packed or tightly packed) Cell charge (negative): • If membrane surface is negative⇒fouling ↓ (repulsive force exists) • If membrane surface is positive⇒fouling ↑ (adhesion force exists) Cell debris: • Mostly smaller than membrane pore size • Internal fouling or pore blockage occurs	• Biomass concentration, extracellular organic matter (EOMs) and extracellular polymeric substances (EPS) are critical factor impacting membrane fouling.	[71,105,110,123–125]
Operating parameters	Transmembrane pressure (TMP): • Direct relationship with membrane flux • At high TMP ⇒microalgae cells break ⇒ release of AOM ⇒ plugging of pores Cross Flow Velocity (CFV): • CFV ↑ ⇒ shear forces ↑⇒Fouling ↓⇒Permeance↑ Feed Temperature (T): • T↑⇒viscosity↓⇒Feed diffusion easy⇒Flux↑⇒Fouling ↓	• TMP operated ideally below critical flux (where no fouling occurs) • High CFV may damage microalgal cell structure • It is challenging to draw conclusions on the relationship between the pH values and the membrane fouling. • A neutral pH seems to be preferred.	[126,127][79,128,129]

1.3. Water reuse for Sustainable Biomass Production

Large scale cultivation of microalgae necessitates substantial amount of fresh water. Though microalgae exhibit greater oil productivity as compared to terrestrial plants, they possess the highest water footprint among various biofuel sources [130]. According to a life cycle analysis, the overall water consumption for producing one ton of biodiesel from *Jatropha curcas* L. and microalgae was reported as 5787 and 31,361 m^3, respectively[131]. Although microalgae can grow in water resources that are not suitable for conventional crops such as saltwater or wastewater, there is still an increased need for a significant volume of water. The costs related to water pumping, nutrients and wastewater treatment can be mitigated by reusing water after the harvesting step. According to a life cycle analysis, reusing water reduced the fresh water and nutrient demand by 84% and 55%, respectively [132,133]. Consequently, reusing water is considered as a crucial measure for sustainable and long-term advancement of microalgae industry.

The diverse effects of reused water on microalgae growth, whether inhibitory, stimulatory or neutral, can be attributed to a combination of numerous factors. These factors include microalgae strain type, conditions of culture, mode of harvesting method, among others. Consequently, although water reuse is desirable, several obstacles hinder its widespread adoption [133].

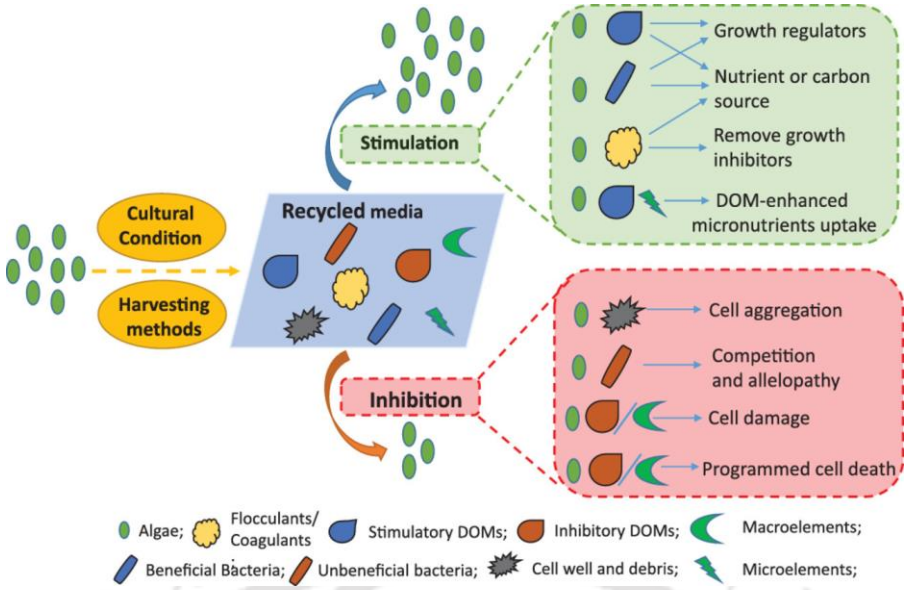

Fig. 1.11 Effects and underlying mechanisms of reused water on microalgal growth (Source: Z. Lu et al., 2020, [1]

1.3.1. Growth inhibition sources and factors responsible for quality of reused water

1.3.1.1. Microalgal species

The impact of water reuse on microalgal growth exhibited variations among different algal species. Also, within a given algal species, there was no consistent trend in response to reused water, as evident by diverse growth patterns in *Chlorella* sp. and *Nannochloropsis* sp. [134]. The variations can be attributed to difference in study conditions. The species-specific impact of reused water is potentially influenced by the distinct compositions and organic matter concentrations released by various microalgae, as indicated by studies conducted by Becker et al. (2014) [135] and Zhuang et al. (2016) [136]. Depraetere et al. (2015) observed elevated concentrations of dissolved organic carbon (DOC) in *Arthrospira* cultures, reaching 100 mg L^{-1} after four cycles of reuse. Similarly, in another study 74 mg L^{-1} of DOC was measured in continuous outdoor culture of *Nannochloropsis gaditana* [137].

Since the majority of microalgae did not exhibit solely neutral, inhibitory, or stimulatory response in reused water, it suggests the presence of additional factors such as culture conditions and harvesting methods, influenced their growth [1].

1.3.1.2. Culture conditions

The quality of reused water can be influenced by various factors such as nutrient concentrations, growth phase, cell density, and growth conditions during harvesting. Despite this, no distinct pattern was observed between the different parameters and growth response in meta-analysis done by Loftus and Johnson (2017) [1]. Nitrogen concentration appears to play a role in influencing the reused water quality. One finding observed that the algae cultivated under lower initial concentrations of nitrogen produced more inhibitory substances than those cultivated at higher nitrogen concentrations. Cell density is another factor influencing the quality of reused water. Zou et al. (2000) observed that highly dense *Nannochloropsis* sp. increased inhibition with the increase of culture density [138]. Growth phase during harvesting is another important factor that affects reused water. Studies have indicated that reused water obtained from late exponential and stationary phase cultures exhibited more adverse properties in comparison to that of exponential phase [1].

1.3.1.3. Harvesting methods

Microalgae harvesting methods include sedimentation, centrifugation, flocculation, filtration or a combination of these methods [139]. The choice of harvesting method influences what is retained in the reused water, thereby impacting its nature as a growth medium. Centrifugation and filtration method exhibits highest concentration of inhibitory substances in the harvested culture. Centrifugation, lower than 5000 g may not remove bacteria, organic matter, or virus, whereas ultrafiltration has the capability to remove bacteria and macromolecules [140]. Additionally, flocculation methods have the capability to remove some of the organic matter [141]. Biorefineries that uses microalgae as source need harvesting techniques that are compatible with generating products of food-grade quality. In this regard, membrane technology is gaining considerable attention as harvesting technology, which would safeguard the harvested biomass and effluent from harmful coagulants and flocculants[142].

1.3.2. Treatment of harvested effluent

Choosing effective pre-treatment method to remove dissolved organic carbon (DOC) becomes crucial while reusing water, along with the selection of suitable harvesting technique [139]. In a study, various methods such as filtration, chlorination, hydrogen peroxide and heating, were tested. The findings indicated that ozonation method proved most effective in reducing bacterial density from the media, thereby facilitating growth of *Nannochloropsis gaditana* [143]. Membranes with pores in the range of 10-50 nm possesses the capability to eliminate bacteria, viruses, and proteins that exceed a size of 50 kDa. Nevertheless, the accumulation of organic matter resulting from multiple recycles may lead to membrane fouling. Activated carbon adsorption, high pH flocculation and $FeCl_3$ flocculation were successful in removal of organic matter from recycled water [1].

The application of activated carbon in the treatment of microalgal harvested effluent offers several noteworthy advantages. Its exceptional adsorption capacity, high porosity, and large surface area plays a vital role in adsorption of diverse organic compounds in the effluent [144]. Furthermore, the flexibility of activated carbon applications, its potential for regeneration, and compatibility with different treatment processes make it a cost-effective and sustainable solution in the long run [1].

1.4. State -of- the Art

1.4.1. Fabrication of tubular ceramic membrane using low-cost kaolin

The cost involved in membrane fabrication has been identified as a significant contributor to the overall cost of algal harvesting using microfiltration membranes. Hence, instead of conventional raw materials such as silica, titania, zirconia, alumina, and zeolite, researchers have started to focus on materials like ball clay, kaolin, fly ash, quartz, apatite, etc., as some of the favoured alternatives for membrane production [19]. It is well documented that the addition

of naturally available raw materials helped to lower the manufacturing cost of ceramic membranes. In one study, a disc shaped membrane with pore size in the microfiltration range was fabricated using kaolin and estimated cost was found to be 130 USD/m^2, taking into account the raw material costs[145]. Kaolin, sawdust and feldspar was used to prepare tubular membranes with an overall estimated membrane cost of 250 USD/m^2[146]. In another study, Goswami et al. (2021) prepared a tubular shaped ceramic membrane using fly ash as the key raw material. The calculated membrane cost was 250 USD/m^2 [147]. Flat ceramic membranes were produced through the extrusion technique, employing Moroccan perlite. These membranes had a pore size of 6.64 µm and were utilized for treatment of baking powder suspension [148]. Achiou et al. (2018) [149] subjected pozzolan material to a sintering temperature of 950 ºC, resulting in the fabrication of MF membranes with pore size of 2 µm and porosity of 30%. These membranes were effectively employed in the treatment of textile wastewater. Numerous studies have explored the use of apatite for the treatment of contaminated soils and aqueous wastes [150].

Of the different types of clay, kaolin has garnered much attention due to its distinctive physical characteristics, such as high refractory properties and low plasticity. Moreover, kaolin exhibits hydrophilic properties, which are highly desirable for preparing membranes for water filtration [17]. Numerous studies have reported the preparation and characterization of kaolin-based ceramic membranes (Table 1.6). Emani et al. (2014) fabricated a 2.16 µm pore size membrane using kaolin as the key raw material for microfiltration of oil-water emulsions [22]. The membrane served its purpose by producing a rejection of 98.52%. In another study, a group of researchers reported the fabrication of low-cost tubular kaolin membranes to treat onshore oilfield produced water [151]. A significant level of TOC and COD was removed through microfiltration under a pressure of 69 kPa, with values of 84% and 78%, respectively. Kaolin, ball clay, quartz, pyrophyllite, and feldspar mixture was also used to prepare tubular

microporous membrane. At 69 kPa of applied pressure, a high oily wastewater rejection (99.98%) was obtained in the study [31]. In a recent work, kaolin was combined with perlite to produce disc-shaped membranes for microfiltration in the treatment of textile and dairy wastewater [18]. 45% and 80% TOC removal was achieved for dairy and textile wastewater, respectively. Considering the potential and techno-economic benefits of kaolin over other raw materials, this work focuses on producing kaolin-based low-cost membranes.

Assam has 0.74 million tonnes of Kaolin deposits in Deopani area of Karbi Anglong district (26.24° N, 93.75° E). However, the clay is not yet exploited for ceramic membrane fabrication or any kind of major application. Characterization of the clay was done in 2003 [152] where it was found that the crude clay contained lower percentage of Al_2O_3 and higher percentage of iron which did not match the standards of pure kaolinite [153]. Henceforth, no research is reported using kaolin of Assam. Also, the properties of any natural clay deposit changes with time because of weathering process. So, in this work, Assam kaolin was characterized in detail in order to see its feasibility to be used in ceramic membrane fabrication. Ceramic membranes were prepared by varying the percentage of kaolin, sodium carbonate, boric acid and sodium metasilicate. Sodium metasilicate creates silicate bonds thereby increasing mechanical strength, sodium carbonate helps in creating homogeneity by improving dispersion properties and boric acid enhances mechanical strength by the creation of metaborates during membrane sintering [154].

Table 1.6 Summary of studies on kaolin-based membrane

Raw material Mixed with kaolin	Membrane configuration	Porosity (%)	Pore size (μm)	Sintering temperature (°C)	Mechanical strength (MPa)	Water permeability (L m^{-2} h^{-1} bar^{-1})	References
Alumina, lignite	Tubular	36	0.7	1200	39	410	[23]
Quartz, ball clay, pyrophyllite feldspar, and calcium carbonate	Tubular	53	0.309	950	12	213.5	[31]
Quartz, sodium carbonate, calcium carbonate, and boric acid	Flat	42	4.58	1000	11.55	49.8	[155]
Quartz, titanium oxide, and calcium carbonate	Tubular	23	0.45	900	10	13.32	[156]
Alumina and aluminium hydroxide	Flat	46	1.3	1300-1550	-	-	[157]
Feldspar, sodium metasilicate and boric acid	Flat	29	0.93	850	8.75	-	[158]
Quartz and calcium carbonate	Flat	30	1.3	900	34	-	[159]
Feldspar, Quartz and saw dust	Flat	36	0.19	850	2	-	[146]

1.4.2. Microalgal harvesting using the prepared membrane

The first and most crucial step in the downstream processing of biomass is the recovery of microalgae from culture. Concentrating the culture into a slurry of 15-25% solid, a cake or solid for further downstream processing, is the goal of harvesting and dewatering [79]. Due to energy and capital costs, selecting and designing an appropriate harvest method for large-scale algae production facilities is crucial [74,117,160]. Harvesting microalgae remains challenging due to their small cell size and growth in highly diluted conditions. While centrifugation is the most effective technique available, it is limited in its use due to its high energy consumption (8 kWh/m^3 to achieve >90% harvesting efficiency) and the risk of cell rupture at high speed [161]. Flocculation-based technique harvests biomass quickly, efficiently, and cheaply without involving any energy. However, it could alter the chemical composition and colour of the algal growth medium, rendering it unusable for some specific applications [72]. Membrane filtration is a reliable method for microalgae harvesting, resulting in nearly 100% cell retention and recovery [69]. Additionally, the absence of chemicals permits the incorporation of membrane technology into the microalgae biorefinery, simplifying the process of extracting products from biomass and culture media. Most researched membrane types for microalgae filtration are ultrafiltration (UF) with pores ranging from 1-100 nm and microfiltration (MF) with pores in the range of 0.1-10 µm, which allow for nearly complete biomass retention while preserving the structural integrity and properties of the harvested cells. The high permeate flux and selectivity of microfiltration membranes are ideal for removing algae from diluted feed [85]

Table 1.7 presents a list of different techniques used for microalgal harvesting. Out of all the techniques, membrane filtration is one technique which does not produce any unwanted products during harvesting. Mustaq et al. (2019) fabricated poly (ether sulphone) support of 0.37 µm pore size for harvesting *Chlorella* sp. HS-2. At a cross-flow velocity of 2 L min^{-1} and 1 bar transmembrane pressure, permeance and rejection of 369 L m^{-2} h^{-1} and 95.6% were

achieved in this study [162]. Several other studies also used polymeric starting material to prepare microfiltration membranes and successfully harvest microalgal cultures[163].

As can be seen from recent studies, the harvesting of microalgae using membrane filtration reveals mainly the use of polymeric membranes. However, ceramic membranes exhibit superior chemical, thermal, and mechanical stability in contrast to polymeric membranes. But their application in microalgal harvesting is restricted due to the substantial capital cost, mainly contributed by the starting raw material.

The present study aims to find a low-cost alternative for the harvesting of microalgal culture. In this regard, the developed kaolin based ceramic membrane can be used for effective microalgal harvesting.

Table 1.7 Summary of studies on techniques used for microalgal harvesting

Microalgal species	Harvesting Technique	Recovery (%)	Initial biomass concentration (mg L^{-1})	Reference
Scenedesmus obliqus	Electro-floatation	95	1000	[164]
Chlorella vulgaris	Inorganic flocculation	79	1000	[165]
Nannochloropsis maritima	Magnetic	95	1020	[166]
Desmodesmus sp. F51	Bioflocculation	95	1500	[167]

Chlorella vulgaris	Autoflocculation	90	680	[165]
Chlorella Vulgaris	Filtration using Polyvinylidene fluoride (PVDF) membrane	100	500	[168]
Chlamydomonas sp.	Filtration using Polyether sulphone (PES) membrane	91	-	[37]

1.4.3. Energy efficient microalgal effluent recycle under circular bioeconomy

Biodiesel as a renewable energy source can provide an alternative to the alarmingly depleting energy from fossil fuels [169]. Biofuels can be extracted from different biomass sources such as agricultural, municipal, and industrial wastes, food crops, woods, and algae. Microalgae is an encouraging third-generation feedstock for the production of biodiesel as it has the capability of oil production throughout the year. Other advantages include non-requirement of arable land, faster-growing cycle, high growth rate, and lipid content as compared to second-generation feedstock [170,171]. Besides several advantages, commercial production of microalgal biomass feedstock is not considered sustainable due to its high production cost. According to the life cycle analysis, the amount of fresh water, nitrogen, and phosphorus required for producing 1 kg of biomass from microalgae is 3726 kg, 0.33 kg, and 0.71 kg respectively [172]. In this context, recycling the culture media carry significant potential to reduce the overall cost for the long-term growth of microalgal industry. One study determined that water recycle can reduce the freshwater water requirement by 84% and also the nutrient consumption by 55% [172].

Several options are explored for recycling the water and nutrients from the exhausted culture media. The influence of reused water on subsequent algal growth may be positive, negative, or neutral depending upon various factors such as microalgal strain selection, culture conditions, harvesting, and water pretreatment methods. Different pretreatment techniques such as auto sedimentation, centrifugation, flocculants, and adsorption are used to date. Out of these techniques, flocculants are used extensively for harvesting as well as pretreatment of recycled water. Growth of *Chlorococcum sp. RAP13* in recycled media was reduced by 10-20% as compared to the growth in standard MA media when flocculants ($AlCl_3$, $FeCl_3$, $KAl(SO_4)_3$, $Al_2(SO_4)_3$) were used for harvesting [53]. Wu et al. (2016) reported a 10-20% reduction in final biomass of *Isochrysis galbana* when flocculants such as $AlCl_3$, $FeCl_3$, $KAl(SO4)_2$, $Al_2(SO_4)_3$ were used for harvesting in 100 mL flasks [173]. Microalgae did not grow by the second reuse of the harvested medium when *Loftus and Johnson* [134] used the filtration technique to harvest *Staurosira sp. C323* in 1 L bottles. A 14% decrease in final dry weight of *Scenedesmus acuminatus GT-2* in 30 mL glass column photobioreactor was observed when cultivation was carried out using supernatant obtained after centrifugation and filtration (0.2 µm) based harvesting. Wang et al. (2018) reported that the dry weight of culture in 30 mL culture tubes was lowered by 13% while using membrane harvested media of *Scenedesmus acuminatus GT-2* [174].

In selecting the suitable harvesting and pretreatment strategies, energy consumption and capital cost are to be considered. In one of the techno-economic evaluations of microalgal harvesting, it was seen that membrane filtration had higher energy consumptions and costs in comparison to flocculation [175]. Water recycling after flocculants assisted harvesting mainly depends on the residual flocculant concentration in the recycled water. But, residual flocculants in supernatant would interfere in its further processing in recycling studies. Using alum as a flocculant have shown negative influence on the growth of several strains in the recycled media

[176]. Increasing amount of organic matter in the effluent while recycling multiple times may increase fouling of membrane and reduce its efficiency.

Activated carbon can adsorb bacteria on its surface thereby limiting the bacterial growth in the harvested media and improving the algal growth henceforth [177]. Strong adsorption, mild reaction conditions, and fewer by-products to achieve efficient and cheap adsorption of micropollutants are the main advantages of PAC [178]. Though several advantages, implementation in the recycling of microalgal culture medium is not studied significantly. According to United States Environmental Protection Agency (USEPA), adsorption using activated carbon is considered as one of the best among the available technologies for the separation of organic compounds from wastewater (Adams and Watson, 1996).

A study performed by Jacoma et al. (2016), showed that combined treatment of the effluent with PAC and flocculants had enhanced the growth of *A. platensis* by 13.5% as compared to growth in the standard medium [179]. A recent study on the growth of *Scenedesmus acuminatus* in modified BG11 media reported that the spent medium when treated with granular activated carbon (GAC) showed almost an equal amount of biomass as compared to fresh BG11 media while a 14.3% decrease was observed after first reuse without any treatment [180]. Additionally, growth of *Nannochloropsis oceanica* microalgae was studied for 4 continuous recycle experiments [181]. It was observed from their study that an yield of 2.7 g L^{-1} (for 64 mg L^{-1} initial nitrogen concentration) and 2.1 g L^{-1} (for 32 mg L^{-1} initial nitrogen concentration) was obtained in standard f/2 medium whereas growth decreased gradually up to 3rd cycle of experiment (1.6 g L^{-1}, for 32 mg L^{-1} initial nitrogen concentration). Hence, to enhance the growth of microalgal biomass, the media from the 3rd cycle was treated with 5 g L^{-1} PAC. This resulted in an increase in biomass yield up to 1.83 g L^{-1}.

This work aims to evaluate the possibility of using different mixtures of fresh and effluent-based culture (EBC) media (obtained after kaolin-based membrane harvesting), treated with powdered activated carbon (PAC). The objectives to achieve this aim are (a) to select the appropriate mixture of fresh and PAC treated EBC media, (b) study the effect of PAC concentration on the optimized media mixture, (c) to conduct multiple cycles of recycling, and (d) study the effect of PAC on biomass composition by performing physicochemical characterization of harvested biomass (proximate, ultimate, biochemical).

Table 1.8 Comparison of studies on effluent based media recycle.

Strain name	Culture media	Cultivation mode	Harvesting and treatment method	Duration or number of recycles	Biomass Yield		Percentage increase/ decrease in maximum biomass yield after the recycling	Nutrient consumed		Reference
					Fresh Media	Recycled Media		NO_3 (mg/L)	PO_4 (mg/L)	
Scenedesmus acuminatus	Modified BG11 media (initial $NaNO_3$ conc. :187 mg L^{-1})	PBR array with 30 ml glass tubes	Centrifugation and 0.2 µm membrane; treatment using 80 g of Granular activated carbon (GAC)	12 days 1 cycle	2.38 g L^{-1}	2.04 g L^{-1} without treatment and 2.33 g L^{-1} after GAC treatment	14.3 % decrease after first reuse without any treatment and almost equal biomass with GAC treatment	-	-	[182]
Staurosira sp. C323	Artificial seawater	Batch mode in 1 L glass media bottles	Vacuum filtration (0.45 µm)	25 days 3 cycles	6.4 mM C	4.8 mM C	No growth after second reuse	-	-	[183]
Scenedesmus SDEC-8, Chlorella SDEC-18	BG11 media	Batch mode in 3 L columns	Centrifugation and ultrasonication	16 days 4 cycles	1.67 g L^{-1} and 109.05 mg L^{-1} d^{-1} (for SDEC- 8); 1.71 g L^{-1} and 105.56 mg L^{-1} d^{-1} (SDEC-18)	1.01 g L^{-1} and 69.84 mg L^{-1} d^{-1} (for SDEC-8); 1.01 g L^{-1} and 80.00 mg L^{-1} d^{-1} (SDEC-18)	62.78 % decrease for SDEC-8 and 55.89 % decrease for SDEC- 18 after 3 media reuses	-	-	[184]
Arthrospira platensis	Schlosser media	Batch mode in Erlenmeyer flasks of 1 L capacity	Microfiltration with 50 µm pore dia. 30 mg L^{-1} PAC and 6 mg L^{-1} $FeCl_3$	10 days 1 cycle	-	1.093 g L^{-1} and 130.6 mg L^{-1} d^{-1} after treatment with 30 mg L^{-1} PAC and 6 mg L^{-1} $FeCl_3$	Growth in treated media almost equal as the control experiment.	-	-	[185]

Synechocystis sp. PCC 6803	Modified BG11 media (P: five times the normal concentration)	Batch mode in 500 mL Erlenmeyer flasks	Microfiltration with 0.45 µm pore dia.	12 days 5 cycles	-	0.63 g L^{-1} for 50:50 recycle to fresh media ratio	Growth inhibition at 3rd cycle due to lack of phosphorous	79 mg L^{-1}	24 mg L^{-1}	[186]
Arthrospira platensis	Zarrouk media	Batch mode in 1 L bottle	Filtration (20 µm pore size)	10 days 4 cycles	0.18-0.26 d^{-1}	0.24 d^{-1} (start of experiment) 0.07 d^{-1} (end of experiment)	68 % decrease after 4 cycles	-	-	[187]
Dunaliella salina	-	Batch mode in 200 mL flasks	NaOH Flocculation	10 days			No growth in reused media	-	-	[52]

1.5. Literature Review Summary

As seen from literature, microalgae emerge as a promising third-generation feedstock for biodiesel production as it has the capability of oil production throughout the year. Other advantages include non-requirement of arable land, faster-growing cycle, high growth rate, and lipid content as compared to second-generation feedstock. However, commercial production of microalgal biomass feedstock is not considered sustainable due to its high production cost. Therefore, recycling the culture media carry significant potential to reduce the overall cost for the long-term growth of microalgal industry. In this context, the choice of harvesting technique as well as pretreatment method plays a key role in deciding the sustainability of microalgal biomass production.

As evident from literature, conventional techniques such as centrifugation, flocculation and floatation are primarily used for microalgal harvesting. These techniques either uses extensive energy or lead to contamination of the effluent and microalgal biomass. Also, the primary factor limiting the commercial utilization of microalgal biomass is an economically effective and chemical free harvesting technique. Hence, low-cost kaolin based ceramic membranes can be recommended due to their ability to harvest microalgae without cell disruption. Furthermore, the permeate obtained from microfiltration of culture can be recycled to cultivation after pretreatment, which minimizes water requirement and need of nutrient replenishment.

For effective reuse of the harvested culture medium, the removal of organic contaminants is necessary. Pretreatment method such as flocculation leads to contamination of the harvested effluent, thereby interfering in further recycle studies. After rigorous literature review it was found that adsorption by powdered activated carbon proved to be the

suitable technique for effective removal of potential organic inhibitors from the harvested effluent.

1.6. Thesis Objectives

In light of the existing literature gap, the following objectives were framed for the thesis:

- Preparation, characterization and efficiency analysis of low-cost ceramic membranes using naturally found inexpensive kaolin along with different binders.
- Application of kaolin based microporous membrane for efficient microalgal harvesting.
- Recycle of harvested effluent and process enhancement using PAC for cost effective algal biomass production
- Economic Viability of the developed low-cost membrane, microalgal harvesting and the energy efficient recycle process

1.7. Thesis Outline

Chapter 1: Introduction, Literature Review and Objectives

The initial part of this chapter provides a concise overview of the basics and classification of membrane technology. The recent advances on the use of low-cost raw material for membrane fabrication are also highlighted with main focus on kaolin as the key precursor. This is succeeded by a detailed discussion on microalgal harvesting with key emphasis on the use of membrane technology for the same. This chapter also provides insights on the treatment of harvested effluent for energy efficient recycle. The meticulous literature review carried out here unveils potential scopes for further research in the above topic, which also shapes the objectives of the thesis. Finally, this chapter outlines the structure of the thesis.

Chapter 2: Preparation and Characterization of Kaolin-based Disc and Tubular Membrane

Chapter 2 discusses about optimization and fabrication of disc and tubular membranes using kaolin as the key precursor. The kaolin clay procured from Deopani area of Assam was initially characterized using techniques like X-ray fluorescence (XRF), Fourier-transform infrared spectroscopy (FTIR), X-ray diffraction (XRD), thermogravimetric analysis (TGA) and particle size distribution (PSD). Then, to optimize the concentration of binders, five different membrane compositions were chosen by varying the amount of kaolin and binders such as sodium carbonate, boric acid and sodium metasilicate. Once the binder composition was fixed in disc membrane, tubular membranes were prepared using the same concentration of binders. Also, porosity agent calcium carbonate was added to enhance the porosity in tubular membranes. The X-ray diffraction analysis, average porosity, chemical stability, flexural strength, surface morphology, pore size distribution and water permeability of the membranes were investigated. Based on the properties, an optimized membrane was fixed for further application in microalgal harvesting.

Chapter 3: Application of Kaolin-based Membrane in Microalgal Harvesting

Chapter 3 portrays a detailed analysis of the application of the developed tubular membrane in harvesting of microalgae *Monoraphidium* sp. KMC4. The membrane performance was evaluated by investing transmembrane pressure, algal recovery, total organic carbon concentration, and the permeate's nutrient concentration. Furthermore, fouling models were fitted to the experimental data to obtain a comprehensive insight into the microfiltration process.

Chapter 4: Energy Efficient Recycle of Harvested Microalgal Effluent

Chapter 4 discusses about the recycle potential of the harvested microalgal effluent. In this regard, the harvested effluent was mixed with different ratios of fresh BG11 media and then microalgae *Monoraphidium* sp. KMC4 was cultivated in those mixtures. To enhance the inhibited growth in those mixtures, powdered activated carbon (PAC) was used as adsorbent to lower the accumulated organic matter. Also, dose of PAC and effluent media concentration was optimized henceforth. Furthermore, to reduce freshwater dependency, five batch recycle study was studied in the optimized effluent media. The biomass characterization such as biomass composition, TGA profile, FTIR profile and FAME profile was studied for the optimal PAC treated effluent media. At last, this chapter proposes a biorefinery model for sustainable production of microalgal biomass.

Chapter 5: Economic Viability of the Developed Low-cost Membrane, Microalgal Harvesting and the Energy Efficient Recycle Process

In the pursuit of developing a cost-efficient and environmentally sustainable technology, this chapter thoroughly examines detailed cost analysis. The chapter starts with the cost analysis of the fabricated membrane followed by the cost analysis involved in the microalgal harvesting using the fabricated membrane. Subsequently, the overall cost of implementing the energy efficient recycle process was determined. Cost estimations for each process are presented for both laboratory-scale and pilot-scale setups.

Chapter 6: Conclusions, Social Imapact and Future Perspectives

Chapter 6 presents a summary of the findings and social impact derived from the preceding chapters and also provides some valuable suggestions for future work.

Chapter 2

Preparation and characterization of kaolin-based disc and tubular membrane

CHAPTER 2

Preparation and characterization of kaolin-based disc and tubular membrane

This chapter commences with a discussion on the raw materials used for the fabrication of ceramic disc and tubular membranes. Naturally available kaolin was selected as the main raw material along with binders such as boric acid, sodium metasilicate, and sodium carbonate. Moreover, calcium carbonate was added to enhance the porosity of the tubular membranes. Kaolin material along with the fabricated membranes were characterized using standard characterization methods. Based on the membrane properties, the optimized membrane was considered for microalgal harvesting.

2.1. Materials

Raw materials selection is a crucial step in the fabrication of ceramic membranes. The significance of raw material selection is highlighted in Table 2.1. The clay used in this study was collected from Deopani area in Karbi Anglong district of Assam, India (26.24° N, 93.75° E). The lumpy clay was greyish-white in colour and the clay after being dried at 120 °C was powdered by Hammer Mill (Model: KCMO-105, K.C Engineers Pvt. Ltd.). Sodium metasilicate (Loba Chemie Pvt. Ltd.), boric acid (Merck Specialities Pvt. Ltd.) and sodium carbonate (HiMedia Laboratories Pvt. Ltd.) were used as binders in membrane fabrication. Cacium carbonate (HiMedia Laboratories Pvt. Ltd.) was used as a pore former.

Table 2.1 Significance of raw materials used in membrane fabrication

Raw material	Significance	Ref.
Kaolin	Low plasticity and good refractory properties	[17]
Boric acid	Enhances mechanical strength by the creation of metaborates during membrane sintering	[19]
Sodium metasilicate	Creates silicate bonds thereby increasing mechanical strength	[154]
Sodium carbonate	Helps in creating homogeneity by improving dispersion properties	[154]
Calcium carbonate	Act as pore former	[188]

Fig. 2.1 Pictures of kaolin collection site (Deopani area in Karbi Anglong district of Assam, India (26.24° N, 93.75° E)

2.2. Fabrication of Disc Membrane

The disc shaped membranes were prepared using a stainless-steel die of 50 mm diameter and 5 mm thickness by paste casting [155] and the compositions are listed in Table 2.2.

Several membranes of other compositions were also tried but, in some cases, due to less binding material the membrane strength was very poor and, in some cases, due to more binding material the membrane got stick in the furnace and the binders came out of the membrane during sintering. The raw materials were mixed with distilled water to form a paste and then the paste was casted in the die. After drying for 24 h in room temperature, the membrane was taken out from the die carefully and transferred to hot air oven for further drying at 100 °C for 12 h. Finally, the casted membrane was heated in a muffle furnace from room temperature to sintering temperature of 850 °C at 2 °C min^{-1} heating rate. The membrane was kept in hold at the sintering temperature for 6 h and then the muffle furnace temperature was gradually cooled to room temperature. The rigid supports were then polished using silicon carbide abrasive paper to get the final smooth uniform shape. Then the support was ultrasonicated in a water bath for 30 mins to remove any loosely bound particles. The membrane fabrication flow chart is shown in Fig. 2.2. Fig. 2.4 shows the picture of fabricated disc membrane.

Table 2.2 Composition of clay and binders for disc membrane fabrication

Material	M1 (Wt.%)	M2 (Wt.%)	M3 (Wt.%)	M4 (Wt.%)	M5 (Wt.%)
Kaolin	92	88	84	82	80
Sodium metasilicate	2	3	4	4.5	5
Boric acid	2	3	4	4.5	5
Sodium carbonate	4	6	8	9	10

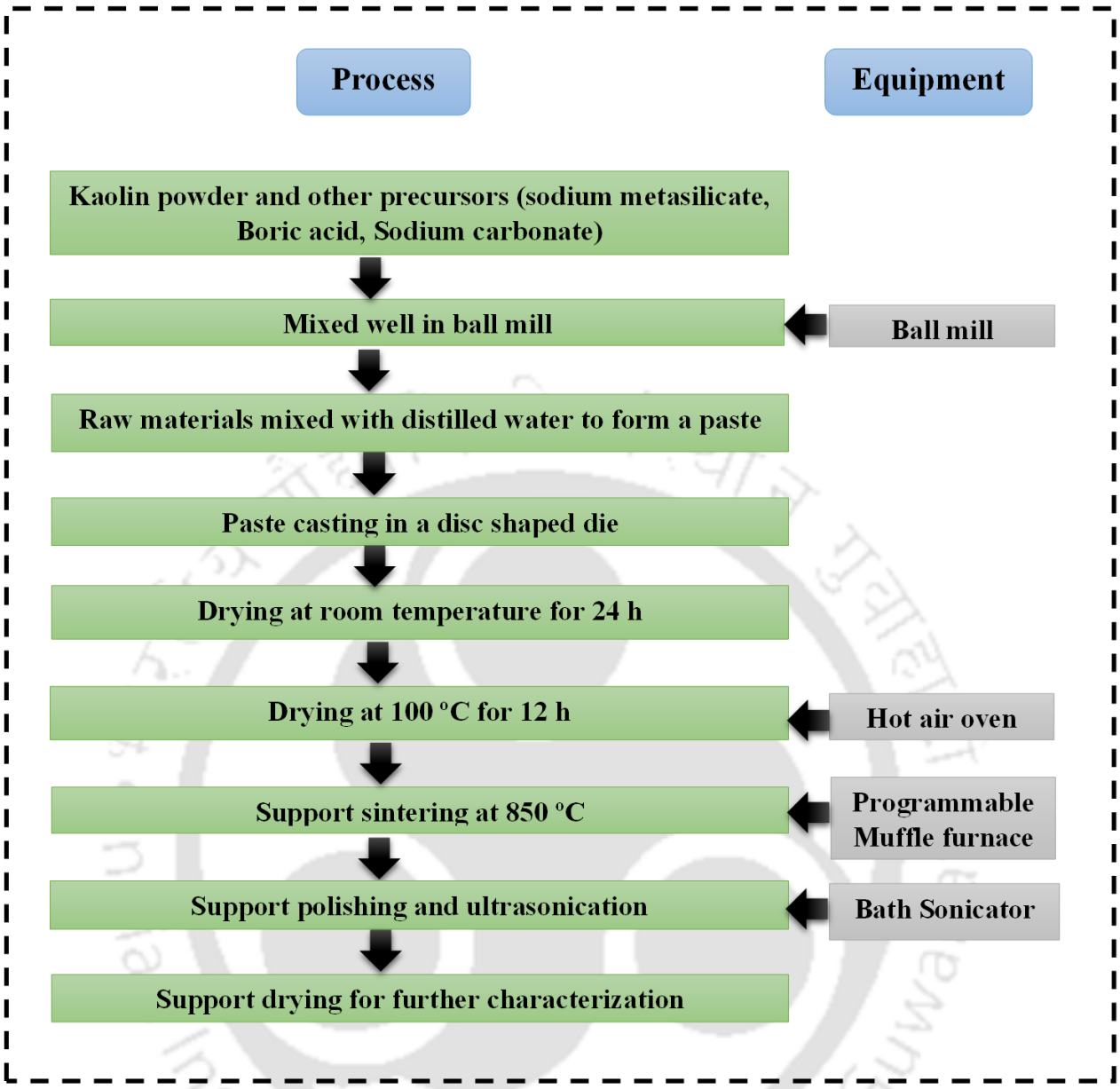

Fig. 2.2 Disc membrane fabrication flow chart

2.3. Fabrication of Tubular Membrane

Kaolin-based tubular ceramic membranes measuring 100 mm in length, 9 mm outer diameter, and 5 mm inner diameter were fabricated using the extrusion technique. Different membrane compositions used are mentioned in Table 2.3. The raw materials were mixed with Millipore water to form a paste, which was then passed through a horizontal extruder (M/s VB Ceramics, Chennai, India) to get the desired membrane shape. The membranes from the extruder were first kept at room temperature for 24 h. Then they were oven dried in two stages: 12 h at 100 °C followed by 12 h at 200 °C. After that, the membranes were sintered in a muffle furnace for 6 h at 950 °C. The heating rate for the sintering process was maintained at 2 °C min^{-1} for avoiding any deformation or bending in the final sintered membrane. Finally, the membrane was smoothened, and surface was furnished using abrasive paper (C-220) and then sonicated to remove any loosely bound particles adhered to the membrane surface. The membranes were then dried at 100 °C and taken for further characterization and experiments [31]. Fabricated tubular membrane is shown in Fig. 2.4.

Table 2.3 Raw material compositions used for tubular membrane fabrication

Raw material	Composition (wt %)				
	M1	M2	M3	M4	M5
Kaolin	92	87	82	77	72
Boric acid	2	2	2	2	2
Sodium metasilicate	2	2	2	2	2
Sodium carbonate	4	4	4	4	4
Calcium carbonate	0	5	10	15	20

2.4. Characterization Techniques

2.4.1. X ray fluorescence analysis (XRF)

The quantitative analysis of major oxides present in the kaolin clay was done by XRF (PAN analytical, Zetium). The analysis was done by mixing the sample with boric acid and then exposing the sample to X-rays to determine the composition of the kaolin clay collected from Deopani. The sample was prepared by mixing 1 g of kaolin with 0.5 g of boric acid binder. Then the mixture was turned into a pellet by 40 kN hydraulic press.

2.4.2. X ray diffraction analysis (XRD)

The phases present in the clay, unsintered and sintered membrane was seen using powder X-ray diffractometer (Rigaku, SmartLab). 40 mA and 40 kV were used as the operating current and analysis voltage, respectively. Measurements were made with a 0.05° step size over a 2θ range of 5° - 80°.

2.4.3. Particle size analysis

The particle size distribution of the raw material was analysed using particle size analyser (Model: Litesizer 500; Make: M/s Anton Paar). The sample was ultrasonicated to avoid any formation of lumps.

2.4.4. Fourier Transform Infrared Spectroscopy (FTIR)

The functional groups present in the clay was characterized by FTIR (Perkin Elmer), The kaolin powder was mixed with KBr and transformed into a pellet.

2.4.5. Thermo-gravimetric analysis (TGA)

The thermal stability and sintering temperature was studied by a thermogravimetric analyzer (Model: TGA 4000, PerkinElmer). For this analysis, sample was placed in platinum crucible and temperature was increased steadily from room temperature to 1100 ^{o}C.

2.4.6. Morphological analysis

Surface morphology and defect analysis of the prepared membranes was studied by Field emission scanning electron microscopy (FESEM, make: Zeiss; Model: Sigma 300). For this analysis, a small fraction of the membrane was taken and gold coated to impart conductivity to the sample.

2.4.7. Mechanical stability

Three-point bending method using Universal Testing Machine (Instron-Dynamic UTM, 100 kN) was used to evaluate the flexural strength of the disc membranes. The flexural strength (σ) was calculated by the formula:

$$\sigma = \frac{3FL}{2bt^2} \tag{2.1}$$

where *F* is the fracture point load, *L* is the span length, *b* is the sample width and *t* is the sample thickness.

The mechanical strength of the fabricated tubular membranes was assessed using the ASTM D695 standard. An Electromechanical Universal Testing Machine (Make: Zwick Roell: Z005TN) equipped with a 5 kN load cell and operated at a crosshead speed of 2 mm min^{-1}, served the purpose. The preparation of samples for this analysis involved a membrane with dimensions of 20 mm in length, 9 mm in outer diameter (OD), and 5 mm in inner diameter (ID).

2.4.8. Chemical stability

Each prepared membrane was tested for its chemical stability by suspending it in a solution of HCl (with a pH of 1.4) and NaOH (with a pH of 13.5). The dry membrane weight (W_i) was determined before the membranes were dissolved in HCl and NaOH. After that, the membranes were immersed in the solutions for a duration of seven days each, at room

temperature and atmospheric pressure [188]. After immersion, the membranes were taken out of the solutions, rinsed with deionized water, and dried in an oven for three hours at 120 °C to determine their final weight (W_f). Eq. (2.2) calculates the amount of weight loss in acidic and alkaline media.

$$\text{Weight loss } \% = \frac{W_i - W_f}{W_i} \times 100 \quad (2.2)$$

2.4.9. Porosity

Archimedes' principle is commonly used to assess membrane porosity. This method necessitates soaking the membrane in deionized water for 48 h. The membrane's pore volume is the variance in weight between the membrane prior to and after being dipped in water. The ratio of the pore volume to the total membrane volume provides the membrane porosity.

$$\text{Porosity } (\%) = \frac{W_{wet} - W_{dry}}{V_m \times \rho} \times 100 \quad (2.3)$$

where W_{wet} is the weight of wet membrane, W_{dry} is the weight of dry membrane, V_m is the membrane volume, and ρ is the water density.

2.4.10. Water permeability and pore size evaluation

Water permeability of the disc membranes was evaluated by dead end filtration setup made of stainless steel. A permeation setup was used to determine the water permeability of the membranes. The permeation setup consists of a top section of capacity 320 mL, an inlet for filling the compartment with water, a small opening to which is connected a pressure gauge and the compressor and an outlet for water permeation. The middle section is a flat base where the membrane is kept. The membrane is tightened carefully using silicon gaskets to avoid any leakage of water from any sides other than the outlet. The time taken for the collection of 50 mL of permeate was noted at different transmembrane pressures. The permeate flux was calculated at different air pressures by using the following equation:

$$J = \frac{Q}{A\Delta t} \quad (2.4)$$

where, J is the water flux, Q is the permeation volume (m^3), A is the membrane area (m^2) and Δt is the water collection time (s).

A cross-flow microfiltration system designed and built entirely in our lab was used as depicted in schematic form (Fig. 2.3). The bypass valve is employed to regulate the feed inlet pressure, and the second valve serves as a controller for maintaining the flow rate of the retentate stream. Water is pumped from the feed tank to the dampener, and the pressure gauge measures the pressure at the entrance of the membrane module. The permeate is collected cross-axially to retentate stream in the permeate tank. By orienting the membrane horizontally in the microfiltration system, an effective filtration area of 15.71×10^{-4} m^2 was obtained to measure pure water flux. Before experiments, membranes were compacted with higher pressure to remove loose particles.

Additionally, after reaching a steady state, water flux measurements were performed. Maintaining a consistent cross-flow rate of 1.11×10^{-5} m^3 s^{-1} and altering transmembrane pressures (69 kPa, 138 kPa, 207 kPa, 276 kPa, and 345 kPa), the permeate sample was taken at regular intervals up to 40 min. The water flux (J_w) of the membrane at each pressure (P) was estimated using the quantity of water collected with time (t) at the permeate side and the membrane area (A) according to Eq. (2.4). Henceforth, the calculated flux (J_w) values for all pressures were used to determine the hydraulic permeability (L_h) of the membrane, which was found to follow Darcy's law (Eq. (2.5)).

$$J_w = L_h \times \Delta P \quad (2.5)$$

The Hagen-Poiseuille equation is then applied to determine the membrane's pore size (Eq. 5)[189].

$$r = \left(\frac{8\mu\tau l L_h}{\varepsilon}\right)^{1/2} \quad (2.6)$$

where r represents the radius of membrane pore, μ stands for water viscosity at 25 °C, l indicates the pore length (l = 0.002 m), L_h is the pure water permeability, ε is the membrane porosity and τ is the membrane tortuosity (Eq. 2.7) [188].

$$\tau^2 = 1 - 2\ln\varepsilon \quad (2.7)$$

Using ImageJ software, the pore size of the membranes was also determined from the FESEM images. Each membrane was examined using four FESEM images, and Eq. (2.8) was used to calculate the average pore size assuming that the pores are cylindrical.

$$d_s = \left[\frac{\sum_{i=1}^{n} n_i d_i^2}{\sum_{i=1}^{n} n_i}\right]^{0.5} \quad (2.8)$$

where d_s represent the average pore diameter, d_i denotes the diameter of the i^{th} pore, n_i stands for the quantity of pores with diameter d_i, and n signifies the overall count of pores taken into consideration.

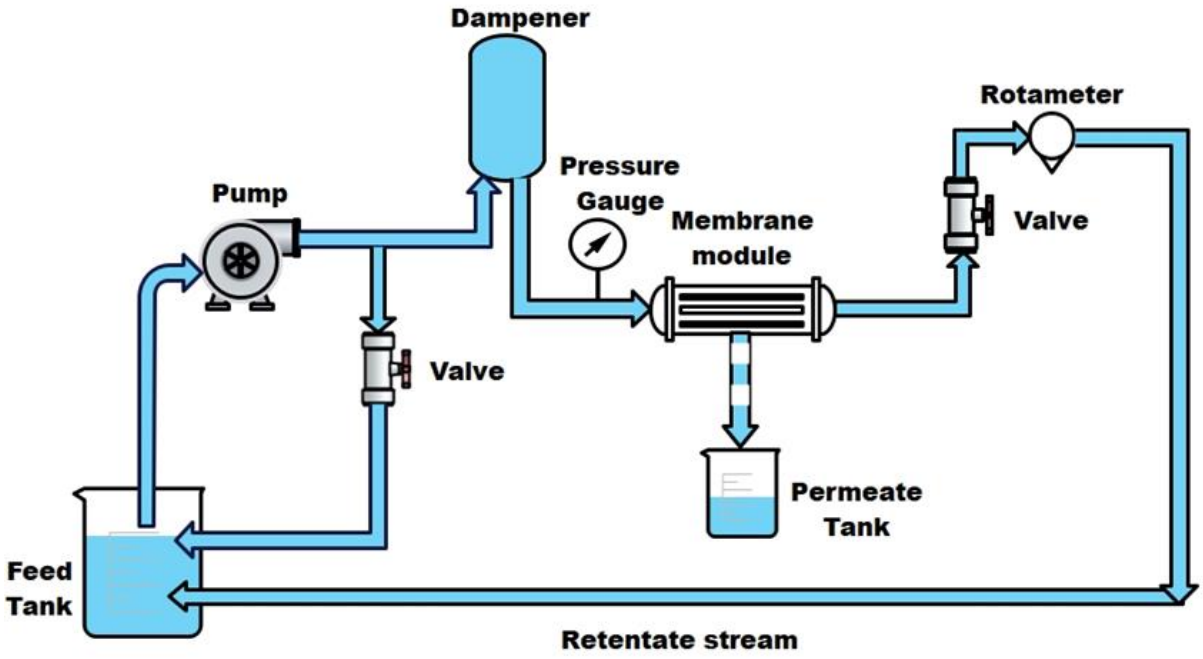

Fig. 2.3 Schematic of microfiltration setup

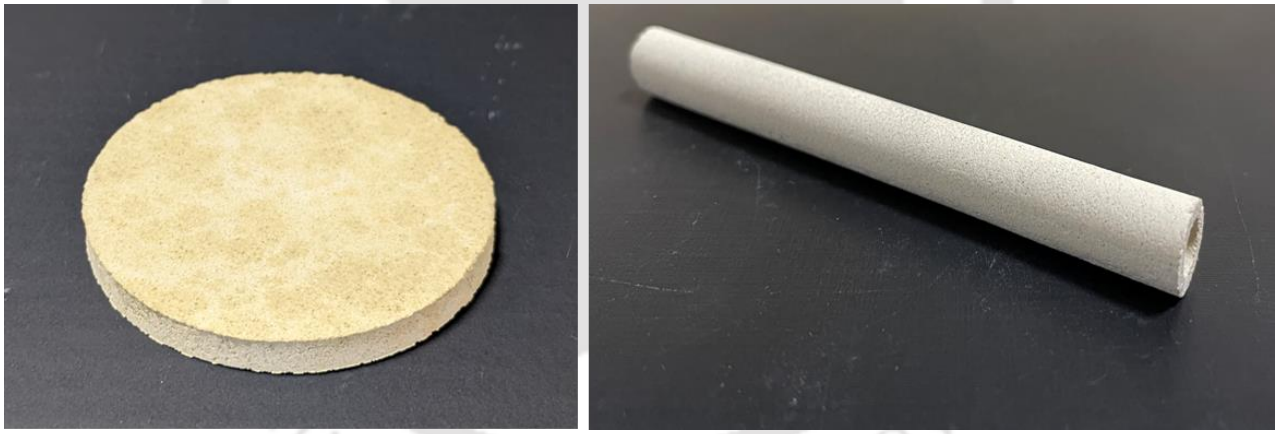

Fig. 2.4. Pictures of fabricated disc and tubular membrane

2.5. Results and Discussions

2.5.1. Characterization of kaolin clay

2.5.1.1. X ray fluorescence analysis (XRF)

Kaolin compositions mainly varies with the geographical location [190,191]. The chemical composition of Assam Kaolin in weight percentage is shown in Table 2.4. The kaolin was rich in SiO_2 (49.98%) and Al_2O_3 (35.03%) along with the presence of alkali metal oxides

such as Na_2O and K_2O; alkaline earth metal oxides such as CaO and MgO and oxides of transition metals like Fe_2O_3, MnO and TiO_2. In addition, non-metallic oxides such as P_2O_5 and SO_3 were also present in trace amounts. The loss on ignition (LOI) of Kaolin was 11.01% at 1000 °C. The mass loss was mainly due to removal of organic substances and water. As compared to the theoretical Kaolinite composition, which is SiO_2 = 46.5% and Al_2O_3 = 39.5% [192], Assam Kaolin was slightly rich in SiO_2 content. The main impurity was Fe_2O_3 (1.57%) which may impart dark color to sintered products.

Table 2.4 Chemical composition of Assam Kaolin

	SiO_2	Al_2O_3	Fe_2O_3	MnO	MgO	CaO	Na_2O	K_2O	TiO_2	P_2O_5	SO_3	LOI
Kaolin(%)	49.98	35.03	1.57	0.015	0.19	0.24	0.06	1.03	0.73	0.09	0.05	11.01

2.5.1.2. X ray diffraction analysis (XRD)

Identification of phase of a clay is of primary importance before using it in any application. Fig. 2.5 represents the XRD spectra of Kaolin. It can be seen from the profile that Kaolinite ($Al_2Si_2O_5(OH)_4$) (JCPDF Card No.: 00-001-0527) and Quartz (SiO_2) (JCPDF card No.: 00-001-0649) were the major components. The presence of Quartz was inevitable because of 49.98% SiO_2 in Assam Kaolin (as seen from XRF data). The peaks for kaolin appeared at 2θ = 12.38°, 19.94°, 24.89°, 35.49°, 35.94°, 38.43°, 45.52°, 47.96°, 59.96°, 62.3°, 72.15°, 73.46° and 76.81° corresponding to d = 7.14, 4.44, 3.57, 2.52, 2.49, 2.34, 1.99, 1.89, 1.54, 1.48, 1.3, 1.28 and 1.22 Å respectively, whereas, peaks for quartz were identified at 2θ = 20.84°, 26.67°, 36.57°, 39.23°, 40.32°, 42.47°, 50.15°, 55.07°, 68.14° and 75.65° for d = 4.25, 3.33, 2.45, 2.29, 2.23, 2.12, 1.81, 1.66, 1.37 and 1.25 Å respectively. No other significant peaks were observed which proved the presence of very less impurities in the Kaolin powder. The diffraction patterns were in accordance with the patterns obtained from literature for kaolin [193,194].

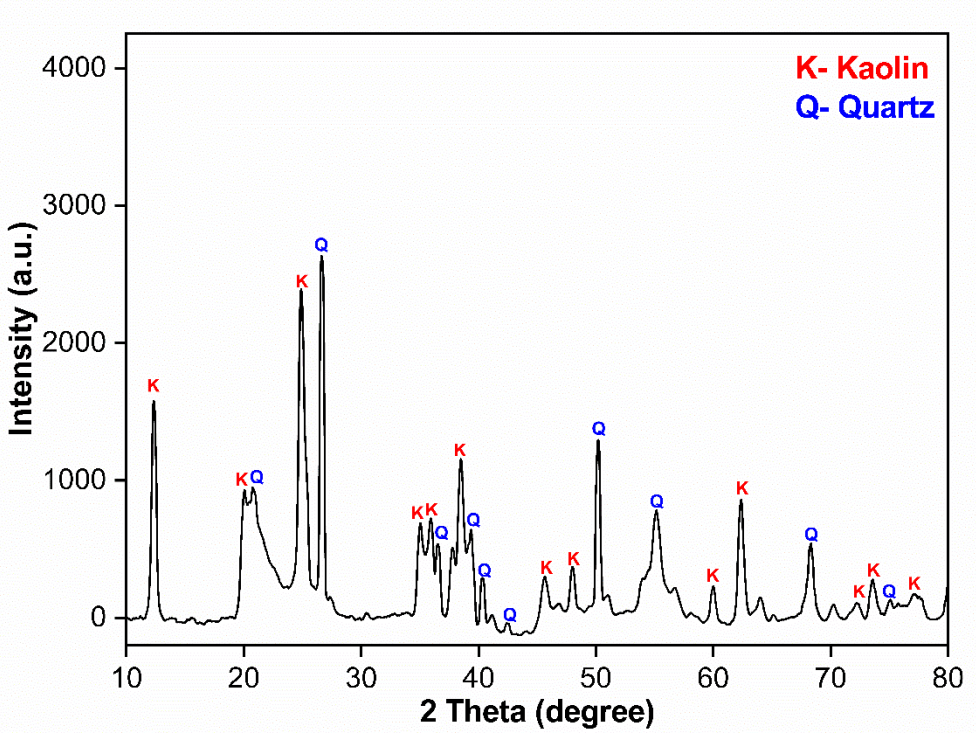

Fig. 2.5. XRD profile of Assam Kaolin

2.5.1.3. Particle size analysis

The particle size distribution of the Kaolin powder was determined by Dynamic Light scattering technique**.** As seen from Fig. 2.6, the average particle size of Kaolin clay was 0.354 µm.

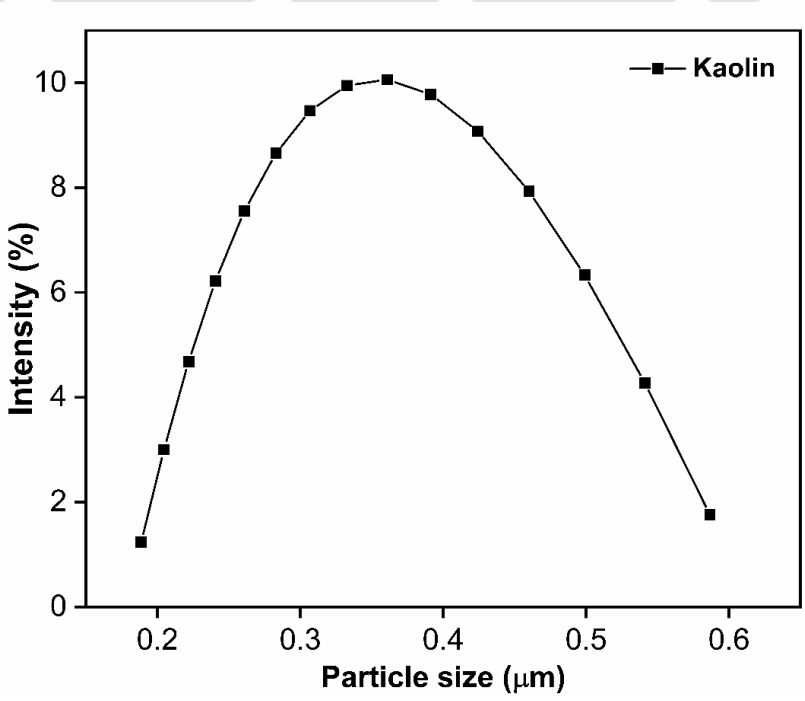

Fig. 2.6 Particle size distribution of Assam kaolin

2.5.1.4. Fourier Transform Infrared Spectroscopy (FTIR)

FTIR of Assam Kaolin powder was done to identify the bonds present in it. The FTIR of kaolin showed peaks at 3694, 3653, 3620, 1110, 1030, 1007, 917, 789, 754, 680, 528 and 469 cm^{-1}

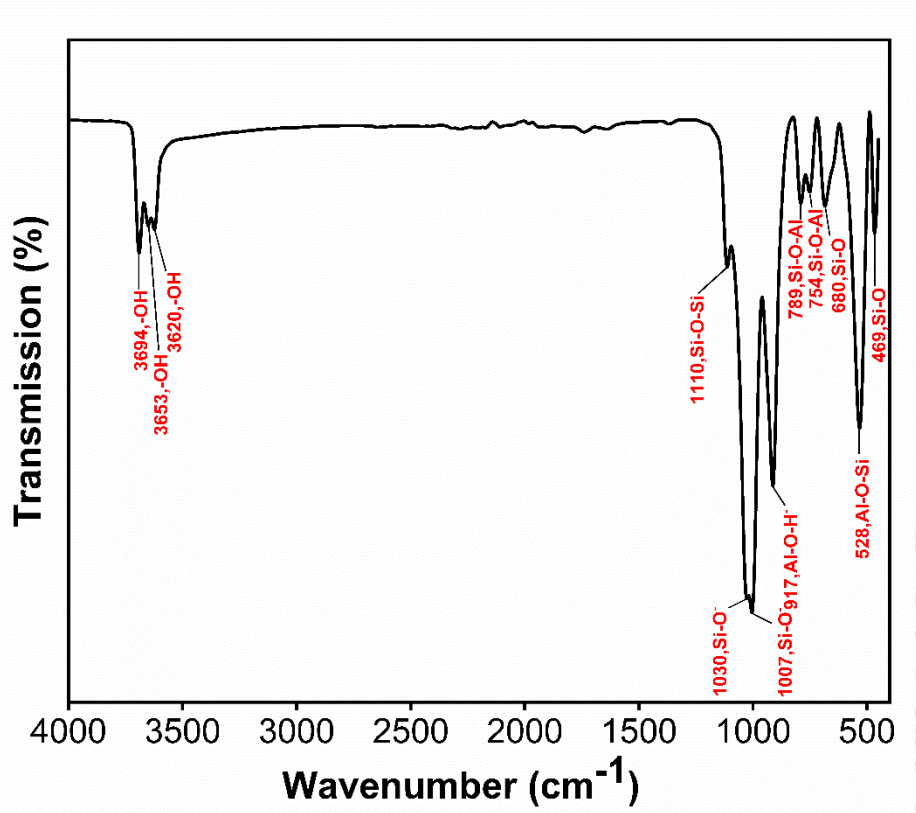

Fig. 2.7 FTIR spectra of Assam Kaolin

respectively (Fig. 2.7). The bands corresponding to OH stretching were 3694, 3653 and 3620 cm^{-1}; bands associated with Si-O stretching were 1030, 1007, 680 and 469 cm^{-1}; for Si-O-Al stretching the bands were 789, 754 and 528 cm^{-1}; for Si-O-Si stretching the band was 1110 cm^{-1} and for Al-OH stretching it was 917 cm^{-1} respectively. Similar peaks for kaolin were observed by Saikia et al. [152].

2.5.1.5. Thermo-gravimetric analysis (TGA)

The thermal stability of Kaolin powder was seen by TGA analysis. The TGA-DTG-DSC curve of Assam Kaolin is shown in Fig. 2.8. It could be clearly seen from the graph that the weight loss occurred in two phases. First one occurred between the ambient temperature (25 °C) and around 120 °C because of the dehydration of Kaolin. This region is very important in the membrane sintering process. The membrane should be dried at 100 °C to avoid any crack formation before further heating it at elevated temperature. The second sharp weight loss (7.5%) occurred between 400 °C and 600 °C due to the dehydroxylation of the clay. The endothermic DSC peak of the Kaolin clay at 580 °C confirmed the same. At this temperature kaolin transforms into amorphous metakaolin (Eq. 2.9) [195]. An exothermic peak at around 990 °C corresponds to the transformation of metakaolinite phase to crystalline Spinel phase ($2Al_2O_3.SiO_2$) [196]. The total weight loss from TGA was 11%, which matches with the loss on ignition data of XRF (Table 2).

$$Al_2Si_2O_5(OH)_4\ (\text{Kaolin}) \xrightarrow{(400-600)^\circ C} 2(Al_2O_3O.2SiO_2)(\text{Metakaolin}) + 2H_2O \quad (2.9)$$

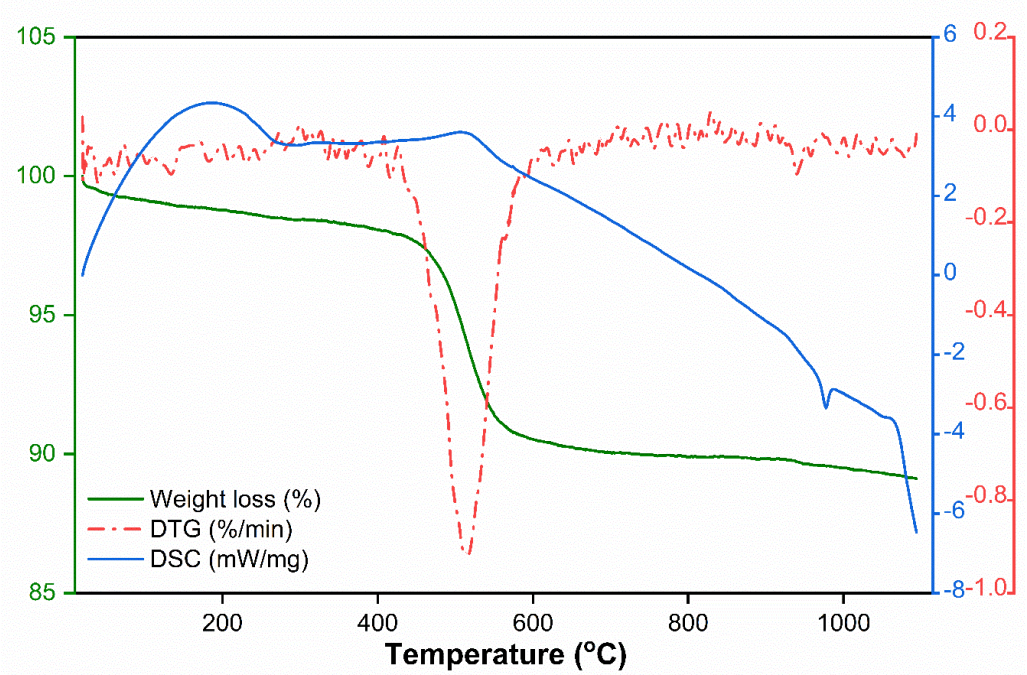

Fig. 2.8 Thermogravimetric analysis of Assam kaolin

2.5.2. Characterization of disc membrane

2.5.2.1. Particle size analysis of raw materials

The particle size distribution analysis of the raw material mixture forming the membrane is shown in Fig. 2.9. The particle size distribution of all the compositions showed a narrow distribution. For M1 and M2 membranes, the size ranges from 0.13 µm to 1.03 µm and for M3, M4 and M5 it ranges from 0.16 µm to 0.68 µm respectively. The average particle size showed a decreasing trend as composition were varied from M1 to M5. For membrane M1, M2, M3, M4 and M5, the average particle size based on intensity distribution was found to be 0.47 µm, 0.45 µm, 0.39 µm, 0.38 µm and 0.36 µm respectively. The particle size determines the pore size as well as porosity of membrane formed. As pores are the vacant spaces formed in between the particles, so a large number of finer particles in a specified volume gives large number of pores, larger transport resistance and high porosity whereas coarser particles occupying the same volume gives small number of pores, lower transport resistance and low porosity.

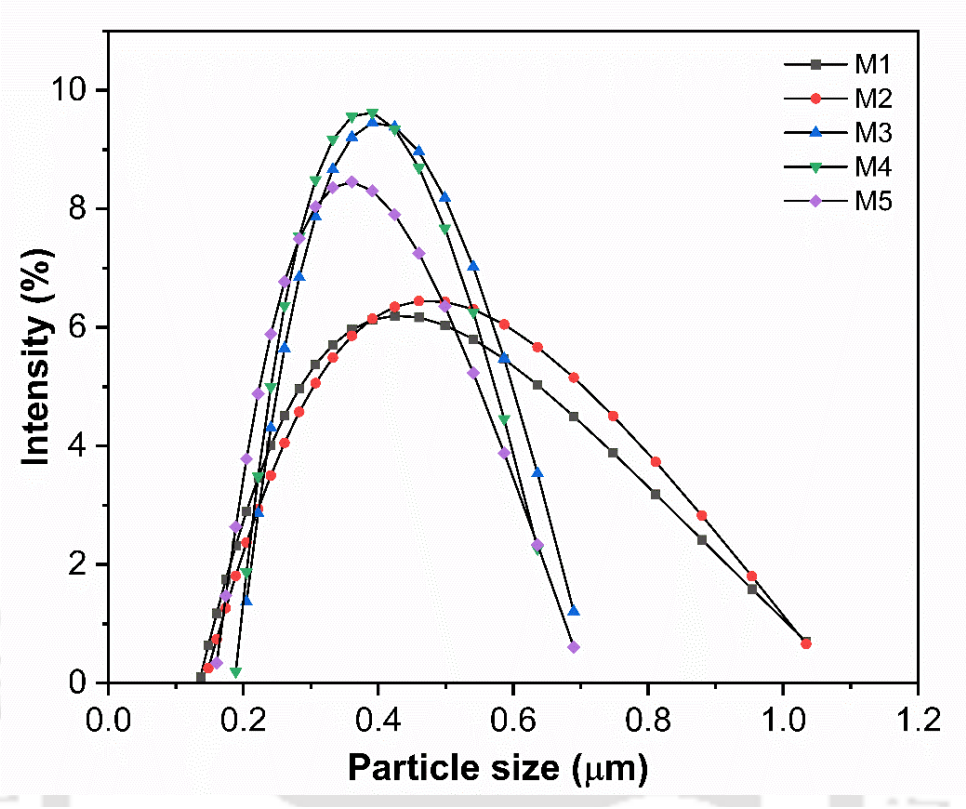

Fig. 2.9 Particle size distribution of membrane raw material mixture

2.5.2.2. Thermogravimetric analysis of membrane composition

Thermogravimetric analysis (TGA) of the membrane composition was done to see the minimum sintering temperature for the membrane fabrication. As can be seen from Fig. 2.10, the first weight loss occurred between the ambient temperature and around 120 °C because of the removal of loosely held molecules of water. The weight loss in this range increased from M1 to M5 compositions because of the increase in the percentage contribution of hygroscopic sodium metasilicate, boric acid and sodium carbonate from M1 to M5 respectively [154]. Secondly, from 150 °C to 450 °C, boric acid dehydrated sequentially forming metaboric acid (HBO_2), tetraboric acid ($H_2B_4O_7$) and boron trioxide (B_2O_3) respectively. The percentage of boric acid was increased subsequently from M1 to M5 and hence weight loss also increased in this range. After 450 °C, a sharp weight loss

was seen up to near about 800 °C. This was due to the transformation of kaolinite to metakaolinite by the release of hydroxyl group. The curve was stagnant after 850 °C for all the five compositions M1, M2, M3, M4 and M5. Hence, it was concluded that the minimum sintering temperature for membrane fabrication can be fixed at 850 °C to obtain a support with higher mechanical and thermal stability. The total percentage weight loss for M1, M2, M3, M4 and M5 compositions was 10.44%, 9.98%, 13.88%, 14.59% and 13.54% respectively.

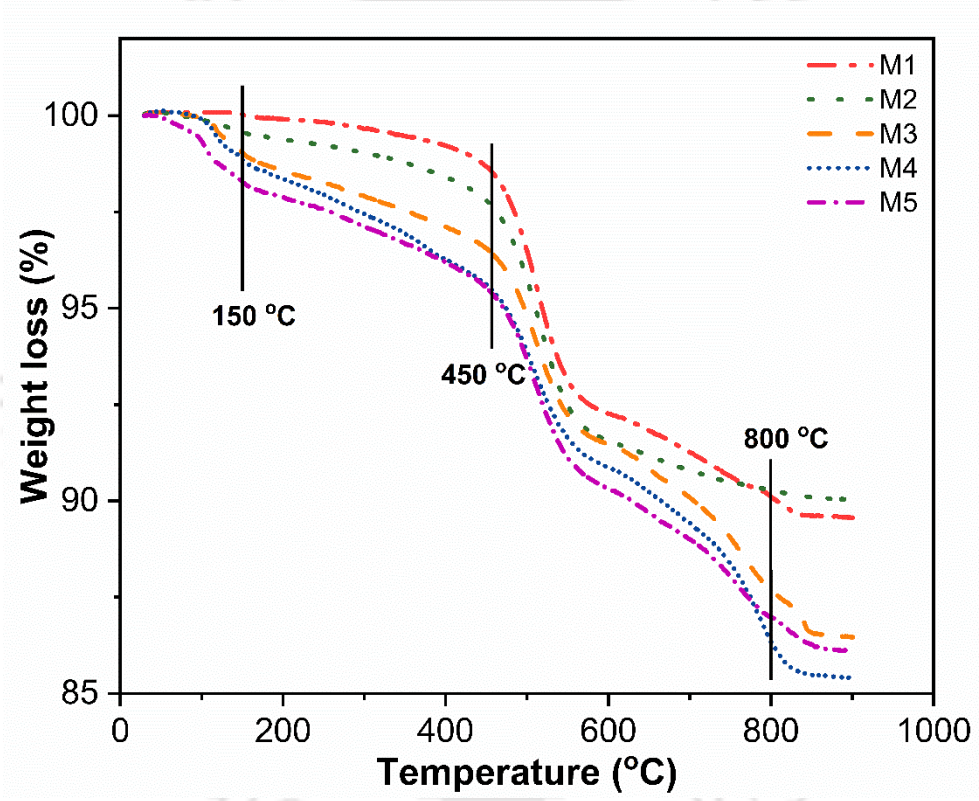

Fig. 2.10 Thermogravimetric analysis of membrane raw material mixture

2.5.2.3. Average porosity

The average porosity was evaluated by the Archimedes principle using the Eq. 2.3. The average porosity calculated was 34.52%, 31.82%, 24.18%, 22.26% and 21.50% for M1, M2, M3, M4 and M5 respectively (Table 2.5). The porosity decreased with decrease in average particle size of membrane raw materials and membrane densification from M1 to

M5. The level of porosity obtained here for M1 is similar to that obtained by others [197,198]. However, in this study, the porosity of 34.52% was obtained without any use of pore-formers.

2.5.2.4. X-ray Diffraction analysis

The phase behaviour of membrane was seen by XRD analysis as depicted in Fig. 2.11. The observed phases of the sintered membrane were Quartz (Q), Corundum (C), Mullite (M) and Nepheline (N). As Kaolin contains a little amount of iron and titanium as impurity so the occurrence of Corundum phase, which is a crystalline phase of Al_2O_3 was justified [155]. The peaks for Nepheline ($K_{0.25}Na_6Al_{6.24}Si_{9.76}O_{32,}$ JCPDF Card No.: 01-070-1260) occurred at 2θ =21.23°, 36.9°, 48.36°, 54.2°, 55.36° and 68.43° for d = 4.18, 2.43, 1.88, 1.69, 1.65 and 1.36 Å respectively. Quartz (SiO_2, JCPDF card No.: 00-001-0649) peaks were seen at 2θ = 26.99° and 64.34° for d = 3.3 and 1.44 Å respectively, whereas, Mullite ($Al_{4.8}Si_{1.2}O_{9.6}$, JCPDF card No.: 05-001-0663) peaks at 2θ = 39.8°, 40.6° and 73.73° for d = 2.26, 2.21 and 1.28 Å respectively and Corundum (Al_2O_3, JCPDF card No.: 00-002-1227) peaks were observed at 2θ = 25.67° and 60.25° for corresponding d = 3.46 and 1.53 Å respectively. As can be seen from Fig. 2.11, all the five membrane composition showed almost same XRD peaks. Kaolinite reflection was not found because of its transformation to metakaolinite, which was also confirmed by TGA analysis of Kaolin powder.

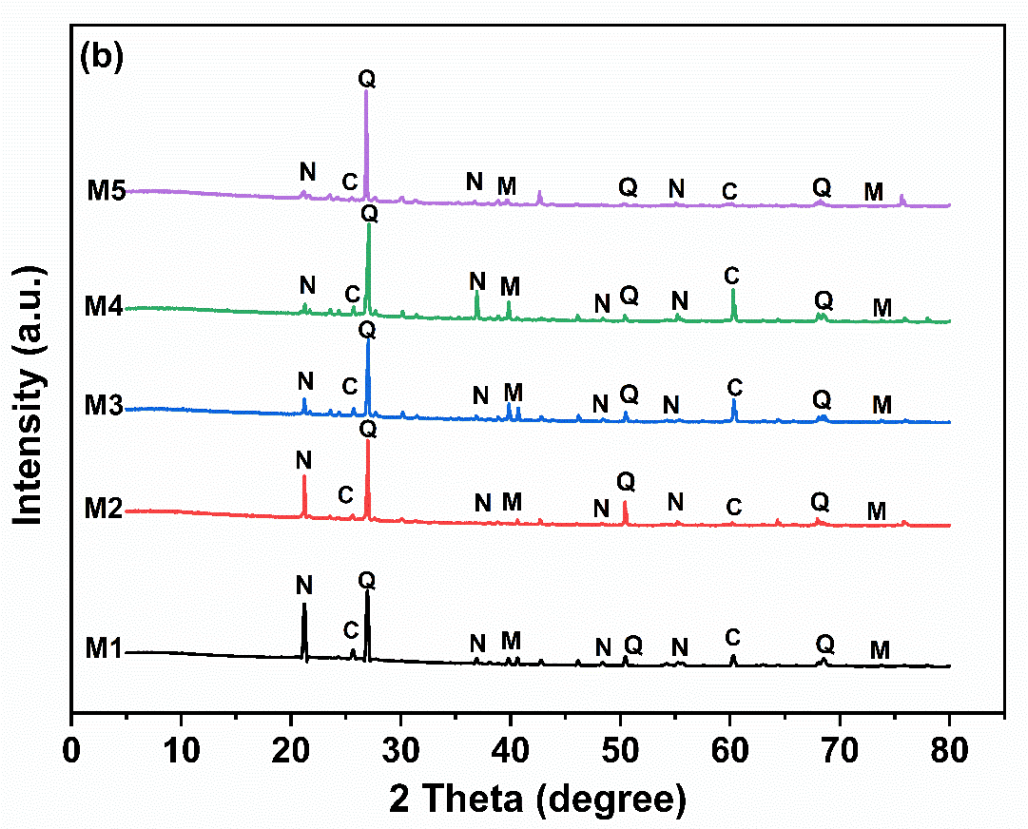

Fig. 2.11 XRD analysis of the prepared disc membranes

2.5.2.5. Chemical stability

The weight loss percentage for base (NaOH) corrosion was found to be 0.21%, 0.19%, 0.22%, 0.13% and 0.11% for M1, M2, M3, M4 and M5 respectively and for acid (HCl) corrosion it was 0.14%, 0.15%, 0.19%, 0.14% and 0.08% respectively (Table 2.5). The results obtained revealed that the fabricated support showed great corrosion resistance and hence it can be used for membrane applications involving acidic and alkaline media. Results for all the supports did not vary much because of the similar XRD peaks.

2.5.2.6. Flexural strength

The flexural strength of the fabricated supports was estimated by three-point bending method using the Eq. 2.1. The span length was 25 mm and membrane thickness 5 mm. The flexural strength of M1, M2, M3, M4 and M5 membranes was calculated as 7.1 MPa, 7.4 MPa, 8.2 MPa, 9 MPa and 9.4 MPa respectively (Table 2.5). The incorporation of sodium

metasilicate crystals results in densification of the membrane support. So, as the XRD analysis of M1, M2, M3, M4 and M5 (Fig. 2.11) was not showing much difference, it could be concluded that the increase in strength was due to more dense structure of M5 membrane (as it has higher percentage of sodium metasilicate) in comparison to M4 membrane and so on. Similar flexural strength was also reported by Jana et al. [155].

2.5.2.7. Surface morphology

To determine the average pore size and pore size distribution of membranes, morphological studies were done using FESEM. By looking at the FESEM images (Fig. 2.12) it was found that the prepared membranes were intact without any visible cracks. The pore size of the membranes decreased from M1 to M5. This was because the particle size of the membrane raw material mixture decreased and the membrane density increased from M1 to M5 respectively. Also, the pore sizes were between 0.05 µm to 10 µm making it suitable for MF applications.

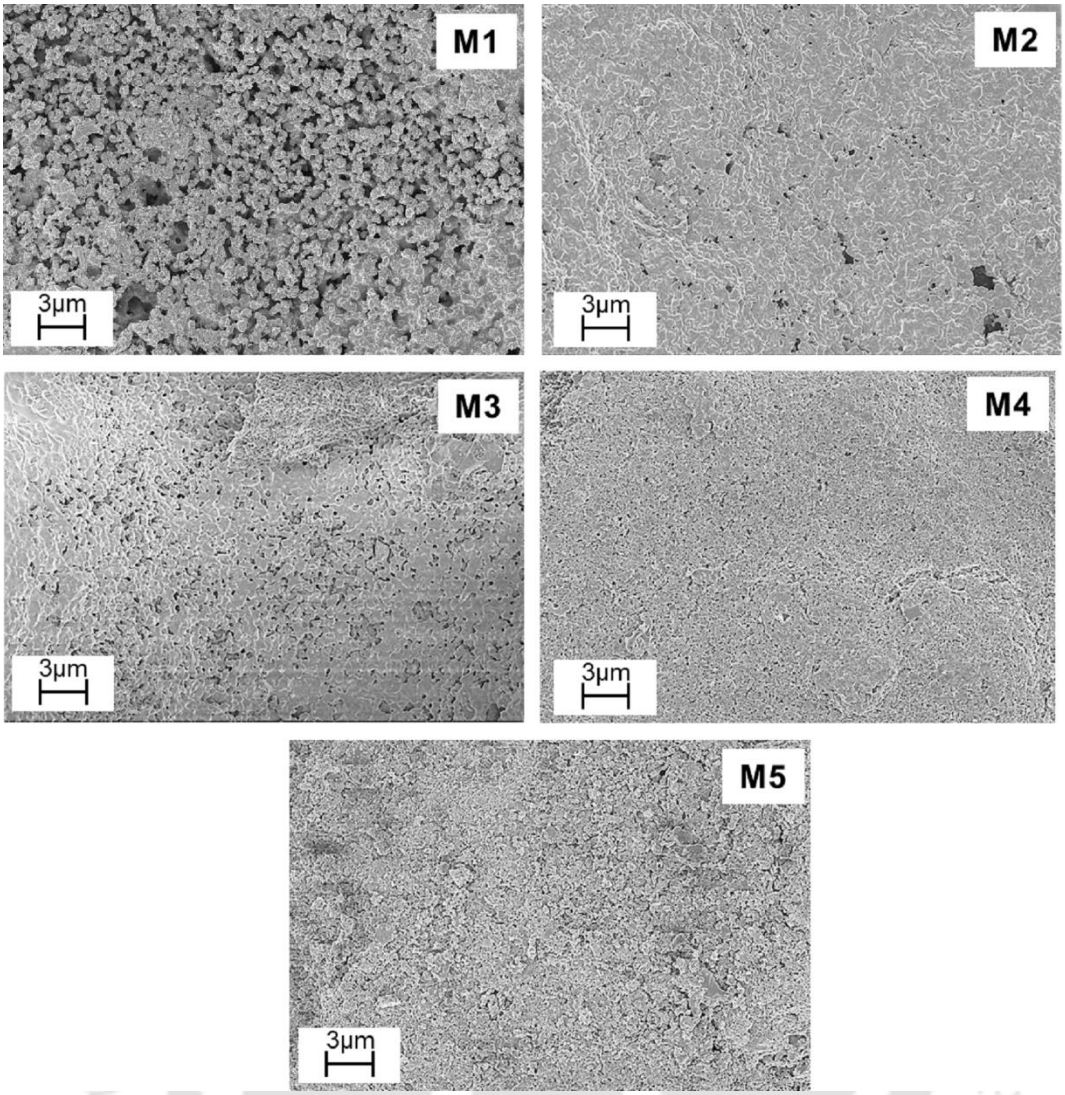

Fig. 2.12 FESEM images of the prepared membranes M1, M2, M3, M4 and M5

2.5.2.8. Pore size distribution

Pore size distribution was determined by using the ImageJ software and the FESEM images. Four FESEM images were taken of each membrane and the pore size was evaluated. Fig. 2.13 shows the pore size distribution of membranes M1, M2, M3, M4 and M5. Assuming that the pores are cylindrical, the average pore size was evaluated using the Eq. 2.6 [154].

The average pore diameter obtained was 2.28 μm, 0.615 μm, 0.605 μm, 0.308 μm and 0.195 μm for membranes M1, M2, M3, M4 and M5 respectively (Table 2.5). The pore size decreased from M1 to M5 due to membrane densification. It was observed that the prepared

membranes had wide pore size distribution with all pores lying within the MF range. These range of pore sizes has been successfully used as support layer [199], oil and bacteria separation [200], mosambi juice clarification [201], solid particles removal [202] , arsenic removal [203], oily wastewater treatment [204].

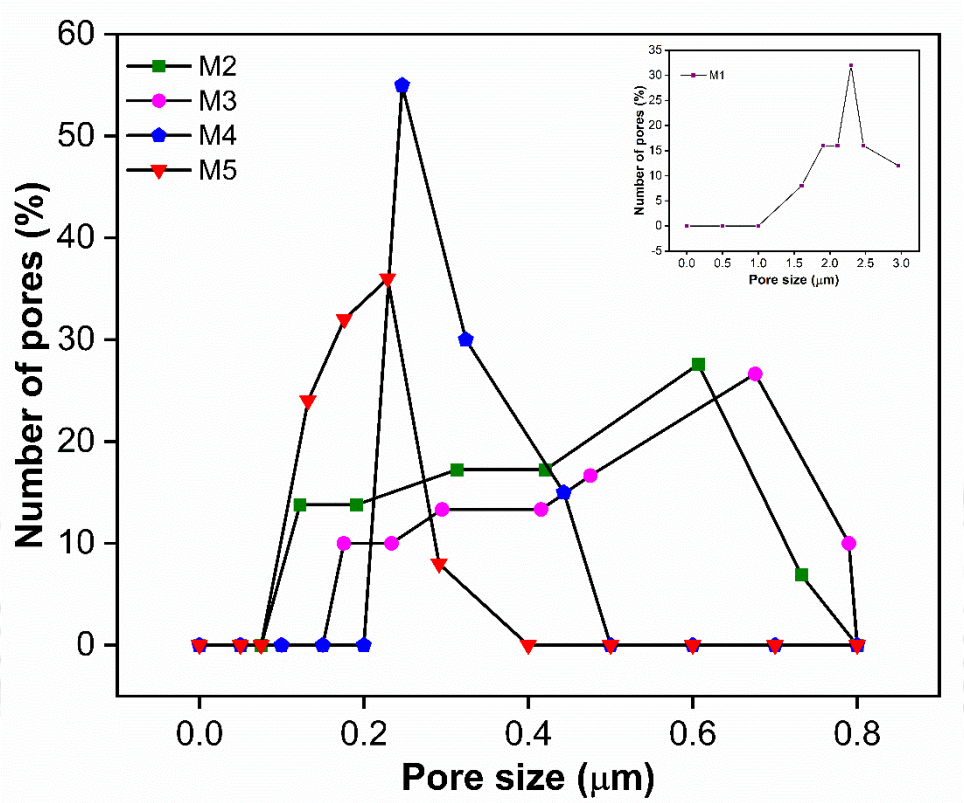

Fig. 2.13 Pore size distribution of M2, M3, M4, M5 and M1 (insert) from FESEM micrographs

2.5.2.9. Water permeability

Pure water flux was calculated using the Eq. 2.4. Fig. 2.14 shows the pure water flux of M1, M2, M3, M4 and M5 at 50 kPa, 100 kPa, 150 kPa, 200 kPa and 250 kPa respectively. The water flux increased linearly as the trans-membrane pressure was increased from 50 kPa to 250 kPa. From the graph it is clear that the water permeability (slope of the graph) decreased from M1 to M5. It was evident because of the decreasing porosity and pore size from M1 to M5. The water permeability values obtained were 6.12×10^{-9}, 5.01×10^{-9},

3.71×10^{-9}, 2.57×10^{-9} and 1.61×10^{-9} m Pa^{-1} s^{-1} for membranes M1, M2, M3, M4 and M5 respectively (Table 2.5). Similar permeability values for kaolin disc type membrane was also reported by others [155,205].

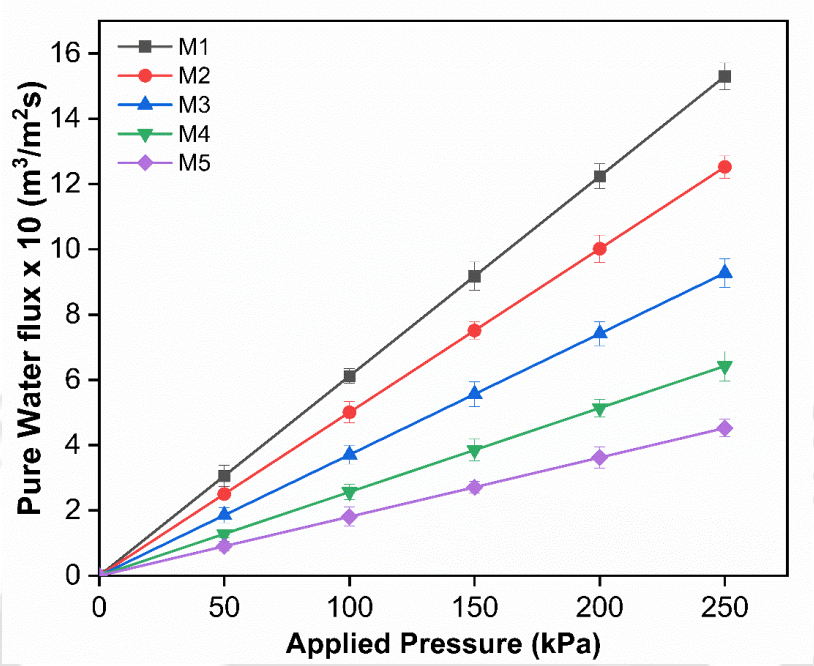

Fig. 2.14 Pure water flux as a function of applied pressure

Table 2.5 Summary of results obtained for the disc membrane compositions.

Membranes	Average Porosity (%)	Flexural strength (MPa)	Average Pore size (µm)	Weigh loss in acid medium (%)	Weight loss in alkaline medium (%)	Water Permeability (m/Pas)
M1	34.52	7.1	2.28	0.14	0.21	6.12×10^{-9}
M2	31.82	7.4	0.615	0.15	0.19	5.01×10^{-9}
M3	24.18	8.2	0.605	0.19	0.22	3.71×10^{-9}
M4	22.26	9	0.308	0.14	0.13	2.57×10^{-9}
M5	21.5	9.4	0.195	0.08	0.11	1.61×10^{-9}

2.5.2.10. Optimization of binder composition

With increase in binder percentage from 8% to 20%, the percentage porosity, average pore size and water permeability decreased from 34.52% to 21.5%, 2.28 µm to 0.195 µm and 6.12×10^{-9} to 1.69×10^{-9} m Pa^{-1} s^{-1} respectively while flexural strength increased slightly from 7.1 MPa to 9.4 MPa. Hence, binder percentage of 8% i.e., 2% boric acid, 2% sodium metasilicate and 4% sodium carbonate was found to be optimum. Thereafter, tubular membranes will be fabricated using this binder concentration.

2.5.3. Characterization of tubular membrane

2.5.3.1. Thermogravimetric analysis of membrane composition

The thermal investigation of the raw materials was carried out to establish the sintering temperature to produce a membrane of high quality. In the TGA results of the kaolin with the binders and pore former $CaCO_3$, the first weight loss occurs at around 100 °C owing to the removal of loosely held water molecules in the sample. Boric acid dehydrated between 150 °C and 400 °C, forming metaboric acid (HBO_2), tetraboric acid ($H_2B_4O_7$), and boron trioxide (B_2O_3) [189]. A sharp DTG peak between 400 °C to 550 °C was attributed to the dehydroxylation of kaolin to amorphous metakaolinite phase [206]. The significant weight loss between 550 °C to 730 °C occured due to the thermal decomposition of calcium carbonate ($CaCO_3$), resulting in calcium oxide (CaO) and carbon dioxide (CO_2) [31]. The membrane porosity mainly depends on the pathway taken by the evolved CO_2 at this temperature range. A negligible weight loss was observed after 850 °C, suggesting that minimum sintering temperature should be 850 °C for fabricating membranes of good mechanical and chemical strength. However, since the flexural strength increases with rise in sintering temperature, the chosen temperature for sintering was 950 °C. Above 950 °C, a reduction in chemical stability of membrane was observed.

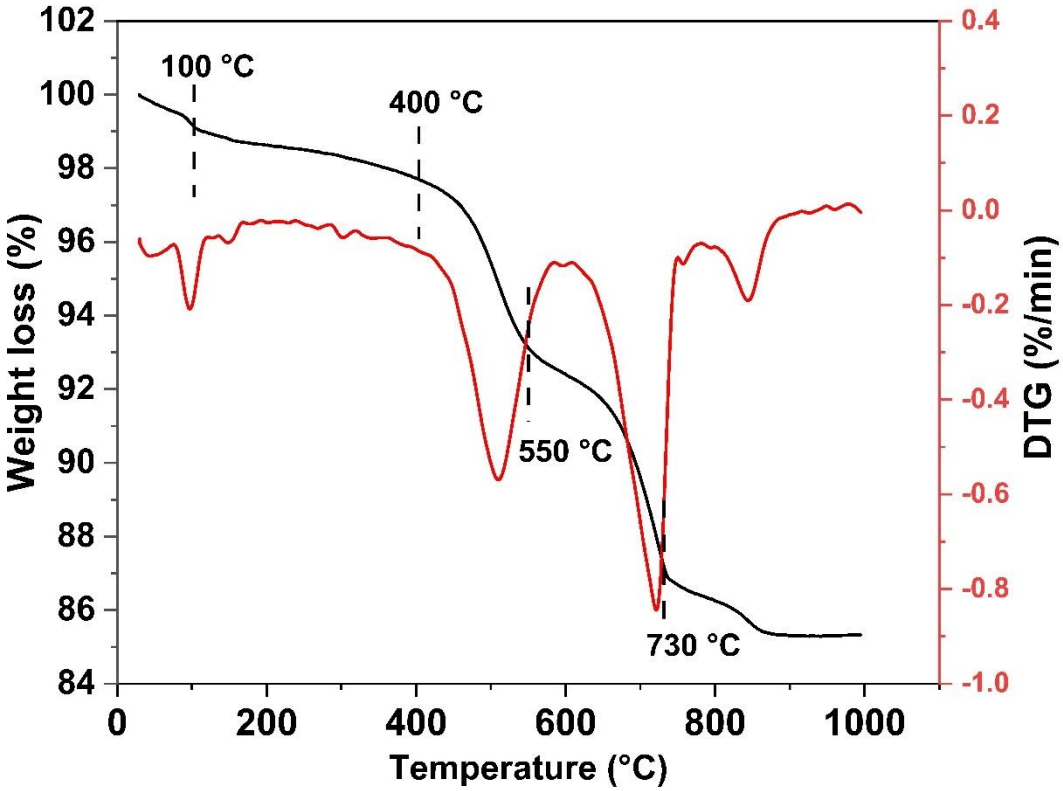

Fig. 2.15 TGA-DTG curve of the membrane raw material mixture

2.5.3.2. Average porosity

The porosity of the membranes calculated using Archimedes' principle revealed that the porosity increases with increasing pore former ($CaCO_3$) concentration (Table 2.6). This happens because the thermal decomposition of higher pore former ($CaCO_3$) concentrations at higher temperatures produces more carbon dioxide (CO_2), which increases membrane porosity [31,207]. Kakali et al. [188] also report a similar relation between the porosity values and concentration of pore former $CaCO_3$. They found the lowest porosity when no $CaCO_3$ was used and the highest porosity at 15% concentration of $CaCO_3$.

2.5.3.3. X-ray Diffraction analysis

Fig. 2.16 depicts the X-ray diffraction analysis of raw material mixtures used to fabricate membranes (M1-M5) before and after the sintering process. As anticipated, high-temperature sintering causes phase transformations. The main phases appearing in the unsintered membranes are kaolinite ($Al_2Si_2O_5(OH)_4$, JCPDF Card No.: 00-001-0527), Quartz (SiO_2, JCPDF card No.: 00-001-0649) and Inyoite ($2CaO.3B_2O_3.13H_2O$, JCPDF Card No.: 00-002-0836) [51]. From the observation and comparison of the XRD profiles of sintered and unsintered membranes, it is seen that the peak corresponding to kaolinite at $2\theta = 12.38°$ disappeared in the sintered membrane due to the phase transformation of kaolinite to metakaolinite and mullite [206]. Also, quartz (SiO_2, JCPDF card No.: 00-001-0649), mullite ($Al_{4.8}Si_{1.2}O_{9.6}$, JCPDF card No.: 05-001-0663), nepheline ($K_{0.25}Na_6Al_{6.24}Si_{9.76}O_{32}$, JCPDF Card No.: 01-070-1260) and corundum (Al_2O_3, JCPDF card No.: 00-002-1227) are the other phases that are visible in the fabricated membrane. The peaks that correspond to quartz remain unchanged throughout the XRD pattern. It means that the sintering temperature does not affect quartz.

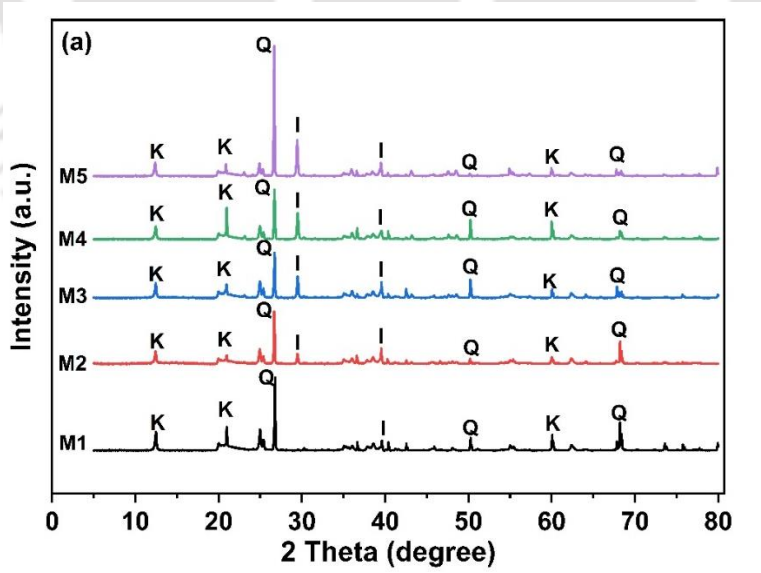

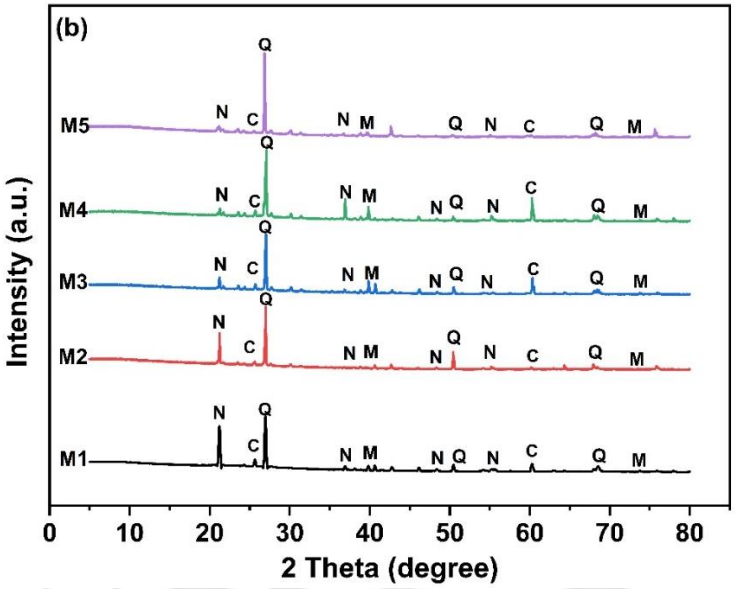

Fig. 2.16 XRD patterns of (a) unsintered and (b) sintered membranes (K: Kaolin, Q: Quartz, I: Inyoite, N: Nepheline, C: Corundum, M: Mullite)

2.5.3.4. Chemical stability

One of the crucial steps in membrane separation process is the chemical cleaning operation. So, in this study, corrosion caused by acid and alkali solutions on the prepared membranes was investigated. All the membranes showed good chemical resistance in alkaline conditions (Table 2.6) owing to the negligible mass loss. However, at acidic conditions, average weight loss percentage continued to rise from M1 to M5. This may be attributed to a trace amount of CaO in the membranes, which, after reacting with HCl, forms calcium chloride ($CaCl_2$) as a precipitate. Also, for membranes with higher pore former concentration, the FESEM images (Fig. 2.17) indicate larger pores which may allow acid solution to penetrate through it, resulting in higher weight losses. A similar trend of weight loss in acidic conditions for $CaCO_3$ as pore former was reported by Vasanth et al. in their research [156]. Consequently, it is advised against using the membranes in highly acidic environments.

2.5.3.5. Flexural strength

From Table 2.6, it is evident that the mechanical strength of membranes decreases with an increase in the quantity of $CaCO_3$ from 0 wt% to 20 wt%. The decrease in porosity values indicates fewer voids in the membrane, making it more rigid. A recent study obtained similar results where the mechanical compressive strength was higher at 5 wt% compared to 15 wt% concentration of $CaCO_3$ [188]. Also, for membrane M1 (mechanical strength ~ 26 MPa), the absence of pore former resulted in a lesser volume of voids, thus making the membrane more rigid.

2.5.3.6. Surface morphology

After the membranes with varying pore former concentrations have been made, their morphology must be examined to ensure they can be used in subsequent separation procedures. Fig. 2.17 corresponds to the surface images of membranes M1, M2, M3, M4, and M5. It is clear that membrane surfaces are smooth without cracks or pinholes. The darker portion marked by red arrows refers to the pores in the membrane, and the lighter portion depicts the clay particles. FESEM images were also used to determine the pore size of the membranes using the ImageJ software. The calculated average diameters of pore for M1, M2, M3, M4, and M5 membranes were 0.934 µm, 1.023 µm, 1.142 µm, 1.323 µm, and 1.376 µm respectively. The increase in pore size with increasing quantity of pore former is due to coalescence of pores leading to abnormally bigger pores.

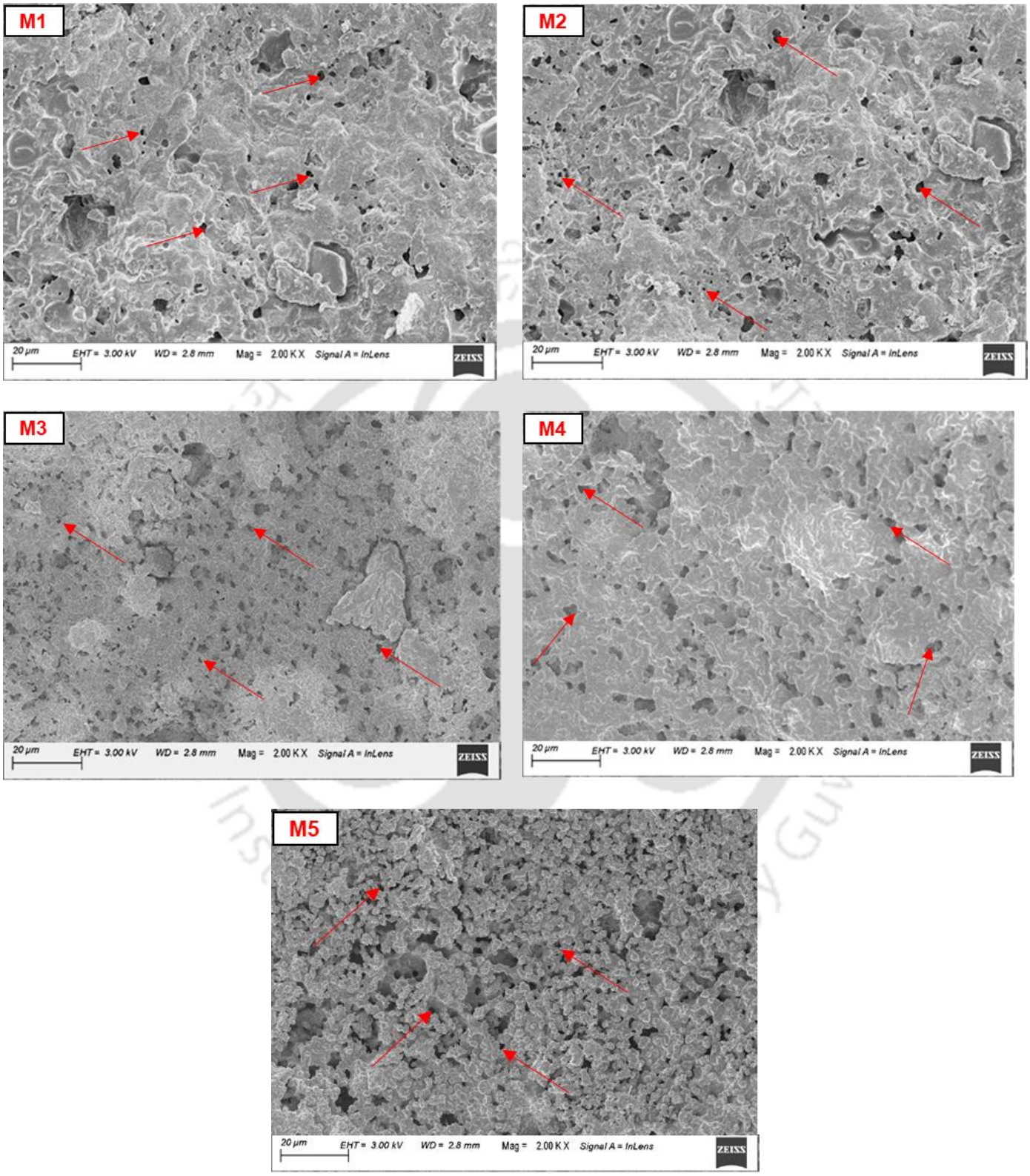

Fig. 2.17 FESEM images of the fabricated membranes

2.5.3.7. Water permeability

The pure water flux experiments were conducted for 40 minutes with five membrane compositions (M1, M2, M3, M4, and M5) at 69, 138, 207, 276, and 345 kPa pressures, respectively. Fig. 2.18 represents the steady-state pure water flux of the membranes at varied pressures. Also, Fig. 2.18 gives the pure water permeability as a function of the applied pressure. Observations indicate that pure water flux increases steadily with a rise in applied pressure due to the increased driving force for all the membranes with varying pore former concentrations. This trend follows Darcy's law (Eq. 2.5). As can be seen from Fig. 5, an increased water flux was observed for higher concentrations of pore former (15% and 20%). This can be attributed to the presence of larger pores and higher porosity for these membranes. The pore size was also calculated by Hagen-Poiseuille equation (Eq. 2.6).

For this, the tortuosity values from Eq. (2.7), the water permeability from Eq. (2.5) and the porosity values from Eq. (2.3) were calculated (Table 2.6). The mean pore size calculated using water permeability tests was 0.123, 0.132, 0.134, 0.179, and 0.182 µm for M1, M2, M3, M4, and M5 membranes, respectively, which was lower than those obtained from FESEM images. The reason for the difference is that the FESEM method only shows the pores on the surface of the membrane, which may get smaller as the membrane gets thicker. Moreover, in the FESEM technique, dead-end pores are also taken into account, and membrane tortuosity is not considered. On the other hand, mean pore size calculated from water flux data gives more genuine data as it considers the permeation pathway of water molecules considering the effect of tortuosity and dead-end pores. The outcomes of the pore size analysis of the membranes using permeation test are quite consistent with the findings of other studies [21,188]. As a result, the pore sizes obtained through water permeability data are considered for further experiments.

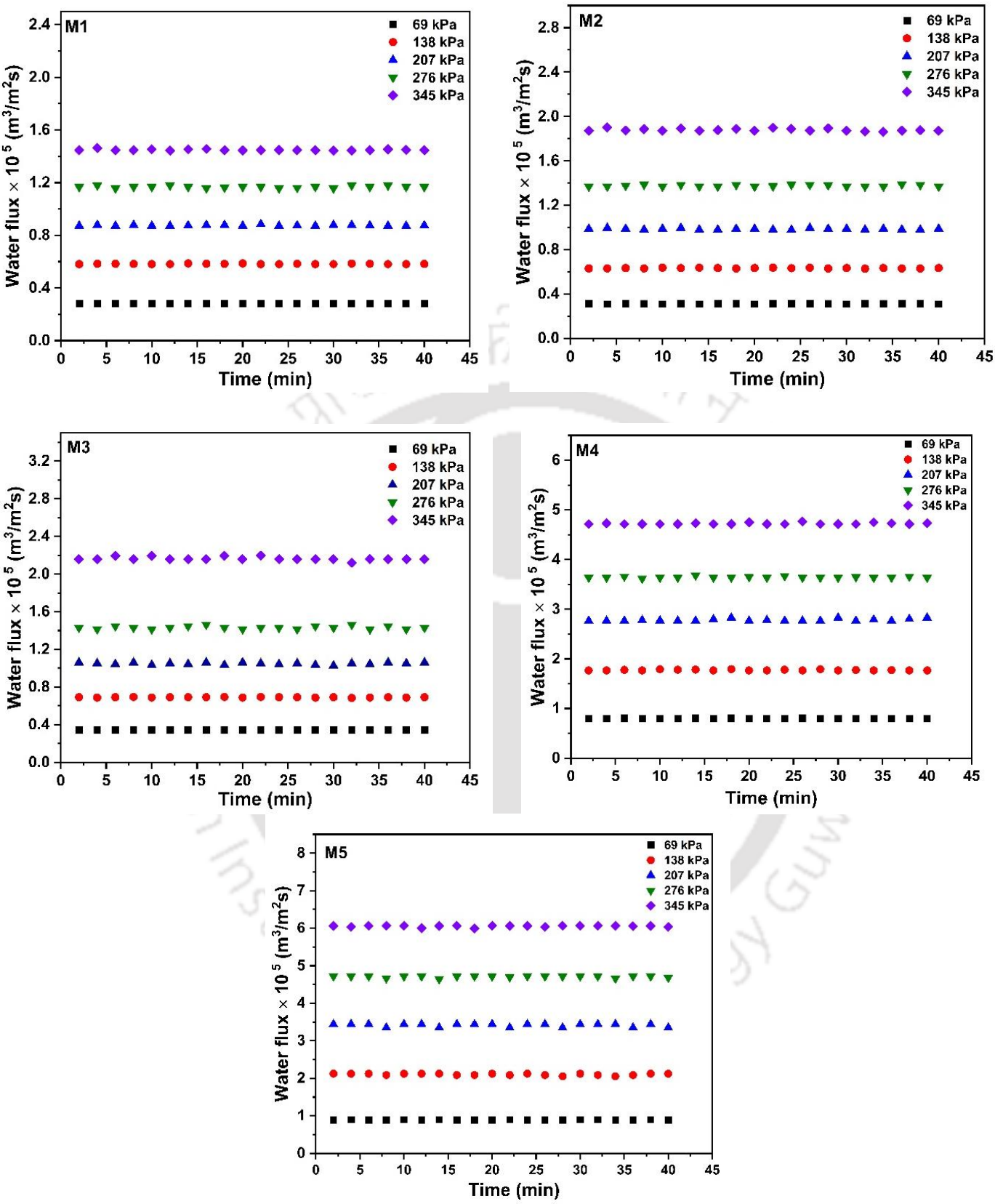

Fig. 2.18 Pure water flux of membranes M1, M2, M3, M4, and M5 at different transmembrane pressures.

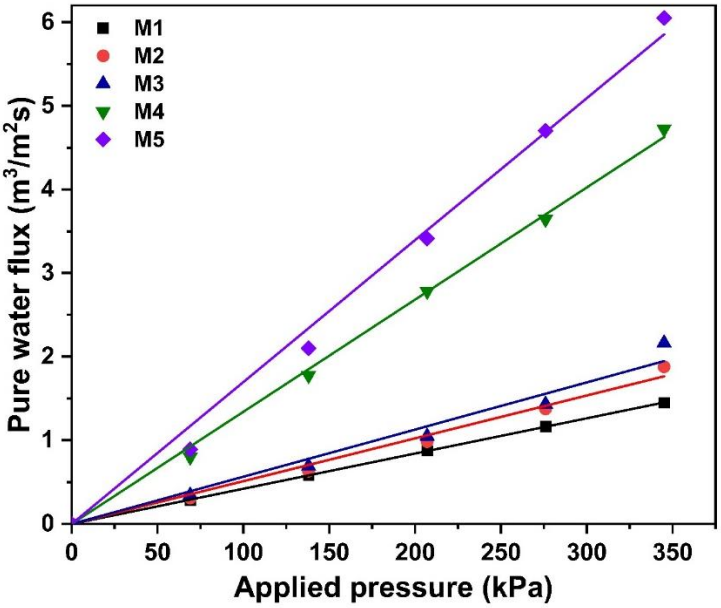

Fig. 2.19 Pure water flux as a function of applied pressure for membranes M1, M2, M3, M4, and M5.

Table 2.6 Summary of properties of fabricated tubular membranes

Membrane	Porosity (%)	Tortuosity	Pure water permeability ($m^3\ m^{-2}\ s^{-1}\ kPa^{-1}$)	Pore size (µm)	Chemical strength (% weight loss)		Mechanical strength (MPa)
					Acid	Base	
M1	25.91±1.32	1.92	4.2×10^{-8}	0.123	1.23 ± 0.57	0.32± 0.04	23.70 ± 2.30
M2	29.97±1.67	1.85	5.1×10^{-8}	0.132	3.24 ± 0.68	0.46 ± 0.15	21.82 ± 2.06
M3	33.64±1.25	1.77	5.6×10^{-8}	0.134	3.57± 0.92	0.86 ± 0.32	20.14 ± 2.32
M4	39.68±1.16	1.68	13.4×10^{-8}	0.179	4.83 ± 0.86	0.64 ± 0.50	18.45 ± 1.59
M5	46.92±0.78	1.58	17.1×10^{-8}	0.182	6.65 ± 0.18	1.12 ± 0.22	12.80± 1.86

2.5.3.8. Optimization of membrane composition

The results obtained from the characterization of all the membranes are summarized in Table 2.6. It is evident that the pore size of the membranes increases slightly with an increase in pore former concentration. Also, porosity followed an increasing trend from M1 to M5. However, membrane M1 performed better than other membranes in terms of mechanical strength and chemical strength. Though mechanical strength increases from M5 to M1, the decreasing porosity restricts the use of M1, M2, and M3 membranes. Membranes M1, M2, and M3 also have comparatively less water permeability when compared with M4 and M5. Hence M4 and M5 proved to be the best options for use in separation process. However, the low mechanical and chemical strength of M5, in contrast to M4, implied that the former could not be used in harsh environments and high pressures. So, with a good range of porosity, water permeability, and mechanical and chemical strength, M4 was chosen for the microfiltration of microalgae

2.5.4. Comparison of fabricated membranes with literature

Table 2.7 compares the characteristics of the membranes fabricated in this study with those of other kaolin-based membranes reported in the scientific literature. In one study, Hedfi et al. (2016) prepared tubular membranes using kaolin, Alumina, and lignite as the raw materials. The optimized membrane had a 0.7 µm and 36% pore size and porosity, respectively. Although the pore size and porosity were suitable for microfiltration applications, the sintering temperature was very high [23]. In another study, pore size, porosity, and sintering temperature were optimal, but the mechanical strength of the membrane was on the lower side [31]. In some instances, the porosity (23%) and mechanical strength (10 MPa) were also unsatisfactory, limiting their industrial application. As evident from Table 4, some of the studies have reported good mechanical strength but at a higher sintering temperature. Also, a large pore size of 4.58 µm was

reported by Jana et al. using kaolin and quartz as the primary raw material [154]. Other studies have used titania and alumina as the starting material, which adds to the production cost of the membrane [19,206] On the contrary, in the present study, kaolin-based low-cost tubular membrane fabricated at low sintering temperatures (950 °C) provided good porosity, low pore size, suitable mechanical strength, and water permeability. Also, tubular membranes have more filtration surface area than flat ones. Thus, it can be said that the low-cost kaolin membrane prepared in this study is comparable to or better than the other reported literature on membranes prepared with kaolin as the primary raw material.

Table 2.7 Comparison of various kaolin-based membranes reported in literature with the present study

Raw material Mixed with kaolin	Membrane configuration	Porosity (%)	Pore size (µm)	Sintering temperature (°C)	Mechanical strength (MPa)	Water permeability (L/m^2hbar)	References
Alumina, lignite	Tubular	36	0.7	1200	39	410	[23]
Quartz, ball clay, pyrophyllite feldspar, and calcium carbonate	Tubular	53	0.309	950	12	213.5	[31]
Quartz, sodium carbonate, calcium carbonate, and boric acid	Flat	42	4.58	1000	11.55	49.8	[154]
Quartz, titanium oxide, and calcium carbonate	Tubular	23	0.45	900	10	13.32	[156]
Alumina and aluminum hydroxide	Flat	46	1.3	1300-1550	-	-	[157]
Sodium carbonate, sodium metasilicate, boric acid, and calcium carbonate	Tubular	40	0.179	950	18.45	48.2	This study

2.5.5. Summary

Indigenous low-cost disc and tubular membranes were fabricated using kaolin as the key precursor. Since fabrication of tubular membrane require excess of main raw material, hence initially disc membranes were fabricated to optimize the binder concentration and simultaneously avoid excess usage of kaolin and binders. In case of disc membranes, by increasing the binder concentration from 8% to 20%, there was a notable decrease in percentage porosity, average pore size, and water permeability. As a result, the optimal binder percentage was identified as 8%, comprising 2% boric acid, 2% sodium metasilicate, and 4% sodium carbonate. Further, using this optimized binder concentration tubular membranes were fabricated. The fabricated tubular membranes had porosity of ~26% - 47%, a pore diameter of 0.123-0.182 µm, water permeability of 4.2×10^{-8} – 17.1×10^{-8} m^3 m^{-2} s^{-1} kPa^{-1}, along with good mechanical and chemical strength. Further, the optimized composition of tubular membrane shall be applied in the harvesting of microalgal culture.

Chapter 3

Application of kaolin-based membrane in microalgal harvesting

CHAPTER 3

Application of kaolin-based membrane in microalgal harvesting

This chapter explores the potential use of tubular membranes made from indigenous kaolin for the microalgal harvesting process. The optimized membrane was tested for microfiltration of microalgae Monoraphidium sp. KMC4 with 1.5 g L^{-1} of initial concentration at a persistent cross-flow rate (1.11 × 10^{-5} m^3 s^{-1}) and various transmembrane pressures (69 kPa - 345 kPa). Fouling mechanism was explained by fitting four distinct pore-blocking models.

Graphical abstract of Chapter 3

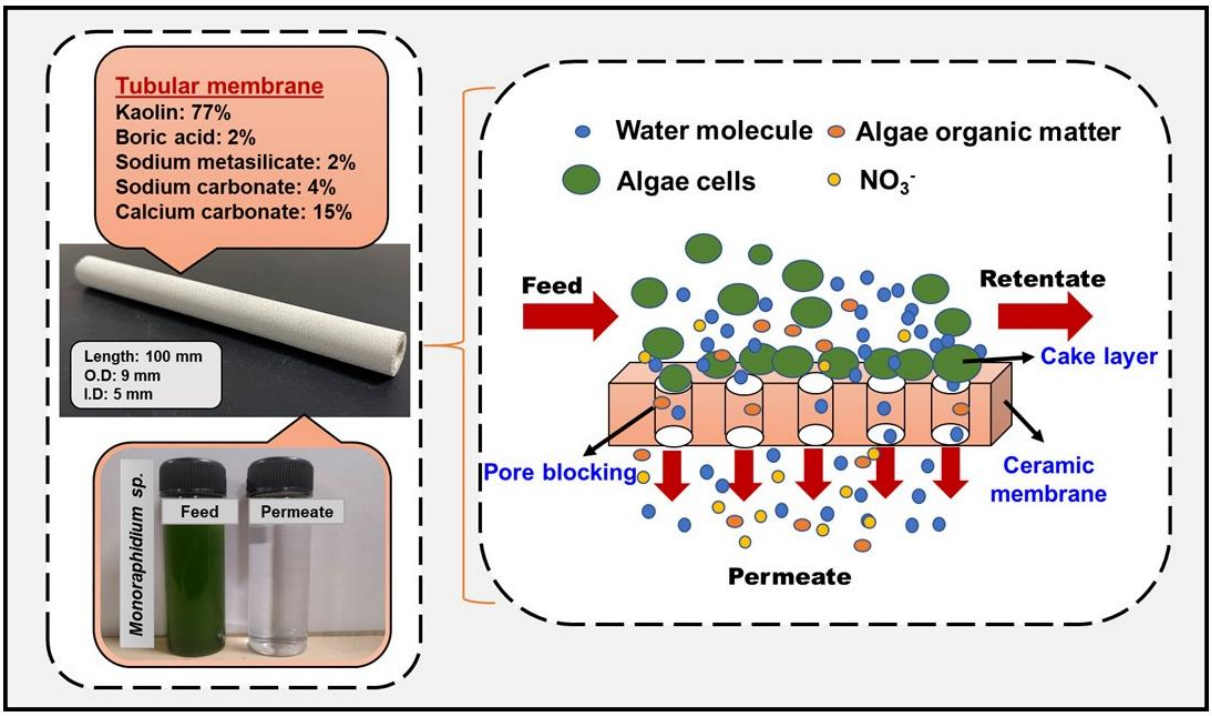

3.1. Chemicals

BG11 media and the reagents required for nitrate estimation was supplied by HiMedia Laboratories Pvt. Ltd. (India).

3.2. Microalgae Cultivation

The strain selected for this study was the previously isolated *Monoraphidium* sp. KMC4. This strain was cultivated in standard BG11 media [189]. The BG11 media is composed of 1.5 g L^{-1} sodium nitrate ($NaNO_3$), 0.04 g L^{-1} dipotassium phosphate (K_2HPO_4), 0.075 g L^{-1} magnesium sulphate ($MgSO_4.7H_2O$), 0.036 g L^{-1} calcium chloride ($CaCl_2.2H_2O$), 0.006 g L^{-1} citric acid, 0.006 g L^{-1} ferric ammonium citrate, 0.001 g L^{-1} EDTA (disodium salt), 0.02 g L^{-1} sodium carbonate (Na_2CO_3) and 1 ml L^{-1} of trace metals. The experiments were conducted using 1 L conical flasks containing 500 mL of growth media and a biomass concentration of 0.02 g L^{-1} at the start. In each trial, the medium was sterilised in an autoclave and cultured for a total of 13 days. The culture temperature was maintained at 25 ± 2 ºC while the pH was controlled at 7–8 by periodically supplying CO_2. For culture mixing, a constant airflow of 0.5 vvm was provided. The ratio of light (100 mol m^{-2} s^{-1}) to dark was maintained at 16 h: 08 h. Additionally, samples were taken each day to calculate growth rates. The growth was measured using a UV-spectrophotometer (Thermo Fisher Scientific, USA), taking culture's optical density (OD) at 680 nm. Eq. (3.1) shows the standard graph equation, which was obtained plotting OD at 680 nm versus the dry cell weigh (DCW).

$$B\ (g\ L^{-1}) = X \times 0.2495 \tag{3.1}$$

where *B* is the dry cell weight (g L^{-1}) and *X* is the OD taken at 680 nm.

The microalgae attained a maximum concentration of around 1.55 g L^{-1}. However, the culture was diluted to 1.5 g L^{-1} to maintain a constant feed concentration for all the microfiltration experiments. The cell size of the cells was studied by microscopic observation (Axio Scope.A1, Zeiss, US).

3.3. Microalgal Harvesting Using Microfiltration Membrane

All the microfiltration experiments were conducted at ~25 °C. The microalgal culture at the end of the 13th day was taken for harvesting using the microfiltration setup. The optimized membrane was inserted in the membrane module, and then the microalgal feed was passed to the inlet of the membrane module using a pump (Fig. 2.3, Chapter 2). The permeate was collected in a different beaker, and the retentate was recycled back to the feed tank. A continuous microfiltration study was done for 2.5 h at each pressure (69 kPa, 138 kPa, 207 kPa, 276 kPa and 345 kPa) and at a constant flow rate of 1.11×10^{-5} m^3 m^{-2} s^{-1}. After each run, the membrane was regenerated according to the protocol in section 3.4.

The membrane performance was assessed in terms of percentage cell recovery, volume reduction factor (VRF), and permeate recovery.

$$\text{Cell Recovery (\%)} = \frac{C_0 - C_p}{C_0} \times 100 \quad (3.2)$$

$$\text{VRF} = \frac{V_i}{V_f} \quad (3.3)$$

$$\text{Permeate recovery (\%)} = \frac{V_p}{V_i} \times 100 \quad (3.4)$$

where C_0 is the initial feed concentration (g L^{-1}), and C_p is the permeate concentration in g L^{-1}. V_i and V_f are the initial and final feed volumes, whereas V_p is the volume of permeate collected.

The primary nutrient i.e., nitrate (NO_3^-) concentration in the permeate stream, was estimated using APHA protocols [208].

Total Organic Carbon (TOC) was used to report the levels of organic matter in the permeate stream after being analyzed by a TOC analyzer (Model No: Aurora 1030 C; Make: M/s O.I. Analytical, USA).

3.4. Membrane Regeneration

Thorough cleaning and regeneration of the membrane followed each experimental run. Initially, the membrane underwent a cleaning process using deionized water for a duration of 30 min. Subsequently, it was subjected to washing with 1 g L^{-1} of surf excel solution for 1 h [31]. This was again followed by rinsing with deionized water to remove any residual detergent molecule present in the membrane. After the cleaning procedure, the membrane's water flux was measured to ensure no significant drop in flux due to partial plugging. The regenerated membranes had a water permeability within ± 2% of the original hydraulic permeability.

3.5. Pore blocking models for analysis of flux decline

Four fouling models, including (a) complete, (b) standard, (c) intermediate pore blocking, and (d) cake filtration model, were analyzed to determine the microfiltration flux decline profile of microalgal harvesting.

When the size of the microalgal cells exceeds the size of the membrane pores, complete pore blocking occurs. It blocks the surface of membrane but does not affect the membrane's interior pores (Eq. 3.5). In the standard pore-blocking model, the algae cell is smaller than the ceramic membrane's pore mouth, which promotes pore channel blocking (Eq. 3.6). When the membrane's particle and pore sizes are nearly equal, intermediate pore blocking predominates. According to this model, the particles are assumed to settle on one another and not significantly obstruct the membrane pores (Eq. 3.7). When the membrane's pore size exceeds the particle size, cake filtration occurs. Consequently, the particles accumulate on the membrane's surface, forming a cake (Eq. 3.8). The schematic of the pore blocking models is shown in Fig. 3.1.

$$\ln J^{-1} = \ln J_0^{-1} + k_b t \qquad (3.5)$$

$$J^{-0.5} = J_0^{-0.5} + k_s t \quad (3.6)$$

$$J^{-1} = J_0^{-1} + k_i t \quad (3.7)$$

$$J^{-2} = J_0^{-2} + k_c t \quad (3.8)$$

where J is the flux, J_0 is the y-intercept of flux, k is the slope, and t is the time, respectively.

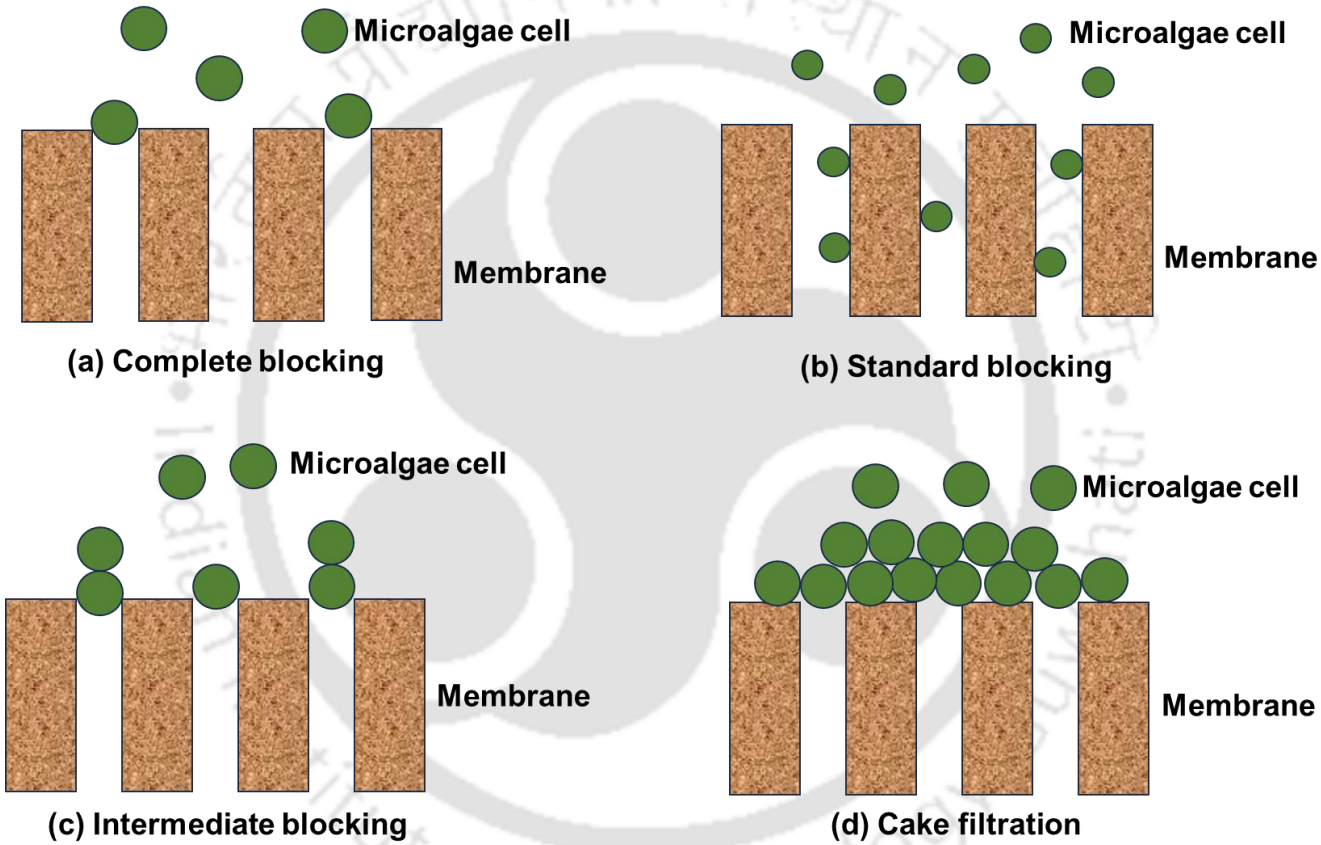

Fig. 3.1. Schematic diagram of pore blocking models

3.6. Growth and nutrient removal study of microalgae *Monoraphidium* sp. KMC4

The microscopic image of *Monoraphidium* sp. KMC4 is shown in Fig. 3.2. The image was taken on the 13th day of cultivation when the growth reached the maximum steady-state value. The microalgae was pear or cylindrical-shaped cells with a length of 6-8

µm and a width of 2-3 µm. The microalgal growth and nitrate removal curve is shown in Fig. 3.3. It was seen that the maximum growth reached 1.548 g L^{-1} with a corresponding nitrate removal of 88%. The residual nutrient in the culture medium was 131.28 mg L^{-1} of NO_3^-. The results observed here were in accordance with our earlier study for the growth of *Monoraphidium* sp. KMC4 [189,208].

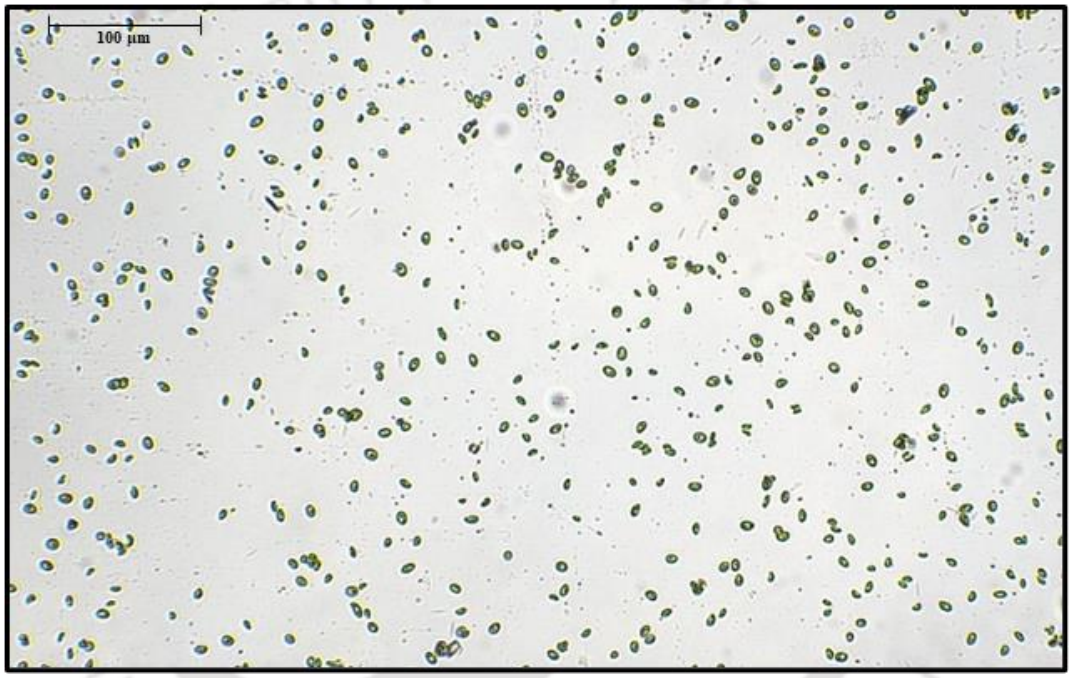

Fig. 3.2. Microscopic image of *Monoraphidium* sp. KMC4

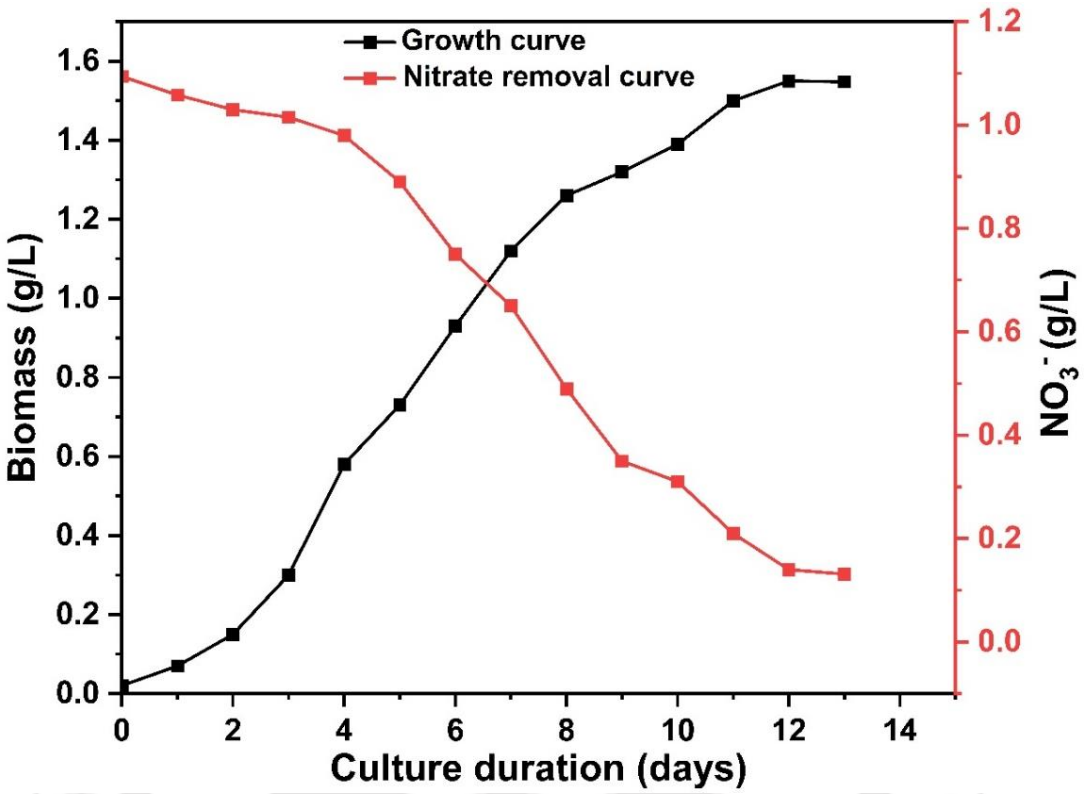

Fig. 3.3. Growth study and nutrient removal profile of *Monoraphdium* sp. KMC4 grown in BG11 media

3.7. Assessment of Membrane Performance in Microalgal Harvesting

The test results reported in Fig. 3.4 investigate the flux pattern of M4 membrane as a function of time for five different applied pressures and for an initial biomass concentration of 1.5 g L^{-1}. The volume reduction factor and final recovery of permeate after 150 min of experiment is shown in Fig. 3.5. The percentage recovery indicates the ratio of the extracted permeate to the initial feed volume. The initial phase (first 20-30 min) of the microfiltration experiment showed a rapid decrease in the permeate flux, but after that, the permeate flux remained relatively constant throughout the experiment. The decline in flux was because of the formation of microalgal cell cake layer during filtration, which eventually covered the entire membrane. This trend is coherent with other literature studies [85,87]. Permeate flux generally increased in tandem with applied pressure up to 276 kPa, but further increasing the pressure to 345 kPa yielded no noticeable improvement in

permeate flux. Also, maximum reduction in permeate flux was observed at higher pressures due to the rapid deposition of the microalgal cake layer. Hence, 276 kPa can be considered the optimum pressure, giving higher flux with less flux decline.

The VRF and the percentage recovery of permeate also increase with an increase in pressure attributed to the enhancement in driving force. The VRF after 2.5 h of microfiltration reached up to 1.38 for 276 kPa pressure. The corresponding permeate recovery was 28.17%. Also, in a recent study by Ricceri et al. (2022), it was observed that the microfiltration membrane of pore size 0.14 µm was able to harvest elongated-shaped *Spiriluna p*. microalgae with a permeate recovery of close to 30% [87]. The VRF/m^2 obtained in our study was 878, which was significantly higher than other polymeric membranes (25 VRF/m^2) [209] and also better than one of the recent articles on kaolin-based harvesting (635 VRF/m^2) of microalgae *Chlorella sorokiniana* [85].

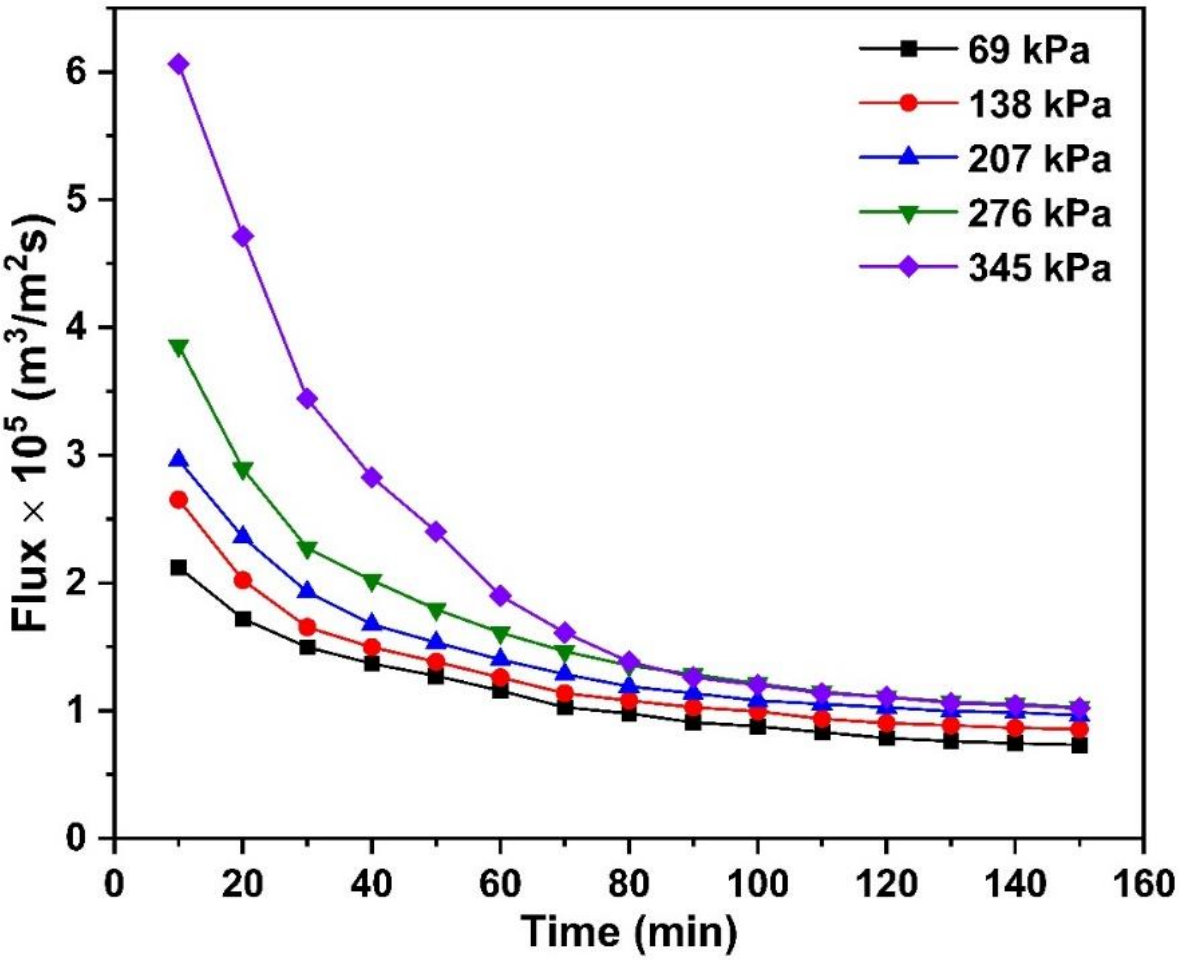

Fig. 3.4. Permeate flux observed for membrane M4 under different pressures as a function of time

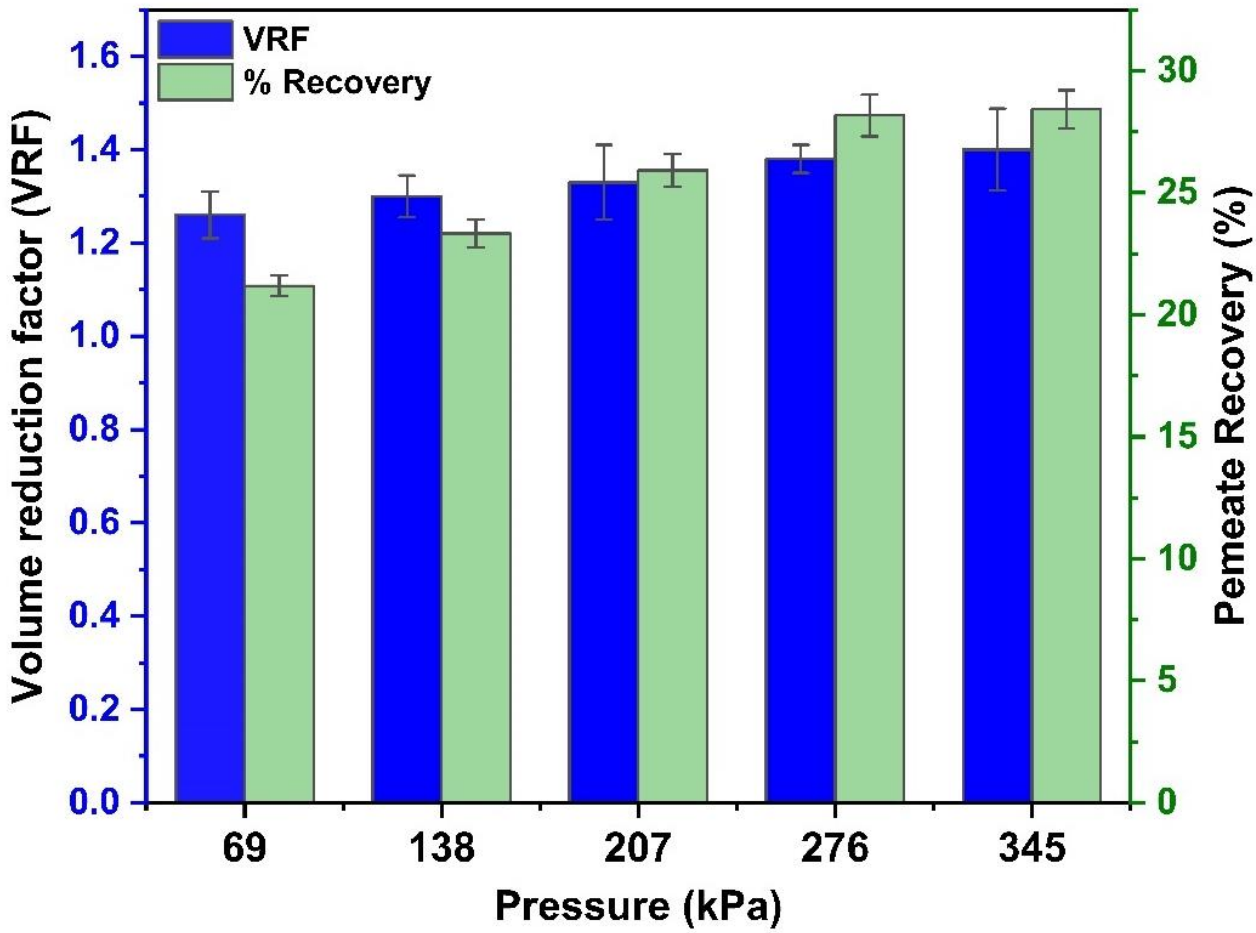

Fig 3.5. Separation performance of membrane M4 in terms of VRF and percentage recovery of permeate

3.8. Fouling Effects

The permeate flux decreased with time for the microfiltration of microalgae. Hence, it is essential to identify the effective mechanism underlying this decline. The decline was investigated using various pore-blocking models. Fig. 3.6 represents the fitness of four pore-blocking models for the optimized membrane M4 at an optimum pressure of 276 kPa. Parameters obtained from pore-blocking models for microalgal microfiltration are listed in Table 3.1. The findings show that the cake filtration model best matches the flux data of the M4 membrane. This is validated by analyzing the R^2 values of various pore-blocking models and comparing them. The cake filtration model offers the highest R^2 value of 0.99 compared to the other models. Similar results have been reported by Purnima et al. (2020),

who inferred that the microfiltration of microalgae followed the cake filtration mechanism when kaolin-based MF membrane was used [85]. Another recent study used a 0.1 µm flat sheet ceramic membrane to harvest microalgae *Chlorella* sp. and *Scenedesmus* sp. Their work also reported the formation of a cake layer that continued to develop with the filtration time [50].

The higher k values for the cake filtration model indicate that pore blockage occurred rapidly once the experiment was initiated. The elongated shape of *Monoraphidium* sp. might be responsible for the more rapid flux decline (Fig. 3.4) and the lower average flux value, which gives rise to a compact cake layer with algalogenic organic matter (AOM). Contrary to it, Ricceri et al. (2022) reported a smoother flux decline for spherical-shaped microalgae *Chlorella s*. and *Scenedesmus o.* [87]. Hence, it can be said that variations in cell shape and physical properties may influence the formation and characteristics of the cake layer, including its compactness and porosity, resulting in distinct filtration resistances.

Table 3.1 Summary of parameters associated with various pore blocking models for M4 membrane

Models	Membrane M4		
	Correlation coefficient (R^2)	Slope (k)	Initial permeate flux, J_0 (m/s)
Complete pore blocking	0.87	$k_b = 0.012\ s^{-1}$	4.80×10^{-5}
Standard pore blocking	0.92	$k_s = 0.013 \times 10^2\ s^{0.5}\ m^{-0.5}$	5.59×10^{-5}
Intermediate pore blocking	0.96	$k_i = 0.050 \times 10^4\ m^{-1}$	3.49×10^{-5}
Cake filtration	0.99	$k_c = 0.066 \times 10^9\ s\ m^{-2}$	$9.28\ 10^{-5}$

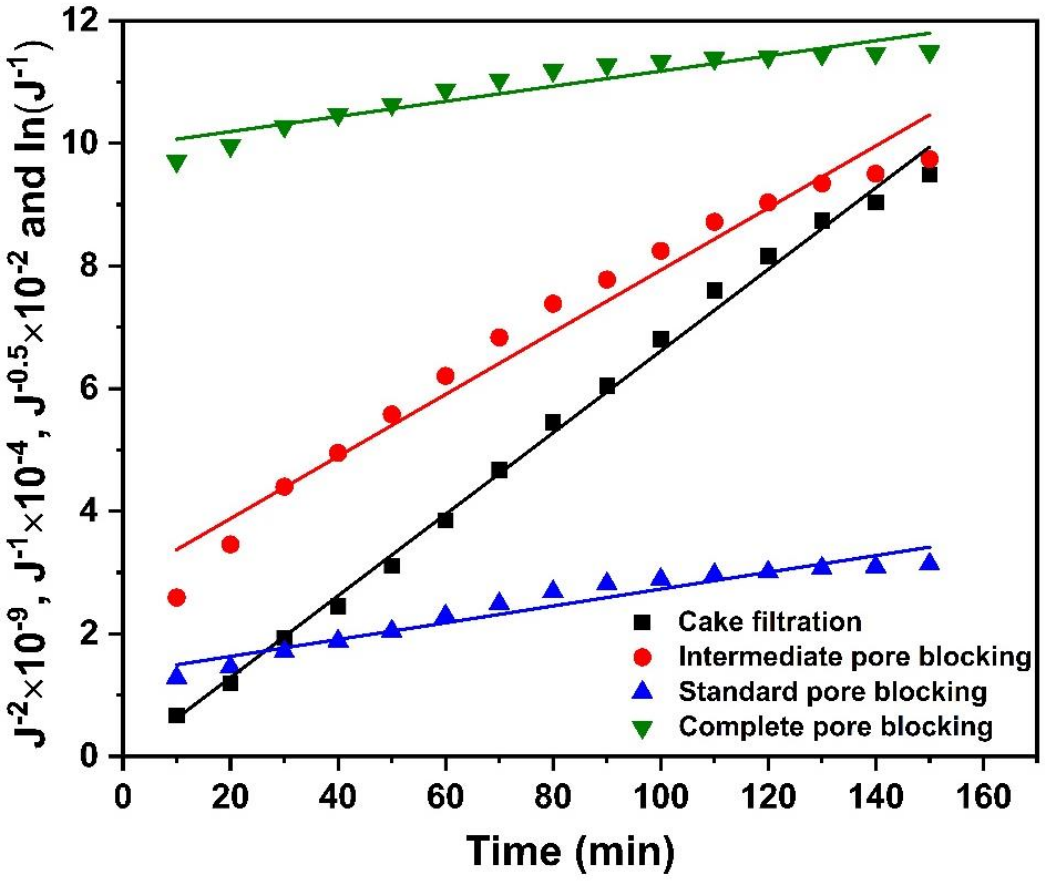

Fig. 3.6. Flux functions vs. time plot for four pore blocking models

(Applied pressure: 276 kPa)

Fig. 3.7 depicts the morphology of inner, outer and the cross section of the fouled membrane. It is apparent that the membrane's inner surface shows the development of algal cake layer. In contrast, there is absence of algae from the membrane's outer surface, further confirming the complete retrieval of algae by the fabricated tubular kaolin membrane.

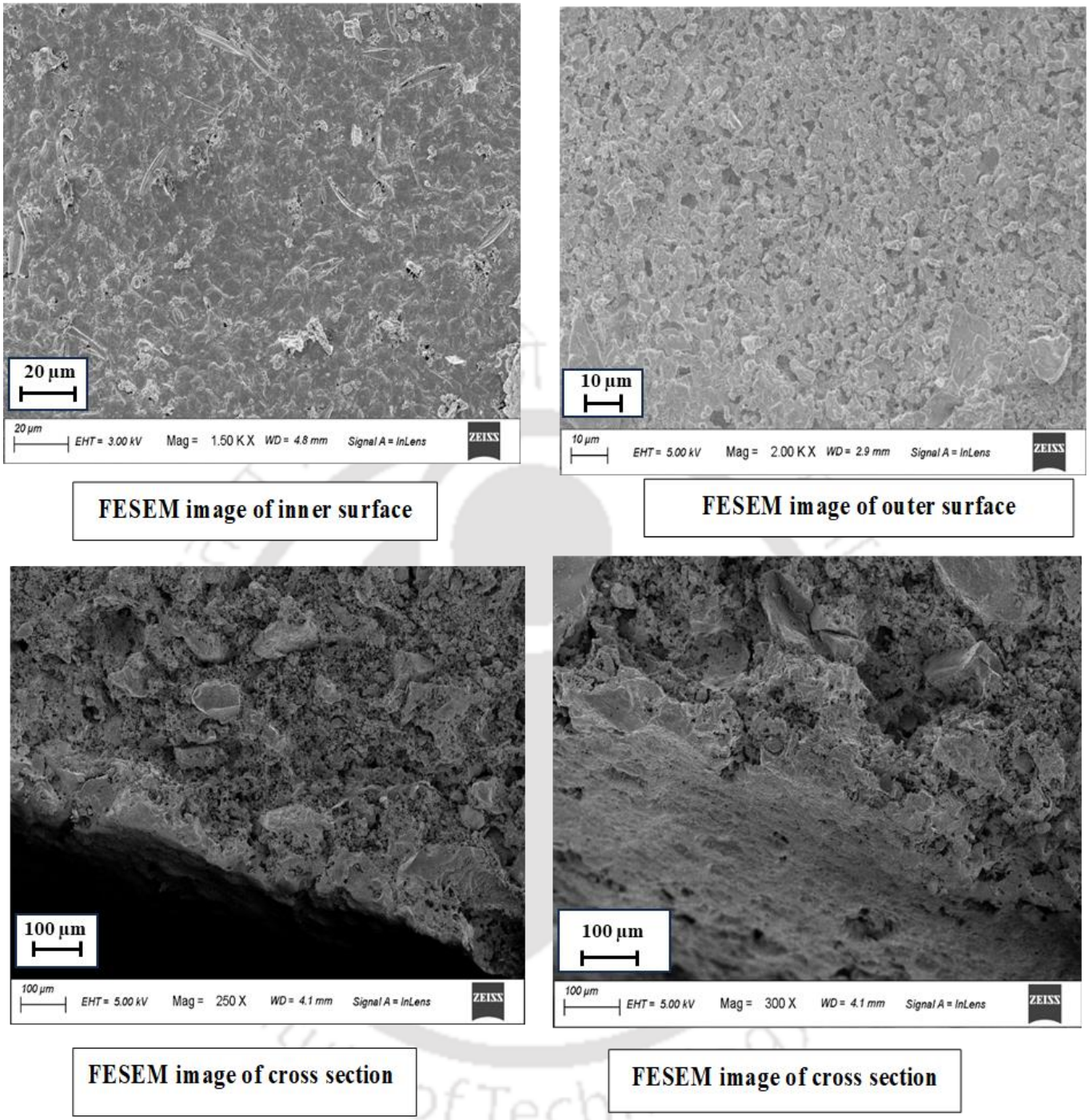

Fig. 3.7. Morphology of inner, outer and cross-section of fouled membrane

3.9. Separation of Algal cells, Nutrients, and Organic Matter

Ideally, the filtration process should retain algal cells and algalogenic organic matter (AOM) while nutrients should be found in the permeate for reuse [87,210]. Fig. 3.8 indicates the concentration of NO_3^-, total organic carbon (TOC) in the permeate stream and the percentage recovery of algal cells at different applied pressures. The cell recovery was 100% at all applied pressures for membrane M4. Fig. 3.9 also indicates that the permeate stream was completely free of microalgal biomass.

It is to be noted the initial nitrate concentration in the feed was 131.28 mg L^{-1}. Data in the Fig. 3.8 suggests that a fraction of NO_3^- was rejected while a major portion passed the membrane unchanged. This was because nitrates are significantly smaller than the membrane's pore size. Also, a slight decrease in concentration was mainly due to the interactions with the cake layer. Other researchers also saw a similar pattern [87] , where the NO_3^- in the permeate stream reached 88-93% of the feed stream. A high passage of nutrients through the membrane indicates a reduced need for salt reintegration before any subsequent cultivation process, which positively impacts the process's economics and sustainability. Thus, the effect of membrane filtration on the reintegration of nutrients and ions was minimal.

To gain a better understanding of membrane fouling and also to evaluate the potential of reusability of permeate stream in further cultivation process, the AOM was evaluated in terms of TOC of the permeate (in mg/L). During the growth phase, microalgal cells release organic matter into the environment. Once the culture reaches the stationary phase, the level of organic matter increases as the cells lyse and release their contents [211]. From Fig. 3.8, it is clear the permeate stream consisted of a subsequent amount of organic compounds at all pressures within a range of 31.6-63.2 mg L^{-1}. TOC continued to increase as the applied pressure was increased from 69 kPa to 345 kPa. The increase in TOC concentration may be

attributed to the enhanced cell breakdown at higher pressures as well as the cake-enhanced polarization effects [85,87]. Though these results were obtained for the specific test involving *Monarphidium sp.* KMC4 and 0.179 µm pore size membrane, they provide insight for further research on the quality of permeate after microfiltration and their potential in further reusability.

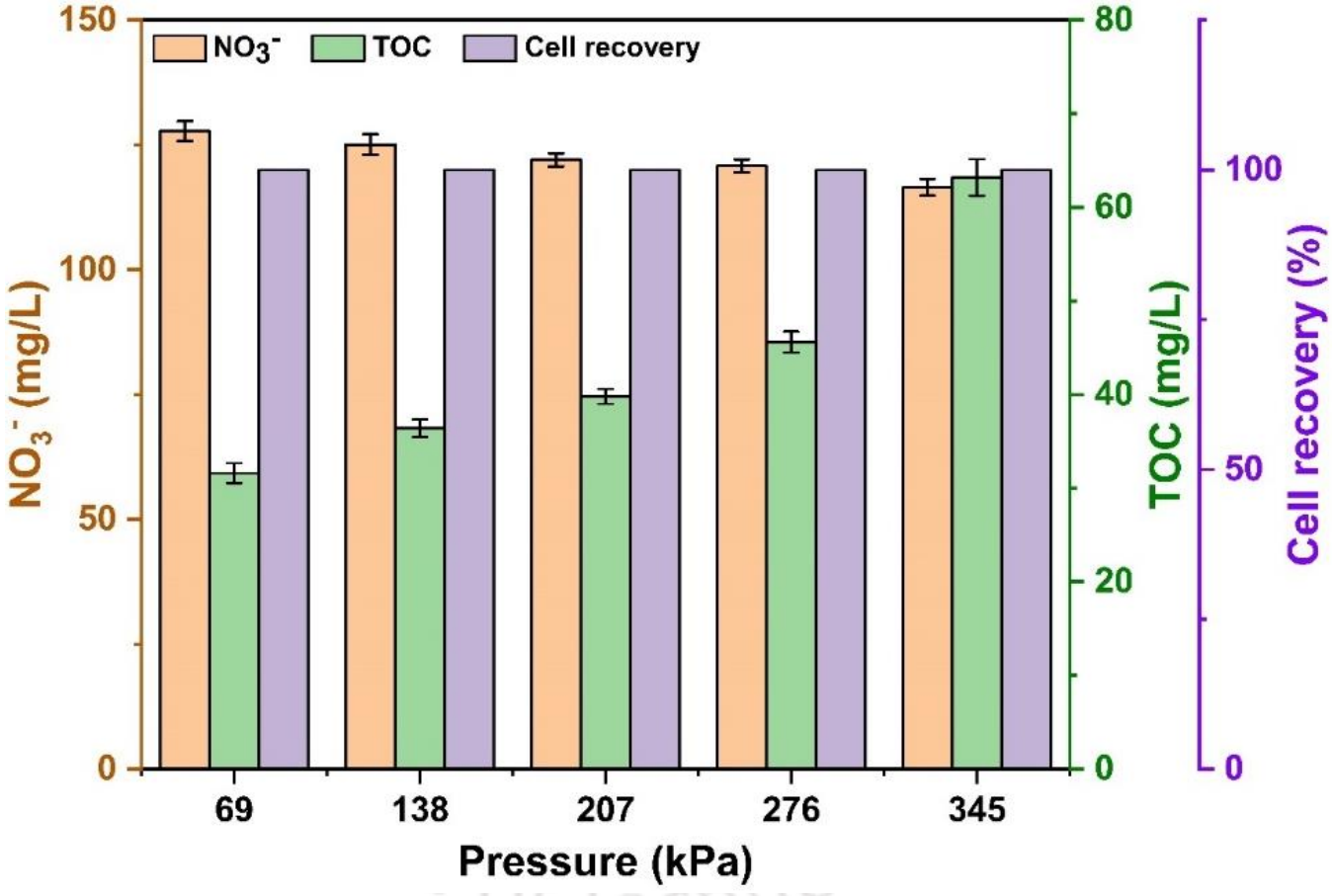

Fig. 3.8. TOC and NO_3^- concentration of M4 permeate at different transmembrane pressures

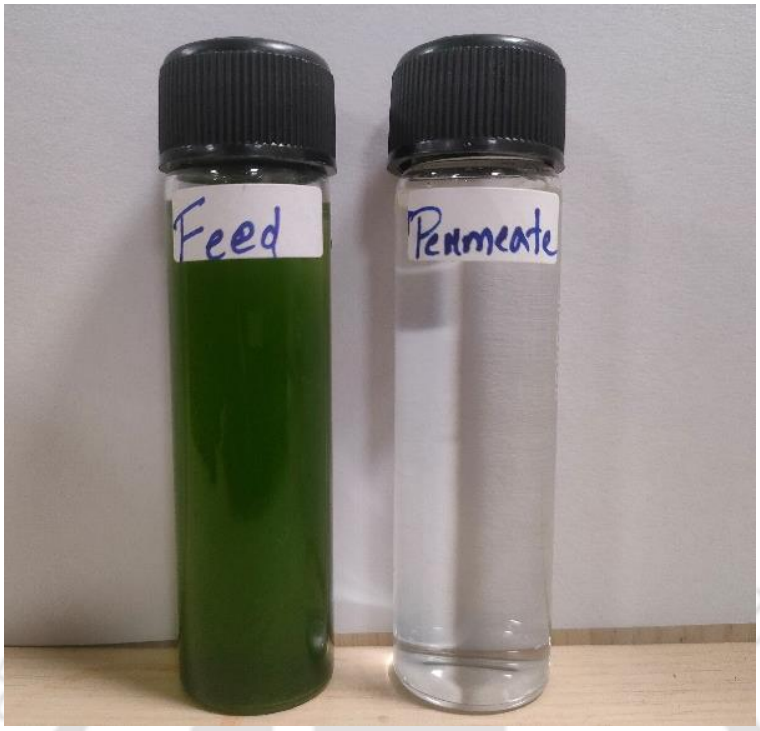

Fig. 3.9. Image of feed and permeate

3.10. Comparison of the Present Study with Prior Literatures

From the application point of view, microalgal harvesting in this study was carried out in a cross-flow system using ceramic membrane. Compared to ceramic membranes, extensive literature is available on the microfiltration of microalgal biomass by polymeric membranes. As seen from Table 5, VRF/m^2 value obtained in this study is significantly higher than other membranes reported earlier. Even though the initial biomass concentration in the present study was higher compared to other reported literature, the average flux was significantly higher. This again proves the potential of the fabricated tubular membrane. Additionally, the separation obtained by Chen et al. [212] and Susanto et al. [101] was lower than that obtained in this study. Compared to polymeric membranes, the current low-cost tubular kaolin-based membranes have superior thermal, chemical, and mechanical properties. The comparison results also show that the prepared ceramic

membrane is superior to polymeric membranes for recovering algae from the culture medium

Table 3.2. Comparison of membrane performance with the existing literature

Membrane		Operating parameters	Microalgae		Performance				Ref.
Material	Pore size		Species	Initial concentration	Average Flux	Recovery	VRF	VRF/m^2	
Polyether sulphone (PES)	0.8 µm	TMP: 20 kPa	*Chlamydomonas sp.*	2.96 × 10^{10} cells/mL	-	91.1%	-	-	[101]
Polyvinylidene fluoride (PVDF)	0.2 µm	TMP: 50 kPa CFV: 4 m/s	*Scenedesmus sp.*	0.305 g/L	-	90%	10	25	[212]
Polyvinylidene fluoride (PVDF)	0.2 µm	TMP: 45 kPa CFV: 0.35-1.57 m/s	*Chlorella Vulgaris*	0.5 g/L	0.33 m^3/m^2s	100%	4.8	347.8	[38]
Kaolin	0.178 µm	TMP: 276 kPa CFV: 0.0065 m/s	*Chlorella sorokiniana*	0.5 g/L	0.94 m^3/m^2s	100%	1.08	635	[85]
Kaolin	0.179 µm	TMP: 276 kPa CFV: 0.007 m/s	*Monoraphidium sp.*	1.5 g/L	1.61 m^3/m^2s	100%	1.38	878	This study

3.10. Summary

The optimized membrane (77% kaolin, 2% boric acid, 2% sodium metasilicate, 4% sodium carbonate, and 15% calcium carbonate) was tested for microfiltration of microalgae *Monoraphidium* sp. KMC4 with 1.5 g L^{-1} of initial concentration at a persistent cross-flow rate (1.11 × 10^{-5} m^3 s^{-1}) and various transmembrane pressures (69 kPa - 345 kPa). The separation results yielded an average permeate flux of 1.85×10^{-5} m^3 m^{-2} s^{-1} at an optimized transmembrane pressure of 276 kPa. The corresponding volume reduction factor and

permeate recovery were 1.38 and 28.17%, respectively. Complete algal cell recovery and substantial nutrient passage (>88%) were observed within the pressure range of 69 kPa to 345 kPa. Fouling mechanism was explained by fitting four distinct pore-blocking models, of which the cake filtration model provided the most accurate fit as compared to the complete, intermediate and standard pore-blocking models. Additionally, the total organic carbon varied in the range of 31.6-63.2 mg L^{-1}. This essentially explained the source of pore blocking. The elongated shape of *Monoraphidium sp.* KMC4 might have contributed to the enhanced fouling of membrane. Lastly, the nitrate passage was almost complete (~88% - 97%), highlighting the prospects of permeate stream in further cultivation process, which will be discussed in detail in the following chapter.

Chapter 4

Energy efficient recycle of harvested microalgal effluent

CHAPTER 4

Energy efficient recycle of harvested microalgal effluent

This chapter discusses the suitability of cultivating Monoraphidium sp. KMC4 in the media obtained after harvesting using kaolin based tubular ceramic membrane. The principal target here is to reduce the concentration of total organic carbon (TOC) from the harvested effluent stream so that it can be used for energy efficient recycle. In this regard, powdered activated carbon (PAC) with a loading of 5-50 mg L^{-1} was employed to aid in the recyclability of the effluent based culture (EBC) media.

Graphical abstract of Chapter 4

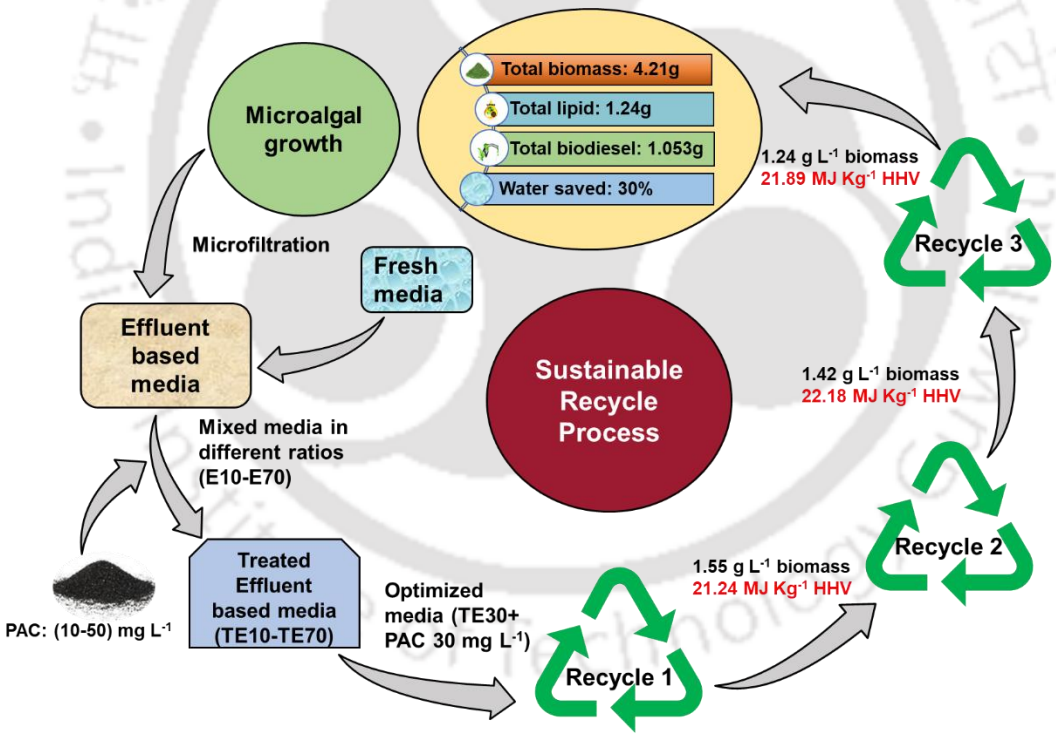

4.1. Microalgal Strain and Culture Media

Previously isolated *Monoraphidium* sp. KMC4 was selected as the potential strain based on its superior biomass and lipid yield [208]. Recycling experiments were performed using KMC4 in a standard BG11 media, which were prepared in Milli-Q water.

4.2. Experimental design

The experiments were performed in 500 mL conical flasks filled with 250 mL of growth media with an initial biomass concentration of 0.02 g L^{-1}. In all the experiments, media was autoclaved and cultured for 13 days. The temperature of the culture was maintained at 25 ± 2 °C and the pH at 7-8 by supplying CO_2 at regular intervals. Continuous air flow of 0.5 vvm was supplied for culture mixing. The light (100 µmol m^{-2} s^{-1}) - dark ratio was kept as 16 h: 08 h. Furthermore, samples were collected each day for the estimation of growth and nutrient consumption rates.

The experimental design is demonstrated in Fig. 4.1. Initially, KMC4 was grown in standard BG11 media and the culture was harvested using kaolin-based membrane after attaining the stationary phase. The biomass feedstock and supernatant (also named Effluent based culture (EBC) media) were stored for further experiments. The EBC media and fresh BG11 were mixed in different volumetric ratios of 10:90, 20:80, 30:70 , 40:60, 50:50, 60:40, and 70:30. The prepared mixture was used to perform two different sets of experiments (a) without any treatment named as E10, E20, E30, E40, E50, E60, and E70; (b) treatment with 10 mg L^{-1} powdered activated carbon (PAC) for 6 h was termed as TE10, TE20, TE30, TE40, TE50, TE60, and TE70. The PAC dose was decided in accordance with the available literature [178,185]. Additionally, the mixture was replenished with nitrates, and phosphates to maintain a concentration equimolar to the control BG11.

Further, the TE30 mixture was treated with six different concentrations of PAC such as 5, 10, 20, 30, 40, and 50 mg L^{-1} respectively. The results obtained from these experiments provided the optimum culture conditions: TE30 with PAC concentration of 30 mg L^{-1}.

The optimum conditions obtained from the above study were further used to perform five recycle experiments (R1, R2, R3, R4, and R5) to see the reusability of the supernatant

(EBC media) and the PAC. Moreover, the PAC that was used in the first recycle was washed and reused for the subsequent cycles.

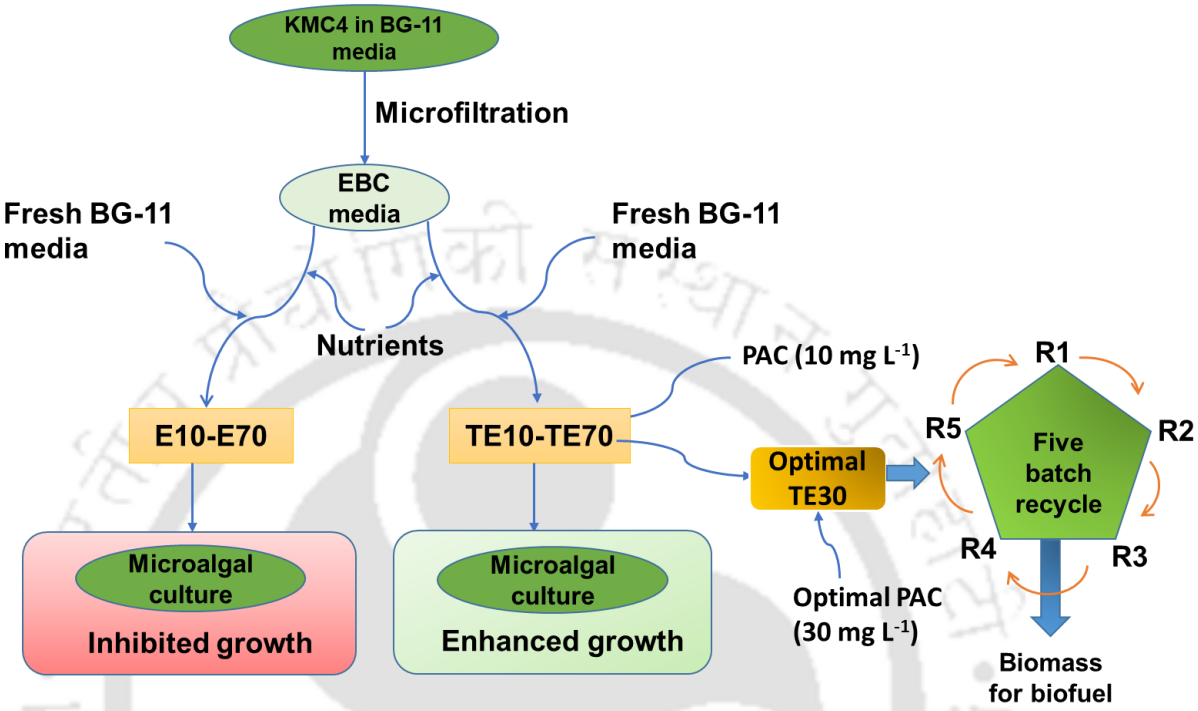

Fig. 4.1. Experimental design of batch recycle study

4.3. Analytical Methods

4.3.1. Growth study

Growth estimation was analyzed using the spectrophotometric method. Culture samples were taken on each day and optical density (OD) was determined at a wavelength of 680 nm using UV-Vis Spectrophotometer (Thermo Fisher Scientific, USA). The cultures were centrifuged (Harmle Z300, Hettich, Germany) at 6000 rpm for 15 min and then oven-dried at 80 °C to obtain the dry cell weight (DCW). Eq. 4.1 shows the standard graph equation, which was obtained plotting OD at 680 nm versus the DCW.

$$B\ (g\ L^{-1}) = X \times 0.2495 \quad (4.1)$$

where *B* is the dry cell weight (g L^{-1}) and *X* is the OD taken at 680 nm.

4.3.2. Nutrient removal study

Nitrates and phosphates as key nutrients in the growth media (BG11 and EBC) were estimated by APHA protocols (APHA, 1998). The nutrient removal efficiency was calculated by using the following equation.

$$RE(\%) = \frac{C_f - C_i}{C_f} \times 100 \quad (4.2)$$

where C_f and C_i are the final and initial nutrient concentrations respectively.

4.3.3. Lipid extraction and quantification

The lipids present in dry microalgal biomass were extracted in a Soxhlet apparatus. During this, methanol and n-hexane were used as an extracting solvent. The quantification was done as reported earlier [213].

4.3.4. Characterization of EBC media

The concentrations of the organics in the EBC media was reported as Total Organic Carbon (TOC), measured using TOC analyzer (Model No: Aurora 1030 C; Make: M/s O.I. Analytical, USA).

4.3.5. Characterization of biomass

4.3.5.1. Physico-chemical characterization of biomass

Proximate analysis of the biomass was done following ASTM standards (E-871, D1102-84). The moisture content of the biomass was analyzed by placing 1.0 g of sample in a hot-air oven at 105 ºC for 1 h. The weight difference was noted to be moisture content. Further, the volatile content was estimated by taking 1.0 g of sample was placed in a muffle furnace at 925 ± 10 ºC for 7 mins. Additionally, biomass was analyzed for ash content by placing 1.0 g in a crucible in a muffle furnace at 575 ± 10 ºC for 4 h. Finally, the fixed carbon content of the biomass was obtained by noting the mass of the residue [214].

$$Fixed\ carbon\ (\%) = 100 - \%\ of\ [Moisture\ content + volatile\ matter + Ash\ content] \quad (4.3)$$

The ultimate (CHNS) analysis of the biomass samples was done in a CHNS Elemental Analyzer (Flash EA 1112 series, Thermo Finnigan, Italy). The difference determines the oxygen content of sample.

4.3.5.2. Thermal decomposition behaviour of biomass

The thermal stability of the biomass sample was determined by the weight loss of the sample with an increase in temperature in a Thermogravimetric analyzer (Model: TGA 4000, Perkin Elmer). Dry biomass of 8-10 mg was loaded in a ceramic crucible and heated from room temperature to 900 °C at a heating rate of 20 °C min^{-1}.

4.3.5.3. FTIR analysis

The functional group present in biomass was investigated using an FTIR spectrometer (Perkin Elmer Spectrum 2 FTIR). The wavenumber range was considered to be 400 cm^{-1} - 4000 cm^{-1}.

4.3.5.4. Transesterification and FAME quantification

Acid-base transesterification reaction consisting of basically two steps, was used to obtain fatty acid methyl esters (FAME). 250 mg of extracted neutral lipid was placed in a 25 mL round bottom flask and methanol was added in a molar ratio of 1:20 (lipid: methanol). The preliminary reaction was done with the acid catalyst H_2SO_4 (1.5 wt % of lipid) whereas in secondary reaction, NaOH of the same concentration was used as the base catalyst. For both the reactions, the reaction time was 3 h and the temperature was maintained at 70 ± 2 °C. After each reaction, FAME was separated from the product using hexane and washed with distilled water to separate glycerol and catalyst. Further, FAME conversion was calculated by the previously prescribed protocol [213].

4.4. Results and Discussions

4.4.1. Microalgal culture in Effluent based culture (EBC) media

4.4.1.1. Growth study

The initial experiment done using EBC media (E10-E70), along with BG11 as control, showed that the biomass yield obtained from E10 (1.51 g L^{-1}) was found comparable to control BG11 (1.55 g L^{-1}). However, increasing the volumetric ratio of harvested media in microalgal culture (E20 to E70) had significantly decreased the biomass yield to 0.68 g L^{-1} (Fig. 4.2 a.). Accordingly, the biomass productivity was also reduced from 0.12 g L^{-1} d^{-1} (BG11) to 0.05 g L^{-1} d^{-1} (E70). Superior biomass productivity for E10 can be attributed to the maximum amount of fresh BG11 media present in it as compared to other EBC media. A decreasing trend in biomass yield with increasing effluent media concentration was found comparable to previous reports. A recent study reported a decrease of 14.3% in final dry weight for the cultivation of *Scenedesmus acuminatus* in reused media of modified BG11 with an initial $NaNO_3$ concentration of 187 mg L^{-1} [180]. An 18.2% reduction in maximum biomass concentration was observed for the first recycle of *Chlorella* sp. SDEC-18 in BG 11 media by Yu et al. [171].

From the results obtained and compared with the previous literature, it is recommended to reduce freshwater dependency and maximize recyclability of EBC media by the selection of higher effluent loading. In this context, PAC-mediated treatment of EBC was performed to enhance recyclability followed by simultaneously enhancing the biomass yield.

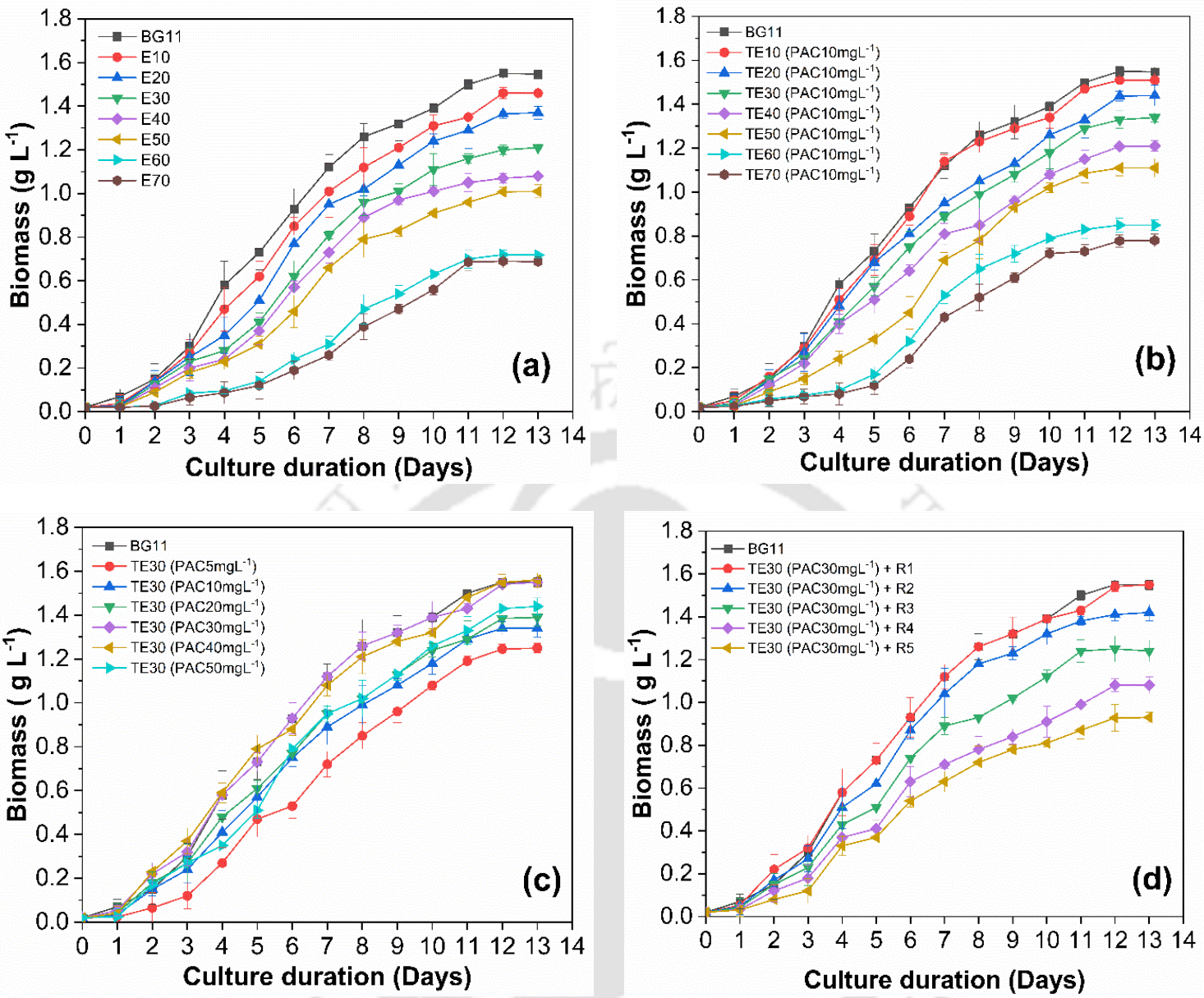

Fig. 4.2. KMC4 growth profile in untreated and treated EBC media (a) Growth in E10-E70 without PAC treatment, (b) Effect of 10 mg L^{-1} PAC on EBC media (E10-E70), (c) Effect of different PAC concentrations (5 mg L^{-1} to 50 mg L^{-1}) on optimal treated EBC media (TE30), (d) Batch recycle study (R1-R5) of treated EBC media (TE30).

4.4.1.2. Nutrient removal profile

To achieve optimal biomass yield, initial nitrate and phosphate concentrations in the growth media were maintained equimolar to the control BG11. From the nitrate removal profile (Fig. 4.3a), it was observed that the maximum removal of 88.4% was achieved from

E10 at a rate of 74.4 mg L^{-1} d^{-1} and it was gradually reduced to 83.6% (70.35 mg L^{-1} d^{-1}) in E30. However, on further increasing the effluent concentrations in EBC media from E40 to E70, a significant reduction in nitrate removal was observed (74.04% to 51%). A decreasing trend in nitrate removal was seen that correlates with the decreasing biomass yield in EBC media (E10-E70).

In contrast to nitrate, low phosphate content (21.8 mg L^{-1}) in all EBC media resulted in its near-complete removal (4.3 mg L^{-1} d^{-1}- 5.4 mg L^{-1} d^{-1}). A low rate of removal (4.3 mg L^{-1} d^{-1}) was due to a decrease in KMC4 growth (0.053 g L^{-1} d^{-1}- 0.051 g L^{-1} d^{-1}) at higher effluent concentrations (E60-E70) (Fig. 4.3b). In a recent report, Hwang et al. in 2017 performed microalgal growth of *Synechocystis sp*. PCC 6803 in different concentrations of effluent media (0-100%), which had an initial phosphate concentration of 23.9-25.1 mg L^{-1}. The study reported more than 95% of phosphate removal for all the effluent media concentrations that was comparable to present study. On the other hand, the nitrate consumption was low (37%-68%), resulting in a decreased biomass yield in the range of 0.55 g L^{-1} - 0.61 g L^{-1} for the effluent concentrations of 0-100%, respectively [183]. In contrast, our study showed a better nitrate removal profile for the EBC media (51%-88%), which enhanced the biomass yield (0.68 g L^{-1} – 1.51 g L^{-1}) for E70-E10 effluent loading.

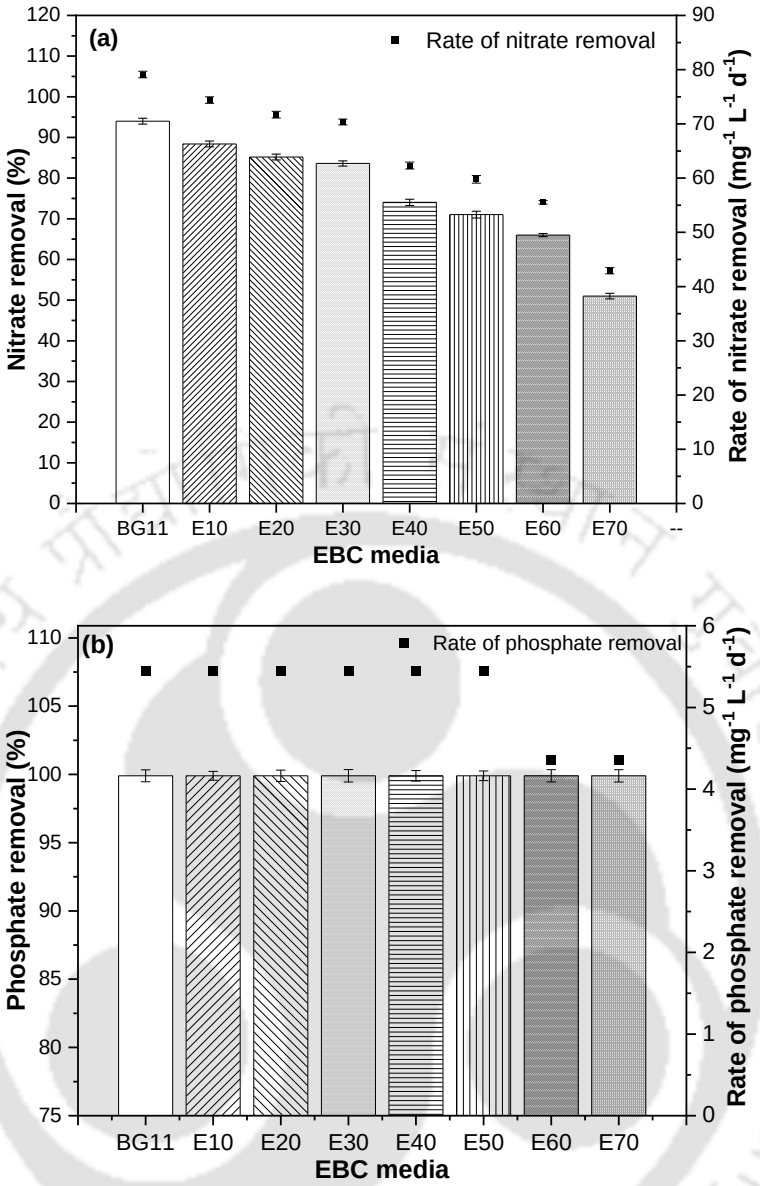

Fig. 4.3. (a) Nitrate and (b) Phosphate consumption profile of KMC4 in different EBC media (E10-E70)

4.4.2. PAC on enhancing KMC4 growth in EBC media

4.4.2.1. Effect of 10 mg L^{-1} PAC

To enhance the growth, EBC media (E10-E70) was treated with 10 mg L^{-1} powdered activated carbon (PAC). The growth profile in Fig. 4.2 (b) followed a trend similar to untreated EBC media (Fig. 4.2a), but the biomass yield for all the EBC loading was enhanced by PAC treatment. The study showed that lower effluent loading (TE10-TE30)

resulted in superior biomass yield, which was consistently reduced with an increase in effluent loading (TE40-TE70). The maximum biomass yield of 1.51 g L^{-1} was obtained from TE10 whereas the lowest (0.78 g L^{-1}) was obtained from TE70. A consistent decrease in biomass yield with increase in effluent loading was in accordance with the literature available [215,216].

The selection of optimum EBC treated media to obtain a higher biomass yield comparable to BG11 media while utilizing minimum water content, is considered to be an important criterion. In the present study, TE10-TE30 had better growth profile compared to TE40-TE70. Further, with regard to simultaneous reduction in water footprint and achieving maximum biomass yield, TE30 was considered as an optimal volumetric ratio of EBC media. The study had shown a 10.74% enhancement in biomass yield (1.34 g L^{-1}) compared to the untreated one (E30). However, the enhanced biomass obtained with 10 mg L^{-1} PAC was found 13.5% less than the control BG11. Hence, it was concluded that there is a potential to further enhance the biomass yield with effect to optimizing PAC loading. In this context, different concentrations of PAC was further optimized along with E30 as optimal EBC media.

4.4.2.2. Effect of different concentrations of PAC on the optimized EBC

The E30 mixture was treated with 5 mg L^{-1} - 50 mg L^{-1} of PAC, and the obtained KMC4 growth profile is depicted in Fig. 4.2c. The study indicated that increase in PAC loading had significantly enhanced the biomass yield (1.25 g L^{-1}- 1.56 g L^{-1}), which was achieved as a consequence of minimal incubation period (1-2 days) of KMC4 in lag phase. Among all, 5 to 40 mg L^{-1} of PAC had shown maximum specific growth rate (0.14 d^{-1}-0.16 d^{-1}) followed by superior biomass productivity (94.6 mg L^{-1} d^{-1}-118.5 mg L^{-1} d^{-1}). But, 30 mg L^{-1} and 40 mg L^{-1} of PAC had shown comparable biomass yield of 1.55 g L^{-1} and 1.56 g L^{-1}, which was 13.5% and 21.9% superior to the TE30 (10 mg L^{-1} PAC) and E30 (without

PAC), respectively. Conversely, further increasing the PAC loading to 50 mg L^{-1} had resulted in a 7.7% reduced biomass yield (1.44 g L^{-1}). The PAC study had shown positive results on enhancing biomass yield, which was in agreement with the previous reported literature [185,217]. In a recent study on the enhancement of biomass growth it was suggested that treatment with PAC resulted in an increase of 12.5% using 5 g L^{-1} PAC loading [217]. Whereas, in the current study, the treatment with PAC enhanced the biomass growth by 21.9% when using only 30 mg L^{-1} PAC (TE30). In order to make the process sustainable, use of low PAC loading to achieve maximum biomass is important. Also, at higher PAC loading, accumulation of particles takes place resulting in lesser exposure to active sites for adsorption of organic matter [178]. The negative effect of higher PAC loading on biomass yield was also reported previously [185]. In this context, 30 mg L^{-1} PAC treated E30 EBC media was found optimum, which was further chosen for recycle batch experiments.

4.4.2.3. Batch recycle study (R1-R5) of treated EBC media (TE30)

To reduce freshwater dependency, recycling potential of EBC media was studied by culturing KMC4 in five recycle batches along with BG11 as the control. During this, E30 (30% EBC media, 70% BG11 media) was considered as growth media, to which 30 mg L^{-1} PAC was supplemented to enhance the recycle efficiency. The biomass concentration for the first recycle was found maximum (1.55 g L^{-1}) with an average productivity of 117.6 mg L^{-1} d^{-1} that was comparable to the control (Fig. 4.2d). However, a consistent decrease in KMC4 growth was recorded with each recycle leading to the lowest biomass yield of 0.93 g L^{-1} (70 mg L^{-1} d^{-1}) for the fifth batch. In a recent study Yu et al. (2018) reported a similar observation where *Scenedesmus* SDEC-8 had shown reduced biomass growth profile with subsequent increase in recycle batches [171]. In another study, 68% (Table 4.3) decreased biomass yield was found while growing *Arthrospira platensis* in recycle

effluent [187]. However, in context to the present study, up to third recycle, KMC4 had shown comparatively superior biomass yield that signifies 30 mg L^{-1} of PAC was found sufficient to retain an optimal KMC4 growth in E30 mixture. The declined biomass growth in subsequent cycles was due to an increase in cell debris and residual nutrients in the media [218]. Moreover, reutilization of the PAC in the recycle experiments reduces the adsorption efficiency of the material resulting in a decrease in biomass growth. For which further studies need to be done on enhancing adsorption efficiency of PAC.

4.4.2.4. Nutrient removal profile

A periodic study of nutrient removal rate was done to correlate the effect of nutrient consumption rate on the biomass yield. From Fig. 4.4a it is evident that significant nitrate removal (92 %) was achieved from TE10 (77.42 mg L^{-1} d^{-1}) that produced the maximum biomass during 10 mg L^{-1} PAC treated EBC media. However, for TE10-TE50, within four days of culture the phosphate consumption reached 99.9% at 5.44 mg L^{-1} d^{-1} (Fig. 4.5a). In accordance to decreased biomass yield from TE10-TE70, the nitrate removal rate also decreased (Fig. 4.4a). It was due to limited utilization of nitrate for cellular metabolism that involves synthesis of protein, nucleic acid, and phospholipid [219]. However, a lower phosphate loading (21.8 mg L^{-1}) in culture medium resulted in a consistent utilization for all except for the TE60 and TE70 mixtures that had a comparatively lower growth rate than others, where the removal reached 99.9% in five days with a rate of 4.35 mg L^{-1} d^{-1}.

As shown in Fig. 4.4b, for the experiment with TE30 and different concentrations of PAC, the maximum assimilation of nitrate (94.6%) was obtained for 40 mg L^{-1} PAC. However, all other PAC loadings had shown comparatively lower nitrate removal (78%-91%), which further validated biomass yield is directly proportional to nitrate consumption. Nevertheless, the phosphate consumption for all (except 5 mg L^{-1} PAC) was 99.9% with a removal rate of 5.44 mg L^{-1} d^{-1} (Fig. 4.5b). In a recent study, Mejia-da-Silva et al. (2018)

also found decreased nitrate consumption rate leading to lower biomass yield due to a higher PAC loading (Table1). In addition, present study used 30 mg L^{-1} PAC which was 40% less than previous report leading to an overall cost-effective process with superior nutrient consumption followed by a biomass yield [185].

Further, the nitrate and phosphate removal profiles in the batch recyle studies of 30 mg L^{-1} PAC treated E30 are depicted in Fig. 4.4c and Fig. 4.5c respectively. The nitrate consumption was reduced from 91% to as low as 68% from R1 to R5, respectively. Also, the phosphate removal reached 99.9% for all the cycles. The number of days required to achieve such a significant phosphate removal was four days for R1 and R2, five days for R3 and R4, and six days for R5.

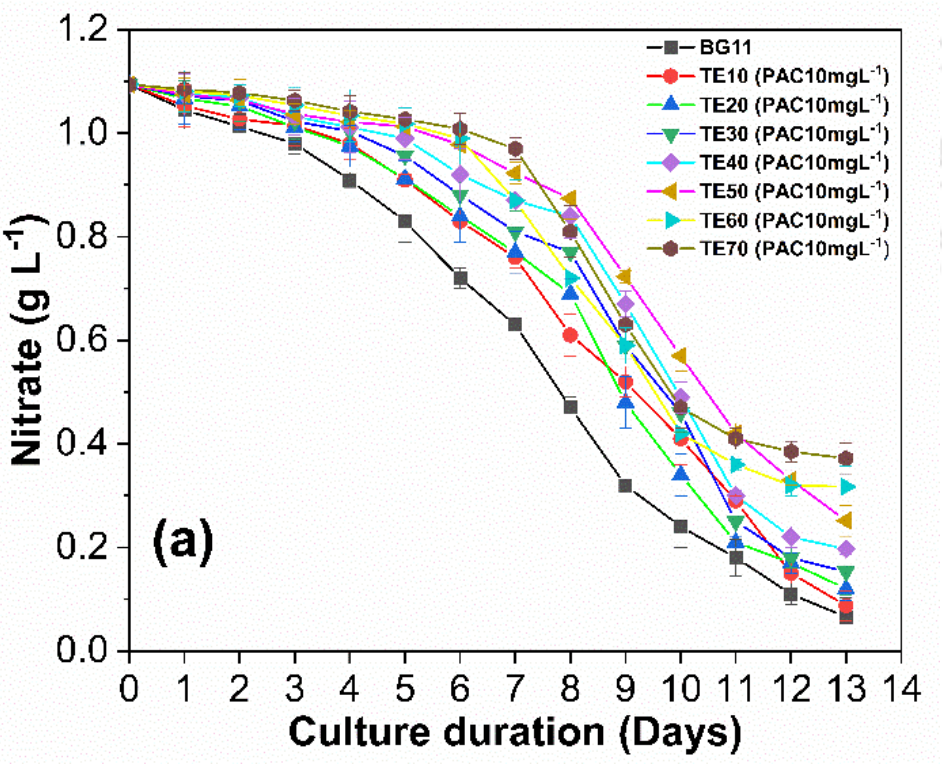

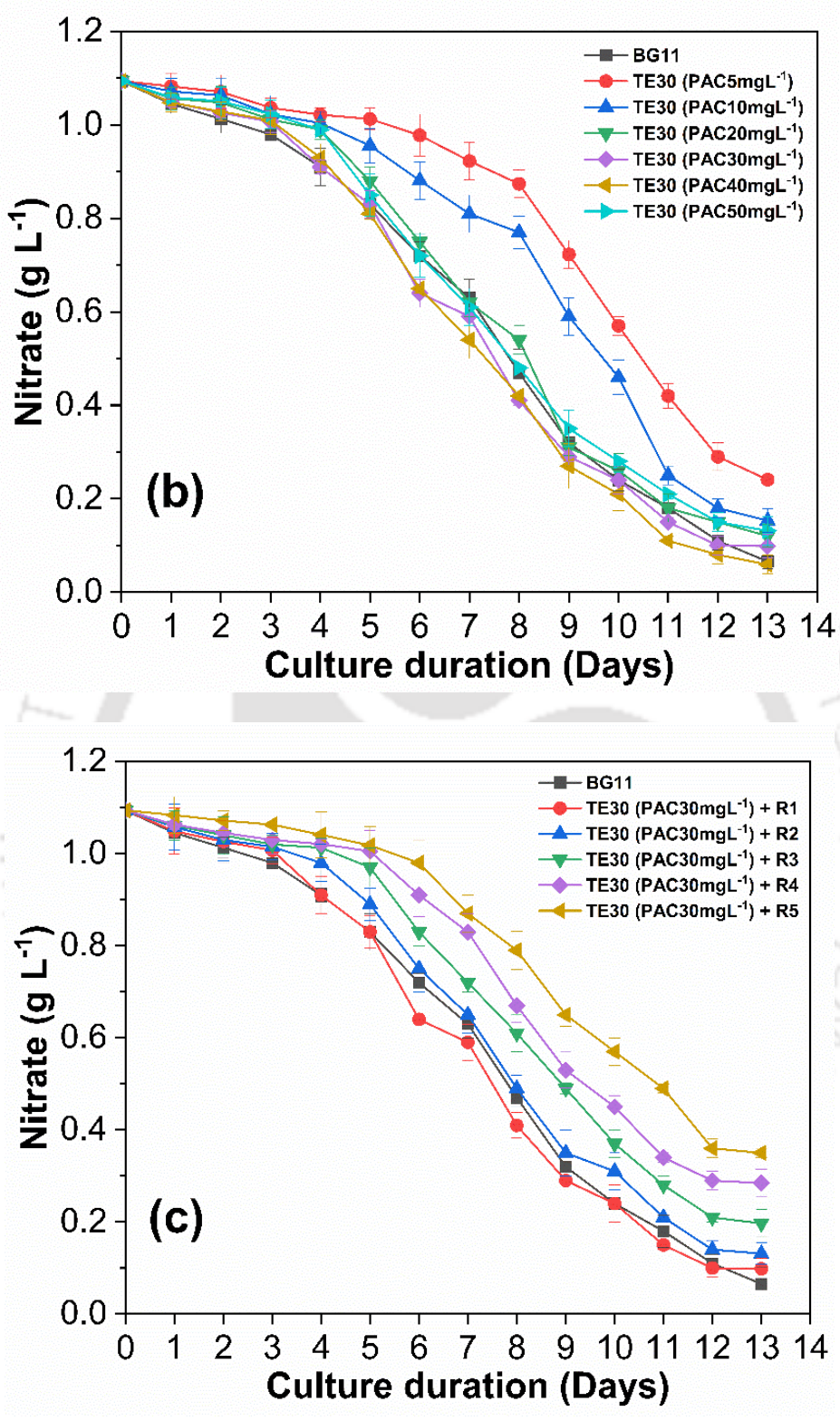

Fig. 4.4. Nitrate consumption profile at different recycle conditions (a) Effect of 10 mg L^{-1} PAC on EBC media (E10-E70), (b) Effect of different PAC concentrations (5 mg L^{-1} to 50 mg L^{-1}) on optimal treated EBC media (TE30), (c) Batch recycle study (R1-R5) of treated EBC media (TE30).

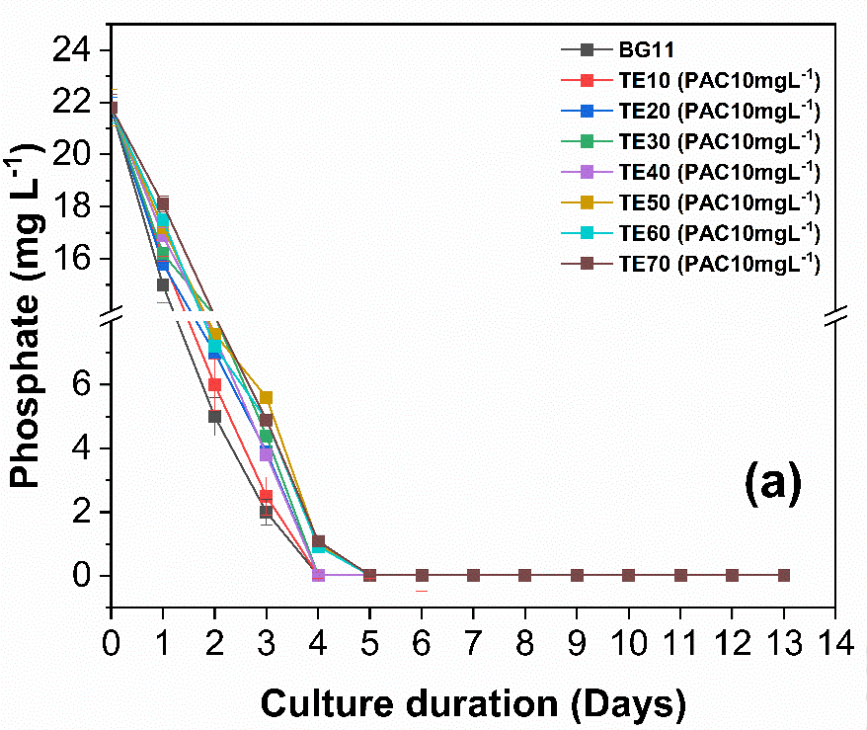
BG11
TE10 (PAC10mgL-1)
TE20 (PAC10mgL-1)
TE30 (PAC10mgL-1)
TE40 (PAC10mgL-1)
TE50 (PAC10mgL-1)
TE60 (PAC10mgL-1)
TE70 (PAC10mgL-1)
Phosphate (mg L-1)
Culture duration (Days)
(a)

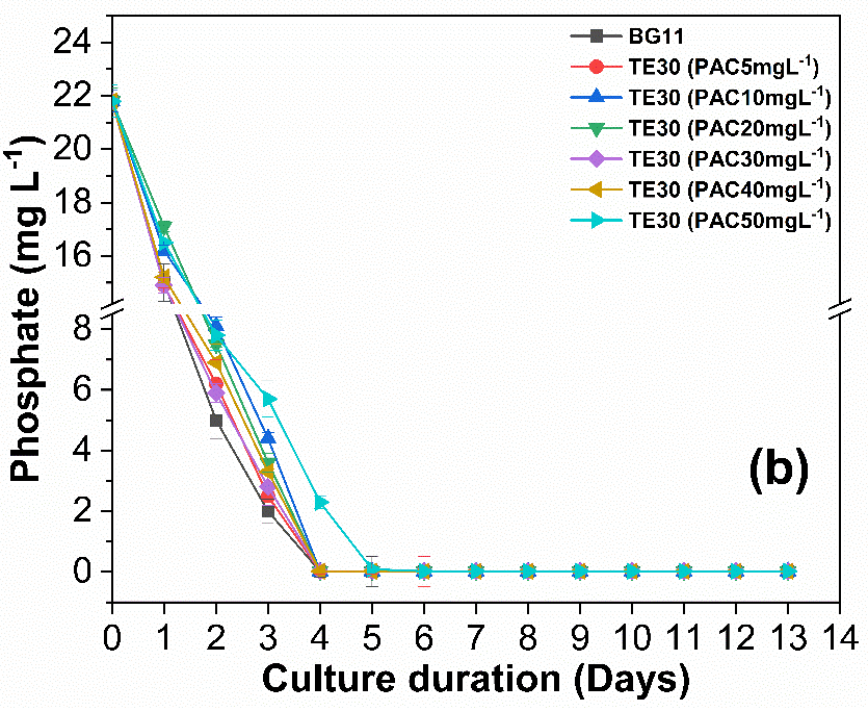
BG11
TE30 (PAC5mgL-1)
TE30 (PAC10mgL-1)
TE30 (PAC20mgL-1)
TE30 (PAC30mgL-1)
TE30 (PAC40mgL-1)
TE30 (PAC50mgL-1)
Phosphate (mg L-1)
Culture duration (Days)
(b)

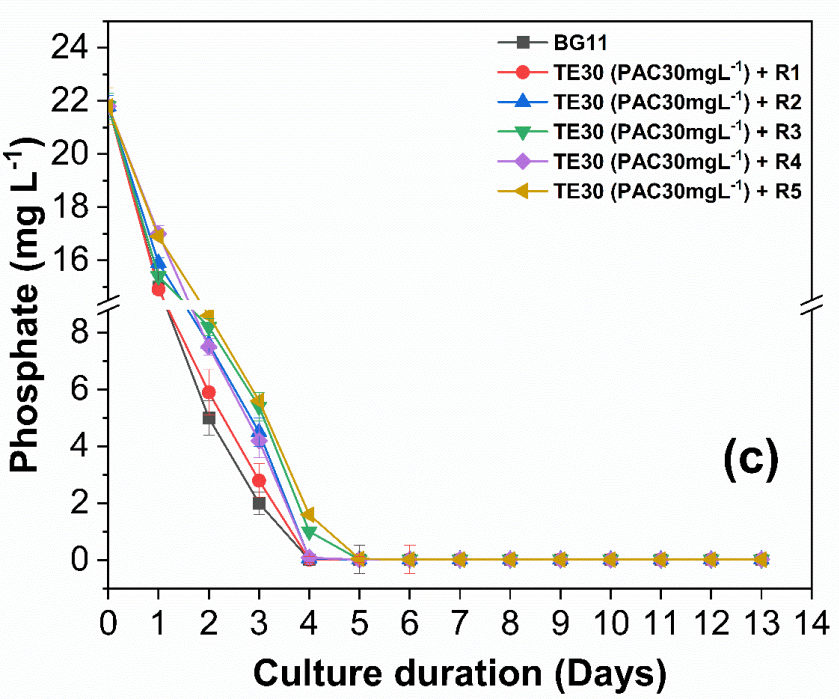

Fig. 4.5. Phosphate consumption profile at different recycle conditions (a) Effect of 10 mg L^{-1} PAC on EBC media (E10-E70), (b) Effect of different PAC concentrations (5 mg L^{-1} to 50 mg L^{-1}) on optimal treated EBC media (TE30), (c) Batch recycle study (R1-R5) of treated EBC media (TE30).

4.4.2.5. Change in total organic carbon (TOC) in the KMC4 cultures

To evaluate the potential of PAC in treating EBC media and enhancing its growth, TOC (mg L^{-1}) was analysed for various culture conditions that includes E30 EBC media (untreated), TE30 EBC media (5 mg L^{-1} - 50 mg L^{-1}), and recycle study (R1-R3). The TOC concentration for E30 EBC media was 13.7 mg L^{-1} which was further reduced using different concentrations of PAC. The TOC values for TE30 were 10.2 mg L^{-1}, 8.78 mg L^{-1}, 7.83 mg L^{-1}, 6.3 mg L^{-1}, 6.41 mg L^{-1}, and 7.29 mg L^{-1} for the PAC range of 5 mg L^{-1}- 50 mg L^{-1}. Organic matter removal continued to increase upto 30 mg L^{-1} and decreased at higher PAC loading (40 mg L^{-1} - 50 mg L^{-1}). The present result was found comparable to previous report by Zhang et al. (2016) that shown optimal PAC loading supported for removal of growth inhibitors through TOC removal leading to enhancing microalgal

growth [181]. At higher PAC concentration, particle accumulation results in less active sites for adsorption of organic matter, thereby negatively effecting the biomass yield [178,185]. The TOC concentration for R1, R2 and R3 was 6.3 mg L^{-1}, 8.4 mg L^{-1} and 10.25 mg L^{-1} respectively at the start of experiment which was increased to 14.0 mg L^{-1}, 15.6 mg L^{-1} and 16.2 mg L^{-1} at the end of experiment, respectively. The organic matter concentration in the recycled EBC media continued to increase consistently as the media was used repeatedly. The reduced growth from R1 to R3 (Fig. 4.2d) further authenticated the obtained TOC results. Similar observations were also reported previously [181].

4.4.3. Characterization of biomass

Aforementioned studies with an optimal PAC treated EBC media (TE30 (PAC 30 mg L^{-1})) was considered for comprehensive characterization. During this, R1, R2, and R3 recycle batch studies that had shown superior biomass yield were considered for proximate, ultimate, thermochemical and FAME analysis and the obtained results are compared with the control BG11 biomass.

4.4.3.1. Biomass composition

The proximate analysis showed that all samples had moisture and ash content of <5 wt% (Table 4.1). However, the ash content was found increasing from 2.8 wt% to 3.71 wt% with an increase in recycle batch from R1 to R3. It might be due an increased cell debris and residual nutrients in the harvested biomass, which can be reduced with improved harvesting procedures. In contrast, comparatively higher proportion of volatile matters (68-79 wt.%) and fixed carbon (15-25 wt.%) in the feedstock, which was found comparable to other microalgal and lignocellulosic biomass feedstocks [220,221]. Besides, increasing the recycle batches reduced volatile matter and increased fixed carbon, which support enhanced biochar production during the thermochemical conversion process [222].

The ultimate analysis suggests that KMC4 grown in recycle media and BG11 both had comparable elemental composition that include carbon (48-52 wt%), hydrogen (7.5-8.5 wt%), and oxygen (33-36 wt%) (Table 4.1) . The present study showed a considerably higher nitrogen and sulfur content in biomass that leads to emission of SOx and NOx. However, it can be significantly reduced with implimenting efficient biomass pretreatment process [223,224]. The biomass samples had energy content (HHV) of 21-22 MJ kg^{-1} that was found comparavely superior than other microalgal and lignocellulosic biomass [221]. Besides proximate and ultimate analysis, present study also estimated lipid content in the havested biomass. The study showed that increasing the recycle batches resulted in consistent reduction in lipid content (30.57 wt% to 28.6 wt%) compared to the control BG11 (31.4 wt%). However, a promissing biomass yield (1.5 g L^{-1} to 1.6 g L^{-1}) during recycle batches supported towards overal lipid producivity of 34-37 mg $L^{-1}d^{-1}$. Besides, implimention of a two-step cultivation process is suggested to significantly enhance overall lipid productivity, where harvested biomass will be transferred to a nitrogen-deficient medium [225].

Table 4.1 Physicochemical characteristics of biomass harvested.

Components	Control (BG11)	Recycle 1	Recycle 2	Recycle 3
Lipid (wt%)[a]	31.4	30.57	29.41	28.16
Proximate composition [a]				
Moisture (wt%)	4.2	3.3	2.6	3.8
Volatile matter (wt%)[a]	73	69.24	78.62	68.02
Fixed carbon (wt%)[a]	19.8	24.66	15.63	24.47
Ash (wt%)[a]	3	2.8	3.15	3.71
Ultimate composition [a]				
C (wt%)[a]	51.04	48.2	49.3	48.94
H (wt%)[a]	7.94	7.81	8.04	7.9
N (wt%)[a]	5.5	6.22	5.9	6.03
S (wt%)[a]	0.08	0.28	0.25	0.27
O (wt%)[b]	35.44	34.69	33.36	33.15
HHV (MJ Kg^{-1})[a]	22.79	21.24	22.18	21.89

4.4.3.2. TGA profile

The KMC4 biomass obtained from recycle study (R1, R2, and R3) and control BG11 were characterized using thermogravimetric analyzer to evaluate its thermal decomposition behavior (pyrolytic profile) and obtained thermogravimetric (TG) curves are depicted in Fig. 4.6. The study suggests that all biomass had three-stage of degradation. The initial weight loss in the first stage (up to 120 °C) was due to moisture removal that accounted for weight loss of 0.8% to 4 wt%. The second stage (120-550 °C) had a weight loss of 68-79 wt%, which was due to the devolatilization of organic matters in biomass. In the third stage (> 550 °C), biomass samples had a minimal weight loss of 1.4-6 wt% and left with char as a residue of 16-26 wt%. The obtained pyrolytic profile was also found comparable to previous reports on various biomass feedstock [220,226].

The present pyrolytic study suggests that KMC4 biomass obtained from the R2 had the maximum volatile matter (78.62 wt%) with least residual content (16.92 wt%) and found comparable to the control BG11 derived biomass. Moreover, increasing the recycle batch had significant effect on reducing the volatile matter content and increased residues, which was due to the transfer of cell debris and residual nutrients in harvested biomass. Thus the study ascertained that two batch recycle (R2) was found optimal to generate energy dense biomass for biofuel application.

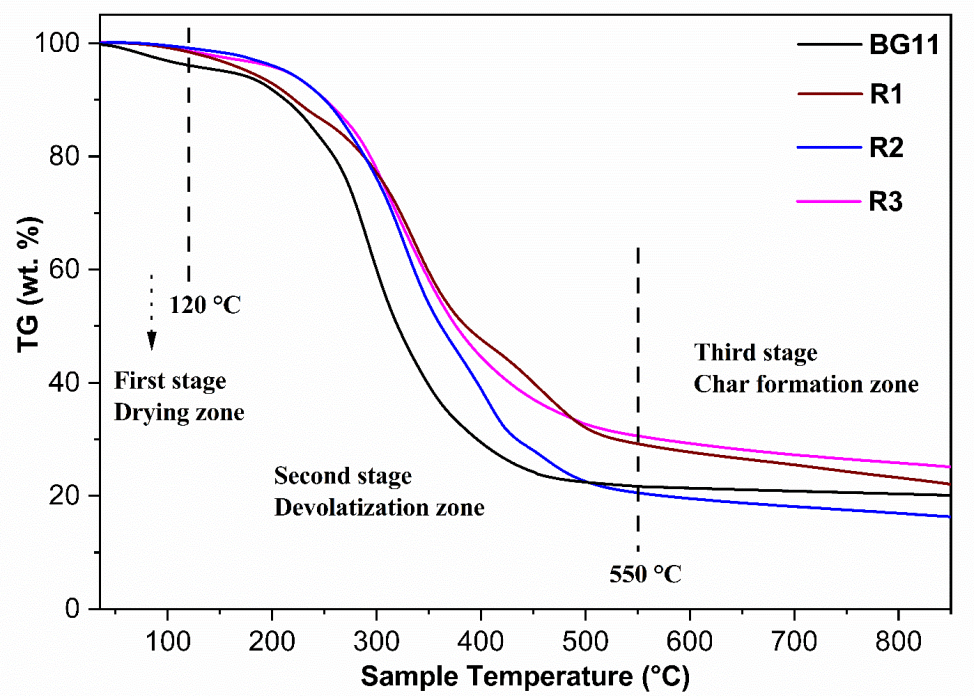

Fig. 4.6. TGA (pyrolysis) profile of KMC4 biomass obtained from different culture conditions

4.4.3.3. FTIR profile

FTIR analysis was performed to identify organic and inorganic compounds presence in the KMC4 biomass (Fig. 4.7). The study showed that the biomass samples were primarily composed of alcohol group (OH), carboxyl group (COOH), amino (NH_2), and other groups associated with organic compounds [220]. Peak at 3550 cm^{-1} - 3200 cm^{-1} observed due to OH stretching that denotes presence of carbohydrates, proteins, lipids (sterols and fatty acids), nucleic acids [227]. Multiple peaks between 2830 cm^{-1} - 2695 cm^{-1}, 1745 cm^{-1} - 1730 cm^{-1}, and 1685 cm^{-1} - 1660 cm^{-1} represents presence of alkane, aldehyde, and ester group compounds [220]. Presence of protein in KMC4 biomass was also confirmed from the peaks shown between 1550 cm^{-1} - 1540 cm^{-1} due to the C-N stretching. Furthermore, presence of carbonate ion (C=O stretching), phospholipids and nucleic acids (P=O), amide group (N-H) compounds were identified from their respective peaks [228].

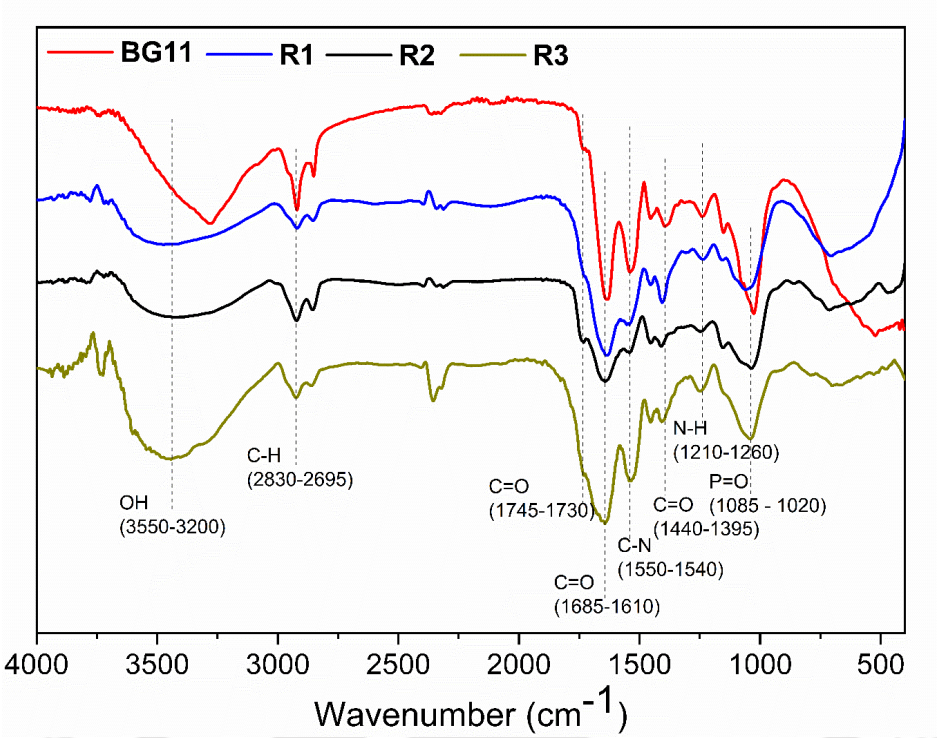

Fig. 4.7. FTIR spectrum of harvested KMC4 biomass from different culture conditions

4.4.3.4. FAME profile

The FAME profile obtained through the two-step transesterification process is depicted in Table 4.2. The study showed that maximum FAMEs were of saturated fatty acid (SFA) that includes, myristic acid (C 14:0), palmitic acid (C 16:0), stearic acid (C 18:0), arachidic acid (C 20:0). Among all samples, recycle derived FAME (R1, R2, R3) had the maximum SFA content (55-56 wt%), and the MUFA and PUFA were comparatively less than the FAME derived from the BG11. This property suggests that the recycle derived biodiesel was ideal for commercial application in tropical regions [229]. The present study showed, 78-80 wt% of total FAME content in the recycle derived biomass was of C16 (42.26 wt% - 43.69 wt%) and C18 (35.8 wt% - 36.35 wt%). This includes oleic acid (C 18:1) of 11-13 wt%, which was lesser than the BG11 derived biomass (11.2 wt%). The above results ascertained that biodiesel derived from recycle media biomass had superior biofuel quality. These results were found to be in accordance with previous studies [230,231].

Table 4.2 FAME profile (wt%) of KMC4 obtained from different culture conditions

	Fatty acids	BG11	R1	R2	R3
C 14:0	Myristic acid	1.14	1.07	1.29	1.31
C 16:0	Palmitic acid	35.9	36.22	36.02	36.47
C 16:1	Palmitoleic acid	6.91	6.04	6.62	7.22
C 18:0	Stearic acid	10.3	11.06	11.83	10.73
C 18:1	Oleic acid	11.2	11.8	11.55	12.77
C 18:2	Linoleic acid	9.77	9.88	9.37	9.44
C 18:3	Linolenic acid	3.5	3.16	3.05	3.41
C 20:0	Arachidic acid	7.61	7.4	6.91	7.44
C 20:1	Eicosenoic acid	4.65	4.81	4.72	5.02
C 22:1	Erucic acid	1.73	1.6	1.38	0.84
C 24:1	Nervonic acid	0.5	0.33	0.32	0.21
Total Saturated fatty acid		54.95	55.75	56.05	55.95
Total unsaturated fatty acid		38.26	37.62	37.01	38.91

4.4.4. Proposed Biorefinery model

A microalgal biorefinery process is an integrated approach that uses upstream and downstream operations for economic production and efficient conversion of microalgal biomass to biofuel. Combining the concept of biorefinery with wastewater treatment helps effectively utilize algal biomass and reduce overall waste generated during the process [232].

The aim of this study is to extract multiple coproducts from harvested microalgal biomass and develop a biorefinery model, which can be implemented at commercial scale. Experimental results (optimal N and P) from the above study were considered in the proposed biorefinery model (Fig. 4.8). During this, 1 million litre of water was considered as the basis for KMC4 cultivation, to which nutrients input were 1500 kg $NaNO_3$ and 40 kg K_2HPO_4 respectively. Furthermore, 70% of the effluent based culture (EBC) media obtained after harvesting was mixed with 30% of fresh BG11 media and treated with PAC

to obtain TE30. The sequencial batch recycle study (R1-R3) in raceway pond of TE30 could generate 5,760 kg of biomass which further generates 1,468 L (113 L d^{-1}) of biodiesel. The obtained biodiesel can be blended at 20% with commercial diesel (B20) and used as a transport fuel that is estimated to run 8 buses for 10 round trips from point A to B of 25 km distance apart. The model estimates to release 3.1 million litre of nutrient rich effluent that can be used for various biorefinery applications such as microalgal cultivation, water supplement for biofuel conversion, and gardening [233]. In addition, the solid residue (deoiled microalgal biomass) can be processed through biochemical and thermochemical conversion processes to obtain biofuels (bio-methane, bio-oil, and biochar), neutraceuticals (mycosporine-like amino acids, Lipophilic antioxidant, Phenolic antioxidant, Astaxanthin, Cantaxanthin, Fucoxanthin, Lutein, Zeaxanthin, Glutathione, Glycerol, Sulphonated polysaccharides, Arachidonic acid, Glycoprotein, Anatoxin, Vitamin B, Vitamin C, Vitamin E), fooder and biofertilizer [234]. Moreover, recycling the waste yielded in the process ensures alternate technologies for fossil production which are environmental-friendly. Also, a total of 0.9 million litre of fresh water was saved through this process which accounted to 22.5% of savings when compared to process without any recycle of EBC media.

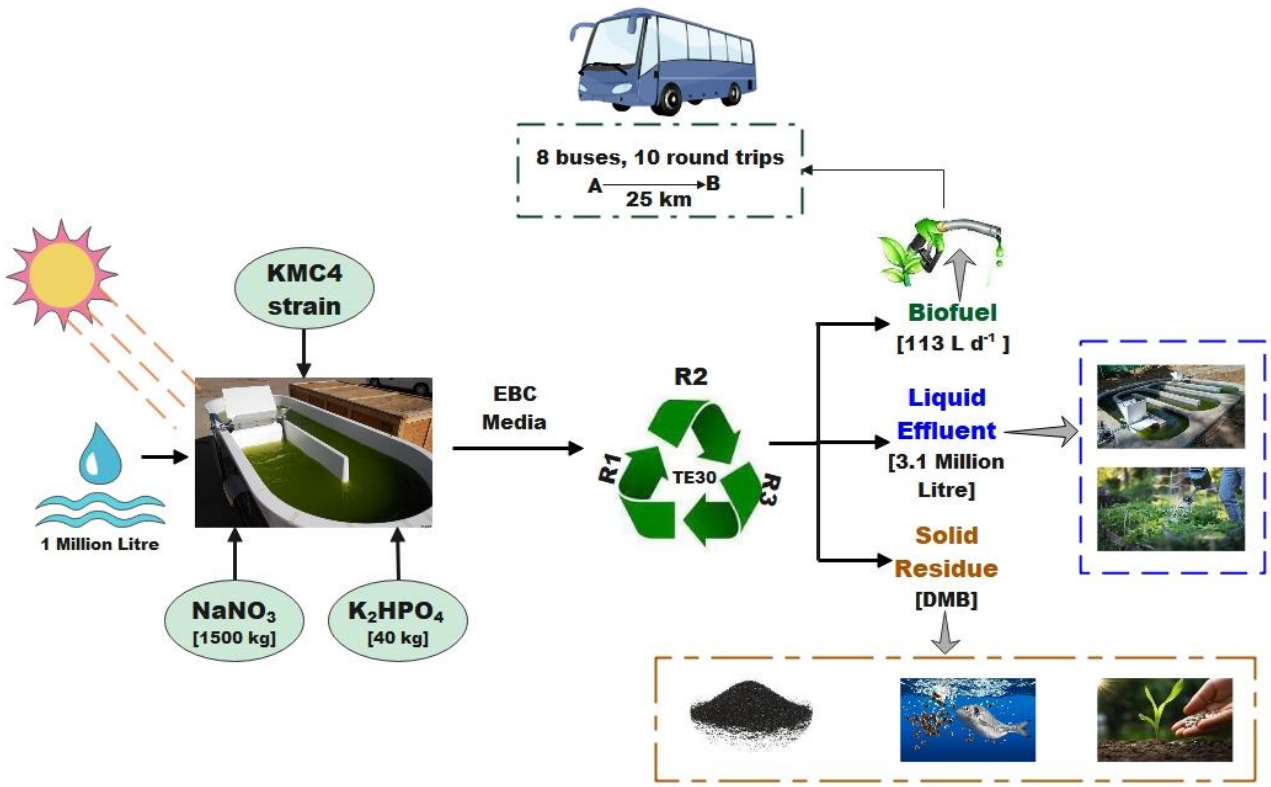

Fig. 4.8. Proposed biorefinery model

4.4.5. Comparison with prior arts

The comparison of different studies on effluent based media recycle is summarized in Table 4.3. Sha et al. in 2019 obtained equal biomass as that of the controlled media after using granular activated carbon (GAC) to treat effluent based media. However, only one cycle of experiment was accomplished in this study using *Scenedesmus acuminatus* microalgae. In a different investigation [185], *Anthrospira platensis* was cultured using Schlosser media. In this case, the culture was harvested using an MF membrane, and the harvested media was treated with PAC and $FeCl_3$. The results indicated that the growth in the treated media closely resembled that of the control experiment. The utilization of flocculation as the harvesting method resulted in no observed growth in the recycled media [52]. This showed the inhibitory impact of flocculation method on the harvested effluent. Conversely, when the filtration method was employed for harvesting, researchers observed growth in the recycled media, as reported by multiple studies. In a study by Depraetere et al. in 2015 [187], four cycles of recycling were conducted, with a 68% decrease in biomass observed in the fourth cycle compared to the initial batch. In another investigation using a 0.45 µm MF membrane, growth inhibition occurred in the third cycle due to a phosphorus deficiency [186]. In our study, combining PAC with MF membrane resulted in almost equal growth for the 1st batch of recycle (1.548 g L^{-1}) in comparison to the control (1.55 g L^{-1}). Nevertheless, a consistent decline in KMC4 growth was observed with each subsequent recycle, reaching the lowest biomass yield of 0.93 g L^{-1} (70 mg L^{-1} d^{-1}) in the fifth batch However, up to third recycle, KMC4 had shown comparatively superior biomass yield (1.24 g L^{-1}) that signifies 30 mg L^{-1} of PAC was found sufficient to retain an optimal KMC4 growth in E30 mixture. The decrease in biomass growth in later cycles was attributed to an accumulation of cell debris and residual nutrients in the media.

Table 4.3 Comparison of studies on effluent based media recycle

Strain name	Culture media	Cultivation mode	Harvesting and treatment method	Duration or number of recycles	Biomass Yield		Percentage increase/ decrease in maximum biomass yield after the recycle cycles	Reference
					Fresh Media	Recycled Media		
Scenedesmus acuminatus	Modified BG11 media (initial $NaNO_3$ conc. :187 mg L^{-1})	PBR array with 30 ml glass tubes	Centrifugation and 0.2 µm membrane; treatment using 80 g of Granular activated carbon (GAC)	12 days 1 cycle	2.38 g L^{-1}	2.04 g L^{-1} without treatment and 2.33 g L^{-1} after GAC treatment	14.3 % decrease after first reuse without any treatment and almost equal biomass with GAC treatment	[180]
Staurosira sp. C323	Artificial seawater	Batch mode in 1 L glass media bottles	Vacuum filtration (0.45 µm)	25 days 3 cycles	6.4 mM C	4.8 mM C	No growth after second reuse	[183]
Scenedesmus SDEC-8, Chlorella SDEC-18	BG11 media	Batch mode in 3 L columns	Centrifugation and ultrasonication	16 days 4 cycles	1.67 g L^{-1} and 109.05 mg L^{-1} d^{-1} (for SDEC-8); 1.71 g L^{-1} and 105.56 mg L^{-1} d^{-1} (SDEC- 18)	1.01 g L^{-1} and 69.84 mg L^{-1} d^{-1} (for SDEC-8); 1.01 g L^{-1} and 80.00 mg L^{-1} d^{-1} (SDEC-18)	62.78 % decrease for SDEC-8 and 55.89 % decrease for SDEC- 18 after 3 media reuses	[171]
Arthrospira platensis	Schlosser media	Batch mode in Erlenmeyer flasks of 1 L capacity	Microfiltration with 50 µm pore dia. 30 mg L^{-1} PAC and 6 mg L^{-1} $FeCl_3$	10 days 1 cycle	-	1.093 g L^{-1} and 130.6 mg L^{-1} d^{-1} after treatment with 30 mg L^{-1} PAC	Growth in treated media almost equal as the control experiment.	[185]

						and 6 mg L^{-1} $FeCl_3$		
Synechocystis sp. PCC 6803	Modified BG11 media (P: five times the normal concentration)	Batch mode in 500 mL Erlenmeyer flasks	Microfiltration with 0.45 µm pore dia.	12 days 5 cycles	-	0.63 g L^{-1} for 50:50 recycle to fresh media ratio	Growth inhibition at 3rd cycle due to lack of phosphorous	[186]
Arthrospira platensis	Zarrouk media	Batch mode in 1 L bottle	Filtration (20 µm pore size)	10 days 4 cycles	0.18-0.26 d^{-1}	0.24 d^{-1} (start of experiment) 0.07 d^{-1} (end of experiment)	68 % decrease after 4 cycles	[187]
Dunaliella salina	-	Batch mode in 200 mL flasks	NaOH Flocculation	10 days			No growth in reused media	[52]
Monoraphidium sp. KMC4	**BG11 Media**	**Batch mode in 500 mL flasks**	**Microfiltration and PAC treatment**	**13 days 5 cycles**	**1.55 g L^{-1} and 117.5 mg L^{-1} d^{-1}**	**1.548 g L^{-1} and 117.6 mg L^{-1} d^{-1}**	**40% decrease after 5 cycles**	**Present study**

4.4.6. Summary

The suitability of cultivating *Monoraphidium* sp. KMC4 was exhibited in different effluent media concentrations (E10-E70), the latter being treated with powdered activated carbon (PAC) with a loading of 5-50 mg L^{-1}. The optimum EBC media (TE30) treated with 30 mg L^{-1} PAC enhanced the biomass yield by 21.9% as compared to the untreated E30 (1.21 g L^{-1}). A recyclability study of TE30 performed in five batches resulted in an optimal growth up to three batches with an overall biomass yield of 4.21 g and a total water savings of 30%. Additionally, physico-chemical characterization and FAME profile of the biomass from recyclability study validated the energy potential of feedstock. Moreover, this chapter proposes a biorefinery model which could recover nutrient rich liquid effluent (3.1 million litre) and solid residue for various applications along with the generation of 5,760 kg of biomass followed by 113 L d^{-1} biodiesel yield.

Chapter 5

Economic viability of the developed low-cost membrane, microalgal harvesting and the energy efficient recycle process

CHAPTER 5

Economic viability of the developed low-cost membrane, microalgal harvesting and the energy efficient recycle process

Conducting an economic feasibility assessment is crucial for effective scaling of any process. In the pursuit of developing a cost-efficient and environmentally sustainable technology, this chapter thoroughly examines detailed cost analysis. The chapter starts with the cost analysis of the fabricated membrane followed by the cost analysis involved in the microalgal harvesting using the fabricated membrane. Subsequently, the overall cost of implementing the energy efficient recycle process was determined. Cost estimations for each process are presented for both laboratory-scale and pilot-scale setups.

5.1. Cost Analysis of Membrane Fabrication

Estimating the cost of membrane requires calculating the different costs incurred during the membrane fabrication across various categories. Direct manufacturing costs and indirect manufacturing costs are the two major heads of any production process. Direct manufacturing costs encompass the costs occurred during the actual production of membrane. These costs involve cost of raw materials, labor, laboratory expenses, electricity consumption and expenditures related to repairs and maintenance [235,236].

In membrane fabrication, the majority of the indirect expenses are attributed to the depreciation costs, which is calculated by the straight-line depreciation method.

Apart from these expenses, the total cost related to the membrane fabrication process will also consider the cost of purchasing the necessary equipment. The equipment cost will be determined using the fixed capital cost, which includes all other costs related to the purchase of equipment, such as site preparation, handling and installation fees, utilities, and laboratory expenses [235,237,238].

The membranes are fabricated using composition: Kaolin (77%), Sodium metasilicate (2%), Boric acid (2%), Sodium carbonate (4%) and Calcium carbonate (15%). Additionally, due to limitations in furnace capacity, each batch can only sinter a maximum of hundred membranes. Therefore, the cost analysis is based on the fabrication of hundred membranes per batch to fully utilize the furnace's capacity. It is important to note that producing hundred membranes requires 1428.57 g of raw material mixture.

5.1.2. Direct manufacturing cost

Raw material cost

While calculating the raw material cost, cost of kaolin, sodium metasilicate, boric acid, sodium carbonate and calcium carbonate was taken into consideration. Additionally, even though kaolin was procured from Deopani area without any charge, the transportation expense was included in this category. The cost of abrasive paper also comes under this head.

The cost involved in obtaining the required raw materials is shown in Table 5.1. Although kaolin is obtained naturally from Deopani area of Assam, the expense of INR 1000 in the transportation of 100 kg of kaolin was considered.

Table 5.1 Summary of raw material cost used in membrane fabrication

Raw material	Price (INR/kg)	Quantity (g)	Cost	
			INR	USD
Kaolin	10	1100	11	0.13
Sodium metasilicate	3377	28.57	96.48	1.16
Boric acid	2000	28.57	57.14	0.69
Sodium carbonate	1440	57.14	82.28	0.99
Calcium carbonate	920	214.28	197.13	2.38
		Total cost	**444.03**	**5.35**

Note: The following conversion was used,1 USD = 82.74 INR

Furthermore, after cutting the membrane to the desired length, abrasive paper (C-220) was employed to smooth them. Considering an average of twenty membranes being smoothened with a single sheet, five sheets of abrasive paper will be needed for 100 membranes.

Cost of one sheet of abrasive paper = 10 INR

Hence, total cost of 5 sheets = 50 INR = 0.604 USD

Therefore, total cost of raw material = (5.35 + 0.604) = 5.97 USD

Labor cost

The labour cost is the payment made to skilled labour for fabricating the membranes working 8 h/day. Assuming that in the fabrication process of one batch of membranes, the labor works for 8 hrs and the daily wage of the labor is estimated as = 500 INR = 6.04 USD.

Laboratory cost

The laboratory cost is typically around 20% of the labour cost [238].

Hence, laboratory cost = (0.2 × 6.04) USD = 1.208 USD

Electricity cost

The electricity consumption of the extruder, hot air oven, ultrasonic bath and muffle furnace was calculated based on the equation below

$$C_e = P \times n_h \times t \quad (5.1)$$

where, C_e represents the electricity consumption cost, n_h is the number of working hours of the equipment and t is the cost of electricity per kWh (0.087 USD/kWh), respectively.

Extruder, muffle furnace, hot air oven and ultrasonic bath mainly contributes to the electricity cost. The tariff for the year 2022-2023 by Assam Power Distribution Limited (APDCL) was 7.25 INR/kWh.

Extruder

Power of motor of extruder = 0.5 HP = (0.5 × 0.7457) kW = 0.3728 kW

For fabrication of hundred membranes, the extruder must operate for 2 hours.

Hence, Power consumption expense = (0.3728 × 2) × 7.25 = 5.40 INR = 0.065 USD

Hot air oven

Heating coil capacity of hot air oven = 1.5 kW

Oven was firstly used at 100 ºC for 12 hours and then at 200 ºC for another 12 hours. Also, it was used for another 6 hours for drying membrane after sonication. Hence, the total operating hours of oven = (12+12+6) hours = 30 hours

Hence, the total power consumption cost of oven = (1.5 × 30 × 7.25) INR = 326.25 INR = 3.943 USD.

Muffle furnace

Power of heating element of furnace = 4.5 kW

Total time it was used during sintering at 2 ºC / min heating rate = {(950-25)/2} = 462.5 min = 7.708 hours

For another 6 hours membrane was kept at 950 ºC. Therefore, total working hour of furnace = (7.708 + 6) hours = 13. 708 hours

Power consumption cost of furnace = (13.708 × 4.5 × 7.25) INR = 447.22 INR = 5.405 USD

Ultrasonic bath

Power rating of ultrasonic bath = 0.15 kW

The bath capacity is 25 membranes per batch for 15 minutes

Hence, for processing 100 membranes, the ultrasonic bath has to be operated for 1 hour.

Therefore, cost of power used by ultrasonic bath = (0.15 × 1 × 7.25) INR = 1,0875 INR = 0.013 USD.

Therefore, total electricity consumption cost = (0.065 + 3.943 + 5.405 + 0.013) = 9.426 USD.

Repair and maintenance cost

The annual repair and maintenance cost are calculated as 2% of the fixed capital investment/year. To determine the fixed capital investment, the book value of equipment is multiplied by Lang factor, as described by Ghodra et al. in 2016 [235]. The book value is the total cost of the equipment minus the accumulated depreciation. The depreciation value is calculated by straight line depreciation method as follows:

$$V_d = \frac{V_0 - V_s}{n_s} \times a \tag{5.2}$$

where, V_d is the accumulated depreciation after a number of years, V_s is the salvage value which is considered as 10% of the original cost, n_s is the service life of the equipment taken as 10 years and a is the number of years equipment was used.

Assumption

1. The service life of all the equipment is set at 10 years, equivalent to 79,200 working hours, based on the assumption of 330 working days in a year.
2. Salvage value is taken as 10% of the original cost.

The Lang factor utilized for determining the fixed capital investment is set at 3.1 for solid processing plants and 3.63 for solid-fluid processing plants.

Table 5.2 Summary of book value of all the equipment

Equipment	Original cost	Installation year	Used year(s) till 2023	Book value	
				INR	USD
Extruder	2,00,000	2015	8	56,000	676.82
Hot air oven	40,000	2022	1	36,400	439.93
Furnace	6,30,000	2022	1	5,67,000	6852.79
Ultrasonic bath	19,000	2021	2	15,580	188.30

Table 5.3 Estimation of annual repair and maintenance cost

Equipment	Book value (USD)	Lang Factor	Fixed capital investment (FCI)(USD)	Service life remaining	FCI/year	Annual repair and maintenance cost (USD/year)
Extruder	676.82	3.1	2098.14	2	1049.07	20.98
Hot air oven	439.93	3.63	1596.94	9	177.43	2.94
Furnace	6852.79	3.63	24875.60	9	2763.95	55.27
Ultrasonic bath	188.30	3.63	683.52	8	85.44	1.71

However, the repair and maintenance cost are entirely reliant on the equipment working hours. This approach to calculating equipment repair and maintenance costs, known as the "Machine Hourly Rate method" [239], is adopted by most industries. A detailed breakdown of the repair and maintenance cost incurred during membrane fabrication is provided in Table 5.4.

Table 5.4 Estimation of repair and maintenance cost for the process duration

Equipment	Annual repair and maintenance cost (USD/year)	Hourly repair and maintenance cost (USD/hour)	Hours used (hours)	Total repair and maintenance cost (USD)
Extruder	20.98	0.0026	2	0.0052
Hot air oven	2.94	0.00037	30	0.0111
Furnace	55.27	0.00697	13.708	0.0955
Ultrasonic bath	1.71	0.00021	1	0.00021
			Total cost	**0.112**

5.1.2. Indirect manufacturing cost

In membrane fabrication, the majority of the indirect expenses are attributed to the depreciation costs, which is calculated by the straight-line depreciation method [239].

Table 5.5 Estimation of depreciation cost of all the equipments

Equipment	Book value	Years of service life remaining	Hourly depreciation cost	Duration of use during fabrication (hrs)	Depreciation cost (USD)
Extruder	676.82	2	0.038	2	0.076
Hot air oven	439.93	9	0.0055	30	0.165
Furnace	6852.79	9	0.086	13.708	1.178
Ultrasonic bath	188.30	8	0.0027	1	0.0027
				Total	**1.4217**

5.1.3. Calculation of equipment cost

Apart from these expenses, the total cost related to the membrane fabrication process will also consider the cost of purchasing the necessary equipment. The equipment cost will be determined using the fixed capital cost, which includes all other costs related to the purchase of equipment, such as site preparation, handling and installation fees, utilities, and laboratory expenses [235,237,238].

Table 5.6 Estimation of equipment cost

Equipment	Fixed capital cost (USD/year)	Hourly fixed capital cost (USD/h)	Duration of use (h)	Equipment cost (USD)
Extruder	1049.07	0.12	2	0.24
Hot air oven	177.43	0.02	30	0.6
Furnace	2763.95	0.32	13.708	4.38
Ultrasonic bath	85.44	0.0097	1	0.0097
			Total	**5.22**

5.1.4. Estimation of total cost involved in membrane fabrication

The total cost involved in membrane fabrication is the sum of the direct and the indirect expenses.

Hence, total cost = (5.97 + 6.04 + 1.21 + 9.42 + 0.112 + 1.42 + 5.22) = 29.99 USD

The estimated cost for producing hundred membranes is 29.99 USD, resulting in a cost of 0.29 USD per membrane. Since the membranes have a surface area of 15.71×10^{-4} m^2, the cost per m^2 of membrane is 190.93 USD. The cost of commercial ceramic membranes based on Al_2O_3 and ZrO_2 is significantly higher; usually ranging from 500 USD to 3,000 USD per m^2 or more [240]. This substantial cost severely limits their general use in various industrial processes. With a raw material cost of 37.11 USD per m^2, the membrane developed in this study is within the price range that is generally associated with low-cost membranes, as reported in the literature [241]. Fig. 5.1 shows the different cost heads as percentage of overall cost. The membranes developed in this study will not only serve as an alternative to traditional microalgal harvesting methods but also provides a viable substitute for the high-cost membranes as mentioned.

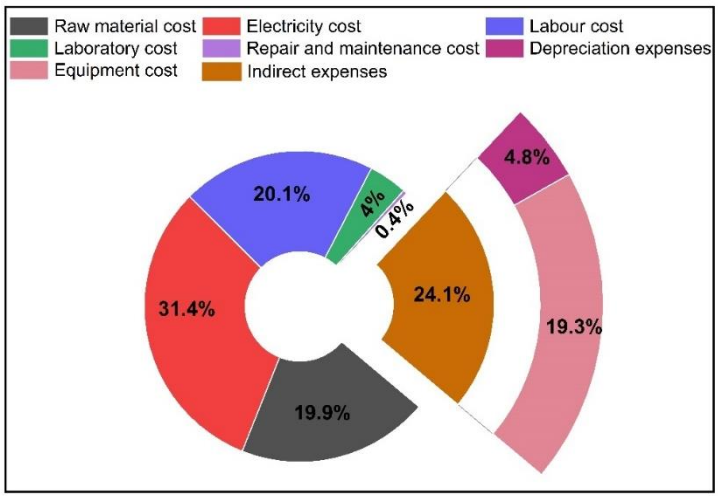

Fig. 5.1. Splitting of membrane fabrication costs as percentages of overall cost. Basis: 100 membranes per batch (1 membrane = 15.71×10^{-4} m^2)

5.2. Estimation of Microalgal Harvesting Cost on Lab Scale

The cost estimation at the laboratory scale is conducted using the existing permeation setup, which includes a membrane housing capable of fitting a single membrane with inner diameter of 5 mm, outer diameter of 9 mm and a length of 100 mm. The cost accrued during the process can be divided into capital costs and operating costs. Capital costs refer to the expenses related to acquisition and installation of equipment, securing required land and service facilities, as well as construction of the plant with all essential pipings and controls[239]. When assessing the capital cost for microalgal harvesting process, expenses related to acquiring the separation setup, necessary equipment, and membrane costs will be evaluated. However, only the costs associated with procuring the permeation setup and essential equipment will be considered as fixed capital costs within the process.

The operating expenses in any chemical process refers to the daily expenses during plant operation such as electricity, labor, maintenance, cleaning and so on.

Calculation basis:

1. The fabricated membranes have a lifespan of 3 years.

2. The microfiltration permeation setup and all essential equipment utilized in the separation process are anticipated to have a durability of 10 years.
3. Each year will consist of 330 working days.

In the lab scale microalgal harvesting, the process spans four and half hours, with two and half hours for filtration and the remaining two hours for cleaning the membrane and setup.

Total number of working days per year for microalgal harvesting = (2.5/4.5) × 330 days = 183.33 days ~ 183 days.

Permeate flux (at 276 kPa) = 1.85×10^{-5} m^3 m^{-2} s^{-1}

Therefore, volume of culture processed in a year using lab scale MF setup with a filtration area of 15.71×10^{-4} m^2 = $1.85\times10^{-5} \times 15.71 \times 10^{-4} \times 183 \times 24 \times 60 \times 60$ m^3 = 0.4595 m^3 = 459.5 L.

5.2.1. Calculation of capital cost

Cost of permeation setup = 35,000.00 INR

Since the setup was installed in the year 2022 and the filtration experiments were also carried out in the same year, so book value at 2022 = 35,000.00 INR

Fixed capital cost (Lang factor = 4.74) = 35,000.00 × 4.74 INR

=165900.00 INR= 2005.07 USD

Fixed capital cost per year (with 10 years of service life) = 2005.07/10 = 200.50 USD/year

Fabrication cost of one membrane = 0.29 USD

Since, membrane have a shelf life of 3 years, hence fabrication cost of single membrane per year = 0.096 USD/year

Therefore, total capital cost for microalgal harvesting process = (200.50 + 0.096) USD/year

= 200.596 USD/year

5.2.2. Calculation of operating cost

Electricity

The power-consuming device utilized in the separation process is a booster pump equipped with a 36 W motor capacity. The pump operates continuously for 330 days, serving both filtration and membrane cleaning processes.

Using the previously mentioned electricity tariff rate (7.25 INR/kWh), the electricity cost incurred by pump = (0.036 × 7.25 × 330 × 24) INR/year

= 2067.12 INR/year = 24.98 USD/year

Cleaning cost

In the separation process, the setup underwent an initial flush with Millipore water for 30 minutes, succeeded by flushing with a 1 g L^{-1} Surf Excel solution for an additional hour. Subsequently, the setup underwent another 30-minute flush with Millipore water.

Considering this cleaning procedure, the cleaning cost is estimated to be 4% of the fixed capital cost incurred during microalgal harvesting.

Hence, cleaning cost = (4/100) × 200.50 USD/year

= 8.02 USD/year

Maintenance cost

Maintenance cost is considered to be 3% of the fixed capital cost incurred during microalgal harvesting[242].

Hence, maintenance cost = (3/100) × 200.50 USD/year

= 6.015 USD/year

Labor cost

Labor cost is considered to be 2% of the fixed capital cost incurred during microalgal harvesting [242].

Hence, labor cost = (2/100) × 200.50 USD/year

= 4.01USD/year

Laboratory cost

Laboratory cost is considered to be 20% of the labor cost incurred during microalgal harvesting[243].

Hence, laboratory cost = (20/100) × 4.01 USD/year

= 0.802 USD/year

Depreciation cost

With a salvage value of 10% of the book value of permeation setup in the year 2022, the depreciation charges calculated using straight line depreciation method (service life of 10 years) = (40,000.00 – 0.10 ×40,000)/10

= 3600 INR = 43.51 USD/year

Hence, total operating cost = (24.98 + 8.02 + 6.015 + 4.01 + 0.802 + 43.51) USD/year

= 87.33 USD/year

5.2.3. Calculation of total cost

The total cost incurred in microalgal harvesting is the sum of the capital expenses and the operating expenses

Hence, total cost = (200.596 + 87.33) USD/year

= 287.926 USD/year

With a total of 459.5 L of microalgal culture harvested per year, the total cost incurred per litre of microalgal culture = (297.926/459.5) = 0.648 USD/L. Fig. 5.2. depicts the splitting of all the costs involved in microalgal harvesting at lab scale.

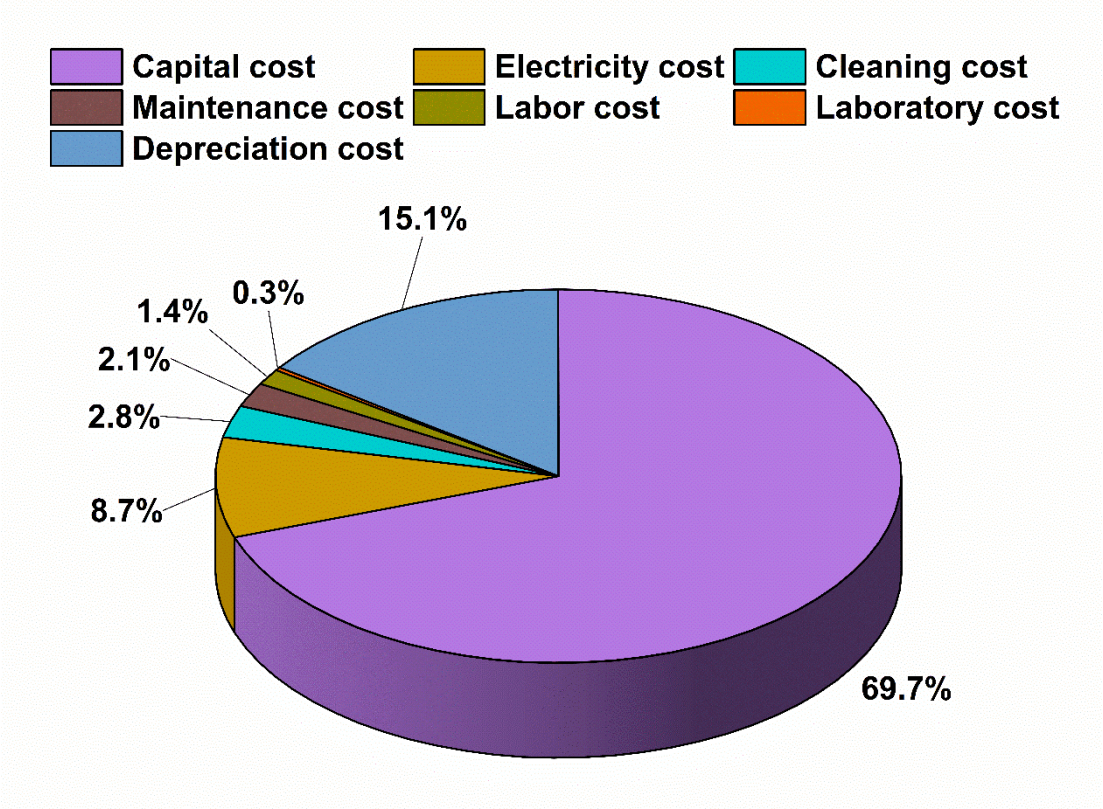

Fig. 5.2. Splitting of microalgal harvesting cost in lab scale as percentage of total cost

5.3. Cost Estimation of Microalgal Harvesting For a Pilot Scale In-house Setup

Considering the efficiency of the lab scale setup and the capacity of the existing equipment to be expanded into a pilot scale setup, the following design is proposed. Also, it is to be noted that the pilot scale setup shall be designed based on the existing facilities in the lab. In this configuration, instead of a single housing for the membrane module, three parallel housings are employed, each measuring 300 mm in length. Given that both the extruder and muffle furnace have a maximum capacity of 300 mm length, this length was selected accordingly. Each housing has the capacity to hold 7 membranes, resulting in a collective utilization of 21

membranes, all with a length of 300 mm. Importantly, both the inner and outer diameters of the membranes remain consistent.

The total membrane filtration area = $21\pi d_1 h = \pi \times 5 \times 10^{-3} \times 30 \times 10^{-2} = 0.0989\ m^2$

The basis of calculation remains the same as for lab scale setup. Also, as this is a proposed setup hence current price of each equipment will be considered negating the depreciation charges.

Permeate flux (at 276 kPa) $= 1.85\times10^{-5}\ m^3\ m^{-2}\ s^{-1}$

Therefore, volume of culture processed in a year using pilot scale MF setup with a filtration area of 0.0989 m^2 $= 1.85\times10^{-5} \times 0.0989 \times 183 \times 24 \times 3600\ m^3$

$= 28.9289$ m3 = 28928.96 L

5.3.1. Calculation of capital cost

Cost of permeation setup = 150,000.00 INR

Fixed capital cost (Lang factor = 4.74) = 150,000.00 × 4.74 INR

= 711000.00 INR= 8593.18 USD

Fixed capital cost per year (with 10 years of service life) = 8593.18/10 = 859.31 USD/year

Fabrication cost per m^2 of membrane = 190.93 USD

Hence, fabrication cost for 0.0989 m^2 of membrane filtration area = 18.88 USD

The capital cost of membrane fabrication per year (with 3 years of service life) = 6.29 USD/year

Therefore, total capital cost for the in-house pilot scale setup = (859.31 + 6.29) USD/year

= 865.60 USD/year

5.3.2. Calculation of operating cost

Electricity

The power-consuming device utilized in the separation process is a booster pump equipped with a 80 W motor capacity. The pump operates continuously for 330 days, serving both filtration and membrane cleaning processes.

Using the previously mentioned electricity tariff rate (7.25 INR/kWh), the electricity cost incurred by pump = (0.080× 7.25 × 330 × 24) INR/year

= 4593.60 INR/year = 55.52 USD/year

Cleaning cost

In the separation process, the setup underwent an initial flush with Millipore water for 30 minutes, succeeded by flushing with a 1 g L^{-1} Surf Excel solution for an additional hour. Subsequently, the setup underwent another 30-minute flush with Millipore water.

Considering this cleaning procedure, the cleaning cost is estimated to be 4% of the fixed capital cost incurred during microalgal harvesting.

Hence, cleaning cost = (4/100) × 859.31 USD/year

= 34.37 USD/year

Maintenance cost

Maintenance cost is considered to be 3% of the fixed capital cost incurred during microalgal harvesting[242].

Hence, maintenance cost = (3/100) × 859.31 USD/year

= 25.77 USD/year

Labor cost

Labor cost is considered to be 2% of the fixed capital cost incurred during microalgal harvesting[242].

Hence, labor cost = (2/100) × 859.31 USD/year

= 17.18 USD/year

Laboratory cost

Laboratory cost is considered to be 20% of the labor cost incurred during microalgal harvesting[243].

Hence, laboratory cost = (20/100) × 10.31 USD/year

= 3.43 USD/year

Depreciation cost

With a salvage value of 10% of the book value of permeation setup in the year 2024, the depreciation charges calculated using straight line depreciation method (service life of 10 years) = (1,50,000.00 – 0.10 ×1,50,000)/10

= 13500 INR = 163.16 USD/year

Hence, total operating cost = (55.52 + 34.37 + 25.77 + 17.18 + 3.43 + 163.16) USD/year

= 299.43 USD/year

5.3.3. Calculation of total cost

The total cost incurred in microalgal harvesting is the sum of the capital expenses and the operating expenses.

Hence, total cost = (865.60 + 299.43) USD/year

= 1165.03 USD/year

With a total of 28928.96 L of microalgal culture harvested per year, the total cost incurred per litre of microalgal culture = (1165.03/28928.96) = 0.04 USD/L. Fig. 5.3. depicts the splitting of all the costs involved in microalgal harvesting at pilot scale.

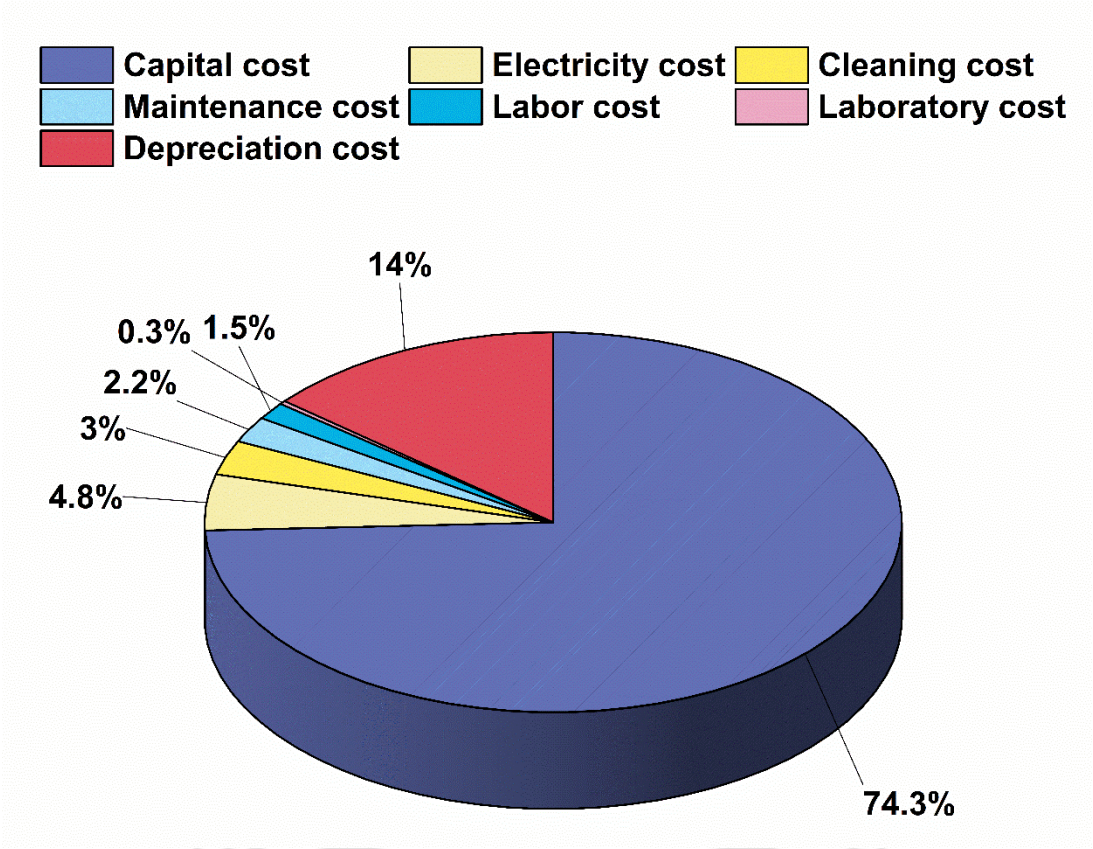

Fig. 5.3. Splitting of microalgal harvesting cost in pilot scale as percentage of total cost

5.4. Cost Estimation of the Developed Energy Efficient Recycle Process at Lab Scale

The energy efficient recycle process is depicted in Fig. 5.4. The cost estimation for the production of biomass shall be calculated both at lab scale as well as pilot scale.

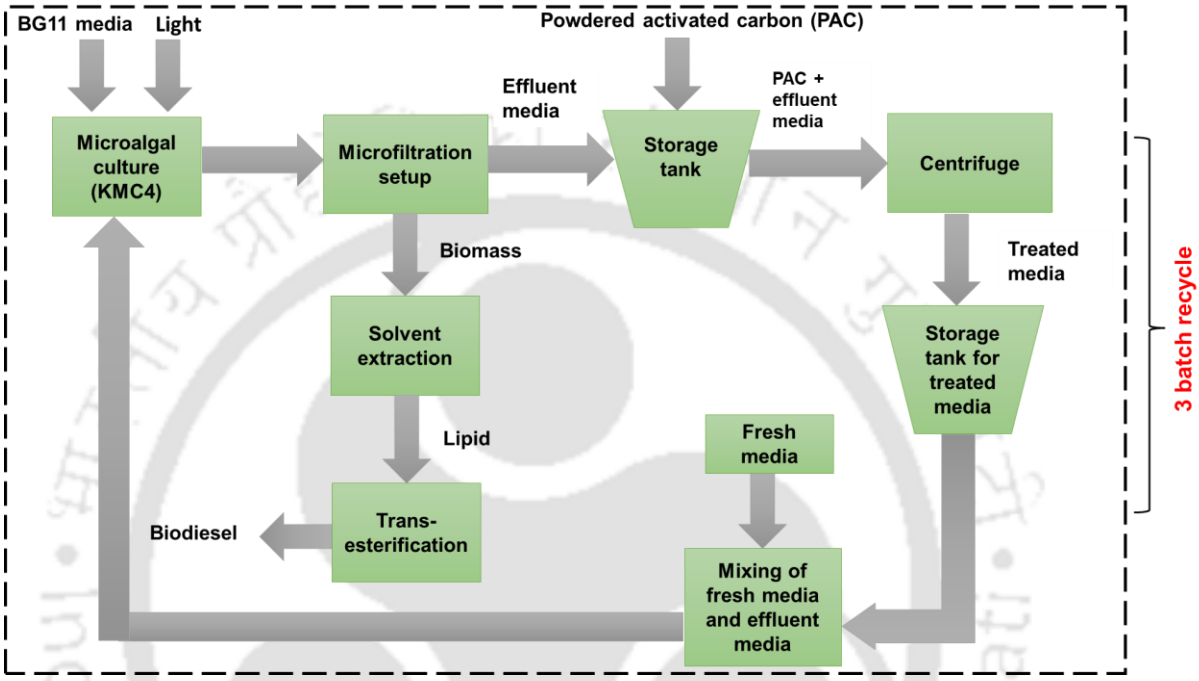

Fig. 5.4. Energy efficient recycle process

Calculation basis:

1. Two litres of working volume was considered for each batch (BG11, R1, R2, R3) of 13 days.
2. One cycle consists of four batches.
3. Number of cycles processed annually: 6
4. The microfiltration permeation setup and all essential equipment utilized in the separation process are anticipated to have a durability of 10 years.
5. Each year will consist of 330 working days.

Table 5.7 Key assumptions and process details

	BG11	R1	R2	R3
Culture density (g L^{-1})	1.55	1.55	1.42	1.24
Biomass lipid content (wt.%)	31.4	30.57	29.41	28.16
Extraction efficiency (%)	85	85	85	85
Biomass per batch (g)	3.1	3.1	2.84	2.48
Annual biomass production (g)	18.6	18.6	17.04	14.88
Annual Lipid production (g)	5.84	5.68	5.01	4.19

5.4.1. Calculation of direct cost

Raw material cost

While calculating the raw material cost, cost of BG11 media, powdered activated carbon, methanol, n-hexane, sulphuric acid and sodium hydroxide was taken into consideration. Additionally, for the transesterification process, a 1:1 mixture of n-hexane and methanol was utilized, with a ratio of 5 mL of each reagent per 1 g of biomass. For FAME production, lipid and methanol were mixed in a ratio of 1:20 along with 1.5 wt.% of H_2SO_4 and NaOH respectively. Table 5.8 summarizes the quantity of raw material used annually along with its cost.

Table 5.8 Summary of raw material cost for energy efficient recycle process at lab scale

Raw material	Quantity	Price (INR/kg)	Quantity used	Cost	
				INR	USD
BG-11 media	500g	4000	60.52 g	484.16	5.85
Powdered activated carbon	500g	270	0.36 g	0.194	0.0023
Methanol	2.5L	897	760 mL	272.68	3.29

n-Hexane	2.5L	4177	345.6 mL	577.42	6.97
Sulphuric acid	2.5L	1227	0.31 mL	0.15	0.0018
Sodium hydroxide	500g	378	0.31 g	0.234	0.0028
			Total cost	**1334.84**	**16.13**

Electricity cost

Air Pump

Power rating of aquarium air pump = 3 W = 0.003 kW

Number of hours of operation = (13 × 4 × 6 × 24) h = 7488 h

Hence, power consumption by air pump = 0.003 × 1248 × 7.25 = 162.86 INR = 1.96 USD / year

Booster pump

In the lab scale microalgal harvesting, the process spans four and half hours, with two and half hours for filtration and the remaining two hours for cleaning the membrane and setup.

In one cycle of experiment, the MF setup will be run 4 times (for BG11, R1, R2, R3)

Number of runs annually = 4 × 6 = 24

Hence, total number of working hours of pump = 4.5 × 24 = 108 h

Power rating of pump = 36 W

Power consumption cost = 0.036 × 108 × 7.25 = 4.698 = 28.188 INR = 0.34 USD / year

Centrifuge

Power rating of centrifuge = 120 W

The centrifuge was used for separating powdered activated carbon from the treated cultures (R1, R2 and R3) for 15 mins.

Hence, number of times it was used annually = 3 × 6 =18 times

Duration of use of centrifuge for single run = 15 minutes

Duration of use = 15 × 18 = 270 minutes = 4.5 h

Also, it was used during transesterification for 10 mins = 0.16 h

Therefore, total duration of use of centrifuge for the entire process = 4.66 h

Therefore, total cost of power consumption of centrifuge = 0.120 × 4.66 ×7.25 = 4.05 INR

= 0.048 USD/year

Hot air oven

Heating coil capacity of hot air oven = 1.5 kW

Oven was used at 80 ºC for 12 hours for drying the microalgal biomass.

Hence, the total power consumption cost of oven = (1.5 × 12 × 7.25) INR = 130.5 INR = 1.57 USD/year.

Vortex

Power rating of vortex equipment = 60 W

Vortex was used for 2 hours during lipid extraction from dried microalgal biomass.

Hence, cost of power consumption of vortex = (0.06 × 2 × 7.25) INR = 0.87 USD/year

Tubelights

Power rating of one tubelight = 40W

Number of tubelights used during microalgal culturing = 4

Total number of days in use = 13 × 4 × 6 = 312 days

Total number of hours in use = 312 × 16 = 4992 hours (16 h: 8 h of light: dark period)

Therefore, power consumption cost due to tubelight = 0.04 × 4992 × 7.25 = 1447.68 INR = 17.49 USD/year.

Air conditioning

Power rating of air conditioner = 1000 W

Duration of use = (13 × 4 × 6 × 12) h = 3744 h

Therefore, power consumption due to air conditioner = 1 × 3744 × 7.25 = 27188 INR = 328.06 USD/year

Rota evaporator

Power rating of Rota evaporator = 900 W

Rota evaporator was used for 30 mins (0.5 h) to separate lipid-solvent mixtures after lipid extraction step

Hence, cost of power consumption due to Rota evaporator = 0.9 × 0.5 × 7.25 = 3.26 INR = 0.039 USD/year

Heating mantle

Power rating of heating mantle = 300 W

Duration of use = 6 h

Hence, cost of power consumption due to heating mantle = 0.3 × 6 × 7.25 = 13.05 INR = 0.157 USD/year.

Total cost of electricity consumption during the entire process = (1.96 + 0.34 + 0.048 + 1.57 + 0.87 + 17.49 + 328.06 + 0.039 + 0.157) USD/year = 350.534 USD/year.

Labor cost

Labor cost is considered to be 2% of the fixed capital cost incurred during microalgal harvesting[242].

Hence, labor cost = (2/100) × 1819.01 USD/year

= 36.38 USD/year

Laboratory cost

Laboratory cost is considered to be 20% of the labor cost incurred during microalgal harvesting[243].

Hence, laboratory cost = (20/100) × 36.38 USD/year

= 7.27 USD/year

Repair and Maintenance cost

The protocol for the calculation of repair and maintenance cost is mentioned in section 5.1.2. Table 5.9 summarizes the book value of all the equipments, which will be henceforth used for the calculation of fixed capital investment and hence the annual repair and maintenance cost. However, the repair and maintenance cost are entirely reliant on the equipment working hours. The detailed cost based on the working hours is summarized in Table 5.11.

Table 5.9 Estimation of book value of all the equipments used

Equipment	Original cost	Installation year	Used year(s) till 2022	Book value	
				INR	USD
Centrifuge	80,000	2017	5	44000	531.78
Vortex	7000	2015	7	2590	31.30
Heating mantle	2,000	2017	5	1100	13.29
Hot air oven	40,000	2022	0	40,000	483.44
Rota evaporator	1,90,000	2018	4	121600	1469.66

MF setup	35,000	2022	0	35000	423.01
Air conditioner	15,000	2014	8	4200	50.76

Table 5.10 Summary of annual repair and maintenance cost

Equipment	Book value (USD)	Lang Factor	Fixed capital investment (FCI)(USD)	Service life remaining	FCI/year	Annual repair and maintenance cost (USD/year)
Centrifuge	531.78	3.63	1930.36	5	386.07	7.72
Vortex	31.30	3.63	113.62	3	37.87	0.75
Heating mantle	13.29	3.63	48.24	5	9.65	0.19
Hot air oven	483.44	3.63	1754.88	10	175.48	3.51
Rota evaporator	1469.66	3.63	5334.86	6	889.14	17.78
MF setup	423.01	4.74	2005.06	10	200.50	4.01
Air conditioner	50.76	4.74	240.60	2	120.30	2.41
				Total	**1819.01**	**33.96**

Table 5.11 Summary of annual repair and maintenance cost based on process duration

Equipment	Annual repair and maintenance cost (USD/year)	Hourly repair and maintenance cost (USD/h)	Hours used (h)	Total repair and maintenance cost (USD)
Centrifuge	7.72	0.00097	4.66	0.0045
Vortex	0.75	0.000095	2	0.00019
Heating mantle	0.19	0.000024	6	0.000144
Hot air oven	3.51	0.00044	12	0.00528
Rota evaporator	17.78	0.00224	0.5	0.00112
MF setup	4.01	0.000506	108	0.05468
Air conditioner	2.41	0.000304	3744	1.138
			Total	**1.205**

5.4.2. Calculation of Indirect expenses

The majority of the indirect expenses are attributed to the depreciation costs, which is calculated by the straight-line depreciation method.

Table 5.12 Estimation of depreciation cost of all the equipments used

Equipment	Book value	Years of service life remaining	Hourly depreciation cost	Duration of use during fabrication (h)	Depreciation cost (USD)
Centrifuge	531.78	5	0.013429	4.66	0.062578
Vortex	31.30	3	0.001317	2	0.002635
Heating mantle	13.29	5	0.000336	6	0.002014
Hot air oven	483.44	10	0.006104	12	0.073248
Rota evaporator	1469.66	6	0.030927	0.5	0.015464
MF setup	423.01	10	0.005341	108	0.576832
Air conditioner	50.76	2	0.003205	3744	11.99782
				Total	**12.73059**

5.4.3. Calculation of equipment cost

In addition to these costs, the total expense will also cover the purchase of required equipment. The equipment cost will be calculated using the fixed capital cost, which includes all associated expenses like site preparation, handling and installation fees, utilities, and laboratory expenses. [235,237,238].

Table 5.13 Estimation of equipment cost of the equipments used

Equipment	Fixed capital cost (USD/year)	Hourly fixed capital cost (USD/h)	Duration of use (h)	Equipment cost (USD)
Centrifuge	386.07	0.0487	4.66	0.226
Vortex	37.87	0.00478	2	0.0095
Heating mantle	9.65	0.001218	6	0.00731
Hot air oven	175.48	0.02215	12	0.265
Rota evaporator	889.14	0.11226	0.5	0.056
MF setup	200.50	0.02531	108	2.734
Air conditioner	120.30	0.01518	3744	56.869
			Total cost	**60.169**

5.4.4. Calculation of total cost

Fabrication cost of one membrane = 0.29 USD

Since, membrane have a shelf life of 3 years, hence fabrication cost of single membrane per year = 0.096 USD/year

Total direct cost = (350.534 + 16.13 + 1.205 + 36.38 + 7.27) USD/year = 411.52 USD/year

Total indirect cost = (60.169 + 12.73 + 0.096) = 72.99 USD/year

Total cost = 411.52 + 72.99 = 484.51 USD/year

Total biomass produced per year = 69.12 g

Therefore, cost of 1 gram of biomass = 7.02 USD

The cost per head in percentage of the total cost at lab scale is depicted in pie diagram in Fig. 5.5.

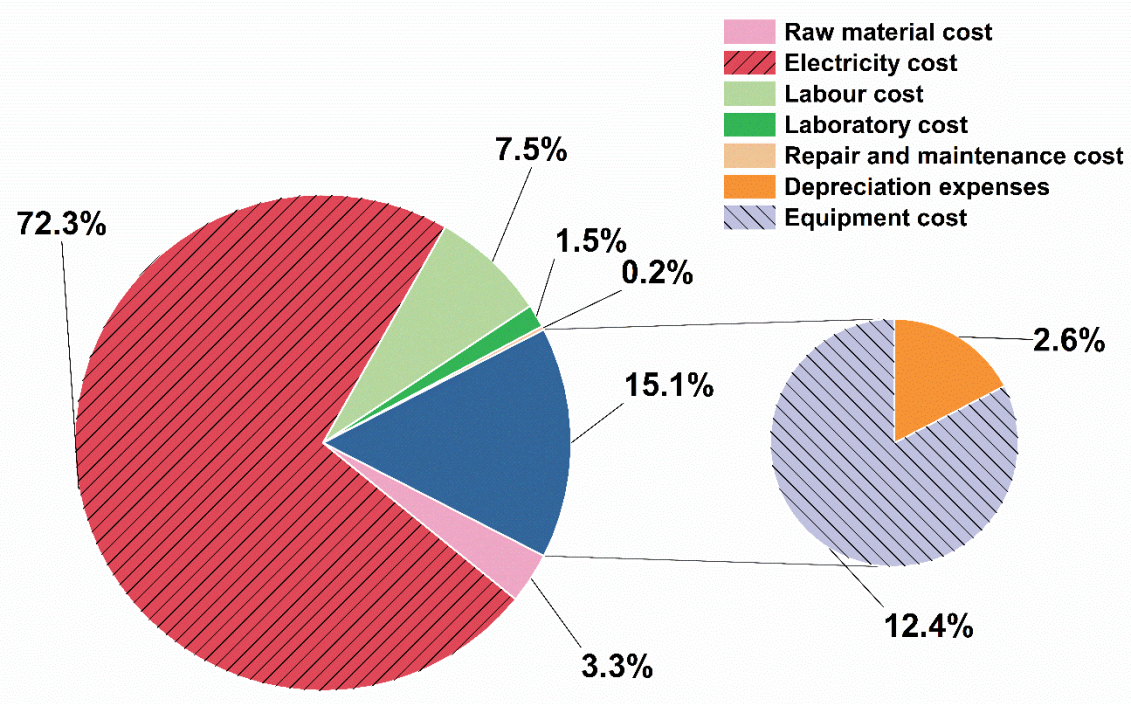

Fig. 5.5. Splitting of overall cost incurred in energy efficient recycle process at lab scale

5.5. Cost Estimation of the Developed Energy Efficient Recycle Process at Pilot Scale

Calculation basis:

1. 500 L of working volume in raceway pond was considered for each batch (BG11, R1, R2, R3).
2. One cycle consists of four batches.
3. Number of cycles processed annually: 6
4. The microfiltration permeation setup and all essential equipment utilized in the separation process are anticipated to have a durability of 10 years.
5. Each year will consist of 330 working days.
6. Commercial sodium nitrate and di-potassium hydrogen phosphate was used as the media instead of high cost BG11 media.
7. The culture density will be low than that of lab scale process.

The microfiltration setup for processing 500 L of culture will differ than that of lab scale setup. In this configuration, instead of a single housing for the membrane module, three parallel housings are employed, each measuring 900 mm in length. Each housing has the capacity to hold 7 membranes, resulting in a collective utilization of 21 membranes, all with a length of 900 mm. Importantly, both the inner and outer diameters of the membranes remain consistent. The membrane module was designed in such a way that the filtration experiment was completed within 24 hours with a flux of 5×10^{-3} m^3 m^{-2} s^{-1}.

The total membrane filtration area = $21\pi d_1 h = \pi \times 5 \times 10^{-3} \times 90 \times 10^{-2} = 0.296$ m^2

Table 5.14 Key assumptions and process details

	BG11	R1	R2	R3
Culture density (g L^{-1})	1.24	1.24	1.136	0.992
Biomass lipid content (wt.%)	31.4	30.57	29.41	28.16
Extraction efficiency (%)	85	85	85	85
Biomass per batch (g)	620	620	568	496
Annual biomass production (g)	3720	3720	3408	2976
Annual Lipid production (g)	1168.08	1137.20	1002.29	838.04

5.5.1. Calculation of direct cost

Raw material cost

While calculating the raw material cost, the commercial cost of sodium nitrate, di-potassium hydrogen phosphate, powdered activated carbon, methanol, n-hexane, sulphuric acid and sodium hydroxide was taken into consideration. Additionally, the protocol for transesterification process as well as for FAME production remains same as mentioned earlier. Table 5.15 summarizes the quantity of raw material used annually along with its cost.

Table 5.15 Summary of raw material cost for energy efficient recycle process at lab scale

Raw material	Quantity	Unit Price (INR)	Quantity used	Cost	
				INR	USD
Sodium nitrate	1 Kg	40	13.95 Kg	558	6.74
Di-potassium hydrogen phosphate	1 Kg	135	0.48 Kg	64.8	0.78
Powdered activated carbon	1 Kg	20	0.09 Kg	1.8	0.021
Methanol	1 L	30	152 L	4560	55.11
n-Hexane	1 L	60	69 L	4140	50.03
Sulphuric acid	1 L	15	62.18 mL	0.93	0.011
Sodium hydroxide	1 Kg	40	62.18 g	2.48	0.029
			Total cost	**9328.01**	**112.74**

Electricity cost

Paddle wheel

Paddle wheel in the raceway pond is used to mix the microalgal culture evenly throughout the year. It will also be used for mixing PAC with the effluent based media.

Power rating of paddle wheel = 0.5 HP = 0.372 kW

Number of hours of operation for culturing = (13 × 4 × 6 × 24) hrs = 7488 h

Number of hours of operation for PAC treatment (12 h / cycle) = (12 × 3 × 6) = 216 h

Hence, power consumption by paddle wheel = 0.372 × 7704 × 7.25 = 20777.68 INR = 251.12 USD/year

Air pump

Power rating of aquarium air pump = 3 W = 0.003 kW

Number of hours of operation = (13 × 4 × 6 × 24) h = 7488 h

Hence, power consumption by air pump = 0.003 × 1248 × 7.25 = 162.86 INR = 1.96 USD/year.

Booster pump

In the pilot scale microalgal harvesting, the process spans twenty-four hours, with extra hours for cleaning the membrane and setup.

In one cycle of experiment, the MF setup will be run 4 times (for BG11, R1, R2, R3)

Number of runs annually = 4 × 6 = 24

Hence, total number of working hours of pump = 26 × 24 = 624 h

Power rating of pump = 80 W

Power consumption cost = 0.08 × 624 × 7.25 = 361.92 INR = 4.37 USD/year

Centrifuge

Power rating of centrifuge = 120 W

The PAC treated media will undergo settling in the raceway pond overnight. Subsequently, the supernatant will be separated using capillary action. The approximately remaining 10 L of PAC treated media will then be centrifuged to recover the PAC for the next cycle of experiment.

The centrifuge was used for separating powdered activated carbon from the treated cultures (R1, R2 and R3) for 15 mins. However, the capacity of centrifuge is 2 L.

Hence, number of times it was used annually = 3 × 6 =18 times

Duration of use of centrifuge for single run = (15 × 5) minutes = 75 minutes

Duration of use = 75 × 18 = 1350 minutes = 22.5 h

Also, it will be used during transesterification for 10 mins = 0.16 h

Therefore, total duration of use of centrifuge for the entire process = 22.66 h

Therefore, total cost of power consumption of centrifuge = 0.120 × 22.66 ×7.25 = 19.71 INR

= 0.238 USD/year

Hot air oven

Heating coil capacity of hot air oven = 1.5 kW

Oven was used at 80 ºC for 12 hours for drying the microalgal biomass.

Hence, the total power consumption cost of oven = (1.5 × 12 × 7.25) INR = 130.5 INR = 1.57 USD/year.

Industrial stirrer

Power rating of stirring equipment = 0.5 HP = 0.372 kW

Stirrer was used for 2 hrs during lipid extraction from dried microalgal biomass

Hence, cost of power consumption of stirrer = (0.372 × 2 × 7.25) INR = 5.39 INR/year

= 0.065 USD/year

LED flood lights

Power rating of one light = 100W

Number of lights used during microalgal culturing = 4

Total number of days in use = 13 × 4 × 6 = 312 days

Total number of hours in use = 312 × 16 = 4992 h (16 h: 8 h of light: dark period)

Therefore, power consumption cost due to light = 0.10 × 4992 × 7.25 = 3619.2 INR

= 43.74 USD/year

Rota evaporator

Power rating of Rota evaporator = 900 W

Rota evaporator will be used approximately 5 times for 30 mins (0.5 h) to separate lipid-solvent mixtures after lipid extraction step.

Hence, cost of power consumption due to Rota evaporator = 0.9 × 0.5 × 5 × 7.25 = 16.3 INR = 0.197 USD/year

Heating mantle

Power rating of heating mantle = 300 W

Duration of use = 6 h

However, to process higher amount of lipid in pilot scale, the heating mantle will be used approximately 5 times.

Hence, cost of power consumption due to heating mantle = 0.3 × 6 × 5 × 7.25 = 65.25 INR = 0.788 USD/year.

Total cost of electricity consumption during the entire process = (251.12 + 1.96 + 4.37 + 0.238 + 1.57 + 0.065 + 43.74 + 0.197 + 0.788) USD/year = 304.04 USD/year.

Labor cost

Labor cost is considered to be 2% of the fixed capital cost incurred during microalgal harvesting.

Hence, labor cost = (2/100) × 3842.08 USD/year

= 76.84 USD/year

Laboratory cost

Laboratory cost is considered to be 20% of the labor cost incurred during microalgal harvesting.

Hence, laboratory cost = (20/100) × 76.84 USD/year

= 15.36 USD/year

Repair and Maintenance cost

The protocol for the calculation of repair and maintenance cost is mentioned in section 5.1.2. Table 5.16 summarizes the book value of all the equipments, which will be henceforth used for the calculation of fixed capital investment and hence the annual repair and maintenance cost. However, the repair and maintenance cost are entirely reliant on the equipment working hours. The detailed cost based on the working hours is summarized in Table 5.18.

Table 5.16 Estimation of book value of all the equipments used

Equipment	Original cost	Installation year	Used year(s) till 2022	Book value	
				INR	USD
Centrifuge	80,000	2017	5	44000	531.78
Stirrer	20,000	2022	0	20000	241.72
Heating mantle	2,000	2017	5	1100	13.29
Hot air oven	40,000	2022	0	40000	483.44
Rota evaporator	1,90,000	2018	4	121600	1469.66
MF setup	2,50,000	2022	0	2,50,000	3021.51
Raceway pond	75,000	2017	5	41250	498.54
Paddle wheel	55,500	2017	5	30525	368.92
Aerator and air pump	2,000	2017	5	1100	13.29

Table 5.17 Summary of annual repair and maintenance cost

Equipment	Book value (USD)	Lang Factor	Fixed capital investment (FCI)(USD)	Service life remaining	FCI/year	Annual repair and maintenance cost (USD/year)
Centrifuge	531.78	3.63	1930.36	5	386.07	7.72
Stirrer	241.72	4.74	1145.75	10	114.57	2.29
Heating mantle	13.29	3.63	48.24	5	9.64	0.19
Hot air oven	483.44	3.63	1754.88	10	175.48	3.50
Rota evaporator	1469.66	3.63	5334.86	6	889.14	17.78
MF setup	3021.51	4.74	14321.95	10	1432.19	28.64
Raceway pond	498.54	4.74	2363.07	5	472.61	9.45
Paddle wheel	368.92	4.74	1748.68	5	349.73	6.99
Aerator and air pump	13.29	4.74	62.99	5	12.59	0.25
				Total	**3842.07**	**76.84**

Table 5.18 Summary of annual repair and maintenance cost based on process duration

Equipment	Annual repair and maintenance cost (USD/year)	Hourly repair and maintenance cost (USD/h)	Hours used (h)	Total repair and maintenance cost (USD)
Centrifuge	7.72	0.00097	22.66	0.02208
Stirrer	2.29	0.00028	2	0.000578
Heating mantle	0.19	2.39899×10^{-5}	30	0.000719
Hot air oven	3.50	0.00044	12	0.00530
Rota evaporator	17.78	0.002244	2.5	0.00561
MF setup	28.64	0.00361	624	2.2564
Raceway pond	9.45	0.001193	7488	8.9345
Paddle wheel	6.99	0.000882	7704	6.7993
Aerator and air pump	0.25	3.15657×10^{-5}	7488	0.2363
			Total	**18.26**

5.5.2. Calculation of Indirect expenses

The majority of the indirect expenses are attributed to the depreciation costs, which is calculated by the straight-line depreciation method.

Table 5.19 Estimation of depreciation cost of all the equipments used

Equipment	Book value	Years of service life remaining	Hourly depreciation cost	Duration of use (h)	Depreciation cost (USD)
Centrifuge	531.78	5	0.01342	22.66	0.30429
Stirrer	241.72	10	0.00305	2	0.00610
Heating mantle	13.29	5	0.000336	30	0.01006
Hot air oven	483.44	10	0.00610	12	0.07324
Rota evaporator	1469.66	6	0.030927	2.5	0.07731
MF setup	3021.51	10	0.03815	624	23.8058
Raceway pond	498.54	5	0.01258	7488	94.2693
Paddle wheel	368.92	5	0.00931	7704	71.7717
Aerator and air pump	13.29	5	0.00033	7488	2.51301
				Total	**192.83**

5.5.3. Calculation of equipment cost

In addition to these costs, the total expense will also cover the purchase of required equipment. The equipment cost will be calculated using the fixed capital cost, which includes all associated expenses like site preparation, handling and installation fees, utilities, and laboratory expenses. [235,237,238].

Table 5.20 Estimation of cost of the equipments used

Equipment	Fixed capital cost (USD/year)	Hourly fixed capital cost (USD/h)	Duration of use (h)	Equipment cost (USD)
Centrifuge	386.07	0.0487	22.66	1.1045
Stirrer	114.57	0.0144	2	0.0289
Heating mantle	9.64	0.00121	30	0.0365
Hot air oven	175.48	0.0221	12	0.2658
Rota evaporator	889.14	0.1122	2.5	0.2806
MF setup	1432.19	0.1808	624	112.83
Raceway pond	472.61	0.0596	7488	446.83
Paddle wheel	349.73	0.0441	7704	340.19
Aerator and air pump	12.59	0.00158	7488	11.90
			Total cost	**913.48**

5.5.4. Calculation of total cost

Fabrication cost per m^2 of membrane = 190.93 USD

Hence, fabrication cost for 0.296 m^2 of membrane filtration area = 56.51 USD

The capital cost of membrane fabrication per year (with 3 years of service life) = 18.83 USD/year

Total direct cost = (112.74 + 304.04 + 76.84 + 15.36 + 18.26) USD/year = 527.24 USD/year

Total indirect cost = (192.83 + 913.48 + 18.83) = 1125.14 USD/year

Total cost = 527.24 + 1125.14 = 1652.38 USD/year

Total biomass produced per year = 13824 g

Therefore, cost of 1 gram of biomass = 0.1195 USD

The cost per head in percentage of the total cost at pilot scale is depicted in pie diagram in Fig. 5.6.

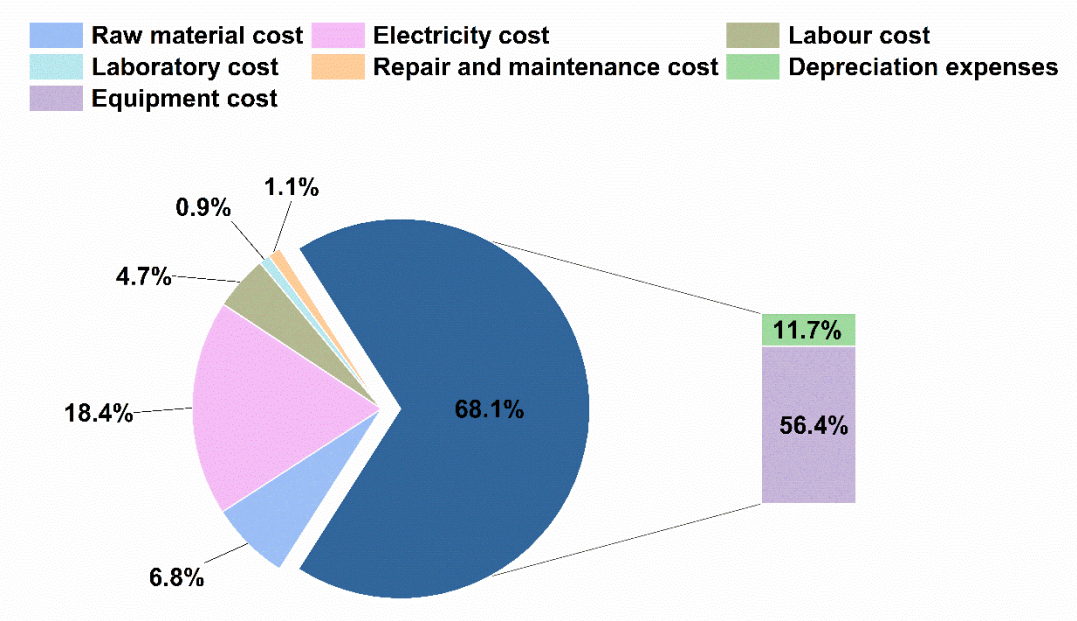

Fig. 5.6. Splitting of overall cost incurred in energy efficient recycle process at lab scale

5.6. Summary

The economic feasibility of low-cost membrane fabrication, microalgal harvesting using the developed membrane and the energy efficient recycle process has been successfully assessed. The initial phase of cost estimation begins with assessing the expenses involved in membrane fabrication, which encompasses equipment costs and manufacturing expenses. The projected cost per square meter of membrane stands at 190.93 USD, falling within the category of low-cost membranes.

Following this, the subsequent stage of cost estimation involves evaluating the cost of microalgal harvesting using the low-cost tubular kaolin membrane, both in lab scale as well as pilot scale. The lab scale setup consists of a single membrane with an effective filtration area of 15.71×10^{-4} m^2, while the pilot scale comprises three parallel membrane housings, each

containing seven membranes, with an effective filtration area of 0.0989 m^2. For the lab scale process, the total cost of harvesting one litre of microalgal culture was estimated to be 0.648 USD/L which lowered to 0.04 USD/L for the pilot scale harvesting setup.

The final step of cost estimation involved the energy efficient recycle process, both in lab scale as well as pilot scale. The cost per gram of biomass was calculated to be 7.02 USD/g for the lab scale configuration while it dropped to 0.1195 USD/g for the pilot scale setup.

Chapter 6

Conclusions, Social Impact and Future Prospect

CHAPTER 6

Conclusions, Social Impact and Future Prospects

This section encapsulates the conclusions drawn from the research conducted in this thesis, along with offering suggestions for future research based on the groundwork laid out in this study. The primary objective of this study was to develop a low-cost tubular ceramic membrane using naturally available kaolin clay as the key precursor. Subsequently, the optimized membrane composition was employed in microalgal harvesting of Monoraphidium sp. KMC4. Additionally, the harvested effluent was treated using powdered activated carbon to develop a sustainable and energy efficient recycle process. All significant findings observed during the membrane fabrication, microalgal harvesting and energy efficient recycle process are detailed in this chapter.

6.1. Conclusions

- Indigenous low-cost disc and tubular membranes were fabricated using kaolin as the key precursor. Since fabrication of tubular membrane require excess of main raw material, hence initially disc membranes were fabricated to optimize the binder concentration, thus, simultaneously avoided excess usage of kaolin and binders.
- In case of disc membranes, by increasing the binder concentration from 8% to 20%, there was a notable decrease in percentage porosity, average pore size, and water permeability. As a result, the optimal binder percentage was identified as 8%, comprising 2% boric acid, 2% sodium metasilicate, and 4% sodium carbonate. Further, using this optimized binder concentration tubular membranes were fabricated.
- The fabricated tubular membranes had porosity of ~26% - 47%, a pore diameter of 0.123-0.182 µm, water permeability of 4.2×10^{-8} – 17.1×10^{-8} m^3 m^{-2} s^{-1} kPa^{-1}, along with good mechanical and chemical strength.

- The optimized membrane (77% kaolin, 2% boric acid, 2% sodium metasilicate, 4% sodium carbonate, and 15% calcium carbonate) was tested for microfiltration of microalgae *Monoraphidium* sp. KMC4 with 1.5 g L^{-1} of initial concentration at a persistent cross-flow rate (1.11×10^{-5} m^3 s^{-1}) and various transmembrane pressures (69 kPa - 345 kPa).
- The separation results yielded an average permeate flux of 1.85×10^{-5} m^3 m^{-2} s^{-1} at an optimized transmembrane pressure of 276 kPa. The corresponding volume reduction factor and permeate recovery were 1.38% and 28.17%, respectively. Complete algal cell recovery and substantial nutrient passage (>88%) were observed within the pressure range of 69 kPa to 345 kPa.
- Fouling mechanism was explained by fitting four distinct pore-blocking models, of which the cake filtration model provided the most accurate fit as compared to the complete, intermediate and standard pore-blocking models. Additionally, the total organic carbon varied in the range of 31.6-63.2 mg L^{-1}. This essentially explained the source of pore blocking. The elongated shape of *Monoraphidium sp.* KMC4 might have contributed to the enhanced fouling of membrane.
- The nitrate passage was almost complete (~88% - 97%), highlighting the prospects of permeate stream in further cultivation process.
- The suitability of cultivating *Monoraphidium* sp. KMC4 was exhibited in different membrane harvested effluent media concentrations (E10-E70), the latter being treated with powdered activated carbon (PAC) with a loading of 5-50 mg L^{-1}.
- The optimum EBC media (TE30) treated with 30 mg L^{-1} PAC enhanced the biomass yield by 21.9% as compared to the untreated E30 (1.21 g L^{-1}).
- A recyclability study of TE30 performed in five batches resulted in an optimal growth up to three batches with an overall biomass yield of 4.21 g and a total water savings of 30%.

- ❖ Additionally, physico-chemical characterization and FAME profile of the biomass from recyclability study validated the energy potential of feedstock.
- ❖ Moreover, a biorefinery model was proposed which could recover nutrient rich liquid effluent (3.1 million litre) and solid residue for various applications along with the generation of 5,760 kg of biomass followed by 113 L d^{-1} biodiesel yield.
- ❖ Lastly, a detailed cost analysis of membrane fabrication was successfully assessed. The projected cost per square meter of membrane stands at 190.93 USD, falling within the category of low-cost membranes.
- ❖ Subsequently, the economic assessment was also done for microalgal harvesting using the fabricated membrane and for the energy efficient recycle process, both in lab scale and pilot scale. In both scenarios, it was determined that the processes were economically viable for implementation in industrial separation operations.

6.2. Social Impact

The social impact of a research is closely related to the UN's Sustainable Development Goals (SDGs) as it directly addresses social challenges and promotes positive changes in various areas. The work carried out in this thesis contributes to several Sustainable Development goals as highlighted in Table 6.1.

Table 6.1 Sustainable Development Goals addressed in the present study

Sl. No.	Sustainable Development Goals	Remarks
1		• Membrane-based microalgal harvesting can help in wastewater treatment and purification processes, thus promoting access to clean water. • Recycling microalgal harvested effluent reduces the demand for freshwater resources and promotes sustainable water management.

2

- Microalgae can be utilized as a feedstock for biofuel production, contributing to the development of affordable and clean energy sources.

3

- Utilizing kaolin, a readily available natural resource in membrane fabrication, promotes innovation in materials science and infrastructure development for sustainable production processes.
- Innovations in membrane technology for microalgal harvesting contribute to advancements in industrial processes and infrastructure.

4

- Kaolin-based membrane fabrication promotes responsible consumption by utilizing a low-cost, abundant material, reducing the environmental footprint associated with manufacturing processes.
- Using low-cost membranes for microalgal harvesting promotes efficient resource use.
- Recycling effluent reduces waste regeneration thereby promoting responsible use.

5

- Kaolin-based membrane fabrication may lead to lower carbon emissions in comparison to processes that rely on more intensive and environmentally harmful materials.
- Use of low-cost membranes reduces the environmental footprint of harvesting processes.

6

- Recycle effluent helps in preserving marine ecosystems by preventing the discharge of harmful contaminants into water bodies.
- Microalgae play a crucial role in marine ecosystems, and sustainable harvesting practices help in preserving biodiversity and marine life.

7

- Utilizing kaolin, a naturally available raw material, reduces the necessity for land disruption associated with the extraction of alternative raw materials.
- By preventing the release of contaminants into the environment, recycling microalgal harvested effluent supports terrestrial ecosystem.

6.3. Future Prospects

- Witnessing the exceptional separation efficiency of the developed tubular microfiltration membrane in microalgal harvesting, there exists a potential to expand its versatility in other liquid phase separation processes.
- Since the fabricated membrane is solely capable of performing microfiltration operations, its utility can be expanded to ultrafiltration and nanofiltration processes. Various coating methods can be employed to modify the membrane, forming a composite structure with one or multiple active layers featuring a narrower pore size distribution across the support membrane. The membranes can then be used for the removal of viruses, bacteria and dissolved organic compounds. The nanofiltration membrane can also be used to valorize the aqueous phase of hydrothermal liquefaction of wet microalgal biomass.
- The results of the pilot plant study of the considered in-house setup is quite promising. Hence, the developed energy efficient process can be used to produce microalgal biomass in pilot scale and for industrial scale applications.

REFERENCES

[1] Z. Lu, S. Loftus, J. Sha, W. Wang, M.S. Park, X. Zhang, Z.I. Johnson, Q. Hu, Water reuse for sustainable microalgae cultivation: Current knowledge and future directions, Resour Conserv Recycl 161 (2020). https://doi.org/10.1016/j.resconrec.2020.104975.

[2] H. Bechhold, Kolloidstudien mit der Filtrationsmethode, Zeitschrift Für Physikalische Chemie 60U (1907) 257–318. https://doi.org/10.1515/zpch-1907-6013.

[3] S. LOEB, S. SOURIRAJAN, Sea Water Demineralization by Means of an Osmotic Membrane, in: 1963: pp. 117–132. https://doi.org/10.1021/ba-1963-0038.ch009.

[4] H.K. Lonsdale, Review THE GROWTH OF MEMBRANE TECHNOLOGY, 1982.

[5] M.B. Asif, Z. Zhang, Ceramic membrane technology for water and wastewater treatment: A critical review of performance, full-scale applications, membrane fouling and prospects, Chemical Engineering Journal 418 (2021). https://doi.org/10.1016/j.cej.2021.129481.

[6] S.P. Nunes, K. Peinemann, eds., Membrane Technology, Wiley, 2001. https://doi.org/10.1002/3527600388.

[7] S.K. Hubadillah, M.R. Jamalludin, M.H. Dzarfan Othman, Y. Iwamoto, Recent progress on low-cost ceramic membrane for water and wastewater treatment, Ceram Int 48 (2022) 24157–24191. https://doi.org/10.1016/j.ceramint.2022.05.255.

[8] A. Manni, B. Achiou, A. Karim, A. Harrati, C. Sadik, M. Ouammou, S. Alami Younssi, A. El Bouari, New low-cost ceramic microfiltration membrane made from natural magnesite for industrial wastewater treatment, J Environ Chem Eng 8 (2020). https://doi.org/10.1016/j.jece.2020.103906.

[9] Y.S. Polyakov, A.L. Zydney, Ultrafiltration membrane performance: Effects of pore blockage/constriction, J Memb Sci 434 (2013) 106–120. https://doi.org/10.1016/j.memsci.2013.01.052.

[10] A.W. Mohammad, Y.H. Teow, W.L. Ang, Y.T. Chung, D.L. Oatley-Radcliffe, N. Hilal, Nanofiltration membranes review: Recent advances and future prospects, Desalination 356 (2015) 226–254. https://doi.org/10.1016/j.desal.2014.10.043.

[11] K.P. Lee, T.C. Arnot, D. Mattia, A review of reverse osmosis membrane materials for desalination-Development to date and future potential, J Memb Sci 370 (2011) 1–22. https://doi.org/10.1016/j.memsci.2010.12.036.

[12] D.M. Warsinger, S. Chakraborty, E.W. Tow, M.H. Plumlee, C. Bellona, S. Loutatidou, L. Karimi, A.M. Mikelonis, A. Achilli, A. Ghassemi, L.P. Padhye, S.A. Snyder, S. Curcio, C.D. Vecitis, H.A. Arafat, J.H. Lienhard, A review of polymeric membranes and processes for potable water reuse, Prog Polym Sci 81 (2018) 209–237. https://doi.org/10.1016/j.progpolymsci.2018.01.004.

[13] Y. Dong, H. Wu, F. Yang, S. Gray, Cost and efficiency perspectives of ceramic membranes for water treatment, Water Res 220 (2022). https://doi.org/10.1016/j.watres.2022.118629.

[14] C.J. Kurth, B.L. Wise, S. Smith, Design considerations for implementing ceramics in new and existing polymeric UF systems, Water Pract Technol 13 (2018) 725–737. https://doi.org/10.2166/wpt.2018.081.

[15] M. Wilf, Membrane Types and Factors Affecting Membrane Performance, 2008.

[16] Z. He, Z. Lyu, Q. Gu, L. Zhang, J. Wang, Ceramic-based membranes for water and wastewater treatment, Colloids Surf A Physicochem Eng Asp 578 (2019). https://doi.org/10.1016/j.colsurfa.2019.05.074.

[17] S.K. Hubadillah, M.H.D. Othman, T. Matsuura, A.F. Ismail, M.A. Rahman, Z. Harun, J. Jaafar, M. Nomura, Fabrications and applications of low cost ceramic membrane from kaolin: A comprehensive review, Ceram Int 44 (2018) 4538–4560. https://doi.org/10.1016/j.ceramint.2017.12.215.

[18] D. El Machtani Idrissi, Z.C. Elidrissi, B. Achiou, M. Ouammou, S. Alami Younssi, Fabrication of low-cost kaolinite/perlite membrane for microfiltration of dairy and textile wastewaters, J Environ Chem Eng 11 (2023) 109281. https://doi.org/10.1016/j.jece.2023.109281.

[19] A. Agarwalla, K. Mohanty, Comprehensive characterization, development, and application of natural/Assam Kaolin-based ceramic microfiltration membrane, Mater Today Chem 23 (2022) 100649. https://doi.org/10.1016/j.mtchem.2021.100649.

[20] M. Rafya, W. Misrar, L. Saâdi, M. Mansori, M. Waqif, A. Hafidi, N. Zehhar, F. Benkhalti, Ceramic membrane support based on kaolin and solid waste from hydrodistillation of Rosmarinus officinalis L, Mater Chem Phys 295 (2023). https://doi.org/10.1016/j.matchemphys.2022.127030.

[21] P. Singh, N.A. Manikandan, M. Purnima, K. Pakshirajan, G. Pugazhenthi, Recovery of lignin from water and methanol using low-cost kaolin based tubular ceramic membrane, Journal of Water Process Engineering 38 (2020) 101615. https://doi.org/10.1016/j.jwpe.2020.101615.

[22] S. Emani, R. Uppaluri, M.K. Purkait, Cross fl ow micro fi ltration of oil – water emulsions using kaolin based low cost ceramic membranes, DES 341 (2014) 61–71. https://doi.org/10.1016/j.desal.2014.02.030.

[23] I. Hedfi, N. Hamdi, M.A. Rodriguez, E. Srasra, Development of a low cost micro-porous ceramic membrane from kaolin and Alumina, using the lignite as porogen agent, Ceram Int 42 (2016) 5089–5093. https://doi.org/10.1016/j.ceramint.2015.12.023.

[24] J. Schwinge, P.R. Neal, D.E. Wiley, D.F. Fletcher, A.G. Fane, Spiral wound modules and spacers: Review and analysis, J Memb Sci 242 (2004) 129–153. https://doi.org/10.1016/j.memsci.2003.09.031.

[25] G. Li, W. Kujawski, R. Válek, S. Koter, A review - The development of hollow fibre membranes for gas separation processes, International Journal of Greenhouse Gas Control 104 (2021). https://doi.org/10.1016/j.ijggc.2020.103195.

[26] W.A. Meulenberg, F. Schulze-Küppers, W. Deibert, T. Van Gestel, S. Baumann, Ceramic Membranes: Materials – Components – Potential Applications, ChemBioEng Reviews 6 (2019) 198–208. https://doi.org/10.1002/cben.201900022.

[27] A. Abdullayev, M.F. Bekheet, D.A.H. Hanaor, A. Gurlo, Materials and applications for low-cost ceramic membranes, Membranes (Basel) 9 (2019). https://doi.org/10.3390/membranes9090105.

[28] S.L. Sandhya Rani, R.V. Kumar, Insights on applications of low-cost ceramic membranes in wastewater treatment: A mini-review, Case Studies in Chemical and Environmental Engineering 4 (2021). https://doi.org/10.1016/j.cscee.2021.100149.

[29] P. Monash, G. Pugazhenthi, P. Saravanan, Various fabrication methods of porous ceramic supports for membrane applications, Reviews in Chemical Engineering 29 (2013) 357–383. https://doi.org/10.1515/revce-2013-0006.

[30] D. Liang, J. Huang, H. Zhang, H. Fu, Y. Zhang, H. Chen, Influencing factors on the performance of tubular ceramic membrane supports prepared by extrusion, Ceram Int 47 (2021) 10464–10477. https://doi.org/10.1016/j.ceramint.2020.12.235.

[31] R. Vinoth Kumar, A. Kumar Ghoshal, G. Pugazhenthi, Elaboration of novel tubular ceramic membrane from inexpensive raw materials by extrusion method and its performance in microfiltration of synthetic oily wastewater treatment, J Memb Sci 490 (2015) 92–102. https://doi.org/10.1016/j.memsci.2015.04.066.

[32] K. Lindqvist, E. Lid&, Preparation of Alumina Membranes by Tape Casting and Dip Coating, Elsevier Science Lmited, 1997.

[33] R.K. Nishihora, P.L. Rachadel, M.G.N. Quadri, D. Hotza, Manufacturing porous ceramic materials by tape casting—A review, J Eur Ceram Soc 38 (2018) 988–1001. https://doi.org/10.1016/j.jeurceramsoc.2017.11.047.

[34] Y. Tang, Y. Lin, D.M. Ford, X. Qian, M.R. Cervellere, P.C. Millett, X. Wang, A review on models and simulations of membrane formation via phase inversion processes, J Memb Sci 640 (2021). https://doi.org/10.1016/j.memsci.2021.119810.

[35] G.M. Urper, R. Sengur-Tasdemir, T. Turken, E. Ates Genceli, V. V. Tarabara, I. Koyuncu, Hollow fiber nanofiltration membranes: A comparative review of interfacial polymerization and phase inversion fabrication methods, Separation Science and Technology (Philadelphia) 52 (2017) 2120–2136. https://doi.org/10.1080/01496395.2017.1321668.

[36] L. Wang, B. Pan, Y. Gao, C. Li, J. Ye, L. Yang, Y. Chen, Q. Hu, X. Zhang, Efficient membrane microalgal harvesting: Pilot-scale performance and techno-economic analysis, J Clean Prod 218 (2019) 83–95. https://doi.org/10.1016/j.jclepro.2019.01.321.

[37] H. Susanto, M. Fitrianingtyas, L. Kurniawan, S. Rusli, I.N. Widiasa, Performance evaluation of flocculation and membrane filtration for microalgae harvesting, Pertanika J Sci Technol 25 (2017) 1159–1172.

[38] H. Elcik, M. Cakmakci, Harvesting microalgal biomass using crossflow membrane filtration: critical flux, filtration performance, and fouling characterization, Environmental Technology (United Kingdom) 38 (2017) 1585–1596. https://doi.org/10.1080/09593330.2016.1237560.

[39] M. Roy, K. Mohanty, A comprehensive review on microalgal harvesting strategies: Current status and future prospects, Algal Res 44 (2019) 101683. https://doi.org/10.1016/j.algal.2019.101683.

[40] M. Ghazvini, M. Kavosi, R. Sharma, M. Kim, A review on mechanical-based microalgae harvesting methods for biofuel production, Biomass Bioenergy 158 (2022) 106348. https://doi.org/10.1016/j.biombioe.2022.106348.

[41] N. Laraib, A. Hussain, A. Javid, T. Noor, Q. ul A. Ahmad, A. Chaudhary, M. Manzoor, M. Akmal, S.M. Bukhari, W. Ali, T.J. Choi, P.M. Schenk, Recent trends in microalgal harvesting: an overview, Springer Netherlands, 2022. https://doi.org/10.1007/s10668-021-01805-2.

[42] G. Singh, S.K. Patidar, Microalgae harvesting techniques: A review, J Environ Manage 217 (2018) 499–508. https://doi.org/10.1016/j.jenvman.2018.04.010.

[43] V.O. Mkpuma, N.R. Moheimani, H. Ennaceri, Microalgal dewatering with focus on filtration and antifouling strategies: A review, Algal Res 61 (2022) 102588. https://doi.org/10.1016/j.algal.2021.102588.

[44] S.K. Choi, J.Y. Lee, D.Y. Kwon, K.J. Cho, Settling characteristics of problem algae in the water treatment process, Water Science and Technology 53 (2006) 113–119. https://doi.org/10.2166/wst.2006.214.

[45] U. Suparmaniam, M.K. Lam, Y. Uemura, J.W. Lim, K.T. Lee, S.H. Shuit, Insights into the microalgae cultivation technology and harvesting process for biofuel production: A review, Renewable and Sustainable Energy Reviews 115 (2019) 109361. https://doi.org/10.1016/j.rser.2019.109361.

[46] Y.S.H. Najjar, A. Abu-Shamleh, Harvesting of microalgae by centrifugation for biodiesel production: A review, Algal Res 51 (2020). https://doi.org/10.1016/j.algal.2020.102046.

[47] M. Ghazvini, M. Kavosi, R. Sharma, M. Kim, A review on mechanical-based microalgae harvesting methods for biofuel production, Biomass Bioenergy 158 (2022). https://doi.org/10.1016/j.biombioe.2022.106348.

[48] C.A. Laamanen, G.M. Ross, J.A. Scott, Flotation harvesting of microalgae, Renewable and Sustainable Energy Reviews 58 (2016) 75–86. https://doi.org/10.1016/j.rser.2015.12.293.

[49] H. Zhang, X. Zhang, Microalgal harvesting using foam flotation: A critical review, Biomass Bioenergy 120 (2019) 176–188. https://doi.org/10.1016/j.biombioe.2018.11.018.

[50] L. Aditya, H.P. Vu, L.N. Nguyen, T.M.I. Mahlia, N.B. Hoang, L.D. Nghiem, Microalgae enrichment for biomass harvesting and water reuse by ceramic microfiltration membranes, J Memb Sci 669 (2023) 121287. https://doi.org/10.1016/j.memsci.2022.121287.

[51] D. Vasanth, G. Pugazhenthi, R. Uppaluri, Fabrication and properties of low cost ceramic microfiltration membranes for separation of oil and bacteria from its solution, J Memb Sci 379 (2011) 154–163. https://doi.org/10.1016/j.memsci.2011.05.050.

[52] K. Pirwitz, L. Rihko-Struckmann, K. Sundmacher, Comparison of flocculation methods for harvesting Dunaliella, Bioresour Technol 196 (2015) 145–152. https://doi.org/10.1016/j.biortech.2015.07.032.

[53] S.B. Ummalyma, A.K. Mathew, A. Pandey, R.K. Sukumaran, Harvesting of microalgal biomass: Efficient method for flocculation through pH modulation, Bioresour Technol 213 (2016) 216–221. https://doi.org/10.1016/j.biortech.2016.03.114.

[54] K.H. Min, D.H. Kim, M.R. Ki, S.P. Pack, Recent progress in flocculation, dewatering, and drying technologies for microalgae utilization: Scalable and low-cost harvesting process development, Bioresour Technol 344 (2022) 126404. https://doi.org/10.1016/j.biortech.2021.126404.

[55] N. Kumar, C. Banerjee, S. Negi, P. Shukla, Microalgae harvesting techniques: updates and recent technological interventions, Crit Rev Biotechnol 43 (2023) 342–368. https://doi.org/10.1080/07388551.2022.2031089.

[56] S.B. Ummalyma, E. Gnansounou, R.K. Sukumaran, R. Sindhu, A. Pandey, D. Sahoo, Bioflocculation: An alternative strategy for harvesting of microalgae – An overview, Bioresour Technol 242 (2017) 227–235. https://doi.org/10.1016/j.biortech.2017.02.097.

[57] M.R. Bilad, H.A. Arafat, I.F.J. Vankelecom, Membrane technology in microalgae cultivation and harvesting: A review, Biotechnol Adv 32 (2014) 1283–1300. https://doi.org/10.1016/j.biotechadv.2014.07.008.

[58] I.L.C. Drexler, D.H. Yeh, Membrane applications for microalgae cultivation and harvesting: a review, Rev Environ Sci Biotechnol 13 (2014) 487–504. https://doi.org/10.1007/s11157-014-9350-6.

[59] A. Mushtaq, H. Cho, M.A. Ahmed, M.S.U. Rehman, J.I. Han, A novel method for the fabrication of silver nanowires-based highly electro-conductive membrane with antifouling property for efficient microalgae harvesting, J Memb Sci 590 (2019) 117258. https://doi.org/10.1016/j.memsci.2019.117258.

[60] Z. Zhao, K. Muylaert, A. Szymczyk, I.F.J. Vankelecom, Harvesting microalgal biomass using negatively charged polysulfone patterned membranes: Influence of pattern shapes and mechanism of fouling mitigation, Water Res 188 (2021) 116530. https://doi.org/10.1016/j.watres.2020.116530.

[61] N.F.M. Khairuddin, A. Idris, L.W. Hock, Harvesting Nannochloropsis sp. using PES/MWCNT/LiBr membrane with good antifouling properties, Sep Purif Technol 212 (2019) 1–11. https://doi.org/10.1016/j.seppur.2018.11.013.

[62] N.I.M. Nawi, N.S.A. Halim, L.C. Lee, M.D.H. Wirzal, M.R. Bilad, N.A.H. Nordin, Z.A. Putra, Improved nylon 6,6 nanofiber membrane in a tilted panel filtration system for fouling control in microalgae harvesting, Polymers (Basel) 12 (2020). https://doi.org/10.3390/polym12020252.

[63] A. Eliseus, M.R. Bilad, N.A.H.M. Nordin, Z.A. Putra, M.D.H. Wirzal, Tilted membrane panel: A new module concept to maximize the impact of air bubbles for membrane fouling control in microalgae harvesting, Bioresour Technol 241 (2017) 661–668. https://doi.org/10.1016/j.biortech.2017.05.175.

[64] H. Ryu, H. Cho, E. Park, J.I. Han, Modeling of forward osmosis for microalgae harvesting, J Memb Sci 642 (2022) 119910. https://doi.org/10.1016/j.memsci.2021.119910.

[65] F. Volpin, H. Yu, J. Cho, C. Lee, S. Phuntsho, N. Ghaffour, J.S. Vrouwenvelder, H.K. Shon, Human urine as a forward osmosis draw solution for the application of microalgae dewatering, J Hazard Mater 378 (2019) 120724. https://doi.org/10.1016/j.jhazmat.2019.06.001.

[66] J. Son, M. Sung, H. Ryu, Y.K. Oh, J.I. Han, Microalgae dewatering based on forward osmosis employing proton exchange membrane, Bioresour Technol 244 (2017) 57–62. https://doi.org/10.1016/j.biortech.2017.07.086.

[67] H. Ryu, K. Kim, H. Cho, E. Park, Y.K. Chang, J.I. Han, Nutrient-driven forward osmosis coupled with microalgae cultivation for energy efficient dewatering of microalgae, Algal Res 48 (2020) 101880. https://doi.org/10.1016/j.algal.2020.101880.

[68] Y. Yang, X. Gao, Z. Li, Q. Wang, S. Dong, X. Wang, Z. Ma, L. Wang, X. Wang, C. Gao, Porous membranes in pressure-assisted forward osmosis: Flux behavior and potential applications, Journal of Industrial and Engineering Chemistry 60 (2018) 160–168. https://doi.org/10.1016/j.jiec.2017.10.054.

[69] Z. Zhao, K. Muylaert, I. F.J. Vankelecom, Applying membrane technology in microalgae industry: A comprehensive review, Renewable and Sustainable Energy Reviews 172 (2023) 113041. https://doi.org/10.1016/j.rser.2022.113041.

[70] I.B. Magalhães, J. Ferreira, J. de S. Castro, L.R. de Assis, M.L. Calijuri, Agro-industrial wastewater-grown microalgae: A techno-environmental assessment of open and closed systems, Science of the Total Environment 834 (2022). https://doi.org/10.1016/j.scitotenv.2022.155282.

[71] I.L.C. Drexler, D.H. Yeh, Membrane applications for microalgae cultivation and harvesting: a review, Rev Environ Sci Biotechnol 13 (2014) 487–504. https://doi.org/10.1007/s11157-014-9350-6.

[72] M. Roy, K. Mohanty, A comprehensive review on microalgal harvesting strategies: Current status and future prospects, Algal Res 44 (2019) 101683. https://doi.org/10.1016/j.algal.2019.101683.

[73] N. Kumar, C. Banerjee, S. Negi, P. Shukla, Microalgae harvesting techniques: updates and recent technological interventions, Crit Rev Biotechnol 43 (2023) 342–368. https://doi.org/10.1080/07388551.2022.2031089.

[74] N. Laraib, A. Hussain, A. Javid, T. Noor, Q. ul A. Ahmad, A. Chaudhary, M. Manzoor, M. Akmal, S.M. Bukhari, W. Ali, T.J. Choi, P.M. Schenk, Recent trends in microalgal harvesting: an overview, Springer Netherlands, 2022. https://doi.org/10.1007/s10668-021-01805-2.

[75] L. Amer, B. Adhikari, J. Pellegrino, Technoeconomic analysis of five microalgae-to-biofuels processes of varying complexity, Bioresour Technol 102 (2011) 9350–9359. https://doi.org/10.1016/j.biortech.2011.08.010.

[76] F. Fasaei, J.H. Bitter, P.M. Slegers, A.J.B. van Boxtel, Techno-economic evaluation of microalgae harvesting and dewatering systems, Algal Res 31 (2018) 347–362. https://doi.org/10.1016/j.algal.2017.11.038.

[77] W. Mo, L. Soh, J.R. Werber, M. Elimelech, J.B. Zimmerman, Application of membrane dewatering for algal biofuel, Algal Res 11 (2015) 1–12. https://doi.org/10.1016/j.algal.2015.05.018.

[78] R. Castro-Muñoz, O. García-Depraect, Membrane-based harvesting processes for microalgae and their valuable-related molecules: A review, Membranes (Basel) 11 (2021) 1–21. https://doi.org/10.3390/membranes11080585.

[79] V.O. Mkpuma, N.R. Moheimani, H. Ennaceri, Microalgal dewatering with focus on filtration and antifouling strategies: A review, Algal Res 61 (2022) 102588. https://doi.org/10.1016/j.algal.2021.102588.

[80] S. Wang, F. Ortiz Tena, R. Dey, C. Thomsen, C. Steinweg, D. Kraemer, A.D. Grossman, Y.Z. Belete, R. Bernstein, A. Gross, S. Leu, S. Boussiba, L. Thomsen, C. Posten, Submerged hollow-fiber-ultrafiltration for harvesting microalgae used for bioremediation of a secondary wastewater, Sep Purif Technol 289 (2022) 120744. https://doi.org/10.1016/j.seppur.2022.120744.

[81] H. Zhou, C. Ji, J. Li, Y. Hu, X. Xu, Y. An, Understanding the interaction mechanism of algal cells and soluble algal products foulants in forward osmosis dewatering, J Memb Sci 620 (2021) 118835. https://doi.org/10.1016/j.memsci.2020.118835.

[82] Q. Zhou, Y. Yang, X. Wang, Q. Wang, S. Wang, X. Gao, C. Gao, Harvesting Microalgae Biomass Using Sulfonated Polyethersulfone (SPES)/PES Porous Membranes in Forward Osmosis Processes, Journal of Ocean University of China 19 (2020) 1345–1352. https://doi.org/10.1007/s11802-020-4382-8.

[83] Z. Zhao, J. Blockx, K. Muylaert, W. Thielemans, A. Szymczyk, I.F.J. Vankelecom, Exploiting flocculation and membrane filtration synergies for highly energy-efficient, high-yield microalgae harvesting, Sep Purif Technol 296 (2022) 121386. https://doi.org/10.1016/j.seppur.2022.121386.

[84] M.T. Hung, J.C. Liu, Microfiltration of microalgae in the presence of rigid particles, Sep Purif Technol 198 (2018) 10–15. https://doi.org/10.1016/j.seppur.2016.10.063.

[85] M. Purnima, N. Arul Manikandan, K. Pakshirajan, G. Pugazhenthi, Recovery of microalgae from its broth solution using kaolin based tubular ceramic membranes prepared with different binders, Sep Purif Technol 250 (2020) 117212. https://doi.org/10.1016/j.seppur.2020.117212.

[86] B. Zhang, C. Peng, S. Zhang, M. Zhang, D. Li, X. Wang, B. Mao, Comprehensive analysis of the combined flocculation and filtration process for microalgae harvesting at various operating parameters, Science of the Total Environment 857 (2023) 159658. https://doi.org/10.1016/j.scitotenv.2022.159658.

[87] F. Ricceri, M. Malaguti, C. Derossi, M. Zanetti, V. Riggio, A. Tiraferri, Microalgae biomass concentration and reuse of water as new cultivation medium using ceramic membrane filtration, Chemosphere 307 (2022) 135724. https://doi.org/10.1016/j.chemosphere.2022.135724.

[88] Z. Zhao, K. Muylaert, I.F.J. Vankelecom, Combining patterned membrane filtration and flocculation for economical microalgae harvesting, Water Res 198 (2021) 117181. https://doi.org/10.1016/j.watres.2021.117181.

[89] Z. Zhao, K. Muylaert, A. Szymczyk, I.F.J. Vankelecom, Harvesting microalgal biomass using negatively charged polysulfone patterned membranes: Influence of pattern shapes and mechanism of fouling mitigation, Water Res 188 (2021) 116530. https://doi.org/10.1016/j.watres.2020.116530.

[90] R. Huang, Z. Liu, B. Yan, Y. Li, H. Li, D. Liu, P. Wang, F. Cui, W. Shi, Layer-by-layer assembly of high negatively charged polycarbonate membranes with robust antifouling property for microalgae harvesting, J Memb Sci 595 (2020) 117488. https://doi.org/10.1016/j.memsci.2019.117488.

[91] L. Hua, H. Cao, Q. Ma, X. Shi, X. Zhang, W. Zhang, Microalgae Filtration Using an Electrochemically Reactive Ceramic Membrane: Filtration Performances, Fouling Kinetics, and Foulant Layer Characteristics, Environ Sci Technol 54 (2020) 2012–2021. https://doi.org/10.1021/acs.est.9b07022.

[92] M.T. Hung, J.C. Liu, Microfiltration of microalgae in the presence of rigid particles, Sep Purif Technol 198 (2018) 10–15. https://doi.org/10.1016/j.seppur.2016.10.063.

[93] A.K. Fard, G. McKay, A. Buekenhoudt, H. Al Sulaiti, F. Motmans, M. Khraisheh, M. Atieh, Inorganic membranes: Preparation and application for water treatment and desalination, Materials 11 (2018). https://doi.org/10.3390/ma11010074.

[94] H. Elcik, M. Cakmakci, Harvesting microalgal biomass using crossflow membrane filtration: critical flux, filtration performance, and fouling characterization, Environmental Technology (United Kingdom) 38 (2017) 1585–1596. https://doi.org/10.1080/09593330.2016.1237560.

[95] M.R. Bilad, A.S. Azizo, M.D.H. Wirzal, L. Jia Jia, Z.A. Putra, N.A.H.M. Nordin, M.O. Mavukkandy, M.J.F. Jasni, A.R.M. Yusoff, Tackling membrane fouling in microalgae filtration using nylon 6,6 nanofiber membrane, J Environ Manage 223 (2018) 23–28. https://doi.org/10.1016/j.jenvman.2018.06.007.

[96] T. De Baerdemaeker, B. Lemmens, C. Dotremont, J. Fret, L. Roef, K. Goiris, L. Diels, Benchmark study on algae harvesting with backwashable submerged flat panel membranes, Bioresour Technol 129 (2013) 582–591. https://doi.org/10.1016/j.biortech.2012.10.153.

[97] J.Y. Li, Z.Y. Ni, Z.Y. Zhou, Y.X. Hu, X.H. Xu, L.H. Cheng, Membrane fouling of forward osmosis in dewatering of soluble algal products: Comparison of TFC and CTA membranes, J Memb Sci 552 (2018) 213–221. https://doi.org/10.1016/j.memsci.2018.02.006.

[98] T. Hwang, M.R. Kotte, J.I. Han, Y.K. Oh, M.S. Diallo, Microalgae recovery by ultrafiltration using novel fouling-resistant PVDF membranes with in situ PEGylated polyethyleneimine particles, Water Res 73 (2015) 181–192. https://doi.org/10.1016/j.watres.2014.12.002.

[99] C. Nurra, E. Clavero, J. Salvadó, C. Torras, Vibrating membrane filtration as improved technology for microalgae dewatering, Bioresour Technol 157 (2014) 247–253. https://doi.org/10.1016/j.biortech.2014.01.115.

[100] N.F.M. Khairuddin, A. Idris, L.W. Hock, Harvesting Nannochloropsis sp. using PES/MWCNT/LiBr membrane with good antifouling properties, Sep Purif Technol 212 (2019) 1–11. https://doi.org/10.1016/j.seppur.2018.11.013.

[101] H. Susanto, M. Fitrianingtyas, L. Kurniawan, S. Rusli, I.N. Widiasa, Performance evaluation of flocculation and membrane filtration for microalgae harvesting, Pertanika J Sci Technol 25 (2017) 1159–1172.

[102] F. Zhao, H. Chu, Z. Yu, S. Jiang, X. Zhao, X. Zhou, Y. Zhang, The filtration and fouling performance of membranes with different pore sizes in algae harvesting, Science of the Total Environment 587–588 (2017) 87–93. https://doi.org/10.1016/j.scitotenv.2017.02.035.

[103] T. De Baerdemaeker, B. Lemmens, C. Dotremont, J. Fret, L. Roef, K. Goiris, L. Diels, Benchmark study on algae harvesting with backwashable submerged flat panel membranes, Bioresour Technol 129 (2013) 582–591. https://doi.org/10.1016/j.biortech.2012.10.153.

[104] M. Larronde-Larretche, X. Jin, Microalgal biomass dewatering using forward osmosis membrane: Influence of microalgae species and carbohydrates composition, Algal Res 23 (2017) 12–19. https://doi.org/10.1016/j.algal.2016.12.020.

[105] Q.V. Ly, T. Maqbool, J. Hur, Unique characteristics of algal dissolved organic matter and their association with membrane fouling behavior: a review, Environmental Science and Pollution Research 24 (2017) 11192–11205. https://doi.org/10.1007/s11356-017-8683-4.

[106] T. Hwang, S.J. Park, Y.K. Oh, N. Rashid, J.I. Han, Harvesting of Chlorella sp. KR-1 using a cross-flow membrane filtration system equipped with an anti-fouling membrane, Bioresour Technol 139 (2013) 379–382. https://doi.org/10.1016/j.biortech.2013.03.149.

[107] A. Alipourzadeh, M.R. Mehrnia, A. Hallaj Sani, A. Babaei, Application of response surface methodology for investigation of membrane fouling behaviours in microalgal membrane bioreactor: The effect of aeration rate and biomass concentration, RSC Adv 6 (2016) 111182–111189. https://doi.org/10.1039/c6ra23188h.

[108] F. Zhao, Y. Su, X. Tan, H. Chu, Y. Zhang, L. Yang, X. Zhou, Effect of temperature on extracellular organic matter (EOM) of Chlorella pyrenoidosa and effect of EOM on irreversible membrane fouling, Colloids Surf B Biointerfaces 136 (2015) 431–439. https://doi.org/10.1016/j.colsurfb.2015.09.031.

[109] H. Yu, F. Qu, H. Liang, Z. shuang Han, J. Ma, S. Shao, H. Chang, G. Li, Understanding ultrafiltration membrane fouling by extracellular organic matter of Microcystis aeruginosa using fluorescence excitation-emission matrix coupled with parallel factor analysis, Desalination 337 (2014) 67–75. https://doi.org/10.1016/j.desal.2014.01.014.

[110] Y. Liao, A. Bokhary, E. Maleki, B. Liao, A review of membrane fouling and its control in algal-related membrane processes, Bioresour Technol 264 (2018) 343–358. https://doi.org/10.1016/j.biortech.2018.06.102.

[111] H. Elcik, M. Cakmakci, Harvesting microalgal biomass using crossflow membrane filtration: critical flux, filtration performance, and fouling characterization, Environmental Technology (United Kingdom) 38 (2017) 1585–1596. https://doi.org/10.1080/09593330.2016.1237560.

[112] X. Sun, C. Wang, Y. Tong, W. Wang, J. Wei, Microalgae filtration by UF membranes: Influence of three membrane materials, Desalination Water Treat 52 (2014) 5229–5236. https://doi.org/10.1080/19443994.2013.813103.

[113] X. Du, Y. Shi, V. Jegatheesan, I. Ul Haq, A review on the mechanism, impacts and control methods of membrane fouling in MBR system, 2020. https://doi.org/10.3390/membranes10020024.

[114] O.T. Iorhemen, R.A. Hamza, J.H. Tay, Membrane bioreactor (Mbr) technology for wastewater treatment and reclamation: Membrane fouling, Membranes (Basel) 6 (2016) 13–16. https://doi.org/10.3390/membranes6020033.

[115] B.S.B. Bamba, C.C. Tranchant, A. Ouattara, P. Lozano, Harvesting of Microalgae Biomass Using Ceramic Microfiltration at High Cross-Flow Velocity, Appl Biochem Biotechnol 193 (2021) 1147–1169. https://doi.org/10.1007/s12010-020-03455-y.

[116] D. Rana, T. Matsuura, Surface modifications for antifouling membranes, Chem Rev 110 (2010) 2448–2471. https://doi.org/10.1021/cr800208y.

[117] M.R. Bilad, H.A. Arafat, I.F.J. Vankelecom, Membrane technology in microalgae cultivation and harvesting: A review, Biotechnol Adv 32 (2014) 1283–1300. https://doi.org/10.1016/j.biotechadv.2014.07.008.

[118] L. Gu, M.Y. Xie, Y. Jin, M. He, X.Y. Xing, Y. Yu, Q.Y. Wu, Construction of antifouling membrane surfaces through layer-by-layer self-assembly of lignosulfonate and polyethyleneimine, Polymers (Basel) 11 (2019) 9–11. https://doi.org/10.3390/polym11111782.

[119] W. Mo, L. Soh, J.R. Werber, M. Elimelech, J.B. Zimmerman, Application of membrane dewatering for algal biofuel, Algal Res 11 (2015) 1–12. https://doi.org/10.1016/j.algal.2015.05.018.

[120] M. Rickman, J. Pellegrino, R. Davis, Fouling phenomena during membrane filtration of microalgae, J Memb Sci 423–424 (2012) 33–42. https://doi.org/10.1016/j.memsci.2012.07.013.

[121] W. Mo, L. Soh, J.R. Werber, M. Elimelech, J.B. Zimmerman, Application of membrane dewatering for algal biofuel, Algal Res 11 (2015) 1–12. https://doi.org/10.1016/j.algal.2015.05.018.

[122] Y. Liao, A. Bokhary, E. Maleki, B. Liao, A review of membrane fouling and its control in algal-related membrane processes, Bioresour Technol 264 (2018) 343–358. https://doi.org/10.1016/j.biortech.2018.06.102.

[123] G. Chen, L. Zhao, Y. Qi, Y.L. Cui, Chitosan and its derivatives applied in harvesting microalgae for biodiesel production: An outlook, J Nanomater 2014 (2014). https://doi.org/10.1155/2014/217537.

[124] W. Mo, L. Soh, J.R. Werber, M. Elimelech, J.B. Zimmerman, Application of membrane dewatering for algal biofuel, Algal Res 11 (2015) 1–12. https://doi.org/10.1016/j.algal.2015.05.018.

[125] Y. Zhang, Q. Fu, Algal fouling of microfiltration and ultrafiltration membranes and control strategies: A review, Sep Purif Technol 203 (2018) 193–208. https://doi.org/10.1016/j.seppur.2018.04.040.

[126] H. Elcik, M. Cakmakci, B. Ozkaya, The fouling effects of microalgal cells on crossflow membrane filtration, J Memb Sci 499 (2016) 116–125. https://doi.org/10.1016/j.memsci.2015.10.043.

[127] H. Elcik, M. Cakmakci, Harvesting microalgal biomass using crossflow membrane filtration: critical flux, filtration performance, and fouling characterization, Environmental Technology (United Kingdom) 38 (2017) 1585–1596. https://doi.org/10.1080/09593330.2016.1237560.

[128] M. Zhang, L. Yao, E. Maleki, B.Q. Liao, H. Lin, Membrane technologies for microalgal cultivation and dewatering: Recent progress and challenges, Algal Res 44 (2019) 101686. https://doi.org/10.1016/j.algal.2019.101686.

[129] A. Udayan, R. Sirohi, N. Sreekumar, B.I. Sang, S.J. Sim, Mass cultivation and harvesting of microalgal biomass: Current trends and future perspectives, Bioresour Technol 344 (2022) 126406. https://doi.org/10.1016/j.biortech.2021.126406.

[130] S.A. Scott, M.P. Davey, J.S. Dennis, I. Horst, C.J. Howe, D.J. Lea-Smith, A.G. Smith, Biodiesel from algae: Challenges and prospects, Curr Opin Biotechnol 21 (2010) 277–286. https://doi.org/10.1016/j.copbio.2010.03.005.

[131] T. Zhang, X. Xie, Z. Huang, Life cycle water footprints of nonfood biomass fuels in China, Environ Sci Technol 48 (2014) 4137–4144. https://doi.org/10.1021/es404458j.

[132] Y. Zhang, C. Zhang, Y. Qiu, B. Li, H. Pang, Y. Xue, Y. Liu, Z. Yuan, X. Huang, Wastewater treatment technology selection under various influent conditions and effluent standards based on life cycle assessment, Resour Conserv Recycl 154 (2020). https://doi.org/10.1016/j.resconrec.2019.104562.

[133] W. Farooq, W.I. Suh, M.S. Park, J.W. Yang, Water use and its recycling in microalgae cultivation for biofuel application, Bioresour Technol 184 (2015) 73–81. https://doi.org/10.1016/j.biortech.2014.10.140.

[134] S.E. Loftus, Z.I. Johnson, Reused Cultivation Water Accumulates Dissolved Organic Carbon and Uniquely Influences Different Marine Microalgae, Front Bioeng Biotechnol 7 (2019) 1–13. https://doi.org/10.3389/fbioe.2019.00101.

[135] J.W. Becker, P.M. Berube, C.L. Follett, J.B. Waterbury, S.W. Chisholm, E.F. DeLong, D.J. Repeta, Closely related phytoplankton species produce similar suites of dissolved organic matter, Front Microbiol 5 (2014). https://doi.org/10.3389/fmicb.2014.00111.

[136] L.L. Zhuang, Y.H. Wu, V.M.D. Espinosa, T.Y. Zhang, G.H. Dao, H.Y. Hu, Soluble Algal Products (SAPs) in large scale cultivation of microalgae for biomass/bioenergy production: A review, Renewable and Sustainable Energy Reviews 59 (2016) 141–148. https://doi.org/10.1016/j.rser.2015.12.352.

[137] O. Depraetere, G. Pierre, W. Noppe, D. Vandamme, I. Foubert, P. Michaud, K. Muylaert, Influence of culture medium recycling on the performance of Arthrospira platensis cultures, Algal Res 10 (2015) 48–54. https://doi.org/10.1016/j.algal.2015.04.014.

[138] N. Zou, C. Zhang, Z. Cohen, A. Richmond, Production of cell mass and eicosapentaenoic acid (epa) in ultrahigh cell density cultures of nannochloropsis sp. (eustigmatophyceae), Eur J Phycol 35 (2000) 127–133. https://doi.org/10.1080/09670260010001735711.

[139] W. Farooq, M. Moon, B. gon Ryu, W.I. Suh, A. Shrivastav, M.S. Park, S.K. Mishra, J.W. Yang, Effect of harvesting methods on the reusability of water for cultivation of chlorella vulgaris, its lipid productivity and biodiesel quality, Algal Res 8 (2015) 1–7. https://doi.org/10.1016/j.algal.2014.12.007.

[140] J.J. Milledge, S. Heaven, A review of the harvesting of micro-algae for biofuel production, Rev Environ Sci Biotechnol 12 (2013) 165–178. https://doi.org/10.1007/s11157-012-9301-z.

[141] P. Das, M.I. Thaher, M.A.Q.M. Abdul Hakim, H.M.S.J. Al-Jabri, G.S.H.S. Alghasal, Microalgae harvesting by pH adjusted coagulation-flocculation, recycling of the

coagulant and the growth media, Bioresour Technol 216 (2016) 824–829. https://doi.org/10.1016/j.biortech.2016.06.014.

[142] R. Castro-Muñoz, O. García-Depraect, Membrane-based harvesting processes for microalgae and their valuable-related molecules: A review, Membranes (Basel) 11 (2021) 1–21. https://doi.org/10.3390/membranes11080585.

[143] C. V. González-López, M.C. Cerón-García, J.M. Fernández-Sevilla, A.M. González-Céspedes, J. Camacho-Rodríguez, E. Molina-Grima, Medium recycling for Nannochloropsis gaditana cultures for aquaculture, Bioresour Technol 129 (2013) 430–438. https://doi.org/10.1016/j.biortech.2012.11.061.

[144] A.L. Morocho-Jácome, G.F. Mascioli, S. Sato, J.C.M. de Carvalho, Continuous cultivation of Arthrospira platensis using exhausted medium treated with granular activated carbon, J Hydrol (Amst) 522 (2015) 467–474. https://doi.org/10.1016/j.jhydrol.2015.01.001.

[145] B.K. Nandi, B. Das, R. Uppaluri, M.K. Purkait, Microfiltration of mosambi juice using low cost ceramic membrane, J Food Eng 95 (2009) 597–605. https://doi.org/10.1016/j.jfoodeng.2009.06.024.

[146] S. Bose, C. Das, Preparation and characterization of low cost tubular ceramic support membranes using sawdust as a pore-former, Mater Lett 110 (2013) 152–155. https://doi.org/10.1016/j.matlet.2013.08.019.

[147] K.P. Goswami, G. Pugazhenthi, Effect of binder concentration on properties of low-cost fly ash-based tubular ceramic membrane and its application in separation of glycerol from biodiesel, J Clean Prod 319 (2021) 128679. https://doi.org/10.1016/j.jclepro.2021.128679.

[148] A. Majouli, S.A. Younssi, S. Tahiri, A. Albizane, H. Loukili, M. Belhaj, Characterization of flat membrane support elaborated from local Moroccan Perlite, Desalination 277 (2011) 61–66. https://doi.org/10.1016/j.desal.2011.04.003.

[149] A. Karim, B. Achiou, A. Bouazizi, A. Aaddane, M. Ouammou, M. Bouziane, J. Bennazha, S. Alami Younssi, Development of reduced graphene oxide membrane on flat Moroccan ceramic pozzolan support. Application for soluble dyes removal, J Environ Chem Eng 6 (2018) 1475–1485. https://doi.org/10.1016/j.jece.2018.01.055.

[150] A. Abdullayev, M.F. Bekheet, D.A.H. Hanaor, A. Gurlo, Materials and applications for low-cost ceramic membranes, Membranes (Basel) 9 (2019). https://doi.org/10.3390/membranes9090105.

[151] M. Purnima, T. Paul, K. Pakshirajan, G. Pugazhenthi, Onshore oilfield produced water treatment by hybrid microfiltration-biological process using kaolin based ceramic membrane and oleaginous Rhodococcus opacus, Chemical Engineering Journal 453 (2023) 139850. https://doi.org/10.1016/j.cej.2022.139850.

[152] N.J. Saikia, D.J. Bharali, P. Sengupta, D. Bordoloi, R.L. Goswamee, P.C. Saikia, P.C. Borthakur, Characterization, beneficiation and utilization of a kaolinite clay from Assam, India, Appl Clay Sci 24 (2003) 93–103. https://doi.org/10.1016/S0169-1317(03)00151-0.

[153] B.A. Kennedy, M. Society for Mining, Exploration, Surface Mining, Second Edition, Society for Mining, Metallurgy, and Exploration, 1990Title, n.d.

[154] S. Jana, M.K. Purkait, K. Mohanty, Applied Clay Science Preparation and characterization of low-cost ceramic micro fi ltration membranes for the removal of chromate from aqueous solutions, Appl Clay Sci 47 (2010) 317–324. https://doi.org/10.1016/j.clay.2009.11.036.

[155] S. Jana, M.K. Purkait, K. Mohanty, S. Jana, M.K. Purkait, K. Mohanty, Preparation and Characterizations of Ceramic Microfiltration Membrane : Effect of Inorganic Precursors on Membrane Morphology Preparation and Characterizations of Ceramic Microfiltration Membrane : Effect of Inorganic Precursors on Membrane Morphology, 6395 (2010). https://doi.org/10.1080/01496395.2010.503669.

[156] D. Vasanth, G. Pugazhenthi, R. Uppaluri, Cross-flow microfiltration of oil-in-water emulsions using low cost ceramic membranes, Desalination 320 (2013) 86–95. https://doi.org/10.1016/j.desal.2013.04.018.

[157] G. Chen, X. Ge, Y. Wang, W. Xing, Y. Guo, Design and preparation of high permeability porous mullite support for membranes by in-situ reaction, Ceram Int 41 (2015) 8282–8287. https://doi.org/10.1016/j.ceramint.2015.02.045.

[158] S. Chakraborty, R. Uppaluri, C. Das, Optimal fabrication of carbonate free kaolin based low cost ceramic membranes using mixture model response surface methodology, Appl Clay Sci 162 (2018) 101–112. https://doi.org/10.1016/j.clay.2018.06.002.

[159] D. Vasanth, G. Pugazhenthi, R. Uppaluri, Fabrication and properties of low cost ceramic microfiltration membranes for separation of oil and bacteria from its solution, J Memb Sci 379 (2011) 154–163. https://doi.org/10.1016/j.memsci.2011.05.050.

[160] G. Singh, S.K. Patidar, Microalgae harvesting techniques: A review, J Environ Manage 217 (2018) 499–508. https://doi.org/10.1016/j.jenvman.2018.04.010.

[161] Z. Zhao, M. Mertens, Y. Li, K. Muylaert, I.F.J. Vankelecom, A highly efficient and energy-saving magnetically induced membrane vibration system for harvesting microalgae, Bioresour Technol 300 (2020) 122688. https://doi.org/10.1016/j.biortech.2019.122688.

[162] A. Mushtaq, H. Cho, M.A. Ahmed, M.S.U. Rehman, J.I. Han, A novel method for the fabrication of silver nanowires-based highly electro-conductive membrane with antifouling property for efficient microalgae harvesting, J Memb Sci 590 (2019) 117258. https://doi.org/10.1016/j.memsci.2019.117258.

[163] N.F. Mohd Khairuddin, A. Idris, M. Irfan, Towards Efficient Membrane Filtration for Microalgae Harvesting: A Review, Jurnal Kejuruteraan si2 (2019) 103–112. https://doi.org/10.17576/jkukm-2019-si2(1)-13.

[164] S. Koley, S. Prasad, S.K. Bagchi, N. Mallick, Development of a harvesting technique for large-scale microalgal harvesting for biodiesel production, RSC Adv 7 (2017) 7227–7237. https://doi.org/10.1039/c6ra27286j.

[165] H. Zheng, Z. Gao, J. Yin, X. Tang, X. Ji, H. Huang, Harvesting of microalgae by flocculation with poly (γ-glutamic acid), Bioresour Technol 112 (2012) 212–220. https://doi.org/10.1016/j.biortech.2012.02.086.

[166] Y.R. Hu, F. Wang, S.K. Wang, C.Z. Liu, C. Guo, Efficient harvesting of marine microalgae Nannochloropsis maritima using magnetic nanoparticles, Bioresour Technol 138 (2013) 387–390. https://doi.org/10.1016/j.biortech.2013.04.016.

[167] Z. Wu, Y. Zhu, W. Huang, C. Zhang, T. Li, Y. Zhang, A. Li, Evaluation of flocculation induced by pH increase for harvesting microalgae and reuse of flocculated medium, Bioresour Technol 110 (2012) 496–502. https://doi.org/10.1016/j.biortech.2012.01.101.

[168] H. Elcik, M. Cakmakci, Harvesting microalgal biomass using crossflow membrane filtration: critical flux, filtration performance, and fouling characterization, Environmental Technology (United Kingdom) 38 (2017) 1585–1596. https://doi.org/10.1080/09593330.2016.1237560.

[169] Y. Li, Z. Zhang, Y. Duan, H. Wang, The effect of recycling culture medium after harvesting of Chlorella vulgaris biomass by flocculating bacteria on microalgal growth and the functionary mechanism, Bioresour Technol 280 (2019) 188–198. https://doi.org/10.1016/j.biortech.2019.01.149.

[170] T.S. Gendy, S.A. El-Temtamy, Commercialization potential aspects of microalgae for biofuel production: An overview, Egyptian Journal of Petroleum 22 (2013) 43–51. https://doi.org/10.1016/j.ejpe.2012.07.001.

[171] Z. Yu, H. Pei, Q. Hou, C. Nie, L. Zhang, Z. Yang, X. Wang, The effects of algal extracellular substances on algal growth, metabolism and long-term medium recycle, and inhibition alleviation through ultrasonication, Bioresour Technol 267 (2018) 192–200. https://doi.org/10.1016/j.biortech.2018.07.019.

[172] J. Yang, M. Xu, X. Zhang, Q. Hu, M. Sommerfeld, Y. Chen, Life-cycle analysis on biodiesel production from microalgae: Water footprint and nutrients balance, Bioresour Technol 102 (2011) 159–165. https://doi.org/10.1016/j.biortech.2010.07.017.

[173] S. Wu, X. Xie, L. Huan, Z. Zheng, P. Zhao, J. Kuang, X. Liu, G. Wang, Selection of optimal flocculant for effective harvesting of the fucoxanthin-rich marine microalga Isochrysis galbana, J Appl Phycol 28 (2016) 1579–1588. https://doi.org/10.1007/s10811-015-0716-0.

[174] W. Wang, J. Sha, Z. Lu, S. Shao, P. Sun, Q. Hu, X. Zhang, Implementation of UV-based advanced oxidation processes in algal medium recycling, Science of the Total Environment 634 (2018) 243–250. https://doi.org/10.1016/j.scitotenv.2018.03.342.

[175] F. Fasaei, J.H. Bitter, P.M. Slegers, A.J.B. van Boxtel, Techno-economic evaluation of microalgae harvesting and dewatering systems, Algal Res 31 (2018) 347–362. https://doi.org/10.1016/j.algal.2017.11.038.

[176] S. Li, T. Hu, Y. Xu, J. Wang, R. Chu, Z. Yin, F. Mo, L. Zhu, A review on flocculation as an efficient method to harvest energy microalgae: Mechanisms, performances, influencing factors and perspectives, Renewable and Sustainable Energy Reviews 131 (2020) 110005. https://doi.org/10.1016/j.rser.2020.110005.

[177] Z.Y. Ni, J.Y. Li, Z.Z. Xiong, L.H. Cheng, X.H. Xu, Role of granular activated carbon in the microalgal cultivation from bacteria contamination, Bioresour Technol 247 (2018) 36–43. https://doi.org/10.1016/j.biortech.2017.07.079.

[178] F. Sher, K. Hanif, A. Rafey, U. Khalid, A. Zafar, M. Ameen, E.C. Lima, Removal of micropollutants from municipal wastewater using different types of activated carbons, J Environ Manage 278 (2021) 111302. https://doi.org/10.1016/j.jenvman.2020.111302.

[179] A.L. Morocho-Jácome, G.F. Mascioli, S. Sato, J.C.M. de Carvalho, Evaluation of physicochemical treatment conditions for the reuse of a spent growth medium in Arthrospira platensis cultivation, Algal Res 13 (2016) 159–166. https://doi.org/10.1016/j.algal.2015.11.022.

[180] J. Sha, Z. Lu, J. Ye, G. Wang, Q. Hu, Y. Chen, X. Zhang, The inhibition effect of recycled Scenedesmus acuminatus culture media: Influence of growth phase, inhibitor identification and removal, Algal Res 42 (2019). https://doi.org/10.1016/j.algal.2019.101612.

[181] X. Zhang, Z. Lu, Y. Wang, P. Wensel, M. Sommerfeld, Q. Hu, Recycling Nannochloropsis oceanica culture media and growth inhibitors characterization, Algal Res 20 (2016) 282–290. https://doi.org/10.1016/j.algal.2016.09.001.

[182] J. Sha, Z. Lu, J. Ye, G. Wang, Q. Hu, Y. Chen, X. Zhang, The inhibition effect of recycled Scenedesmus acuminatus culture media: Influence of growth phase, inhibitor identification and removal, Algal Res 42 (2019). https://doi.org/10.1016/j.algal.2019.101612.

[183] J.H. Hwang, B.E. Rittmann, Effect of permeate recycling and light intensity on growth kinetics of Synechocystis sp. PCC 6803, Algal Res 27 (2017) 170–176. https://doi.org/10.1016/j.algal.2017.09.008.

[184] Z. Yu, H. Pei, Q. Hou, C. Nie, L. Zhang, Z. Yang, X. Wang, The effects of algal extracellular substances on algal growth, metabolism and long-term medium recycle, and inhibition alleviation through ultrasonication, Bioresour Technol 267 (2018) 192–200. https://doi.org/10.1016/j.biortech.2018.07.019.

[185] L. del C. Mejia-da-Silva, M.C. Matsudo, A.L. Morocho-Jacome, J.C.M. de Carvalho, Application of Physicochemical Treatment Allows Reutilization of Arthrospira platensis Exhausted Medium: An Investigation of Reusing Medium in Arthrospira platensis Cultivation, Appl Biochem Biotechnol 186 (2018) 40–53. https://doi.org/10.1007/s12010-018-2712-8.

[186] J.H. Hwang, B.E. Rittmann, Effect of permeate recycling and light intensity on growth kinetics of Synechocystis sp. PCC 6803, Algal Res 27 (2017) 170–176. https://doi.org/10.1016/j.algal.2017.09.008.

[187] O. Depraetere, G. Pierre, W. Noppe, D. Vandamme, I. Foubert, P. Michaud, K. Muylaert, Influence of culture medium recycling on the performance of Arthrospira platensis cultures, Algal Res 10 (2015) 48–54. https://doi.org/10.1016/j.algal.2015.04.014.

[188] K.P. Goswami, G. Pugazhenthi, Treatment of poultry slaughterhouse wastewater using tubular microfiltration membrane with fly ash as key precursor, Journal of Water Process Engineering 37 (2020) 101361. https://doi.org/10.1016/j.jwpe.2020.101361.

[189] A. Agarwalla, S. Mishra, K. Mohanty, Treatment and recycle of harvested microalgal effluent using powdered activated carbon for reducing water footprint and enhancing biofuel production under a biorefinery model, Bioresour Technol 360 (2022) 127598. https://doi.org/10.1016/j.biortech.2022.127598.

[190] M. Messaoudi, N. Tijani, S. Baya, A. Lahnafi, H. Ouallal, H. Moussout, L. Messaoudi, South African Journal of Chemical Engineering Characterization of ceramic pieces shaped from clay intended for the development of filtration membranes, S Afr J Chem Eng 37 (2021) 1–11. https://doi.org/10.1016/j.sajce.2021.03.004.

[191] S. Bouzid, S. Gassara, J. Bouaziz, A. Deratani, S. Baklouti, Applied Clay Science Development and characterization of porous membranes based on kaolin / chitosan composite, 143 (2017) 1–9. https://doi.org/10.1016/j.clay.2017.03.008.

[192] MURRAY H. H. Applied clay mineralogy. Occurrences, processing and application of kaolins, bentonites, palygorskite-sepiolite and common clays. Elsevier, 2007. 180p., n.d.

[193] H. Douiri, S. Louati, S. Baklouti, M. Arous, Z. Fakhfakh, Structural and dielectric comparative studies of geopolymers prepared with metakaolin and Tunisian natural clay, Appl Clay Sci 139 (2017) 40–44. https://doi.org/10.1016/j.clay.2017.01.018.

[194] E. Klosek-Wawrzyn, J. Malolepszy, P. Murzyn, Sintering behavior of kaolin with calcite, Procedia Eng 57 (2013) 572–582. https://doi.org/10.1016/j.proeng.2013.04.073.

[195] H. Wang, C. Li, Z. Peng, S. Zhang, Characterization and thermal behavior of kaolin, J Therm Anal Calorim 105 (2011) 157–160. https://doi.org/10.1007/s10973-011-1385-0.

[196] Brindley, G.W., Nakahira, M. The KaoIinite-Mullite Reaction Series: I, A Survey of Outstanding Problems (1959), (2021) 2021.

[197] A. Agarwal, A. Samanta, B.K. Nandi, A. Mandal, Synthesis, characterization and performance studies of kaolin-fly ash-based membranes for microfiltration of oily waste water, J Pet Sci Eng 194 (2020) 107475. https://doi.org/10.1016/j.petrol.2020.107475.

[198] B.K. Nandi, R. Uppaluri, M.K. Purkait, Preparation and characterization of low cost ceramic membranes for micro-filtration applications, Appl Clay Sci 42 (2008) 102–110. https://doi.org/10.1016/j.clay.2007.12.001.

[199] G. Chen, X. Ge, Y. Wang, W. Xing, Y. Guo, Design and preparation of high permeability porous mullite support for membranes by in-situ reaction, Ceram Int 41 (2015) 8282–8287. https://doi.org/10.1016/j.ceramint.2015.02.045.

[200] D. Vasanth, G. Pugazhenthi, R. Uppaluri, Fabrication and properties of low cost ceramic microfiltration membranes for separation of oil and bacteria from its solution, J Memb Sci 379 (2011) 154–163. https://doi.org/10.1016/j.memsci.2011.05.050.

[201] S. Emani, R. Uppaluri, M.K. Purkait, Preparation and characterization of low cost ceramic membranes for mosambi juice clarification, Desalination 317 (2013) 32–40. https://doi.org/10.1016/j.desal.2013.02.024.

[202] M. Arzani, H.R. Mahdavi, M. Sheikhi, T. Mohammadi, O. Bakhtiari, Ceramic monolith as microfiltration membrane: Preparation, characterization and performance evaluation, Appl Clay Sci 161 (2018) 456–463. https://doi.org/10.1016/j.clay.2018.05.021.

[203] S.K. Hubadillah, M.H.D. Othman, A.F. Ismail, M.A. Rahman, J. Jaafar, A low cost hydrophobic kaolin hollow fiber membrane (h-KHFM) for arsenic removal from aqueous solution via direct contact membrane distillation, Sep Purif Technol 214 (2019) 31–39. https://doi.org/10.1016/j.seppur.2018.04.025.

[204] R. Vinoth Kumar, A. Kumar Ghoshal, G. Pugazhenthi, Elaboration of novel tubular ceramic membrane from inexpensive raw materials by extrusion method and its performance in microfiltration of synthetic oily wastewater treatment, J Memb Sci 490 (2015) 92–102. https://doi.org/10.1016/j.memsci.2015.04.066.

[205] P. Monash, G. Pugazhenthi, Development of Ceramic Supports Derived from Low-Cost Raw Materials for Membrane Applications and its Optimization Based on Sintering Temperature, 238 (2011). https://doi.org/10.1111/j.1744-7402.2009.02443.x.

[206] S.K. Hubadillah, M.H.D. Othman, T. Matsuura, A.F. Ismail, M.A. Rahman, Z. Harun, J. Jaafar, M. Nomura, Fabrications and applications of low cost ceramic membrane from kaolin: A comprehensive review, Ceram Int 44 (2018) 4538–4560. https://doi.org/10.1016/j.ceramint.2017.12.215.

[207] A. Harabi, F. Zenikheri, B. Boudaira, F. Bouzerara, A. Guechi, L. Foughali, A new and economic approach to fabricate resistant porous membrane supports using kaolin and CaCO3, J Eur Ceram Soc 34 (2014) 1329–1340. https://doi.org/10.1016/j.jeurceramsoc.2013.11.007.

[208] S. Mishra, K. Mohanty, Comprehensive characterization of microalgal isolates and lipid-extracted biomass as zero-waste bioenergy feedstock: An integrated bioremediation and biorefinery approach, Bioresour Technol 273 (2019) 177–184. https://doi.org/10.1016/j.biortech.2018.11.012.

[209] X. Chen, C. Huang, T. Liu, Fl Uoride Microfi Ltration Membrane, 45 (2012) 177–181.

[210] Z. Lu, J. Sha, W. Wang, Y. Li, G. Wang, Y. Chen, Q. Hu, X. Zhang, Identification of auto-inhibitors in the reused culture media of the Chlorophyta Scenedesmus acuminatus, Algal Res 44 (2019) 101665. https://doi.org/10.1016/j.algal.2019.101665.

[211] X. Zhang, Z. Lu, Y. Wang, P. Wensel, M. Sommerfeld, Q. Hu, Recycling Nannochloropsis oceanica culture media and growth inhibitors characterization, Algal Res 20 (2016) 282–290. https://doi.org/10.1016/j.algal.2016.09.001.

[212] X. Chen, C. Huang, T. Liu, Harvesting of microalgae Scenedesmus sp. using polyvinylidene fluoride microfiltration membrane, Desalination Water Treat 45 (2012) 177–181. https://doi.org/10.1080/19443994.2012.692034.

[213] M. Gebremedhin, S. Mishra, K. Mohanty, Augmentation of native microalgae based biofuel production through statistical optimization of campus sewage wastewater as low-cost growth media, J Environ Chem Eng 6 (2018) 6623–6632. https://doi.org/10.1016/j.jece.2018.08.061.

[214] A. Singh, D.B. Pal, S. Kumar, N. Srivastva, A. Syed, A.M. Elgorban, R. Singh, V.K. Gupta, Studies on Zero-cost algae based phytoremediation of dye and heavy metal from simulated wastewater, Bioresour Technol 342 (2021) 125971. https://doi.org/10.1016/j.biortech.2021.125971.

[215] C. V. González-López, M.C. Cerón-García, J.M. Fernández-Sevilla, A.M. González-Céspedes, J. Camacho-Rodríguez, E. Molina-Grima, Medium recycling for Nannochloropsis gaditana cultures for aquaculture, Bioresour Technol 129 (2013) 430–438. https://doi.org/10.1016/j.biortech.2012.11.061.

[216] A.L. Morocho-Jácome, G.F. Mascioli, S. Sato, J.C.M. de Carvalho, Continuous cultivation of Arthrospira platensis using exhausted medium treated with granular activated carbon, J Hydrol (Amst) 522 (2015) 467–474. https://doi.org/10.1016/j.jhydrol.2015.01.001.

[217] X. Zhang, Z. Lu, Y. Wang, P. Wensel, M. Sommerfeld, Q. Hu, Recycling Nannochloropsis oceanica culture media and growth inhibitors characterization, Algal Res 20 (2016) 282–290. https://doi.org/10.1016/j.algal.2016.09.001.

[218] W. Farooq, Sustainable production of microalgae biomass for biofuel and chemicals through recycling of water and nutrient within the biorefinery context: A review, GCB Bioenergy 13 (2021) 914–940. https://doi.org/10.1111/gcbb.12822.

[219] E. Daneshvar, L. Antikainen, E. Koutra, M. Kornaros, A. Bhatnagar, Investigation on the feasibility of Chlorella vulgaris cultivation in a mixture of pulp and aquaculture

effluents: Treatment of wastewater and lipid extraction, Bioresour Technol 255 (2018) 104–110. https://doi.org/10.1016/j.biortech.2018.01.101.

[220] M. Arif, Y. Li, M.M. El-Dalatony, C. Zhang, X. Li, E.S. Salama, A complete characterization of microalgal biomass through FTIR/TGA/CHNS analysis: An approach for biofuel generation and nutrients removal, Renew Energy 163 (2021) 1973–1982. https://doi.org/10.1016/j.renene.2020.10.066.

[221] G. Su, H.C. Ong, Y.Y. Gan, W.H. Chen, C.T. Chong, Y.S. Ok, Co-pyrolysis of microalgae and other biomass wastes for the production of high-quality bio-oil: Progress and prospective, Bioresour Technol 344 (2022) 126096. https://doi.org/10.1016/j.biortech.2021.126096.

[222] B. Samal, K.R. Vanapalli, B.K. Dubey, J. Bhattacharya, S. Chandra, I. Medha, Influence of process parameters on thermal characteristics of char from co-pyrolysis of eucalyptus biomass and polystyrene: Its prospects as a solid fuel, Energy 232 (2021) 121050. https://doi.org/10.1016/j.energy.2021.121050.

[223] G. Venkata Subhash, M. Rajvanshi, G. Raja Krishna Kumar, U. Shankar Sagaram, V. Prasad, S. Govindachary, S. Dasgupta, Challenges in microalgal biofuel production: A perspective on techno economic feasibility under biorefinery stratagem, Bioresour Technol 343 (2022) 126155. https://doi.org/10.1016/j.biortech.2021.126155.

[224] G. Jha, S. Soren, K.D. Mehta, Life cycle assessment of sintering process for carbon footprint and cost reduction: A comparative study for coke and biomass-derived sintering process, J Clean Prod 259 (2020) 120889. https://doi.org/10.1016/j.jclepro.2020.120889.

[225] M.M.A. Aziz, K.A. Kassim, Z. Shokravi, F.M. Jakarni, H.Y. Lieu, N. Zaini, L.S. Tan, S. Islam, H. Shokravi, Two-stage cultivation strategy for simultaneous increases in growth rate and lipid content of microalgae: A review, Renewable and Sustainable Energy Reviews 119 (2020) 109621. https://doi.org/10.1016/j.rser.2019.109621.

[226] A.I. Osman, Mass spectrometry study of lignocellulosic biomass combustion and pyrolysis with NOx removal, Renew Energy 146 (2020) 484–496. https://doi.org/10.1016/j.renene.2019.06.155.

[227] S. Basu, A.S. Roy, K. Mohanty, A.K. Ghoshal, Enhanced CO2 sequestration by a novel microalga: Scenedesmus obliquus SA1 isolated from bio-diversity hotspot region of Assam, India, Bioresour Technol 143 (2013) 369–377. https://doi.org/10.1016/j.biortech.2013.06.010.

[228] S. Basu, A.S. Roy, K. Mohanty, A.K. Ghoshal, Enhanced CO2 sequestration by a novel microalga: Scenedesmus obliquus SA1 isolated from bio-diversity hotspot region of Assam, India, Bioresour Technol 143 (2013) 369–377. https://doi.org/10.1016/j.biortech.2013.06.010.

[229] A.E.F. Abomohra, H. Eladel, M. El-Esawi, S. Wang, Q. Wang, Z. He, Y. Feng, H. Shang, D. Hanelt, Effect of lipid-free microalgal biomass and waste glycerol on growth and lipid production of Scenedesmus obliquus: Innovative waste recycling for extraordinary lipid production, Bioresour Technol 249 (2018) 992–999. https://doi.org/10.1016/j.biortech.2017.10.102.

[230] L. Han, H. Pei, W. Hu, L. Jiang, G. Ma, S. Zhang, F. Han, Integrated campus sewage treatment and biomass production by Scenedesmus quadricauda SDEC-13, Bioresour Technol 175 (2015) 262–268. https://doi.org/10.1016/j.biortech.2014.10.100.

[231] M. Nayak, A. Karemore, R. Sen, Sustainable valorization of flue gas CO 2 and wastewater for the production of microalgal biomass as a biofuel feedstock in closed and open reactor systems, RSC Adv. 6 (2016) 91111–91120. https://doi.org/10.1039/C6RA17899E.

[232] B. Cheirsilp, W. Maneechote, Insight on zero waste approach for sustainable microalgae biorefinery: Sequential fractionation, conversion and applications for high-to-low value-added products, Bioresour Technol Rep 18 (2022) 101003. https://doi.org/10.1016/j.biteb.2022.101003.

[233] S. Venkata Mohan, G.N. Nikhil, P. Chiranjeevi, C. Nagendranatha Reddy, M. V. Rohit, A.N. Kumar, O. Sarkar, Waste biorefinery models towards sustainable circular bioeconomy: Critical review and future perspectives, Bioresour Technol 215 (2016) 2–12. https://doi.org/10.1016/j.biortech.2016.03.130.

[234] S. Venkata Mohan, M. Hemalatha, D. Chakraborty, S. Chatterjee, P. Ranadheer, R. Kona, Algal biorefinery models with self-sustainable closed loop approach: Trends and

prospective for blue-bioeconomy, Bioresour Technol 295 (2020) 122128. https://doi.org/10.1016/j.biortech.2019.122128.

[235] M. Ghodrat, M.A. Rhamdhani, G. Brooks, S. Masood, G. Corder, Techno economic analysis of electronic waste processing through black copper smelting route, J Clean Prod 126 (2016) 178–190. https://doi.org/10.1016/j.jclepro.2016.03.033.

[236] E. Tito, G. Zoppi, G. Pipitone, E. Miliotti, A. Di Fraia, A.M. Rizzo, R. Pirone, D. Chiaramonti, S. Bensaid, Conceptual design and techno-economic assessment of coupled hydrothermal liquefaction and aqueous phase reforming of lignocellulosic residues, J Environ Chem Eng 11 (2023). https://doi.org/10.1016/j.jece.2022.109076.

[237] K.P. Goswami, G. Pugazhenthi, Effect of binder concentration on properties of low-cost fly ash-based tubular ceramic membrane and its application in separation of glycerol from biodiesel, J Clean Prod 319 (2021) 128679. https://doi.org/10.1016/j.jclepro.2021.128679.

[238] O. Winter, Preliminary Economic Evaluation of Chemical Processes at the Research Level, Ind Eng Chem 61 (1969) 45–52. https://doi.org/10.1021/ie50712a009.

[239] PRODUCT AND PROCESS DESIGN PRINCIPLES, n.d.

[240] Y. Dong, H. Wu, F. Yang, S. Gray, Cost and efficiency perspectives of ceramic membranes for water treatment, Water Res 220 (2022) 118629. https://doi.org/10.1016/j.watres.2022.118629.

[241] A. Abdullayev, M.F. Bekheet, D.A.H. Hanaor, A. Gurlo, Materials and applications for low-cost ceramic membranes, Membranes (Basel) 9 (2019). https://doi.org/10.3390/membranes9090105.

[242] N. Singh, M. Cheryad, Process Design and Economic Analysis of a Ceramic Membrane System for Microfiltration of Corn Starch Hydrolysate, 1998.

[243] O. Winter, Preliminary Economic Evaluation of Chemical Processes at the Research Level, Ind Eng Chem 61 (1969) 45–52. https://doi.org/10.1021/ie50712a009.

List of Publications

and

Conference Presentation

Publications in International Journals

- A. Agarwalla, K. Mohanty, Fabrication and characterization of low-cost kaolin based tubular ceramic membrane for microalgal harvesting, ***Journal of Environmental Chemical Engineering***, 12,2024, 112089, doi: https://doi.org/10.1016/j.jece.2024.112089

- A. Agarwalla, K. Mohanty, Comprehensive characterization, development, and application of natural/Assam Kaolin-based ceramic microfiltration membrane, ***Materials Today Chemistry***, 23, 2022, 100649, ISSN 2468-5194, doi: https://doi.org/10.1016/j.mtchem.2021.100649

- A. Agarwalla, S. Mishra, K. Mohanty, Treatment and recycle of harvested microalgal effluent using powdered activated carbon for reducing water footprint and enhancing biofuel production under a biorefinery model, ***Bioresource Technology***, 360, 2022, 127598, doi: https://doi.org/10.1016/j.biortech.2022.127598

- A. Agarwalla, J Komandur, K. Mohanty, Current trends in the pretreatment of microalgal biomass for efficient and enhanced bioenergy production. ***Bioresource Technology***, *369,* 2023, 128330, doi: https://doi.org/10.1016/j.biortech.2022.128330

- A. Agarwalla, K. Mohanty, A critical review on the application of membrane technology in microalgal harvesting and extraction of value-added products. ***Separation and Purification Technology,*** 344, 2024, 127180, doi: https://doi.org/10.1016/j.seppur.2024.127180

Presentation in International/National Conferences

- A. Agarwalla, K. Mohanty, Comprehensive characterization, development, and application of natural/Assam kaolin-based ceramic microfiltration membrane, 74th Annual Session of Indian Institute of Chemical Engineers **(CHEMCON - 2021),** CSIR - Institute of Minerals and Materials Technology, Bhubaneswar, India, 26th – 30th Dec, 2021.

- A. Agarwalla, K. Mohanty, Comprehensive characterization, development, and application of natural/Assam kaolin-based ceramic microfiltration membrane, **NERC 2022**, IIT Guwahati.

- A. Agarwalla, K. Mohanty, Powdered activated carbon based treatment of harvested microalgal culture effluent for reducing water footprint and enhancing biofuel production, **India-Dalhousie Student Research Symposium 2022**, Dalhousie University, Dalhousie, 21st July 2022.

- A. Agarwalla, K. Mohanty, Powdered activated carbon based treatment of harvested microalgal culture effluent for reducing water footprint and enhancing biofuel production, **World water Day Celebration 2023, PDEU**, Gandhinagar, Gujarat, 22nd March 2023.

- A. Agarwalla, K. Mohanty, Fabrication and characterization of low-cost kaolin based tubular ceramic membrane for microalgal harvesting, **Advances in Algal Research Symposium 2023**, IIT Guwahati, 12th June 2023.

- A. Agarwalla, K. Mohanty, Fabrication and characterization of low-cost kaolin based tubular ceramic membrane for microalgal harvesting, **Membrane Science and Technology 2023**, Phuket, Thailand, September 2023.